รายงานการวิจัยฉบับสมบูรณ์

โครงการ การพัฒนาและการประยุกต์ใช้วิธีการทางเคมีวิเคราะห์
ในการศึกษาการกระจายขนาดของอนุภาคขนาดนาโนเมตรในตัวอย่างอาหาร
เพื่อความเข้าใจเกี่ยวกับความสามารถในการนำไปใช้งาน
และความเป็นพิษของอนุภาคขนาดนาโนเมตร

โดย ผศ.ดร. อทิตยา ศิริภิญญานนท์ และคณะ

กรกฎาคม 2558

สัญญาเลขที่ RSA5580011

รายงานการวิจัยฉบับสมบูรณ์

การพัฒนาและการประยุกต์ใช้วิธีการทางเคมีวิเคราะห์ในการศึกษาการกระจายขนาดของอนุภาคขนาดนาโนเมตรในตัวอย่างอาหาร เพื่อความเข้าใจเกี่ยวกับความสามารถในการนำไปใช้งานและความเป็นพิษของอนุภาคขนาดนาโนเมตร

คณะผู้วิจัย	สังกัด
1. ผศ.ดร. อทิตยา ศิริภิญญานนท์	ภาควิชาเคมี คณะวิทยาศาสตร์ มหาวิทยาลัยมหิดล
2. นางสาว วิไลวรรณ สมเชื้อ	ภาควิชาเคมี คณะวิทยาศาสตร์ มหาวิทยาลัยมหิดล
3. นางสาว พรวิลาส เอ็มเอ็ม	ภาควิชาเคมี คณะวิทยาศาสตร์ มหาวิทยาลัยมหิดล
4. นางสาว ระเบียบ สุวรรณเพ็ชร	ภาควิชาเคมี คณะวิทยาศาสตร์ มหาวิทยาลัยมหิดล
5. นาย มธุรส อ่อนไทย	ภาควิชาเคมี คณะวิทยาศาสตร์ มหาวิทยาลัยมหิดล

นักวิจัยที่ปรึกษา	สังกัด
ศ.ดร. ยุวดี เชี่ยววัฒนา	ภาควิชาเคมี คณะวิทยาศาสตร์ มหาวิทยาลัยมหิดล

สนับสนุนโดยสำนักงานกองทุนสนับสนุนการวิจัย

(ความเห็นในรายงานนี้เป็นของผู้วิจัย สกว. ไม่จำเป็นต้องเห็นด้วยเสมอไป)

สารบัญ

กิตติกรรมประกาศ

ขอขอบคุณสำนักงานกองทุนสนับสนุนการวิจัยที่ได้สนับสนุนทุนการวิจัย “ทุนพัฒนานักวิจัย” เพื่อใช้ในการดำเนินงานวิจัยในโครงการ “การพัฒนาและการประยุกต์ใช้วิธีการทางเคมีวิเคราะห์ในการศึกษาการกระจายขนาดของอนุภาคขนาดนาโนเมตรในตัวอย่างอาหารเพื่อความเข้าใจเกี่ยวกับความสามารถในการนำไปใช้งานและความเป็นพิษของอนุภาคขนาดนาโนเมตร” โดยมีระยะเวลาของโครงการ 3 ปี ตั้งแต่ กรกฎาคม 2555 ถึง กรกฎาคม 2558 และขอขอบคุณศูนย์ความเป็นเลิศด้านนวัตกรรมทางเคมี โครงการพัฒนาบัณฑิตศึกษาและการวิจัยทางเคมี โครงการพัฒนาเภสัชภัณฑ์จากทรัพยากรธรรมชาติและการจัดการ (NRU) และภาควิชาเคมี คณะวิทยาศาสตร์ มหาวิทยาลัยมหิดล สำหรับทุนการศึกษาของนักศึกษา วัสดุวิจัยและครุภัณฑ์บางส่วนในโครงการวิจัย เครื่องมือและอุปกรณ์ต่างๆ

คณะผู้วิจัย

บทคัดย่อ

รหัสโครงการ: **RSA5580011**

ชื่อโครงการ: **การพัฒนาและการประยุกต์ใช้วิธีการทางเคมีวิเคราะห์ในการศึกษาการกระจายขนาดของอนุภาคขนาดนาโนเมตรในตัวอย่างอาหารเพื่อความเข้าใจเกี่ยวกับความสามารถในการนำไปใช้งานและความเป็นพิษของอนุภาคขนาดนาโนเมตร**

ชื่อนักวิจัย: ผศ.ดร.อทิตยา ศิริภิญญานนท์

ภาควิชาเคมี คณะวิทยาศาสตร์ มหาวิทยาลัยมหิดล

Email Address: atitaya.sir@mahidol.ac.th

ระยะเวลาโครงการ: กรกฎาคม 2555 – กรกฎาคม 2558

งานวิจัยนี้สามารถสรุปได้ใน 3 บท บทที่ 1 กล่าวถึงการศึกษาขนาดและการกระจายขนาดของอนุภาคนาโนของธาตุเงินในผลิตภัณฑ์อุปโภค ได้แก่ เสื้อนาโนและผลิตภัณฑ์ซักล้าง ได้ประยุกต์เทคนิคการแยกแบบไหลภายใต้สนามร่วมกับเทคนิคการวิเคราะห์ปริมาณธาตุเงิน พบว่าธาตุเงินที่ถูกชะออกมาจากการซักล้างนั้น ประมาณเกือบ 100 เปอร์เซ็นต์อยู่ในรูปของไอออน และเพียง 1 เปอร์เซ็นต์อยู่ในรูปของอนุภาคขนาดนาโนเมตร และได้ทำการวิเคราะห์ขนาดของอนุภาคนาโนของธาตุเงินในผลิตภัณฑ์ซักล้าง ปรากฏว่าไม่สามารถตรวจวิเคราะห์ได้ด้วยเครื่องมือวิเคราะห์ขนาดอนุภาคแบบเทคนิคการแยกแบบไหลภายใต้สนามประเภทอาศัยแรงหนีศูนย์กลาง ซึ่งคาดว่าเกิดจากการที่อนุภาคนาโนเปลี่ยนรูปฟอร์ม ทำการพิสูจน์ด้วยการเติมอนุภาคนาโนของธาตุเงินขนาด 47 นาโนเมตร ลงในผลิตภัณฑ์ซักล้าง พบว่าประมาณ 75 เปอร์เซ็นต์ของอนุภาคนาโนของธาตุเงินเกิดการเปลี่ยนสภาพไปเป็นไอออน

บทที่ 2 กล่าวถึงการประยุกต์เทคนิคการแยกแบบไหลภายใต้สนามในการวิเคราะห์ขนาดและการกระจายขนาดของอนุภาคนาโนของธาตุซีลีเนียมในสภาวะจำลองของการย่อยและดูดซึมสารอาหาร โดยได้ศึกษาอนุภาคนาโนของธาตุซีลีเนียมหลายประเภท ที่มีสารเพิ่มความเสถียรต่างๆ กัน ได้แก่ เพคติน สารผสมระหว่างเพคตินและอัลจิเนท โอวัลบูมิน และเบต้าแลคโทโกบูลิน พบว่าขนาดและการกระจายขนาดของอนุภาคนาโนของธาตุซีลีเนียมชนิดต่างๆ เกิดการเปลี่ยนแปลงแตกต่างกันภายใต้สภาวะจำลองของการย่อยและดูดซึมสารอาหาร ทั้งประเภทที่มีและไม่มีการเติมเอ็นไซม์ โดยที่ประมาณมากกว่า 90 เปอร์เซ็นต์ของธาตุซีลีเนียม ยังคงอยู่ในสภาพที่เป็นอนุภาคขนาดนาโนเมตร

บทที่ 3 กล่าวถึงการประยุกต์เทคนิคการแยกแบบไหลภายใต้สนามร่วมกับเทคนิคการวิเคราะห์ปริมาณธาตุแบบอินดัคทีฟลีคัพเพิลพลาสมาแมสสเปกโทรเมตรี สำหรับการศึกษาการเกิดการเกาะจับกันระหว่างอนุภาคนาโนของธาตุเงินกับโปรตีน ได้แก่ โปรตีนอัลบูมินจากซีรัมของวัว โกบูลิน และไฟบริ

โนเจน ได้วิเคราะห์ค่าคงที่การเกาะจับกันระหว่างอนุภาคนาโนของธาตุเงินกับโปรตีนต่างๆ รวมถึงการศึกษาถึงปัจจัยต่างๆ ที่มีผลต่อการเกาะจับ ได้แก่ เวลาและความเข้มข้นของอนุภาคนาโนของธาตุเงิน พบว่าการเกาะจับกันมากขึ้นเมื่อเวลาเพิ่มนานขึ้น และความเข้มข้นของอนุภาคนาโนของธาตุเงินมากขึ้น และได้วิเคราะห์อัตราส่วนโดยโมลของการเกาะจับกันระหว่างโปรตีนอัลบูมินกับอนุภาคนาโนของธาตุเงิน

คำหลัก: การวิเคราะห์ขนาดอนุภาค เทคนิคการแยกแบบไหลภายใต้สนาม
อนุภาคนาโนของธาตุเงิน อนุภาคนาโนของธาตุซีลีเนียม การเกาะจับกับโปรตีน

ABSTRACT

Project Code: **RSA5580011**

Project Title: **Development and Application of Analytical Method for Investigation of Particle Size Distribution of Nanoparticles in Food Samples to Gain an Insight into Their Bioavailability and Toxicity**

Investigator: Atitaya Siripinyanond

Department of Chemistry, Faculty of Science, Mahidol University

Email Address: atitaya.sir@mahidol.ac.th

Project Period: July 2012 – July 2015

The works in this study are divided into three chapters. Chapter one is related to the study of particle size distribution of silver nanoparticles (AgNPs) in consumer product. Two field-flow fractionation (FFF) subtechniques with electrothermal atomic absorption spectrophotometry (ETAAS) were employed to characterize silver nanoparticles (AgNPs) in consumer products, i.e., cotton textile and cleaning products. Size characterization of silver leached from the cotton textile was carried out. Nearly 100% of the silver released was found to be silver ions, whereas only 1% was AgNPs. Further, size distribution of AgNPs in cleaning products, i.e., detergent and shampoo, was examined. Silver nanoparticles were not detectable in those samples by SdFFF. The known size of AgNPs (47 nm) were then spiked into the cleaning products and found that approximately 75% of AgNPs transformed into silver ion after exposure to the cleaning products.

Chapter two discusses about the application of flow field-flow fractionation for particle size characterization of selenium nanoparticles incubated in gastrointestinal conditions. Various types of selenium nanoparticles were examined, including those stabilized by pectin, mixed alginate/pectin, ovalbumin, and β-lactoglobulin. Upon incubation of selenium nanoparticles in gastrointestinal conditions, both in enzymatic and non-enzymatic media, particle size distributions and the surface of selenium nanoparticles changed differently. Nonetheless, more than 90 % of selenium was still presented in nanometer range after gastrointestinal digestion for the nanoparticles prepared by all types of stabilizers.

Chapter three describes the application of flow field-flow fractionation coupled with inductively coupled plasma mass spectrometry (FlFFF-ICP-MS) for investigation of AgNPs and plasma protein association. In this work, bovine serum albumin (BSA), globulin, and fibrinogen were

the model proteins studied. The apparent association constants between BSA and AgNPs of various sizes were determined. Factors influencing protein-AgNPs association were investigated including effect of incubation time and effect of AgNPs concentration. Association between protein and AgNPs increased as incubation time and concentration of AgNPs increased. Further, the binding stoichiometry between BSA and AgNPs was determined.

Keywords: size characterization, field-flow fractionation, silver nanoparticles, selenium nanoparticles, protein association

Executive Summary

Project Title: Development and Application of Analytical Method for Investigation of Particle Size Distribution of Nanoparticles in Food Samples to Gain an Insight into Their Bioavailability and Toxicity

Investigaor: Atitaya Siripinyanond

Department of Chemistry, Faculty of Science, Mahidol University

Email Address: atitaya.sir@mahidol.ac.th

Project Period: July 2012 – July 2015

This research focused on the development and application of an efficient analytical method based on the use of field-flow fractionation (FFF) to perform size characterization of nanoparticles in complex samples. The developed method was used for investigation of particle size distribution of silver nanoparticles in consumer products, e.g., cotton textile, cleaning products. Further, the method was develop to examine changes of selenium nanoparticles in gastrointestinal conditions to offer a systematic in vitro approach to gain more understanding in the nanoparticle properties when they enter human body. Further, when the nanoparticles enter into human body, they will interact with proteins in biological fluid. Therefore, an efficient method based on the use of field-flow fractionation coupled with inductively coupled plasma mass spectrometry was applied to examine the association between silver nanoparticles and proteins. The benefits of this research work are two folds. One is to obtain a new analytical approach for detection of nanoparticles in complex samples. The second is to gain more understanding of how nanoparticles interact with biological system. The results of this study can be considered as an updated scientific evidence of bioavailability and toxicity of nanoparticles, which should be of great concern.

Three papers have been published in the international journals as follows:

1. Wimuktiwan, P., Shiowatana, J., Siripinyanond, A., “Investigation of silver nanoparticles and plasma protein association using flow field-flow fractionation coupled with inductively coupled plasma mass spectrometry (FlFFF-ICP-MS)” (2015) Journal of Analytical Atomic Spectrometry, 30 (1), pp. 245-253. (impact factor 2013 = 3.396)

2. M-M, P., Somchue, W., Shiowatana, J., Siripinyanond, A., "Flow field-flow fractionation for particle size characterization of selenium nanoparticles incubated in gastrointestinal conditions" (2014) Food Research International, 57, pp. 208-209. (impact factor 2013 = 3.05)
3. M-M, P., Siripinyanond, A., "Field-flow fractionation with inductively coupled plasma mass spectrometry: Past, present, and future" (2014) Journal of Analytical Atomic Spectrometry, 29 (10), pp. 1739-1752. (impact factor 2013 = 3.396)

One manuscript has been published as a book chapter as follows:

1. Suwanpetch, R., Techarang, T., Ornthai, M., M-M, P., Siripinyanond, A., "Field-flow fractionation with atomic spectrometric detection for characterization of engineered nanoparticles", in Encyclopedia of Analytical Chemistry, John Wiley & Sons, Ltd., DOI: 10.1002/9780470027318.a9427.

Four papers have been presented at the international conferences during the past three years as follows:

1. Field-Flow Fractionation for Engineered Nanoparticles Characterization, The 2nd Taiwan-Thailand Bilateral Mini-Symposium: Chemistry for Creative Economy 17 - 18 January, 2013, Stang Mongkolsuk Building, Faculty of Science, Mahidol University, Thailand
2. Field-Flow Fractionation with Atomic Spectrometric Detection for Characterization of Engineered Nanoparticles, 2013 European Winter Conference on Plasma Spectrometry, 10 – 15 February, 2013, The Auditorium Maximum of Jagiellonian University, Krakow, Poland
3. Field-Flow Fractionation for Engineered Nanoparticles Characterization, The 1st Academic Science and Technology Conference (ASTC), 18 March, 2013, Ambassador Hotel Bangkok, Thailand
4. Hyphenated Inductively Coupled Plasma Mass Spectrometry Approaches for Bioaccessibility Study and Size-Based Fractionation, The 4th Asia Oceania Mass Spectrometry Conference and 10th Taiwan Society for Mass Spectrometry Annual Conference (4th AOMSC & 10th TSMS Annual Conference), 10 – 12 July, 2013, Taipei International Convention Center, Taipei, Taiwan

Chapter 1

Field-Flow Fractionation (FFF) with Electrothermal Atomic Absorption Spectrophotometric Detection for Particle Size Characterization of Silver Nanoparticles in Consumer Product

1.1 Introduction

Owing to the rapid growth of nanotechnology, nanoparticles (NPs) have been widely used in many area, including catalysis [1], sensor application [2], cosmetic [3], and pharmaceutics [4-5]. In biomedical application the use of silver nanoparticles (AgNPs) is generally known to improve antibacterial property [6-10]. Therefore, AgNPs have been applied in many commercial products such as room sprays, laundry detergents, water purificants, and wall paint [11-12]. Silver nanoparticles are also incorporated into textiles for manufacture of clothing, underwear, and socks [13-14]. Chances of AgNPs discharge into the environment are increasing which can exhibit ecotoxicity [15], and also greatly increase the risk of human exposure. Therefore, it is crucial to quantify and characterize the release of AgNPs from commercial products.

The information on concentration and physicochemical properties (size, shape, surface area etc.) of AgNPs under realistic conditions are important to gain understanding in their fate, behavior, toxicity, and stability in the natural aquatic environment. Their toxicity is related to particle size and size distribution, surface area, charge, solubility, reactivity, state of aggregation, elemental composition as well as structure and shape [16]. Moreover the information on particle size and size distribution are useful for prediction of AgNPs transport behavior. Owing to the importance of particle size of AgNPs, several analytical techniques have been applied to investigate their particle size such as transmission electron microscopy (TEM) [17-19], scanning electron microscopy (SEM) [20], dynamic light scattering (DLS) [20], field-flow fractionation (FFF) [21-23], and other related techniques [24-25].

In this work, two FFF subtechniques, i.e., flow FFF (FlFFF) and sedimentation FFF (SdFFF), were employed for characterization of AgNPs in consumer products. Field-flow fractionation offers wide window for particle size detection ranging from 2 nm to 20 μm, and hence is suitable for nanoparticle characterization. Further, FFF can be used with elemental detectors such as ETAAS [25], ICP-OES [26], ICP-MS [27], etc. to provide information on elemental concentration as a function of diameter or size-based distribution of elements. This work aims to demonstrate the applicability of FFF for characterization of AgNPs. Two FFF subtechniques were chosen to demonstrate their novel applications. The first part presents an application of on-channel FlFFF preconcentration coupled off-line with ETAAS for quantification and characterization of AgNPs release from cotton textile. Large volume introduction based on an on-channel FlFFF preconcentration was developed for two purposes. One was for the characterization of silver released from cotton fabric by using various washing solutions, i.e., doubly deionized water; tap water; and detergent in tap water. Another was for the classification of silver as AgNPs or silver ions released in detergent. The second part presents the application of SdFFF for size

characterization of AgNPs in cleaning products, which were detergent and shampoo. Also, changes in the particle size of AgNPs in the medium of cleaning products were investigated.

1.2 Experimental

1.2.1 Instrumentation

Two types of field-flow fractionation (FFF) were used. These included a flow FFF (FlFFF), which was used for size characterization of AgNPs from the cotton textile, and a sedimentation FFF (SdFFF), which was used for size characterization of AgNPs in cleaning products. A FlFFF system (Model PN-1021-FO, Postnova Analytics, Landsberg, Germany) with the dimension of 27 cm long, 2.0 cm wide, and 0.0254 cm thick was used. This FlFFF channel was equipped with a 1,000 Da molecular weight cut-off regenerated cellulose acetate membrane (Postnova Analytics). Two high-pressure liquid chromatography (HPLC) pumps (Model PN 2101, Postnova Analytics) were employed to deliver the flows, one for the channel (forward) flow and another one for the cross flow or the focusing (backward) flow. The operating conditions of FlFFF are summarized in Table 1. The SdFFF system used in this study was the model S-101 Particle/Colloid Fractionator purchased also from Postnova Analytics. The SdFFF channel was 89.5 cm long, 2.0 cm wide, and 0.0254 cm thick, with a rotor radius of 15.1 cm. The channel volume was calculated to be 4.45 mL. The carrier solution was introduced into the SdFFF channel by an HPLC pump (model PN1122, Postnova Analytics). Light attenuation by the eluted particles was monitored by a UV detector at the fixed wavelength of 400 nm (model UV2075, Jasco, Tokyo, Japan). Samples of 50 µL were introduced into a Rheodyne model 7725i loop injector. A carrier liquid was deionized water containing 0.02% (v/v) FL-70 detergent (Fisher Scientific, USA) and 0.02% (w/v) NaN_3 (Merck, Germany) to prevent bacterial growth, with the final pH of 10.5. The SdFFF instrument operating parameters are also summarized in Table 1.

Table 1 FFF operating conditions

FlFFF Model PN-1021-FO (Postnova Analytics, Landsberg, Germany)	
FlFFF channel dimensions	27.7 cm long x 2.0 cm wide x 0.02 cm thick
Carrier liquid	0.02% FL-70 and 0.02 NaN_3 (pH 9.5)
FlFFF with conventional sample introduction	
Channel flow rate	1.0 mL min^{-1}
Cross flow rate	2.0 mL min^{-1}
Equilibration time	1.0 min
FlFFF with large volume sample introduction	
Channel flow rate (forward)	0.24 mL min^{-1}
Cross flow rate (backward)	3.0 mL min^{-1}
Focusing time	7.0 min
SdFFF Model S-101 (Postnova Analytics, Landsberg, Germany)	
SdFFF channel dimensions/	89.5 cm long x 2.0 cm wide x 0.0254 cm thick
SdFFF rotor radius	15.1 cm
Carrier liquid	0.02% FL-70 and 0.02 NaN_3 (pH 9.5)
Channel flow rate	0.5 mL min^{-1}
Equilibration time	15 min
Power field programming	Initial field strength of 1200 RPM, predecay time for 8 min, field decay parameter of -64 min and final field strength of 150 RPM

A Perkin–Elmer Analyst 100 atomic absorption spectrophotometer equipped with a deuterium arc background corrector and a Perkin–Elmer HGA-800 heated-graphite atomizer was employed for silver determination. The Perkin–Elmer Model AS-72 autosampler was used to introduce standard and necessary solutions into the graphite tube. Pyrolytically coated graphite tubes with integrated platforms from the same manufacturer were used throughout and measurements were based on peak area. A silver hollow-cathode lamp was operated at 4 mA and the wavelength 328.1 nm was used. The spectral bandwidth was 0.7 nm. The furnace operating conditions for silver measurement are given in Table 2.

Table 2 Electrothermal atomic absorption spectrometer operating condition for silver detection

ETAAS: Perkin Elmer Analyst 100-HGA-800				
Step		Temperature (°C)	Ramp time (sec)	Hold time (sec)
1	Drying	130	20	30
2	Ashing	800	20	30
3	Atomization	1800	0	8
4	Clean up	2600	1	5

1.2.2 Chemicals and samples

AgNPs were purchased from Fluka (Buchs, Switzerland), Fisher Scientific (Leicestershire, UK), and Merck (Darmstadt, Germany), respectively. Silver nanoparticles (80 mg L^{-1}) were prepared by the following method. 100 mL of 0.1% (w/v) alginate was dissolved in 50 mL of 1 M ascorbic acid. The mixture was stirred for 3 min. Consequently, 50 mL of 2 M $AgNO_3$ was added and also stirred for 3 min by vortex. Then, 0.3 M of NaOH was added into the mixture until yellow solution of AgNPs was obtained.

To perform particle size characterization by FlFFF, gold colloidal standard of 10 nm (Sigma-Aldrich, Missouri, USA) was used for checking the FlFFF channel. With the large volume sample introduction method, the standard was diluted with carrier liquid 25 times

before introduction into FlFFF channel. FL-70 detergent and NaN_3 for the preparation of carrier liquid were from Fisher Scientific and Merck, respectively. In this case, the test sample was a nanosilver cotton textile purchased from a local company in Thailand.

To perform particle size characterization by SdFFF, polystyrene standards of various sizes including 0.2, 0.35, 0.53, and 0.72 μm purchased from Postnova Analytics were used for SdFFF calibration. In this case, the test samples were commercial detergent and shampoo purchased from a local supermarket, which were labeled to contain AgNPs.

To quantify the total amount of silver in the test samples, concentrated HCl, concentrated HNO_3, and 30% H_2O_2 were used to aid the digestion of the samples. All types of acid were from Merck.

1.2.3 Application of flow field-flow fractionation (FlFFF) for AgNPs characterization in cotton textile

The applicability of FlFFF for characterization of AgNPs was demonstrated for the nanosilver cotton textile sample. The leaching of AgNPs from the textile sample upon washing was investigated and the particle size was characterized. Experimental details are given as follows:

Washing of cotton fabric in various media

The modified ISO 105-method for washing procedure was applied [28]. A 50 mL centrifuge tube was used to contain the sample and the washing solution of 50 mL. Mechanical stress was exerted by three ceramic balls at approximately 0.6 cm. diameters. Three types of washing solution (doubly deionized water, tap water, and 4% AgNPs free detergent dissolved in tap water) were used for leaching study of AgNPs from cotton fabric. An accurately weighed 0.9 g sample (4 cm wide and 10 cm long) was placed in the centrifuge tube with ceramic balls, followed by addition of 50 mL of washing solution into the centrifuge tube. The centrifuge tube was then screw tightened with a lid. The centrifuge tube was agitated for 1-h contact time at room temperature on a horizontal platform shaker (IKA-Horizontal Shaker, Model HS 250 Basic, Germany) with the speed of approximately 250 RPM. Three washing cycles were applied. After the specified

contact time of 1-h, the fabric sample was removed and the sample was placed in a new centrifuge tube for the next washing cycle. The supernatant part was kept for particle size characterization by FlFFF and silver detection by ETAAS. Before introducing the sample to FlFFF, the obtained solution was filtered through a 0.45 μm nitrocellulose-cellulose acetate membrane filter (Lubitech, Shanghi, China) to remove some debris and big particles which can clog FlFFF tubings.

Acid digestion of cotton fabric sample

Acid digestion was performed before ETAAS determination of the amount of silver in the sample. Three pieces of cotton fabric were cut from various parts of the cotton fabric shirt including the front, back, and arm. A known amount of sample (approximately 0.5 g) was digested using 8.0 mL concentrated HNO_3 and 24.0 mL concentrated HCl mixture at approximately 100°C to obtain clear solution. The solution was allowed to cool, and then 3 mL of 30% H_2O_2 was added to complete the digestion process. The accurately weighed digested samples were diluted with deionized water and the total Ag contents were determined by ETAAS.

Particle size characterization of silver released from cotton fabric in various washing media

In order to improve the signal of AgNPs for a very diluted sample, sample preconcentration is necessary. Opposing-flow large-volume sample introduction (500 μL) was used for on-channel FlFFF preconcentration and size characterization. The system set up was similar to that reported by Hassellöv et al. [29] and Lyvén et al. [30]. This approach consists of three steps, which are sample loading and focusing; equilibration; and fractionation. In the sample loading and focusing step, the sample was introduced into the FlFFF channel and two opposing flow streams were used to focus the sample zone into a narrow band near the inlet of FlFFF channel. After a suitable focusing time, by which the whole sample volume was loaded and focused in the FlFFF channel, the forward and backward flow pumps were disengaged and the cross flow stream was introduced, so that the sample could reach steady state equilibrium. After that the sample was fractionated by applying cross and channel flows. The diagram of FlFFF set up for fractionation is depicted in Figure 1.

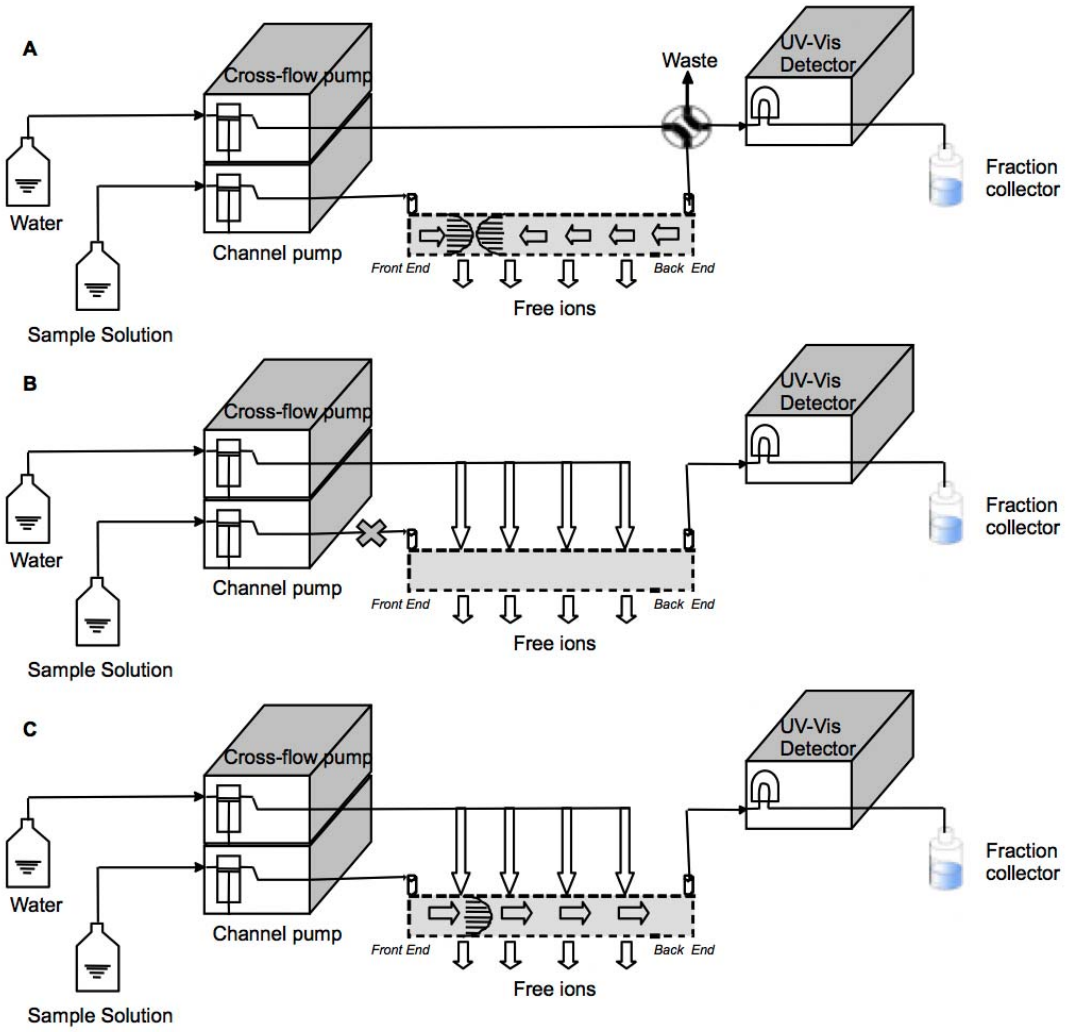

Figure 1 Schematic diagram illustrating FlFFF setup for AgNPs size characterization.

Classification of silver as AgNPs or silver ion release from the cotton fabric in detergent medium

To classify silver as AgNPs or silver ions released from the cotton shirt in various media, opposing-flow large-volume sample introduction (3.0 mL) was used for an on-channel FlFFF preconcentration and collection for silver determination by ETAAS. The system set up was similar to that reported by Sangsawong et al [31]. This approach consists of two steps, including sample loading and focusing; and collection.

In the sample loading and focusing step, the sample was introduced into the FlFFF channel and two opposing flow streams were used to focus the sample zone into a narrow band near the outlet of FlFFF channel. During sample loading and focusing step, silver

ions were removed through membrane whereas AgNPs or particles of larger size than the membrane pore size (1,000 Da or 1 nm) were retained. After a suitable focusing time, the sample was eluted and collected in a PTFE bottle. In the collection step, only AgNPs not silver ions were collected at the channel outlet. The diagram of FlFFF set up for classification of silver as AgNPs or silver ions from the cotton shirt in various media is shown in Figure 2.

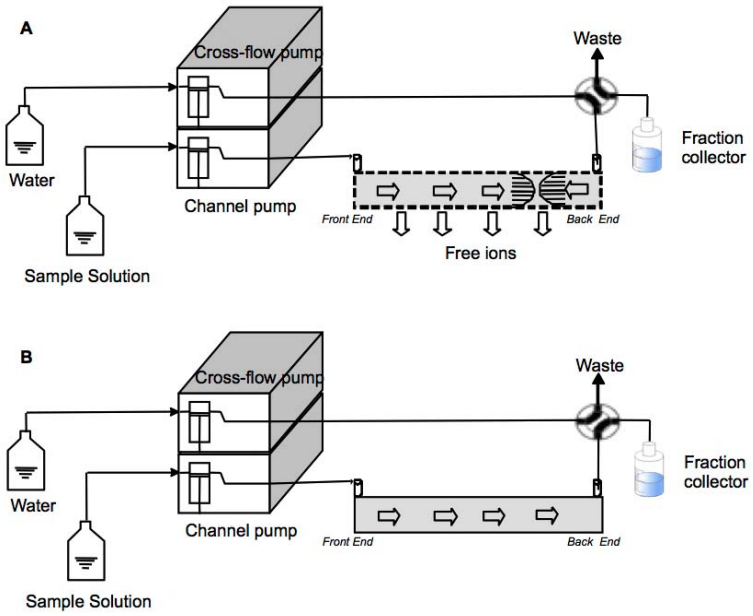

Figure 2 Schematic diagram illustrating FlFFF setup for separation of silver as AgNPs or silver ions.

1.2.4 Application of sedimentation field-flow fractionation (SdFFF) for AgNPs in detergent and shampoo

The applicability of SdFFF for characterization of AgNPs in the commercial detergent and shampoo was demonstrated. Changes of AgNPs in those media were examined. Experimental details are given as follows:

Preparation of detergent and shampoo for SdFFF analysis

Detergent and shampoo containing AgNPs were examined in this study. Detergent was weighed and dissolved in deionized water to obtain the concentration of 10% (w/v).

Shampoo was weighed and dissolved in deionized water to obtain the concentration of 10% (v/v). Then the detergent and shampoo solutions were shaken using a platform shaker for 30 minutes and left until settle. Only the supernatant part was used for subsequent analysis, which was shaken again using a platform shaker for 30 minutes before use. A 50 µL-volume of these samples was introduced into SdFFF for size characterization of AgNPs.

Preparation of AgNPs spiked detergent and shampoo

Silver nanoparticles were added into detergent and shampoo to the final concentration of 64 mg L^{-1} in 0.5, 1, and 2% (w/v) detergent and in 0.5, 1, 2% (v/v) shampoo. A 50 µL-volume of these samples was introduced into SdFFF for size characterization of AgNPs after thorough mixing by vortex.

Observation of changes in the form of AgNPs in the spiked detergent and shampoo

To examine if the spiked AgNPs are converted into silver ion upon in contact with detergent and shampoo, the mixture was filtered through a 1,000 Da regenerated cellulose acetate membrane for separation of silver ion from AgNPs [32]. The filtrate contained only the silver ion and was determined for their silver content using ETAAS.

Determination of total silver concentration of AgNPs spiked cleaning products using ETAAS

The concentrations of silver in AgNPs spiked cleaning products were determined by using ETAAS after acid digestion of the samples using aqua regia. The samples were mixed with aqua regia at the ratio of 1:1, and the mixture was left at room temperature until the colorless solution was obtained.

1.3 Results and discussion

1.3.1 AgNPs characterization in cotton fabric

Quantification of silver released from cotton fabric in various washing media

For the cotton textile sample used in this study, the total amount of silver was found to be 52.1 ± 8.3 µg g^{-1}. By subjecting this textile sample into various washing solutions,

including doubly deionized water, tap water, and 4% detergent dissolved in tap water, the released amounts of silver from the textile were determined by ETAAS. A comparison of cotton fabric based on the released amount of silver in Table 3 indicates that the silver release in tap water was higher than in doubly deionized water. After one washing cycle, the released amounts of silver were 0.73 ± 0.03 μg g^{-1} (1.4 % of the total amount) and 0.26 ± 0.01 μg g^{-1} (0.5% of the total amount) by tap water and doubly deionized water, respectively. Clearly, the silver released by detergent medium, calculated as 66% from the total silver content in cotton fabric, was significantly higher than by the other two washing solutions. This may be due to the complexity of detergent composition such as hypochlorite, oxygen bleaching etc., which can oxidize silver [33] in cotton fabric causing the leaching of silver into the washing solution. This result indicates that non-detergent is less aggressive than the detergent media at stripping silver from the cotton fabric. The study suggests that silver from cotton fabric could be leached into domestic wastewater upon washing with detergent, which mimicked the real situation.

Table 3 The release amount and particle size of the AgNPs from the cotton fabric using various washing solutions (n = 3)

washing solution	released silver (μg g^{-1})	% release*	diameter (nm)**
Deionized water	0.26 ± 0.01	0.5	1.2 ± 0.02, 2.5 ± 0.07
Tap water	0.73 ± 0.03	1.4	1.2 ± 0.04, 2.4 ± 0.05
Detergent in tap water	34.6 ± 1.4	66	1.5 ± 0.01

* The concentration of Ag in the cotton fabric is 52.1 ± 8.3 μg g^{-1}.

** The particle diameter was determined by FlFFF.

Moreover, three consecutive washing cycles were designed to study the silver content released from cotton fabric sample into washing media. Figure 3 shows that doubly deionized and tap water gradually leached silver from the fabric sample whereas detergent medium leached silver more effectively in the first washing and dramatically decreased as a function of washing times. Approximately after three washing cycles with detergent medium, most of silver could be leached out from the cotton fabric sample. Assuming

constant leaching efficiency by doubly deionized and tap water, approximately 200 and 70 washing cycles, respectively, are required to completely leach silver from the sample.

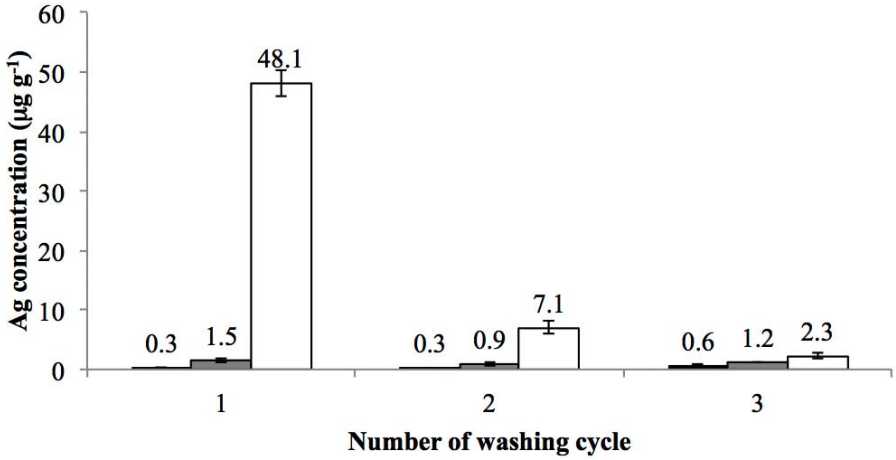

Figure 3 Silver contents released in various washing media: doubly deionized water (solid bar); tap water (grey bar); and detergent in tap water (white bar) using three consecutive washing cycles.

Characterization of silver leached by various washing media

In this study, FlFFF was used to obtain particle size information of the released silver from the fabric sample. However, as AgNPs were present in very low concentration in washing solution and dilution occurs along fractionation step, sample preconcentration step is important. Thus, FlFFF was adapted for preconcentration and fractionation to characterize particle size of AgNPs release from the washing process. A raw fractogram of AgNPs was obtained, as shown in Figure 4(a). The raw fractogram was translated into particle size distribution, using the method described earlier [34], as shown in Figure 4(b). With this plot, the particle size at peak maximum (dp) was measured. The effect of washing media (doubly deionized water, tap water, and 4% detergent dissolved in tap water) on particle size of the released silver was examined as summarized in Table 3. For AgNPs leached by doubly deionized and tap water media bimodal distributions were observed (Figures 4(a) and 4(b)), whereas a distinct monomodal distribution was obtained for AgNPs leached by detergent medium. The peak at retention time of approximately 3 min disappeared which might be due to the fact that AgNPs were oxidized to silver ions in detergent medium.

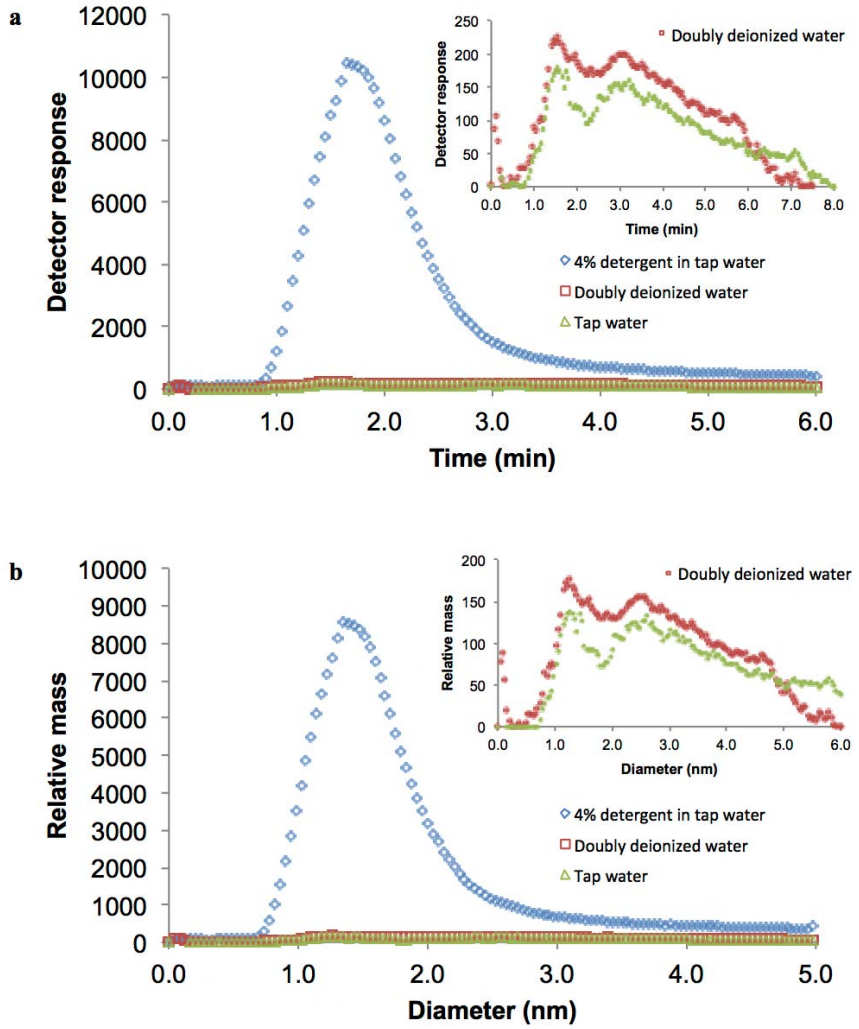

Figure 4 (A) Raw fractograms by FlFFF and (B) the corresponding particle-size distribution of AgNPs obtained from the cotton sample washed in doubly deionized (□), tap water (□), and 4% detergent in tap water (□).

To attain more information, size based fractionation of silver was examined by FlFFF coupled off-line with ETAAS. The fractions collected from tap and doubly deionized water did not show any observable silver signal with ETAAS detection because of the small amount of silver being leached from the cotton shirt sample. Thus, only the fractions collected from the sample washed with detergent were subjected to ETAAS detection of silver. With ETAAS detection as shown in Figure 5, silver was mostly found in sub-fraction 4, corresponding to the retention time of 2 min. The UV fractogram of the retained nanoparticles in Figure 4 showed similar profiles to that of the size based distribution of silver in Figure 5.

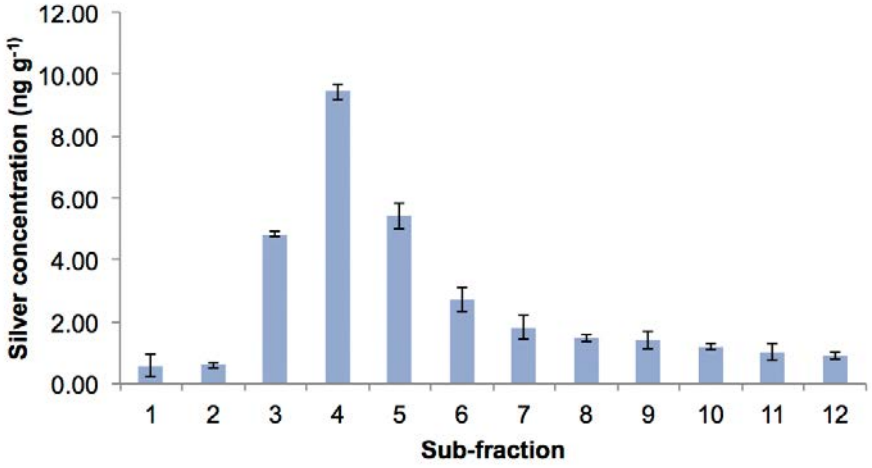

Figure 5 Ag distribution in various size fractions collected from FlFFF of the sample leached by 4% detergent in tap water. Each sub-fraction corresponds to the consecutive times of 0.5 minute.

Classification of silver as AgNPs or silver ions from the cotton fabric in detergent medium

Classification of silver as AgNPs or silver ions from the cotton shirt in detergent medium was carried out using FlFFF. As the FlFFF comprises the membrane having a 1,000 Da molecular-weight inside the FlFFF channel, it can be used to classify form of silver as AgNPs or silver ions after being released from cotton shirt sample. In this study, the soluble silver ions were removed by filtering off through the FlFFF membrane whereas AgNPs retained in the FlFFF channel owing to their larger size than the pore size of membrane cut-off. After washing the cotton sample with 4% detergent in tap water, large-volume sample introduction (3.0 mL) with the opposing-flow on-channel FlFFF preconcentration and collection for off-line silver determination by ETAAS was performed. The soluble silver ion was calculated by subtracting the value between total silver and the AgNPs concentrations. Nearly 100% of the silver released was silver ions, whereas only 1% was AgNPs, suggesting that AgNPs from the cotton fabric studied herein were oxidized into a dissolved ionic form when exposed to detergent medium.

1.3.2 AgNPs characterization in detergent and shampoo

Observation of SdFFF capability for characterization of AgNPs size distribution

To apply SdFFF for size characterization of AgNPs, various experimental conditions were examined to demonstrate the reproducibility and reliability of SdFFF. Various initial field strengths (1200, 1500, and 1800 RPM) were applied to fractionate AgNPs as illustrated in Figure 6a with the resulting particle size distributions shown in Figure 6b. To transform the fractogram to particle size distribution, the average density of AgNPs of 10.490 g mL^{-1} was used. The particle size distributions in Figure 6b obtained from various experimental conditions were all similar showing the particle size range of 30 – 70 nm with the peak maximum at around 47 nm. This suggests that the particle size determination of AgNPs is possible with SdFFF. Moreover, the reliability of particle size information from SdFFF was confirmed by comparing the information with those obtained from FlFFF, by which the results were presented in another manuscript [35]. The particle size distributions from the two techniques were similar. For SdFFF in this work, therefore, the initial field strength of 1200 RPM was selected for further use as it was sufficient to separate the particles from the void fraction with minimal analysis time. SdFFF can be successfully used to determine the particle size distributions of AgNPs with diameter as low as 10 nm because the density of AgNPs was high.

Characterization of AgNPs in detergent and shampoo

With the selected SdFFF operating conditions, fractionation of AgNPs in detergent and shampoo of various concentrations was carried out. Raw fractograms of AgNPs in detergent and shampoo of various concentrations showed only one peak at approximately 9 min of elution time (void fraction), suggesting that if AgNPs were present in the detectable level, their particle sizes were relatively small.

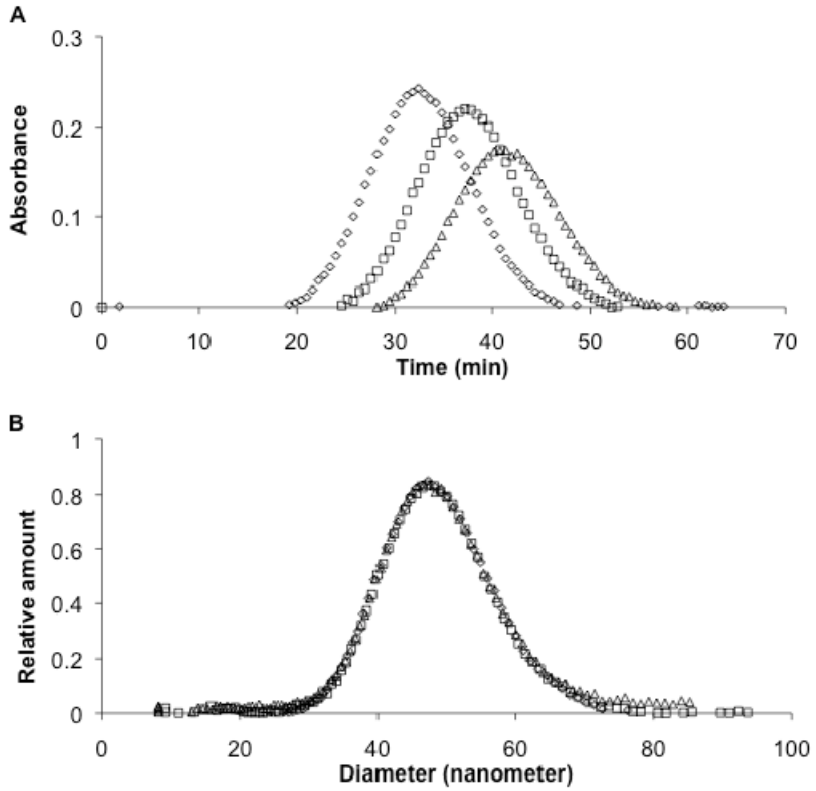

Figure 6 Effect of SdFFF field strength on fractionation of AgNPs: (A) raw fractograms; and (B) particle size distributions of AgNPs, obtained from various initial field strengths as 1200 (◊), 1500 (□), and 1800 RPM (Δ). The SdFFF operating condition was as follows: initial field strength hold time 8 min; field decay parameter -64; final field strength 50 rpm, and $\Delta\rho$ = 9.490 g mL^{-1}. The channel flow rate was constant at 0.5 mL min^{-1}.

As the detergent contains hypochlorite which can oxidize silver [33], it was questioned whether AgNPs could be oxidized into silver ions. To evaluate this, the AgNPs of known particle size (47 nm) was spiked into the detergent and shampoo samples. Raw fractograms of AgNPs spiked detergent (2%, w/v) and shampoo (2%, v/v) are illustrated in Figure 7. Obviously, the signals at the peak of AgNPs were decreased significantly in detergent and shampoo media comparing to that in deionized water, suggesting the changes in AgNPs size in detergent and shampoo. This is consistent with the report by Impellitteri [33] that AgNPs could convert to silver ion and silver chloride after exposure to the hypochlorite/detergent solution and in the presence of an oxidizer. Therefore the next experiment was then performed to examine the changes of AgNPs in these cleaning products.

To examine the change of AgNPs in these cleaning products, ETAAS was applied to determine silver concentrations after two sample preparation approaches as follows: direct detection of silver in the acid digested samples; and detection of silver in the filtrate of the AgNPs spiked detergent (2%, w/v) and shampoo (2%, v/v) from a filtration unit with 1,000 Da regenerated cellulose acetate membrane. The silver concentrations from all approaches are presented in Figure 8. Approximately 75% of AgNPs compared with their original concentrations detected in the digested samples were found in the filtrates, suggesting that AgNPs were transformed into silver ion and silver chloride after exposure to the hypochlorite/detergent solution and in the presence of an oxidizer.

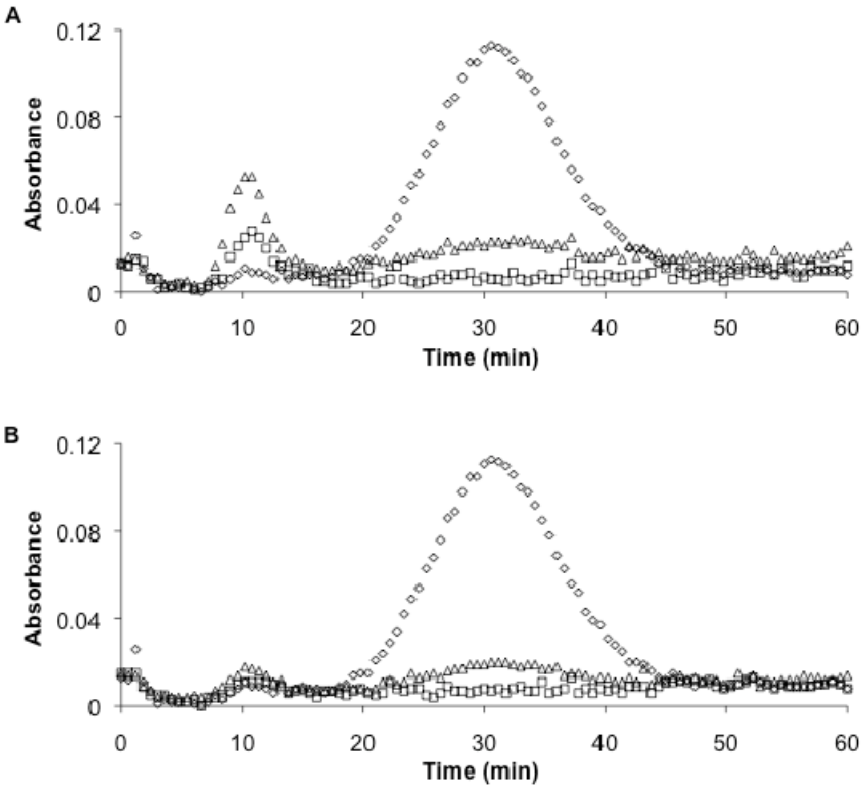

Figure 7 Fractograms of spiked-AgNPs in cleaning products by SdFFF: (A) detergent; and (B) shampoo, where (◊), (□), and (Δ) represent 64 mg L^{-1} AgNPs standard addition to 2% (w/v) detergent, and 2% (w/v) shampoo, respectively.

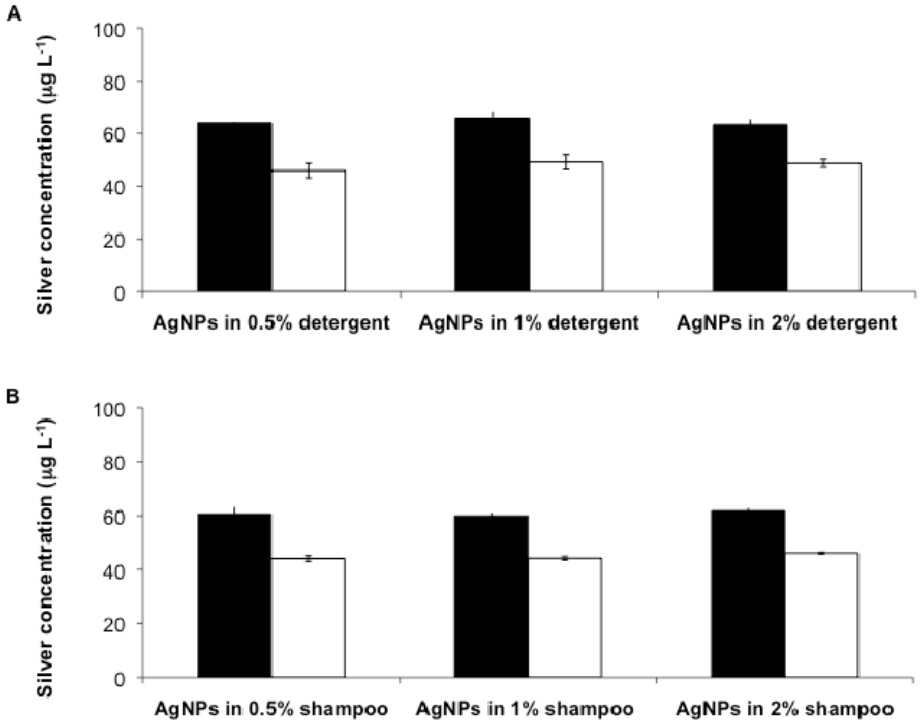

Figure 8 Silver concentration (mg L^{-1}) with ETAAS determination: (A) 64 mg L^{-1} AgNPs in 0.5, 1, and 2% (w/v) detergent; and (B) 64 mg L^{-1} AgNPs in 0.5, 1, and 2% (v/v) shampoo, where black and white bars represent silver concentration from acid digestion and released fraction after filtration, respectively.

1.4 Summary

The applicability of FFF for investigation of AgNPs in consumer products was investigated. Two FFF subtechniques, i.e., FlFFF and SdFFF, were employed to characterize AgNPs in various types of samples. FlFFF was successfully used in the characterization of very low concentration of AgNPs in the leaching study of AgNPs from the cotton fabric during washing process. The finding that AgNPs could be leached during washing is useful for the cotton shirt manufacturer, and also suggests that FlFFF may be used as an efficient tool in the quality control and research and development processes in the garment industry.

Further, SdFFF was effectively used to investigate size distribution of AgNPs in the larger size scale. Detergent and shampoo, which were labeled to contain AgNPs, were used as samples. Silver nanoparticles were not detectable in those samples by SdFFF, which might be due to their smaller size (< 10 nm) than the observable size range by SdFFF or their presence in very low amount and therefore not detectable. Further, it was proven that in those cleaning products, approximately 75% of AgNPs transformed into silver ion after exposure to the hypochlorite/detergent solution and in the presence of an

oxidizer. The information obtained from SdFFF can be useful for quality control of the finished cleaning products.

1.5 References

1. J. Zhensheng, X. Chanjuan, Z. Qingmei, Y. Feng, Z. Jiazheng; X. Jinzhen. J. Mol. Cata. A: Chem. 2003, 191, 61-66.
2. M. Fuke, P. Kanitkar, M. Kulkarni, B. Kale; R. Aiyer. Talanta 2010, 81, 320-326.
3. S. Kokura, O. Handa, T. Takagi, T. Ishikawa, Y. Naito; T. Yoshikawa. Nanomed- Nanotechnol. 2010, 6, 570-574.
4. R. Singh; J. Lillard Jr. Exp. Mol. Pathol. 2009, 86, 215-223.
5. X. Chen; H. Schluesener. Toxicol. Lett. 2008, 176, 1-12.
6. I. Sondi, B; Salopek-Sondi. J. Colloid Interf. Sci. 2004, 275, 177-182.
7. P. Prema; R. Raju. Biotechnol. Bioproc. E. 2009, 14, 842-847.
8. J. S. Kim, E. Kuk, K. N. Yu, J. H. Kim, S. J. Park, H. J. Lee, S. H. Kim, Y. K. Park, Y. H. Park, C. Y. Hwang, Y. K. Kim, Y. S. Lee, D. H. Jeong; M. H. Cho. Nanomed- Nanotechnol. 2007, 3, 95-101.
9. L. Juan, Z. Zhimin, M. Anchun, L. Lei; Z. Jingchao. Int. J. Nanomed. 2010, 5, 261-267.
10. A. Petica, S. Gavriliu, M. Lungu, N. Buruntea; C. Panzaru. Mater. Sci. Eng. B 2008, 152, 22-27.
11. K. Tiede, A. B. A. Boxall, S. P. Tear, J. Lewis, H. David; M. Hassellöv. Food Addit. Contam. A 2008, 25, 795-821.
12. D. Cheng, J. Yang; Y. Zhao. Chin. Med. Equip. J 2004, 4, 26-32.
13. H. Y. Lee, H. K. Park, Y. M. Lee, K. Kim; S. B. Park. Chem. Commun. 2007, 28, 2959-2961.
14. N. Vigneshwaran, A. A. Kathe, P. V. Varadarajan, R. P. Nachane; R. H. Balasubramanya. J. Nanosci. Nanotechnol. 2007, 7, 1893-1897.
15. R. Handy, F. von der Kammer, J. Lead, M. Hassellöv, R. Owen; M. Crane. Ecotoxicology 2008, 17, 287-314.
16. K. Tiede, A. B. A. Boxall, S. P. Tear, J. Lewis, H. David; M. Hassellöv. Food Addit.Contam. A 2008, 25, 795-821.
17. O. Choi; Z. Hu. Environ. Sci.Technol. 2008, 42, 4583-4588.
18. K. Tiede, A. B. A. Boxall, D. Tiede, S. P. Tear, H. David; J. Lewis. J. Anal. Atom. Spectrom. 2009, 24, 964-972.
19. S. A. Cumberland; J. R. Lead. J. Chromatogr. A 2009, 1216, 9099-9105.
20. C. W. Shen; T. Yu. J. Chromatogr. A 2009, 1216, 5962-5967.

21. L. E. Oppenheimer; G. A. Smith. Langmuir 1988, 4, 144-147.
22. S. T. Kim, D. Y. Kang, S. Lee, W. S. Kim, J. T. Lee, H. S. Cho; S. H. Kim. J. Liq. Chromatogr. R. T. 2007, 30, 2533-2544.
23. A. P. Weber, U. Baltensperger, H. W. Gäggeler; A. Schmidt-Ott. J. Aerosol Sci. 1996, 27, 915-929.
24. P. H. McMurry, M. Litchy, P.-F. Huang, X. Cai, B. J. Turpin, W. D. Dick; A. Hanson. Atmos. Environ. 1996, 30, 101-108.
25. G. Blo, C. Contado, F. Fagioli, M. Bollain Rodriguez; F. Dondi. Chromatographia 1995, 41, 715-721.
26. C. Contado; A. Pagnoni. Anal. Chem. 2008, 80, 7594-7608.
27. H. E. Taylor, J. R. Garbarino, D. M. Murphy; R. Beckett. Anal. Chem. 2002, 64, 2036-2041.
28. ISO. Textilesstests for Colour Fastnessspart C06: Colour Fastnessto Domestic and Commercial Laundering, ISO 105-C06; International Organization for Standardization: Geneva, 1997.
29. M. Hassellöv, B. Lyvén, C. Haraldsson; W. Sirinawin. Anal. Chem. 1999, 71, 3497-3502.
30. B. Lyven, M. Hassellöv, C. Haraldsson; D. Turner. Anal. Chim. Acta 1997, 357, 187-196.
31. S. Sangsawong, J. Shiowatana; A. Siripinyanond. J. Anal. Atom. Spectrom. 2006, 21, 1336-1339.
32. J. Fabrega, S. R. Fawcett, J. C. Renshaw; J. R. Lead. Environ. Sci. Technol. 2009, 43, 7285-7290.
33. C. A. Impellitteri, T. M. Tolaymat; K. G. Scheckel. J. Environ. Qual. 2009, 38, 1528-1530.
34. A. Siripinyanond; R. M. Barnes. Spectrochim. Acta B 2002, 57, 1885-1896.
35. K. Songsilawat, J. Shiowatana; A. Siripinyanond. J. Chromatogr. A 2011, 1218, 4213-4218.

Chapter 2

Flow Field-Flow Fractionation for Particle Size Characterization of Selenium Nanoparticles Incubated in Gastrointestinal Conditions

2.1 Introduction

2.2 Experimental

2.2.1 Instrumentation

2.2.2 Chemicals

2.2.3 Preparation of selenium nanoparticles

2.2.4 Gastrointestinal incubation of selenium nanoparticles

2.2.5 Quantification of fractionated selenium nanoparticles by ICP-MS

2.3 Results and discussion

2.3.1 Size characterization of selenium nanoparticles by FlFFF

2.3.2 Selenium nanoparticles in gastrointestinal conditions: effect of pH (without enzyme addition)

2.3.3 Selenium nanoparticles in gastric conditions: pH 2 with and without pepsin addition

2.3.4 Selenium nanoparticles in intestinal conditions: pH 7 with and without pancreatin bile extract addition

2.4 Summary

2.5 References

2.1 Introduction

Selenium is considered as an essential element and it can also be toxic. The recommended dietary allowances (RDAs) and maximum level of daily nutrient intake of selenium for both man and woman are 55-400 μg/day as specified by The Food and Nutrition Board of US National Academy of Sciences (Monsen, 2000). Selenium is essential as it is an important component in many functional selenoproteins required for normal health (Combs Jr & Combs, 1986; Dumont, Vanhaecke, & Cornelis, 2006; Navarro-Alarcon & Cabrera-Vique, 2008; Rayman, Infante, & Sargent, 2008; Thomson, 2004). Selenium nanoparticles show benefits as antioxidant and anticancer agents with low toxicity (Chen, Wong, Zheng, Bai, et al., 2008; Jia, Li, & Chen, 2005; Peng, Zhang, Liu, & Taylor, 2007; Wang, 2009; Wang, Zhang, & Yu, 2007; Zhang, Gao, Zhang, & Bao, 2001; Zhang, Wang, Bao, & Zhang, 2004; Zhang, Wang, Yan, & Zhang, 2005). At nutritional dose levels in mice, selenium nanoparticles (20-60 nm) were reported to have similar bioavailability to that of selenite, but the toxicity of selenium nanoparticles was 7-fold lower than sodium selenite considering from the LD50 of 113 and 15 mg Se/kg body weight for selenium nanoparticles and selenite, respectively (Zhang, Gao, Zhang, & Bao, 2001). In case of selenium nanoparticles ingestion into human gastrointestinal tract, the absorption, translocation, and excretion of nanoparticles in human body are controlled by various parameters including size and surface properties (Teow, Asharani, Prakash Hande, & Valiyaveettil, 2011).

The interaction with proteins influences the surface chemistry of nanoparticles and lead to changes in their charge and agglomeration state (Chithrani, Ghazani, & Chan, 2006; Kittler, Greulich, Gebauer, Diendorf, et al., 2010; Zook, MacCuspie, Locascio, Halter, et al., 2011). Change in pH under the gastrointestinal condition may trigger agglomeration of nanoparticles inside the gastrointestinal tract (Wang, Feng, Wang, Jia, et al., 2006), and the particle size influenced on efficiency of particle uptake (Desai, Labhasetwar, Amidon, & Levy, 1996). Size characterization of silver nanoparticles in gastrointestinal tract was reported (Mwilu, El Badawy, Bradham, Nelson, et al., 2013; Walczak, Fokkink, Peters, Tromp, et al., 2013). The rate of dye and dextran nanoparticle diffusion across the mucus layers to the enterocyte surface was determined (Hoet, Brüske-Hohlfeld, & Salata, 2004; Szentkuti, 1997). Particles with 14 nm diameter permeated within 2 min, while 415 nm particles took 30 min, whereas 1000 nm particles were unable to translocate this barrier. Until now the information about size characterization of selenium nanoparticles on human digestive conditions are still lacking. Therefore, changes in the particle size of selenium nanoparticles in gastrointestinal condition should be examined.

Selenium nanoparticles can be prepared by various methods. The most widely used method for synthesis of selenium nanoparticles is the chemical reduction approach. Several exogenous reducing

agents can be used such as ascorbic acid, glutathione, and sodium thiosulfate (Lin & Chris Wang, 2005; Mees, Pysto, & Tarcha, 1995; Zhang, Gao, Zhang, & Bao, 2001; Zhang, Wang, Bao, & Zhang, 2004). To control the formation and the dispersion of nanoparticles, stabilizing agents are normally required. Many reagents have been used for stabilizing selenium nanoparticles such as polyvinyl alcohol (Barnaby, Frayne, Fath, & Banerjee, 2011; Shah, Kumar, & Bajaj, 2007), chitosan (Bai, Wang, Zhou, Li, et al., 2008; Zhang, Wang, Bao, & Zhang, 2004; Zhang, Wang, Yan, & Zhang, 2005), surfactant (Li & Hua, 2009; Mehta, Chaudhary, Kumar, Bhasin, et al., 2008; Min-Hsiung, 2004), and bovine serum albumin (Zhang, Gao, Zhang, & Bao, 2001). In this work, stabilizing agents, which are generally recognized as safe (GRAS), were used for the preparation of selenium nanoparticles. These included pectin, mixed alginate/pectin, ovalbumin, and β-lactoglobulin, as these reagents have been characterized and used as thickening, emulsifying, and stabilizing agents in food technology (Akhtara, Dickinson, Mazoyer, & Langendorff, 2002; Matto, & Husain, 2006; Medina-Torres, Calderas, Gallegos-Infante, Gonzalez-Laredo, et al., 2010; Dickinson, 2010; respectively).

Several analytical techniques have been used for size characterization of nanoparticles. These include transmission electron microscopy (TEM) (Lin & Chris Wang, 2005; Li & Hua, 2009; Min-Hsiung, 2004), scanning electron microscopy (SEM) (Chen, Wong, Zheng, Bai, et al., 2008; Lee, Choi, Myung, Kim, et al., 2008), and UV-Visible spectrophotometry (UV-Vis) (Lin & Chris Wang, 2005; Mees, Pysto, & Tarcha, 1995). With UV-Vis absorption spectrophotometry, some researchers showed that the absorption peak of selenium nanoparticles was only observed when the particle size was larger than 100 nm (Lin & Chris Wang, 2005). Alternatively, flow field-flow fractionation (FlFFF) has been reported for characterization of several particles with nano scale range (Kammer, Legros, Hofmann, Larsen, et al., 2011; Poda, Bednar, Kennedy, Harmon, et al., 2011). The FlFFF provides not only a relatively gentle separation process, but also it allows for collection of the fractionated samples for further analysis by other techniques.

Although size characterization of selenium nanoparticles has been documented, most publications focused on size in the as synthesized condition medium (Ingole, Thakare, Khati, Wankhade, et al., 2010; Lin & Chris Wang, 2005). None has reported size characterization of selenium nanoparticles in more complex gastrointestinal fluids. With these, the objectives of this work were two-fold. The first was to examine the feasibility of FlFFF for size characterization of selenium nanoparticles with subsequent ICP-MS to provide element specific detection of selenium, and the second was to examine the changes in particle size distribution of selenium under gastrointestinal conditions, both without and with digestive enzymes.

2.2 Experimental

2.2.1 Instrumentation

A symmetrical flow field-flow fractionation (FlFFF) system (Model PN-1021-FO; Postnova Analytics, Landsberg, Germany) coupled to an inductively coupled plasma quadrupole mass spectrometer (ICP-MS, Elan 6000 Perkin Elmer/Sciex, Toronto, Canada) was employed. The FlFFF system equipped with a 1 kDa molecular weight cut-off regenerated cellulose acetate membrane (RC) from Postnova Analytics was used for size characterization of selenium nanoparticles. The FlFFF channel was rectangular in shape with the dimensions being 27 cm long, 2.0 cm wide, and 0.0254 cm thick. Sample volume of 20 μL was introduced into FlFFF via the Rheodyne injector valve. A high-pressure liquid chromatography (HPLC) pump (Model PN 2101, Postnova Analytics, Germany) was used to deliver the channel flow. The cross flow rate was delivered by another HPLC pump of the same model. The optimum operating conditions of FlFFF-ICP-MS are listed in Table 1. A UV-Visible detector (Model S3210, Postnova Analytics) was set at 410 nm for detection of the fractionated selenium nanoparticles samples, considering from the absorption spectra of the synthesized selenium nanoparticles. The ICP-MS was used as an element detector sequentially after the UV-Visible absorption detector. Owing to the similarity of the FlFFF channel and ICP-MS sample flow rates typically used for analysis, the ICP-MS cross-flow nebulizer was connected directly to the UV-Visible detector outlet with a 60 cm length of poly(tetrafluoroethylene) tubing (PTFE, 0.58 mm id).

Zeta potential measurements were carried out using the Zetasizer Nano ZS (Malvern Instruments Zetasizer1000 Hs, Worcestershire, UK). A transmission electron microscope FEI model TECNAI T20 G^2, (FEI Company Corporate, Hillsboro, Oregon, USA was used to observe the size and morphologies of selenium nanoparticles.

Table 1 FlFFF-ICP-MS operating condition

FlFFF: PN-1021-FO	
Channel dimension/cm×cm×cm	27.7 long x 2.0 wide x 0.02 thick
Carrier liquid	0.02% -FL-70 and 0.02 NaN_3 (pH 11.7)
Channel flow rate/ mL min^{-1}	1.4
Cross flow rate/ mL min^{-1}	0.8
Equilibration time/ min	2.4
Membrane	1 kDa MWCO poly(regenerated cellulose acetate)
ICP-MS: Perkin Elmer ELAN 6000	
Torch	Fassel type with alumina ceramic injector
Rf generator frequency	40 MHz
Rf power	1,100 W
Nebulizer gas flow rate	0.9 L/min
Coolant gas flow rate	15 L/min
Auxiliary gas flow rate	0.9 L/min
Scanning mode	peak hopping
Isotopes monitored (m/z)	^{77}Se, ^{78}Se, ^{80}Se, ^{82}Se (^{78}Se for quantification)

2.2.2 Chemicals

The chemicals used in this study include sodium selenite, pectin from apples (30-100 kDa) with 70-75% degree of esterification, alginic acid sodium salt from brown algae (100 – 200 kDa), albumin from chicken egg white (ovalbumin) with molecular weight of 44.3 kDa, β-lactoglobulin from bovine milk (90% PAGE), pepsin (P-7000, porcine stomach mucosa), pancreatin (P-1750, porcine pancreas) and bile extract (B-6831, porcine). All aforementioned chemicals were purchased from Sigma-Aldrich, Inc., MO, USA. L-ascorbic acid was purchased from Fisher Scientific UK Limited, Leicestershire, UK. De-ionized water (18.2 MΩ cm^{-1}) obtained from a water-purification system (Barnstead

International, Dubuque, IA, USA) was used to prepare all chemical reagents. For the preparation of selenium nanoparticles, 2.5% (w/w) of stabilizers (pectin, alginate, ovalbumin, and β-lactoglobulin) and 300 mM ascorbic acid reducing agent were dissolved in de-ionized water. FL-70, a mixture of anionic and non-ionic compounds, was purchased from Fisher Scientific UK Limited, Leicestershire, UK. A 0.02% (v/v) solution of FL-70 was prepared by diluting concentrated FL-70 with de-ionized water and was used as a carrier liquid. A commercial gold nanoparticle of 10 nm used for checking the performance of FlFFF channel was purchased from Sigma, St. Louis, MO, USA.

2.2.3 Preparation of selenium nanoparticles

Ascorbic acid was used as a reducing agent for synthesis of selenium nanoparticles. For the preparation of pectin, ovalbumin, and β-lactoglobulin stabilized selenium nanoparticles, 1 mL of 2.5% (w/w) stabilizing agent was mixed with 8 mL of 300 mmol L^{-1} ascorbic acid reducing agent under magnetic stirring at the speed of 1,000 rpm. With the stirring speed reduced to 100 rpm, 1 mL of 30 mmol L^{-1} aqueous sodium selenite solution was slowly added into the mixtures to initiate the reaction (Chen, Wong, Zheng, Bai, et al., 2008). For mixed alginate/pectin stabilized selenium nanoparticles, 0.5 mL of 2.5% (w/w) alginate solution was mixed with 300 mmol L^{-1} ascorbic acid. Then, 1 mL of 30 mmol L^{-1} aqueous sodium selenite solution was slowly added into the mixtures to initiate the reaction, and 0.5 mL of 2.5% (w/w) pectin was added after 15 min incubation time. The reaction solution therefore contained 3 mmol L^{-1} sodium selenite, 0.25% (w/w) stabilizers, i.e., pectin; mixed alginate/pectin; ovalbumin; or β-lactoglobulin, and 240 mmol L^{-1} ascorbic acid. Upon mixing all reagents together at room temperature, the solutions converted from colorless into red immediately with pH approximately 2.8-2.9. The obtained selenium nanoparticles were stored at 4°C for 2 hours (at least) before size characterization by FlFFF and TEM.

2.2.4 Gastrointestinal incubation of selenium nanoparticles

A pepsin solution was prepared by dissolving 0.16 g of pepsin in 1 mL of 0.1 mol L^{-1} HCl. A pancreatin-bile extract (PBE) mixture was prepared by dissolving 0.004 g of pancreatin and 0.025 g of bile extract in 5 mL of 0.001 mol L^{-1} $NaHCO_3$. Enzymatic

digestion was performed according to the procedure of Miller (Miller, Schricker, Rasmussen, & Van Campen, 1981). 7.5 g of de-ionized water were added to 5 g of selenium nanoparticles as synthesized, adjusted to pH 2.0 with 6 mol L^{-1} HCl. To carry out pepsin-HCl digestion (gastric digestion), 375 μL of pepsin solution was added. The mixture was then incubated for 2 h at 37°C in a shaking water bath. For intestinal digestion, a portion of the mixture after gastric digestion (5 g) was adjusted to pH 7.0 by 5 M NaOH solution. Then 625 μL of PBE mixture was added into the solution. The solution (intestinal fraction) was incubated for 2 h at 37 °C. Non-enzymatic digestion of selenium nanoparticles was also performed with the same procedure described above but without addition of pepsin and PBE mixture solution. These selenium nanoparticles after incubation in the gastrointestinal conditions were directly introduced into FlFFF channel for particle size characterization. Duplicate experiments were performed for each type of selenium nanoparticles.

2.2.5 Quantification of fractionated selenium nanoparticles by ICP-MS

A fractogram from FlFFF experiment was plotted between the intensity of selenium (y-axis) as a function of retention time (x-axis). The quantification of fractionated selenium from FlFFF was performed by an external calibration with sodium selenite standards using the peak height data from ICP-MS peak profile. Therefore, the intensity of selenium in the fractogram was then translated into the concentration. With the fixed flow rate used in the FlFFF experiment, the retention time was then translated into the retention volume. The total concentration of selenium in the fractionated selenium nanoparticles was calculated by area integration of graph which was plotted between the concentration of Se and retention volume.

2.3 Results and discussion

2.3.1 Size characterization of selenium nanoparticles by FlFFF

In our work, selenium nanoparticles were prepared by using ascorbic acid to reduce selenite to selenium with zero valent as shown in the following chemical reaction (Lin & Chris Wang, 2005):

$$SeO_3^{2-} + 2C_6H_8O_6 + 2H^+ \longrightarrow Se + 2C_6H_6O_6 + 3H_2O$$

Various stabilizing agents were employed in the synthesis to control the formation and dispersion stability, and to prevent nanoparticles from aggregation (Donati, Travan, Pelillo, Scarpa, et al., 2009). In this study, two types of stabilizing agents, which are generally recognized as safe (GRAS), were used. Those included the polysaccharide and protein types. The former included pectin and mixed alginate/pectin and the latter included ovalbumin and β-lactoglobulin. The reactive hydroxyl, carboxyl, and amino groups in polysaccharides and proteins show great potential for facilitating the formation and stabilization of selenium nanoparticles (Zhang, Zhang, Wang, & Chen, 2004). Without stabilizing agents, nanoparticles in solution are more susceptible to either oxidation or attractive interparticle Van der Waal's forces which cause them to aggregate and precipitate (Cozzoli & Manna, 1996).

Particle size distributions of selenium nanoparticles prepared by ascorbic acid reducing agent with the use of various stabilizing agents are illustrated in Figure 1. Two types of detector were used including UV-Visible (410 nm) and ICP-MS detectors, as illustrated in Figure 1a and 1b, respectively. The peak profiles obtained from the two detectors were similar. Selenium nanoparticles stabilized with pectin yielded the peak maximum at 64 nm (Figure 1, blue) and those stabilized with mixed alginate/pectin showed the peak maximum at 37 nm (Figure 1, red). For protein based selenium nanoparticles, the peaks appeared at 30 nm (Figure 1, green) and 23 nm for selenium nanoparticles with ovalbumin and β-lactoglobulin stabilizers (Figure 1, purple), respectively. Nonetheless, the ICP-MS was used as a detector for further investigation as it provided element specific information. It is clear that the type of stabilizers shows significant effect on the obtained particle size, as different stabilizers resulted in different degrees of steric repulsion and charge stabilization or electrostatic interaction. Steric repulsion is normally governed by the molecular mass of the stabilizing agent. The differences in electrostatic interaction from various stabilizing agents are due to the differences in amino, hydroxyl, or carboxyl groups in different proteins and polysaccharides (Zhang, Zhang, Wang, & Chen, 2004).

FlFFF-ICP-MS provides not only particle size information, but it can also give quantitative information. To demonstrate this, the amount of selenium detected during

fractionation was compared with the amount introduced into FlFFF. (The amount of selenium detected during fractionation was calculated based on the method described in Section 2.5, and the amount introduced into FlFFF was calculated based on the injection volume of 20 μL.) It was found that 88.4%, 102.5%, 100.5%, and 88.5% were detected during fractionation for pectin, mixed alginate/pectin, ovalbumin, and β-lactoglobulin, respectively.

In addition to the results observed by FlFFF, TEM was also used to monitor the size of selenium nanoparticles. Figure 2a and 2b show the TEM images of pectin stabilized- and ovalbumin stabilized-selenium nanoparticles, respectively. The results show good agreement between the particle size observed from the two techniques, considering by comparing Figure 1 (blue line) with Figure 2a (as synthesized) for pectin stabilized selenium nanoparticles, and Figure 1 (green line) with Figure 2b (as synthesized) for ovalbumin stabilized selenium nanoparticles. With FlFFF, the particle size at peak was 64 nm and 30 nm for pectin stabilized- and ovalbumin stabilized-selenium nanoparticles, respectively. TEM images also show that pectin gave larger particle size than that with ovalbumin.

2.3.2 Selenium nanoparticles in gastrointestinal conditions: effect of pH (without enzyme addition)

To gain an insight into changes in selenium nanoparticles in gastrointestinal conditions, selenium nanoparticles were incubated in the gastric (pH = 2) and intestinal pH (pH = 7), both with and without addition of enzyme. These particles were subjected to FlFFF-ICP-MS, TEM characterization, and zeta potential measurement. The zeta potential values of selenium nanoparticles in various conditions are summarized in Table 2.

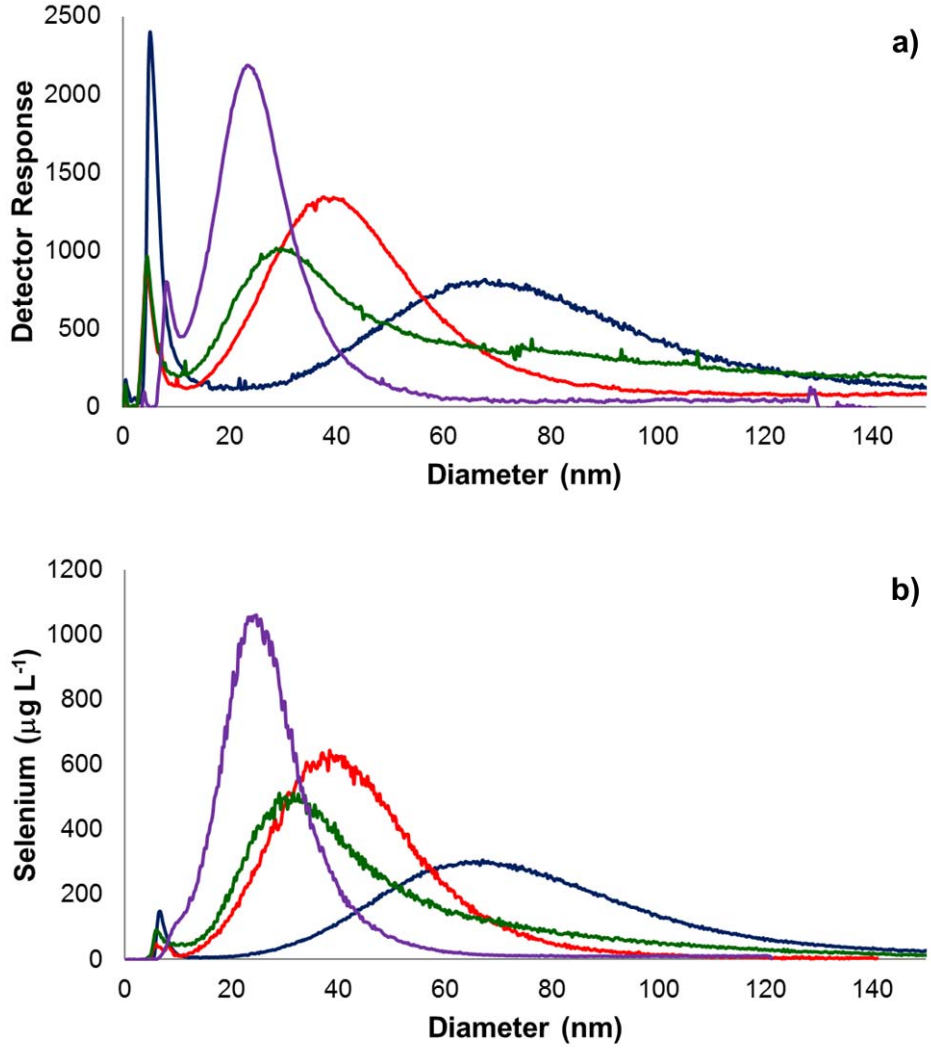

Figure 1 Particle size distributions of selenium nanoparticles synthesized with various stabilizing agents: i.e., pectin (blue); mixed alginate/pectin (red); ovalbumin (green); and β-lactoglobulin (purple), characterized by FlFFF with a) UV-visible detector and b) ICP-MS.

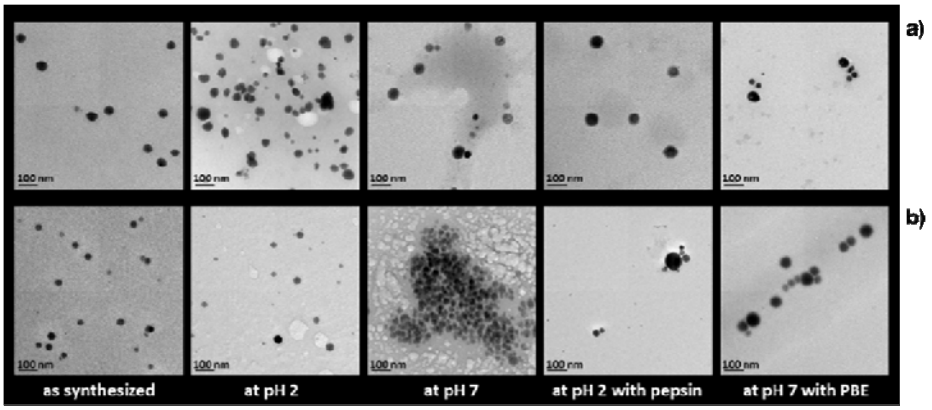

Figure 2 TEM images of selenium nanoparticles under various conditions: a) pectin stabilized selenium nanoparticles; and b) ovalbumin stabilized selenium nanoparticles. (PBE is pancreatin bile extract)

Table 2 Zeta potential values of selenium nanoparticles in various conditions

	Zeta potential (mV)			
	Selenium nanoparticles with various stabilizing agents			
Condition	pectin	mixed alginate/pectin	ovalbumin	β-lactoglobulin
as synthesized	-17.2	-27.6	33.3	24.3
at pH 2	-14.2	-28.4	37.9	25.8
at pH 7	-20.4	-33.0	-20.4	-35.0
at pH 2 with pepsin (gastric)	-11.4	-11.0	1.9	3.0
at pH 7 with PBE (intestinal)	-50.1	-47.0	-48.2	-43.1

Selenium nanoparticles with polysaccharide-based stabilizing agents

Two types of polysaccharide-based stabilized selenium nanoparticles were examined with the particle size distributions shown in Figure 3.

By adjusting the solution pH from 2 to 7, the zeta potential values of selenium nanoparticles with all stabilizers were more negatively charged. For polysaccharide stabilized selenium nanoparticles, increasing pH value from 2 to 7 changed the zeta potential values from -14.2 mV to -20.4 mV and -28.4 mV to -33.0 mV, for pectin stabilized and mixed alginate/pectin stabilized selenium nanoparticles, respectively. It can be realized that free carboxylic groups were deprotonated and changed to carboxylate anions at pH value of 7 (pKa of pectin is between 3 to 4, and pKa of alginic acid is between 1.5 to 3.5). The more negative charge at pH 7 than at pH 2 indicates more electrostatic repulsion with increasing pH, which can inhibit the agglomeration of nanoparticles. Therefore, the particle size at peak of pectin stabilized selenium nanoparticles was smaller at pH 7 (72 nm as shown in Figure 3a, brown) than that at pH 2 (84 nm as shown in Figure 3a, purple). The TEM images of pectin stabilized selenium nanoparticles are illustrated in Figure 2a, which show the same trend as the results from FlFFF.

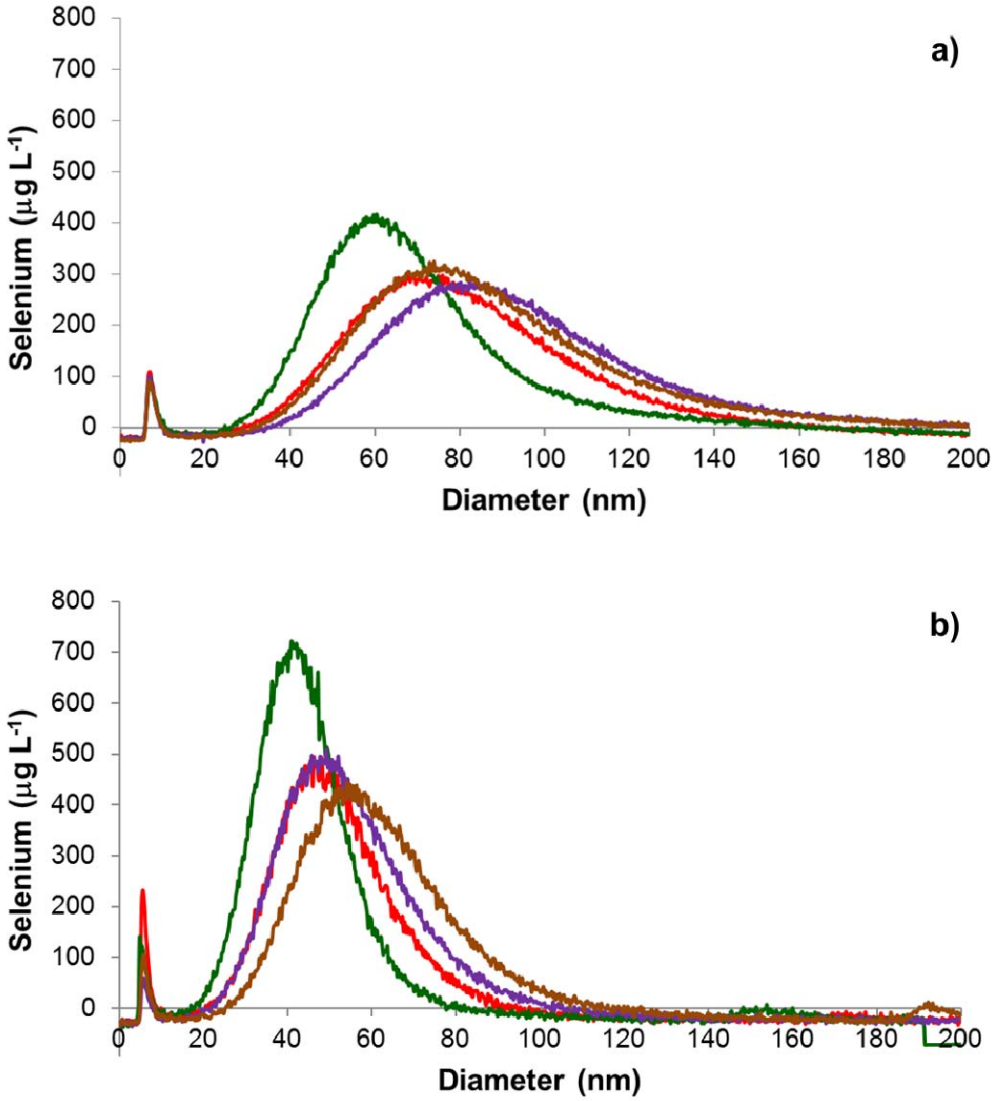

Figure 3 Particle size distributions of a) pectin stabilized selenium nanoparticles and b) mixed alginate/pectin stabilized selenium nanoparticles, under various conditions: i.e., at pH 2 (purple); at pH 7 (brown); at pH 2 with pepsin (red); and at pH 7 with pancreatin-bile extract (green), characterized by FlFFF with ICP-MS.

Although selenium nanoparticles with mixed alginate/pectin stabilizer also exhibited slightly higher negative charge at pH of 7, the particle size at peak was slightly larger than at pH of 2 (46 nm at pH 2 as shown in Figure 3b, purple and 53 nm at pH 7 as shown in Figure 3b, brown). This may be due to the nature of alginate that at pH below 4 alginate is likely to form a high-viscosity acid gel (Bu, Kjøniksen, Knudsen, & Nyström, 2004; Dentini, Rinaldi, Barbetta, Risica, et al., 2006). Therefore, at pH 2, the solution was highly viscous, resulting in the decrease in the collision rate of molecule. At pH 7, however, the

lowering in viscosity of the solution promoted the possibility for particle-particle collision, leading to larger particle size.

Selenium nanoparticles with protein-based stabilizing agents

Ovalbumin and β-lactoglobulin were selected to be a model study of protein stabilized selenium nanoparticles. Gastrointestinal digestion of selenium nanoparticles with protein-based stabilizing agent was also performed in both non-enzymatic and enzymatic media. Two types of protein-based stabilized selenium nanoparticles were examined with the particle size distributions shown in Figure 4. To understand the effect of pH on selenium nanoparticles, experiment without addition of enzymes is first considered.

By adjusting the solution pH from 2 to 7, the zeta potential values of selenium nanoparticles stabilized with proteins switched from the positive values to the negative values, as 37.9 to -20.4 and 25.8 to -35.0 mV for ovalbumin and β-lactoglobulin stabilized selenium nanoparticles, respectively (Table 2). This is due to the fact that the isoelectric points (pI) of both proteins are higher than 2 and lower than 7. The pI of ovalbumin is 4.75 and that of β-lactoglobulin is 5.2. Therefore, at pH 2, both proteins carry a net positive charge. At pH 7, both proteins exhibit a net negative charge.

Considering the particle size observed for ovalbumin stabilized selenium nanoparticles, increasing the pH from 2 to 7 caused the particle size at peak shifted from 52 nm (Figure 4a, purple) to disappearance from the observable size range (1 to 160 nm) as shown in Figure 4a (brown). Nonetheless, the signal of selenium showed up after stopping the cross flow indicating the particle of larger than 160 nm (results not shown). This may be caused by the precipitation of ovalbumin during the pH adjustment from 2 to 7, causing agglomeration of selenium nanoparticles. The TEM image in Figure 2b also implies that ovalbumin stabilized nanoparticles were agglomerated to larger size.

Considering the particle size observed for β-lactoglobulin stabilized selenium nanoparticles, particle size distribution exhibited a peak maximum at 46 nm with a shoulder at around 30 nm (Figure 4b, purple). This bimodal characteristic may be arisen from the fact that β-lactoglobulin is normally found as dimers and other larger aggregates. However at pH below 3 and above pH 8, the dimers can be dissociated into monomers (Kuwata, Era, Hoshino, Forge, et al., 1999; Sakurai, Oobatake, & Goto, 2001). Therefore, at pH 2 β-lactoglobulin was presented as both monomer and other non-native larger aggregates causing the selenium nanoparticles to be stabilized by two different groups of

stabilizer, leading to bimodal distribution. At pH 7, however, the shoulder peak at approximately 30 nm disappeared showing only monomodal peak at 46 nm (Figure 4b, brown).

2.3.3 Selenium nanoparticles in gastric conditions: pH 2 with and without pepsin addition

In gastric condition, not only that the pH should be adjusted to 2, but also pepsin should be added to better mimic the digestive system. Pepsin is enzyme produced in the mucosal lining of the stomach that acts to degrade protein. Pepsin is negatively charged at pH of 2 (pI of pepsin = 1) (Sepelyak, Feldkamp, Moody, White, et al., 1984). With pepsin addition, the surface charge of all types of selenium nanoparticles studied herein changed in such a way that the zeta potential values were less negative and less positive for polysaccharide stabilized and protein stabilized selenium nanoparticles, respectively (Table 2).

Selenium nanoparticles with polysaccharide-based stabilizing agents

Adding pepsin into polysaccharide stabilized selenium nanoparticles cannot digest pectin or mixed alginate/pectin to the smaller unit. Although pepsin addition caused the zeta potential values of polysaccharide stabilized selenium nanoparticles become less negative (-14.2 to -11.4 mV and -28.4 to -11.0 mV for pectin stabilized and mixed alginate/pectin stabilized selenium nanoparticles, respectively), the particle size at peak of pectin stabilized selenium nanoparticles shifted to the smaller particle size (84 nm without pepsin as shown in the purple line to 72 nm with pepsin as shown in the red line of Figure 3a) whereas that of the mixed alginate/pectin remained unchanged (48 nm in the purple and red line of Figure 3b). The decrease in particle size and the unchanged particle size, despite the less negatively surface charge, suggested that under this condition the particle stability of polysaccharide stabilized selenium nanoparticles was governed by steric stabilization rather than electrostatic repulsion. The TEM images of pectin stabilized selenium nanoparticles are illustrated in Figure 2a, which show the same trend as the results from FlFFF.

Selenium nanoparticles with protein-based stabilizing agents

Addition of pepsin at stomach pH of 2 caused the zeta potential values of both protein stabilized selenium nanoparticles become less positively charged (37.9 to 1.9 mV and 25.8 to 3.0 mV for ovalbumin and β-lactoglobuin stabilized selenium nanoparticles, respectively). This can be realized that at this pH both ovalbumin and β-lactoglobulin carry a net positive charge whereas pepsin carries a net positive charge. Therefore, addition of negatively charged pepsin caused charge neutralization of the positively charged proteins resulting in the overall reduction in the zeta potential values.

Ovalbumin is known to be resistant to pepsin digestion (Martos, Contreras, Molina, & López-FandiÑo, 2010). Considering ovalbumin stabilized selenium nanoparticles, the particle size was shifted to larger size (52 nm without pepsin as shown in the purple line and 64 nm with pepsin as shown in the red line of Figure 4a). This may be due to the decrease in electrostatic repulsion between the particles (as evidenced by the decrease in zeta potential values) causing particle agglomeration. The TEM images of ovalbumin stabilized selenium nanoparticles are illustrated in Figure 2b, which show the same trend as the results from FlFFF.

Considering β-lactoglobulin stabilized selenium nanoparticles, the bimodal distribution at pH 2 without pepsin addition (30 and 46 nm as shown in Figure 4b, purple) became monomodal at 30 nm with pepsin addition (Figure 4b, red). The disappearance of the peak at 46 nm may be realized from the fact that the high-molecular weight nonnative aggregates were digested rapidly, whereas the dimers and monomer were resistant to peptic digestion (Peram, Loveday, Ye, & Singh, 2013). The resistance of native β-lactoglobulin to pepsin hydrolysis is attributed to its particular folded calyx structure where the target amino acid residues are buried in the protein core (Malaki Nik, Wright, & Corredig, 2010). Therefore, the peak at 46 nm which is believed to be the selenium nanoparticles stabilized by the high-molecular weight nonnative aggregates, was shifted to the smaller particles stabilized by only the dimeric and monomeric forms of β-lactoglobulin.

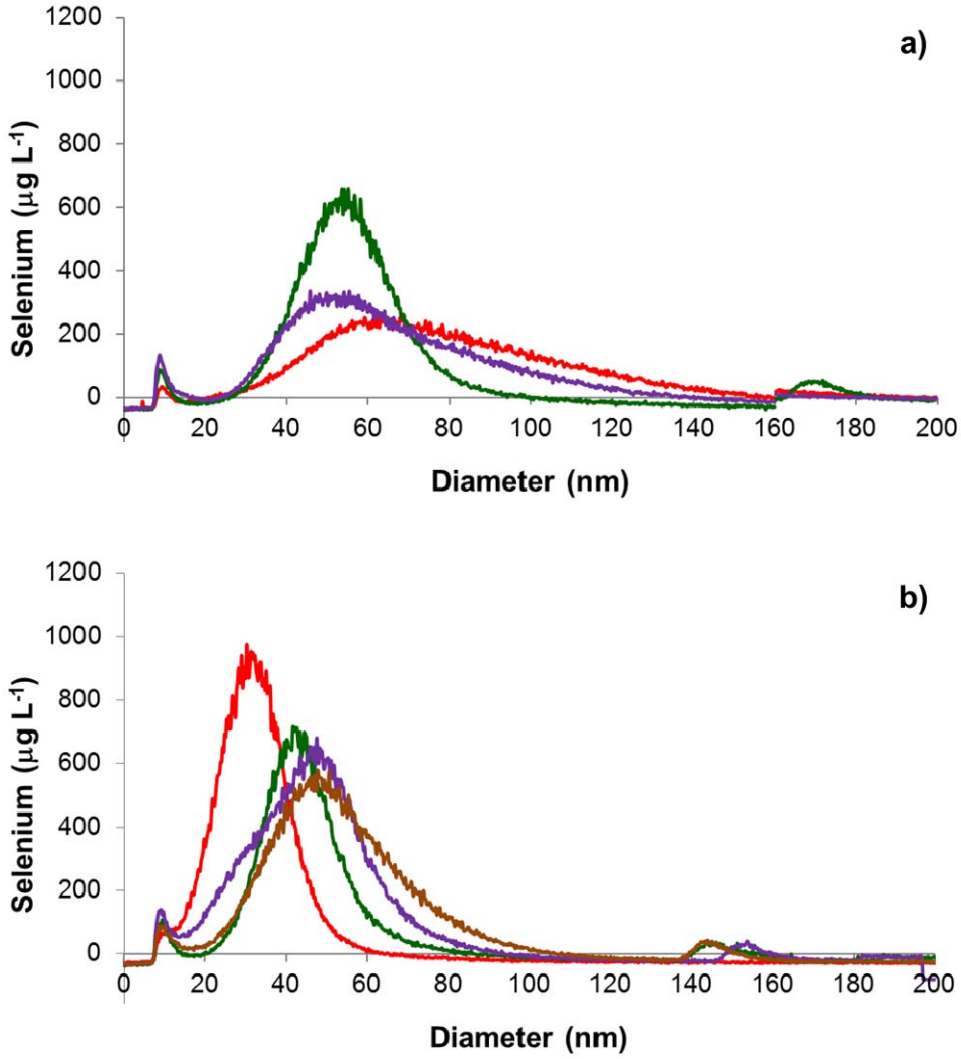

Figure 4 Effect of $ZnCl_2$ concentration on encapsulation efficiency of α-TOC (50 mM) in 4.0% (w/v) HEW particles.

2.3.4 Selenium nanoparticles in intestinal conditions: pH 7 with and without pancreatin bile extract addition

In intestinal condition, not only that the pH should be adjusted to 7, but also pancreain bile extract should be added to better mimic the intestinal system. Pancreatin is a mixture of several digestive enzymes produced by the exocrine cells of pancreas. It is composed of amylase, trypsin, lipase, ribonuclease and protease. The amylase found in pancreatin works to hydrolyze carbohydrate into oligosaccharides and the disaccharide maltose. Moreover, bile solution is hydrophilic on one side and hydrophobic on the other side. The hydrophilic sides are negatively charged, and this charge can prevent nanoparticles from aggregation. With pancreatin bile extract addition, the surface charge of all types of selenium

nanoparticles studied herein became more negatively charge as evidenced by the zeta potential values shown in Table 2.

At pH 7, selenium nanoparticles stabilized with all types of stabilizing agents studied herein carry overall negative charge. Addition of pancreatin bile extract, which consists of a group of negatively charged molecules, results in the overall increase in electrostatic repulsion of the same charge molecules. Therefore, the particles shifted to smaller size as depicted in Figures 3 and 4 (the brown lines and the green lines, without and with pancreatin bile extract, respectively). The TEM images of pectin and ovalbumin stabilized selenium nanoparticles show the same trend as the results from FlFFF.

2.4 Summary

Flow field-flow fractionation was found effective for size characterization of selenium nanoparticles. With the use of an on-line ICP-MS detection, element specific information was obtained and the quantification of selenium indicated that the total of approximately 88-103% of the original selenium nanoparticles were detected during fractionation. Upon incubation of selenium nanoparticles in gastrointestinal conditions, particle size distributions shifted differently depending on the type of stabilizing agent used in the preparation of selenium nanoparticles. The changes in particle size are governed by the resulting particle surface charge and the monomeric/dimeric nature of the stabilizing molecules at different pH values. Ionic strength and the presence of enzyme also affected on the particle surface charge and electrostatic interaction. Despite the shift in particle size distribution, more than 90 % of selenium was still presented in nanometer range after gastrointestinal digestion.

2.5 References

1. Akhtara, M., Dickinson, E., Mazoyer, J., & Langendorff, V. (2002). Emulsion stabilizing properties of depolymerized pectin. Food Hydrocolloids, 16 (3), 249-256.
2. Bai, Y., Wang, Y., Zhou, Y., Li, W., & Zheng, W. (2008). Modification and modulation of saccharides on elemental selenium nanoparticles in liquid phase. Materials Letters, 62 (15), 2311-2314.
3. Barnaby, S. N., Frayne, S. H., Fath, K. R., & Banerjee, I. A. (2011). Growth of Se nanoparticles on kinetin assemblies and their biocompatibility studies. Soft Materials, 9 (4), 313-334.

4. Bu, H., Kjøniksen, A.-L., Knudsen, K. D., & Nyström, B. (2004). Rheological and structural properties of aqueous alginate during gelation via the Ugi multicomponent condensation reaction. Biomacromolecules, 5 (4), 1470-1479.
5. Chen, T., Wong, Y.-S., Zheng, W., Bai, Y., & Huang, L. (2008). Selenium nanoparticles fabricated in Undaria pinnatifida polysaccharide solutions induce mitochondria-mediated apoptosis in A375 human melanoma cells. Colloids and surfaces B: Biointerfaces, 67 (1), 26-31.
6. Chithrani, B. D., Ghazani, A. A., & Chan, W. C. (2006). Determining the size and shape dependence of gold nanoparticle uptake into mammalian cells. Nano Letters, 6 (4), 662-668.
7. Combs Jr, G. F., & Combs, S. B. (1986). Selenium in human nutrition and health. In G. F. Combs & S. B. Combs (Eds.), The role of selenium in nutrition (pp. 327-399): Academic Press.
8. Cozzoli, P. D., & Manna, L. (1996). Nanostructure and biomolecule synthesis. In W.C. Chan (Ed.), Bio-Applications of nanoparticles (pp. 1-14). New York: Springer.
9. Dentini, M., Rinaldi, G., Barbetta, A., Risica, D., & Skjåk-Bræk, G. (2006). Acid gel formation in (pseudo) alginates with and without G blocks produced by epimerising mannuronan with C5 epimerases. Carbohydrate Polymers, 63 (4), 519-526.
10. Desai, M. P., Labhasetwar, V., Amidon, G. L., & Levy, R. J. (1996). Gastrointestinal uptake of biodegradable microparticles: effect of particle size. Pharmaceutical Research, 13 (12), 1838-1845.
11. Dickinson, E. (2010). Flocculation of protein-stabilized oil-in-water emulsions. Colloids and Surfaces B: Biointerfaces, 81 (1), 130-140.
12. Donati, I., Travan, A., Pelillo, C., Scarpa, T., Coslovi, A., Bonifacio, A., Sergo, V., & Paoletti, S. (2009). Polyol synthesis of silver nanoparticles: mechanism of reduction by alditol bearing polysaccharides. Biomacromolecules, 10 (2), 210-213.
13. Dondi, F., & Martin, M. (2000). Physicochemical measurements and distributions from field–flow fractionation. In M.E. Schimpf, J.C. Caldwell, & J.C. Giddings (Eds.), Field-flow fractionation handbook (pp. 103-132). New York: Wiley.
14. Dumont, E., Vanhaecke, F., & Cornelis, R. (2006). Selenium speciation from food source to metabolites: a critical review. Analytical and Bioanalytical Chemistry, 385 (7), 1304-1323.
15. Hoet, P. H., Brüske-Hohlfeld, I., & Salata, O. V. (2004). Nanoparticles–known and unknown health risks. Journal of Nanobiotechnology, 2 (1), 12.
16. Ingole, A. R., Thakare, S. R., Khati, N., Wankhade, A., & Burghate, D. (2010). Green synthesis of selenium nanoparticles under ambient condition. Chalcogenide Letters, 7, 485-489.
17. Jia, X., Li, N., & Chen, J. (2005). A subchronic toxicity study of elemental Nano-Se in Sprague-Dawley rats. Life sciences, 76 (17), 1989-2003.

18. Kammer, F. v. d., Legros, S., Hofmann, T., Larsen, E. H., & Loeschner, K. (2011). Separation and characterization of nanoparticles in complex food and environmental samples by field-flow fractionation. TrAC Trends in Analytical Chemistry, 30 (3), 425-436.

19. Kittler, S., Greulich, C., Gebauer, J., Diendorf, J., Treuel, L., Ruiz, L., Gonzalez-Calbet, J., Vallet-Regi, M., Zellner, R., & Köller, M. (2010). The influence of proteins on the dispersability and cell-biological activity of silver nanoparticles. Journal of Materials Chemistry, 20 (3), 512-518.
20. Kuwata, K., Era, S., Hoshino, M., Forge, V., Goto, Y., & Batt, C. A. (1999). Solution structure and dynamics of bovine β-lactoglobulin A. Protein Science, 8 (11), 2541-2545.
21. Lee, U., Choi, J., Myung, N., Kim, I. H., Chenthamarakshan, C. R. N., De Tacconi, N. R., & Rajeshwar, K. (2008). Synthesis of monodisperse selenium nanospheres and self-assembled monolayers using poly(vinyl pyrrolidone) as dual reductant/colloid stabilizer. Bulletin of the Korean Chemical Society, 29 (3), 689-692.
22. Li, Z.-L., & Hua, P.-M. (2009). Mixed surfactant template method for preparation of nanometer selenium. Journal of Chemistry, 6 (S1), S304-S310.
23. Lin, Z.-H., & Chris Wang, C. (2005). Evidence on the size-dependent absorption spectral evolution of selenium nanoparticles. Materials Chemistry and Physics, 92 (2), 591-594.
24. Malaki Nik, A., Wright, A. J., & Corredig, M. (2010). Surface adsorption alters the susceptibility of whey proteins to pepsin-digestion. Journal of Colloid and Interface Science, 344 (2), 372-381.
25. Martos, G., Contreras, P., Molina, E., & López-FandiÑo, R. (2010). Egg white ovalbumin digestion mimicking physiological conditions. Journal of Agricultural and Food Chemistry, 58 (9), 5640-5648.
26. Matto, M., & Husain, Q. (2006). Entrapment of porous and stable concanavalin A–peroxidase complex into hybrid calcium alginate–pectin gel. Journal of Chemical Technology and Biotechnology, 81 (7), 1316–1323.
27. Medina-Torres, L., Calderas, F., Gallegos-Infante, J. A., Gonzalez-Laredo, R. F., Rocha-Guzman, N. E., & Harte, F. (2010). Mechanical properties of ovalbumin gels formed at different conditions of concentration, ionic strength, pH, and aging time. Food and Bioprocess Technology, 3 (1), 150-154.
28. Mees, D. R., Pysto, W., & Tarcha, P. J. (1995). Formation of selenium colloids using sodium ascorbate as the reducing agent. Journal of Colloid and Interface Science, 170 (1), 254-260.
29. Mehta, S. K., Chaudhary, S., Kumar, S., Bhasin, K. K., Torigoe, K., Sakai, H., & Abe, M. (2008). Surfactant assisted synthesis and spectroscopic characterization of selenium nanoparticles in ambient conditions. Nanotechnology, 19 (29).

30. Miller, D. D., Schricker, B. R., Rasmussen, R. R., & Van Campen, D. (1981). An in vitro method for estimation of iron availability from meals. The American Journal of Clinical Nutrition, 34 (10), 2248-2256.
31. Min-Hsiung, C.-Y. (2004). Observation in the growth of selenium nanoparticles. Journal of the Chinese Chemical Society, 51, 239-242.
32. Monsen, E. R. (2000). Dietary reference intakes for the antioxidant nutrients: vitamin C, vitamin E, selenium, and carotenoids. Journal of the American Dietetic Association, 100 (6), 637-640.
33. Mwilu, S. K., El Badawy, A. M., Bradham, K., Nelson, C., Thomas, D., Scheckel, K. G., Tolaymat, T., Ma, L., & Rogers, K. R. (2013). Changes in silver nanoparticles exposed to human synthetic stomach fluid: Effects of particle size and surface chemistry. Science of The Total Environment, 447, 90-98.
34. Navarro-Alarcon, M., & Cabrera-Vique, C. (2008). Selenium in food and the human body: a review. Science of the Total Environment, 400 (1), 115-141.
35. Peng, D., Zhang, J., Liu, Q., & Taylor, E. W. (2007). Size effect of elemental selenium nanoparticles (Nano-Se) at supranutritional levels on selenium accumulation and glutathione S-transferase activity. Journal of Inorganic Biochemistry, 101 (10), 1457-1463.
36. Peram, M. R., Loveday, S. M., Ye, A., & Singh, H. (2013). In vitro gastric digestion of heat-induced aggregates of β-lactoglobulin. Journal of Dairy Science, 96 (1), 63-74.
37. Poda, A. R., Bednar, A. J., Kennedy, A. J., Harmon, A., Hull, M., Mitrano, D., Ranville, J., & Steevens, J. (2011). Characterization of silver nanoparticles using flow-field flow fractionation interfaced to inductively coupled plasma mass spectrometry. Journal of Chromatography A, 1218 (27), 4219-4225.
38. Rayman, M. P., Infante, H. G., & Sargent, M. (2008). Food-chain selenium and human health: spotlight on speciation. British Journal of Nutrition, 100 (02), 238-253.
39. Sakurai, K., Oobatake, M., & Goto, Y. (2001). Salt-dependent monomer–dimer equilibrium of bovine β-lactoglobulin at pH 3. Protein Science, 10 (11), 2325-2335.
40. Sepelyak, R. J., Feldkamp, J. R., Moody, T. E., White, J. L., & Hem, S. L. (1984). Adsorption of pepsin by aluminum hydroxide I: Adsorption mechanism. Journal of Pharmaceutical Sciences, 73 (11), 1514-1517.
41. Shah, C. P., Kumar, M., & Bajaj, P. N. (2007). Acid-induced synthesis of polyvinyl alcohol-stabilized selenium nanoparticles. Nanotechnology, 18 (38).

42. Szentkuti, L. (1997). Light microscopical observations on luminally administered dyes, dextrans, nanospheres and microspheres in the pre-epithelial mucus gel layer of the rat distal colon. Journal of Controlled Release, 46 (3), 233-242.
43. Teow, Y., Asharani, P. V., Prakash Hande, M., & Valiyaveettil, S. (2011). Health impact and safety of engineered nanomaterials. Chemical Communications, 47 (25), 7025-7038.
44. Thomson, C. (2004). Assessment of requirements for selenium and adequacy of selenium status: a review. European Journal of Clinical Nutrition, 58 (3), 391-402.
45. Walczak, A. P., Fokkink, R., Peters, R., Tromp, P., Herrera Rivera, Z. E., Rietjens, I. M. C. M., Hendriksen, P. J. M., & Bouwmeester, H. (2013). Behaviour of silver nanoparticles and silver ions in an in vitro human gastrointestinal digestion model. Nanotoxicology, 7 (7), 1198-1210.
46. Wang, B., Feng, W.-Y., Wang, T.-C., Jia, G., Wang, M., Shi, J.-W., Zhang, F., Zhao, Y.-L., & Chai, Z.-F. (2006). Acute toxicity of nano-and micro-scale zinc powder in healthy adult mice. Toxicology Letters, 161 (2), 115-123.
47. Wang, H., Zhang, J., & Yu, H. (2007). Elemental selenium at nano size possesses lower toxicity without compromising the fundamental effect on selenoenzymes: comparison with selenomethionine in mice. Free Radical Biology and Medicine, 42 (10), 1524-1533.
48. Wang, Y. (2009). Differential effects of sodium selenite and nano-Se on growth performance, tissue Se distribution, and glutathione peroxidase activity of avian broiler. Biological Trace Element Research, 128 (2), 184-190.
49. Zhang, J. S., Gao, X. Y., Zhang, L. D., & Bao, Y. P. (2001). Biological effects of a nano red elemental selenium. BioFactors (Oxford, England), 15 (1), 27-38.
50. Zhang, J., Wang, H., Bao, Y., & Zhang, L. (2004). Nano red elemental selenium has no size effect in the induction of seleno-enzymes in both cultured cells and mice. Life Sciences, 75 (2), 237-244.
51. Zhang, J., Wang, H., Yan, X., & Zhang, L. (2005). Comparison of short-term toxicity between Nano-Se and selenite in mice. Life Sciences, 76 (10), 1099-1109.
52. Zhang, S.-Y., Zhang, J., Wang, H.-Y., & Chen, H.-Y. (2004). Synthesis of selenium nanoparticles in the presence of polysaccharides. Materials Letters, 58 (21), 2590-2594.
53. Zook, J. M., MacCuspie, R. I., Locascio, L. E., Halter, M. D., & Elliott, J. T. (2011). Stable nanoparticle aggregates/agglomerates of different sizes and the effect of their size on hemolytic cytotoxicity. Nanotoxicology, 5 (4), 517-530.

Chapter 3

Investigation of Silver Nanoparticles and Plasma Protein Association Using Flow Field-Flow Fractionation Coupled with Inductively Coupled Plasma Mass Spectrometry (FlFFF-ICP-MS)

3.1 Introduction

Many consumer products nowadays are claimed to contain engineered nanoparticles. Owing to its strong antimicrobial activity, silver nanoparticles (AgNPs) have been used in several applications, such as food packing materials; textile; cosmetic; household items; and wound dressing. However, the wide usage of AgNPs increases the possibility for these nanomaterials to enter into environment and human body. Human exposure to AgNPs can be from various routes, including ingestion; inhalation; dermal contact; and through therapeutic applications [1, 2].

Some researchers reported different transdermal penetration rates of AgNPs through the intact and damaged skins, which were controlled by intrinsic parameters of the skin [3]. Once entering the body, AgNPs were rapidly in contact with biological fluids such as saliva, mucus, lung lining fluid, and plasma protein [4, 5]. Therefore, the assessment of the interactions between AgNPs and plasma proteins is a very important issue. Considering the plasma proteins, the majority is albumin (55%), followed by globulin (38%) and fibrinogen (7%). Various analytical techniques were exploited to examine plasma protein-nanoparticles association in order to gain an insight into the binding between plasma proteins and AgNPs. Those techniques include ultraviolet-visible spectroscopy (UV-Vis) [6], fluorescence spectroscopy [7], dynamic light scattering (DLS) [8], atomic force microscopy (AFM) [9], and size exclusion chromatography (SEC) [10]. In this work, we proposed the use of flow field-flow fractionation (FlFFF) online with inductively coupled plasma mass spectrometry (ICP-MS) as an alternative technique for investigation of AgNPs-plasma protein association. This hyphenated technique has been successfully applied to examine freshwater oligochaete exposure to AgNPs [11], study the effects of particle size and the coating on the bioaccumulation and depuration of AgNPs within the gut cavities of aquatic invertebrates [12], investigate the effect of UV irradiation on the stability of AgNPs [13], analyze AgNPs in chicken meat [14], and examine the association of AgNPs with HepG2 cells [15].

The aim of this work was to apply a conventional symmetrical flow field-flow fractionation (FlFFF) with online inductively coupled plasma mass spectrometry (ICP-MS) for investigation of plasma protein-silver nanoparticles (AgNPs) association. Plasma proteins studied herein included bovine serum albumin (BSA), globulin, and fibrinogen. The key parameters affecting the association between plasma proteins and AgNPs were examined, including incubation time and AgNPs concentration. The novel finding from this technique also includes the information on stoichiometric binding between AgNPs and BSA.

3.2 Experimental

3.2.1 Instrumentation

A symmetrical FlFFF system (Model PN-1201-FO, Postnova Analytics, Landsberg, Germany) equipped with a 1,000 Da molecular weight cut-off regenerated cellulose acetate membrane (Postnova) was used. The geometry of the FlFFF channel is 27.7 cm long, 2.0 cm wide, and 0.0254 cm thick. Sample volume of 20 μL was introduced into FlFFF via the Rheodyne® injector valve. Two high pressure liquid chromatography (HPLC) pumps (Model PN 2101, Postnova Analytics, Germany) were used to regulate the channel flow and the cross flow, respectively. In our experiment, a channel flow was set at 1 $mLmin^{-1}$ and a cross flow of 2 $mLmin^{-1}$ was used. After fractionation, the effluent was directed through a UV detector (Model Water 2487 Dual λ Absorbance Detector, Waters, Milford, MA, USA) which was set at 280 nm for detection of the plasma proteins. The UV detector outlet was coupled to an ICP-MS instrument (Sciex/Elan 6000, PerkinElmer Instruments, Shelton, CT, USA) using a cross-flow nebulizer with 50-cm poly (tetrafluoroethylene) tubing (PTFE, 0.58 mm id). The eluted fraction from FlFFF was introduced into the ICP-MS sample introduction system for further determination of element. Both silver isotopes (^{107}Ag and ^{109}Ag) were monitored and an integration dwell time of 25 ms was set for each isotope. The total number of readings per replicate was chosen such that data were collected for the entire fractograms. To assure no drift of instrument, 20 $\mu g\ L^{-1}$ AgNPs was used for checking the stability of the signal once after every five run. The FlFFF-ICP-MS operating conditions are given in Table 1.

A UV/Visible spectrophotometer (Model V-530, Jasco, Easton, Maryland, USA) was used for acquisition of the UV/Visible absorption spectra of AgNPs, plasma protein, and protein-AgNPs association.

Table 1 FlFFF-ICP-MS operating conditions

FlFFF: Model PN-1021-FO	
Channel flow rate/mL min^{-1}	1.0
Cross flow rate/mL min^{-1}	2.0
Equilibration time/min	1.1
Carrier liquid	30 mM Tris-HNO_3 (buffered at pH 9)
Membrane	1 kDa MWCO, poly(regenerated cellulose acetate)
ICP-MS: Sciex/Elan 6000 Perkin Elmer	
RF generator frequency/MHz	40
RF power/W	1100-1300
Nebulizer gas flow rate/L min^{-1}	0.90-0.95
Coolant gas flow rate/L min^{-1}	15.0
Auxiliary gas flow rate/L min^{-1}	0.90
Mode	Peak hopping
Dwell time/measurement/isotope	25
Torch	Fassel type
Torch injector	Ceramic alumina
Spray chamber	Ryton® Scott-type
Nebulizer	Gem-tip® cross flow
Isotopes monitored	^{107}Ag, ^{109}Ag

3.2.2 Chemicals

Bovine serum albumin (BSA) and tannic acid were purchased from Fluka (Buchs, Switzerland). γ- globulin and fibrinogen were purchased from Sigma–Aldrich (Steinheim, Germany). Silver nitrate, sodium azide and nitric acid (65%) were from Merck (Darmstadt, Germany). Tris (hydroxymethyl aminomethane) and FL-70® detergent (AR 98% assay) were from Fisher Scientific (Leicestershire, U.K.). De-ionized water (18.2 MΩ cm^{-1}) obtained from a water purification system (Barnstead International, Dubuque, IA, U.S.A.) was used throughout the experiment. All glassware was washed and soaked overnight in 30% HNO_3, and rinsed again with de-ionized water before use.

Two types of carrier liquid were used in the experiment. A 0.02% (w/v) FL-70 with 0.02% (w/v) sodium azide was used for size characterization of AgNPs. Another carrier liquid was a 30 mM tris (hydroxymethyl aminomethane), Tris, buffered at pH 9, which was used for investigation of AgNPs-plasma protein association.

Silver nanoparticles were prepared by using the method described by Sivaraman et al. [16]. While stirring, 25 mL of 0.3 mM tannic acid adjusted pH by K_2CO_3 and 5 mL of 3 mM silver nitrate were mixed in a conical flask. Three pH conditions were used, including pH of 8, 9, and 10 to prepare AgNPs of various sizes. A brown yellow solution appeared immediately, indicating the formation of tannic stabilized AgNPs. Albumin of 5.2 x 10^{-1} M, γ- globulin of 6.2 x 10^{-2} M, and fibrinogen of 5.8 x 10^{-3} M were prepared in Tris-buffer.

3.2.3 Calculation of AgNPs concentration

The concentration of the synthesized AgNPs was calculated by the method described by Mariam et al. [7]. By assuming that AgNPs are spherical in shape, the number of silver atoms was calculated by considering that the volume ratio of silver atom to AgNPs is 74.1% in the cubic structure. The radius of silver atom is 0.144 nm, and therefore its volume is 0.0125 nm^3. For AgNPs with the diameter of d nm, its volume is $(\pi/6)d^3$ nm^3. Thus, the number of silver atoms (N) in each AgNPs is equal to $\frac{74.1}{100} x \frac{\pi}{6} d^3 x \frac{1}{0.0125}$, which is calculated to be 31 d^3 [7]. The concentration of the AgNPs was then calculated by taking the ratio of the total number of silver atoms added to the reaction solution (N_{Total}) and the product between the number of silver atoms present in each nanoparticle (N) and the volume of the reaction solution in liters (V) and the Avogadro's constant (N_A). By assuming that all silver atoms were converted to AgNPs completely, therefore, the concentrations of various AgNPs sizes of 2.6, 10, 23 nm were calculated to be 9.2 x 10^{-7}, 1.6 x 10^{-8}, 1.3 x 10^{-9} M, respectively.

3.2.4 Observation of incubation time and concentration of AgNPs with plasma proteins

Two parameters influencing protein-nanoparticles association were investigated. These included the effects of incubation time and AgNPs concentration on protein binding. To examine the effect of incubation time, 2.6 nm tannic stabilized AgNPs of 4.6 x 10^{-7} M was incubated with either 2.6 x 10^{-1} M BSA, 3.1 x 10^{-2} M globulin, or 2.9 x 10^{-3} M

fibrinogen at 37 °C for 5 min, 2, and 24 h. To examine the effect of AgNPs concentration on its binding with proteins, 2.6 nm tannic stabilized AgNPs of various concentrations as 9.2×10^{-8}, 2.7×10^{-7}, and 4.6×10^{-7} M were incubated with either 2.6×10^{-1} M bovine serum albumin, 3.1×10^{-2} M globulin, or 2.9×10^{-3} M fibrinogen at 37°C for 24 h. After incubation, the mixture was introduced into FlFFF for characterization. After fractionation, the effluent was directed through a UV detector and sequentially to ICP-MS.

3.2.5 Observation of stoichiometric binding between AgNPs and BSA

The stoichiometric binding between AgNPs with BSA was investigated by incubating different concentrations of bovine serum albumin with 2.6 nm tannic stabilized AgNPs of 9.2×10^{-8} M at 37 °C for 5 min. To confirm the stoichiometric binding between AgNPs with BSA, various concentrations of tannic stabilized AgNPs were incubated with BSA of 1.5×10^{-2} M. After incubation, the mixture was introduced into FlFFF-ICP-MS. The mole ratio between AgNPs and BSA was examined by keeping AgNPs and BSA constant as shown in Table 2 and 3, respectively.

Table 2 Mole ratio method for determination of stoichiometric binding between BSA and AgNPs. The concentration of AgNPs was kept constant.

Concentration of AgNPs (M)	Concentration of BSA (M)
9.2×10^{-8}	1.49×10^{-2}
	7.46×10^{-2}
	1.49×10^{-1}
	1.79×10^{-1}
	2.08×10^{-1}
	2.38×10^{-1}
	2.98×10^{-1}

Table 3 Mole ratio method for determination of stoichiometric binding between BSA and AgNPs. The concentration of BSA was kept constant.

Concentration of BSA (M)	Concentration of AgNPs (M)
1.49×10^{-2}	1.84×10^{-9}
	3.68×10^{-9}
	4.60×10^{-9}
	5.52×10^{-9}
	5.98×10^{-9}
	6.44×10^{-9}
	7.36×10^{-9}
	8.28×10^{-9}
	9.20×10^{-9}
	1.10×10^{-8}

3.3 Results and discussion

3.3.1 Characterization of silver nanoparticles

Characterization of the synthesized AgNPs was performed using UV-visible absorption spectrophotometry and FlFFF. With UV-visible absorption spectrophotometry, the blank solution containing tannic acid at the same pH as the tannic stabilized AgNPs was filled in a reference cuvette for background subtraction. The absorption spectra of AgNPs displayed the surface plasmon resonance bands at 400, 410, and 420 nm for tannic stabilized AgNPs at pH 8, 9, and 10, respectively, as displayed in Figure 1a. These peaks indicated the formation of AgNPs. With FlFFF, the particle size distributions showed the peaks at 23.0 ± 0.2, 10.0 ± 0.3, and 2.6 ± 0.1 nm for tannic stabilized AgNPs at pH 9, 10, and 11, respectively, as illustrated in Figure 1b. The large void peaks observed in the fractograms shown in Figure 1b were due to the incomplete removal of the negatively charged tannic acid through the negatively charged cellulose acetate membrane during a very short time equilibration step (1.1 min, Table 1). The trends of particles sizes obtained from UV-visible absorption spectrophotometry and FlFFF were in good agreement. As can

be seen, the smaller particles size of AgNPs exhibited plasmon resonance peak at shorter wavelength as compared to the bigger particle. These AgNPs were used in further experiments to observe the association between these particles and proteins.

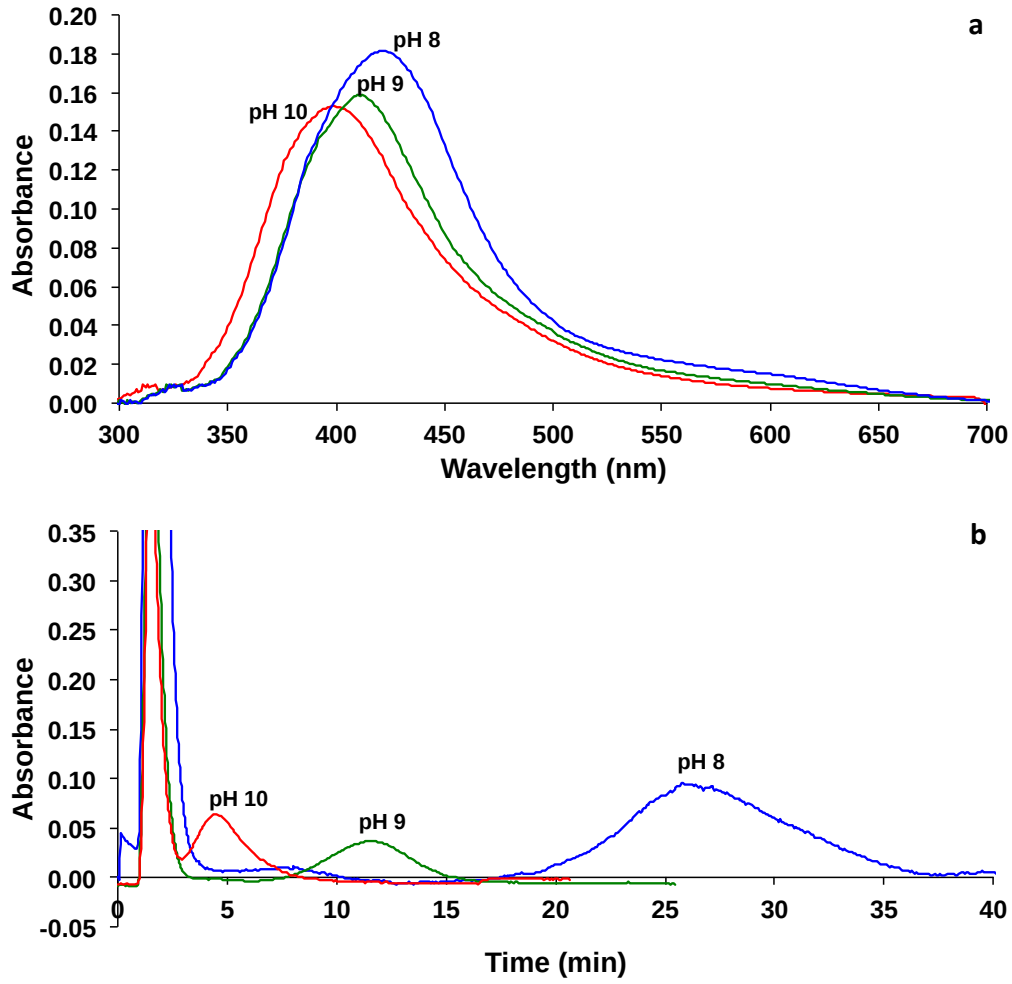

Figure 1 (a) UV-visible absorption spectra and (b) fractograms of tannic stabilized AgNPs synthesized at pH 8 (blue), 9 (green), 10 (red).

As reported by other investigators [7, 17], the complex formation of BSA and AgNPs could be characterized by UV-visible absorption spectrophotometry. The absorption spectrum of BSA displayed a peak maximum at 278 nm (Figure 2). In the presence of AgNPs as illustrated in Figure 2a, 2b, 2c for AgNPs of 2.6, 10, and 23 nm, respectively, the absorbance at 278 nm of BSA increased with increasing in AgNPs concentrations, suggesting the formation of the ground state complex between BSA and AgNPs [7]. The apparent association constant (K_{app}) for the complex formation between BSA and AgNPs

was then calculated using the method reported by Benesi and Hildebrand [17], as illustrated in Figure 2d. The slope of the graph represents the reciprocal of K_{app} (A_c-A_0) and the intercept represents the reciprocal of (A_c-A_0), where A_c is the absorbance of the AgNPs-BSA complex and A_0 is the absorbance of BSA. Therefore, the values of K_{app} for AgNPs size of 2.6, 10, and 23 nm were calculated to be 5.2 x 10^7, 8.8 x 10^7, and 9.8 x 10^8 L mol^{-1}, respectively. This trend suggests that the bigger the particle size, the higher the value of the apparent association constant. The increase of the K_{app} value was found to linearly depend on the increase of the particle volume ($K_{app} \propto d^3$).

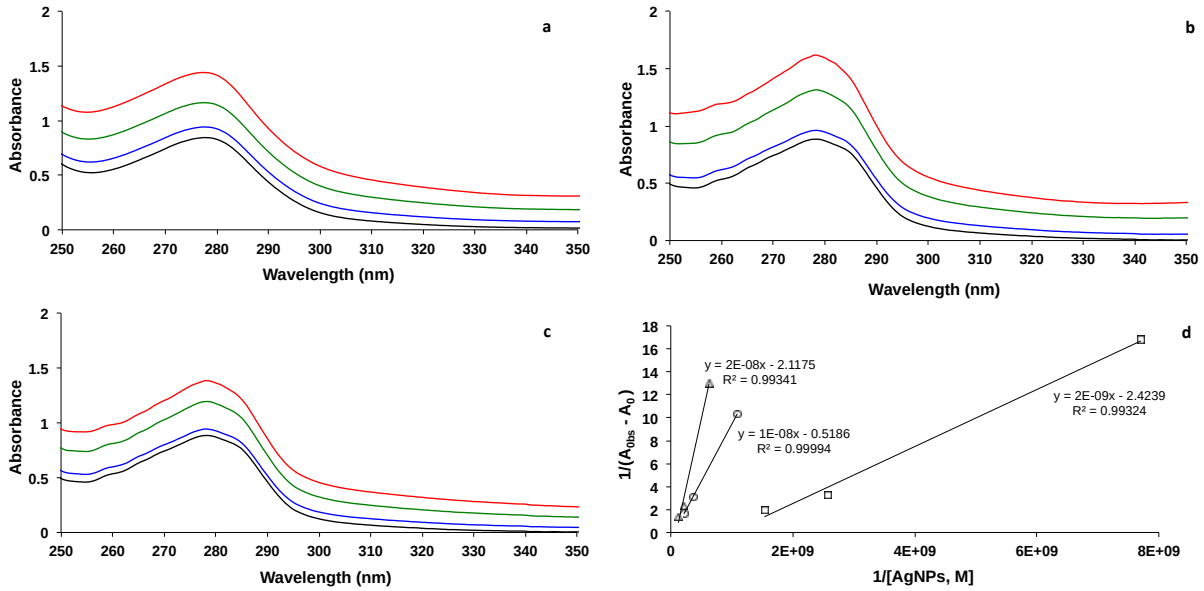

Figure 2 UV-visible absorption spectra of 2.6 x 10^{-1} M BSA (black) and BSA in the presence of AgNPs of (a) 2.6 nm with the concentration of 9.2 x 10^{-8} M (blue), 2.7 x 10^{-7} M (green), and 4.6 x 10^{-7} M (red); (b) 10 nm with the concentration of 1.6 x 10^{-9} M (blue), 4.8 x 10^{-9} M (green), and 8.0 x 10^{-9} M (red); and (c) 23 nm with the concentration of 1.3 x 10^{-10} M (blue), 3.9 x 10^{-10} M (green), and 6.5 x 10^{-10} M (red). [Note – increasing concentration of AgNPs resulted in higher absorbance] (d) Linear plots for calculation of K_{app} between BSA and AgNPs of 2.6 nm (○), 10 nm (△), and 23 nm (□).

3.3.2 FlFFF-ICP-MS for observation of protein-AgNPs association

The effects of incubation time and AgNPs concentration on the binding of the protein to AgNPs were examined using FlFFF-ICP-MS. The proteins investigated were BSA, globulin, and fibrinogen. The particle size of AgNPs was 2.6 nm. In order to understand if

the binding was due to the binding between the proteins and AgNPs, or the free dissolved Ag ions which were not converted into AgNPs, the remaining dissolved Ag ions were estimated. The estimation was performed by calculating the amount of Ag detected under the fractogram compared with the amount of Ag from AgNPs suspension, which was nebulized directly into the ICP-MS without flowing through the FlFFF channel. By taking into consideration that the sample recovery of AgNPs fractionation in the FlFFF channel was approximately 80%, the remaining dissolved Ag ion in the AgNPs were estimated to be approximately 5%. Therefore, the binding behavior discussed hereafter is mainly due to the binding between the protein and AgNPs.

Effect of incubation time

The fractograms of tannic stabilized AgNPs are illustrated in Figure 3a (with UV detection at 400 nm) and Figure 3b (with ICP-MS detection). Two peaks were observed in Figure 3a, by which the first peak (1.6 min) was assigned to the excess tannic acid whereas the second peak (4.8 min) was assigned to AgNPs, which was confirmed by one distinct peak at 5.5 min as observed in Figure 3b with ICP-MS detection. With UV detection, the large void peak was observed (1.6 min), owing to the incomplete removal of negatively charged tannic acid through the negatively charged cellulose acetate membrane during a 1.1 min equilibration step. The fractograms of BSA are illustrated in Figure 3c (with UV detection at 280 nm) and Figure 3d (with ICP-MS detection). One distinct peak was observed at 3.4 min with UV detection (Figure 3c, red) and this was clearly the peak of BSA. No signal was observed with the ICP-MS detection (Figure 3d, red). Different incubation times at 5 min, 120 min, and 24 h were given to allow BSA to interact with AgNPs. For the mixture, the fractograms with varying incubation times are shown in Figure 3c (with UV detection at 280 nm) and Figure 3d (with ICP-MS detection). With ICP-MS detection, it was clearly seen that the peaks illustrating the signal of Ag were shifted from 5.5 min (Figure 3b) to approximately 3 min retention time (Figure 3d), indicating the interaction between AgNPs and BSA. The association between AgNPs and BSA can be the formation of a “nanoparticle-protein corona” which has been documented in many published articles [18, 19]. The formation of a "protein-corona" would affect the interactions with the membrane, resulting in shift of the retention times [14, 20]. Nonetheless, the formation of a “nanoparticle-protein corona” was unlikely as it should result in larger particle formation. Alternatively, the peak at 3 min might be due to the

binding between BSA with the released Ag ion from the AgNPs, as reported by other investigators [21].

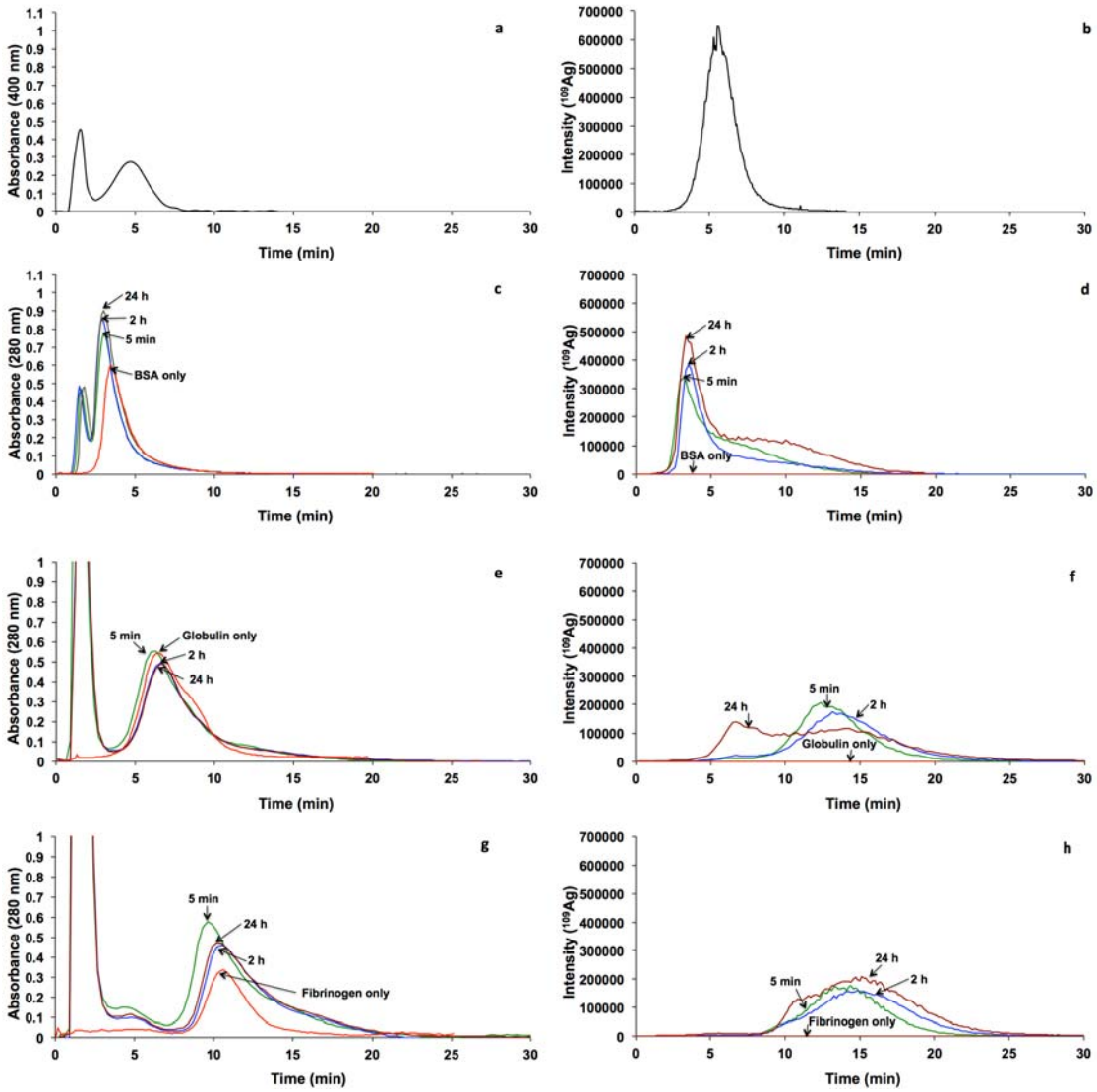

Figure 3 Fractogram of 2.6 nm tannic stabilized AgNPs 4.6 x 10^{-7} M: (a) with UV detection; and (b) with ICP-MS detection. Fractograms of BSA 2.6 x 10^{-1} M (c and d, red); globulin 3.1 x 10^{-2} M (e and f, red); fibrinogen 2.9 x 10^{-3} M (g and h, red), mixed with 2.6 nm tannic stabilized AgNPs 4.6 x 10^{-7} M: (c,e,g) with UV detection; and (d,f,h) with ICP-MS detection, at various incubation times of 5 min (green), 120 min (blue), and (brown) 24 h.

As evidenced by Cedervall et al. [18], the nanoparticle-protein corona formation is a complex and time-dependent process, which is governed by thermodynamic and kinetic factors. Under the condition studied herein, the association between BSA and AgNPs or

the released Ag ion from the AgNPs occurred within 5 min of incubation time. With longer incubation time at 24 h, bimodal characteristic was observed by the appearance of the peak at approximately 10 min, implying that AgNPs might grow bigger. The shift to bigger size may either be caused by three reasons. The first plausible reason is due to the nanoparticle-protein corona formation, yielding larger particle size. The second plausible reason is due to the displacement of tannic acid stabilizing agent with BSA, which is more steric leading to larger particle size. The displacement of stabilizing agent with BSA might occur through the ligand-exchange or place-exchange reaction as reported by the other investigators for AuNPs [22]. The third plausible reason is due to the interaction between tannic acid and BSA as the association between tannic acid and proteins has been widely known by food scientists to cause astringency perception [23].

To demonstrate the effect of incubation time on AgNPs binding with globulin, the fractograms as shown in Figures 3e and 3f are considered. The fractograms of globulin are illustrated in Figure 3e (with UV detection at 280 nm) and Figure 3f (with ICP-MS detection). With UV detection (Figure 3e, red), the peak of globulin appeared at retention time of 6.2 min with a shoulder at 8.7 min. Clearly, no signal was observed with the ICP-MS detection (Figure 3f, red). Different incubation times at 5 min, 120 min, and 24 h were given to allow globulin to interact with AgNPs. For the mixture, the fractograms with varying incubation times are shown in Figure 3e (with UV detection at 280 nm) and Figure 3f (with ICP-MS detection). At incubation times of 5 and 120 min, monomodal distribution was observed at the retention time of 13.2 min. It is interesting to note that the peak at 13.2 min shifted significantly from the peak of individual AgNPs at 5.5 min (Figure 3b), suggesting the rapid occurrence of the binding between AgNPs and globulin. This globulin-AgNPs corona formation resulted in larger particle size. Alternatively, the peak at 13.2 min might be assigned to the binding between the released Ag ion with the dimeric form of globulin as the monomeric form of globulin displayed a peak at approximately 6.2 min (Figure 3e). One might wonder why this dimeric peak was not distinct with the absorbance detection at 280 nm, as shown in Figure 3e. We believed that the dimeric form was present in a relatively lower concentration than the monomeric form of globulin. Nonetheless, the released Ag ion from AgNPs showed preferential association with the globulin dimer, leading to the more distinct peak of the dimeric form when ICP-MS was used for silver detection. The dimerization of globulin on the AgNPs surface might be caused by structural perturbation of globulin by the high surface-to-volume ratios of

nanoparticles, which resulted in high concentration of globulin adsorbed at the particle surface of low dimensionality, enhancing the probability of partial unfolding of globulin, as described by Linse et al [24]. Nonetheless, bimodal distribution was observed when the incubation time reached 24 h, by displaying peaks at 6.6 and 13.2 min. This suggested that in our experiment the dimerization occurred rapidly within 5 min and was found reversible as the monomeric peak at 6.6 min retention time was observed at the incubation time of 24 h. Alternatively, the peak at 6.6 nm might be due to binding of the released Ag ion from AgNPs with the monomeric fraction.

The effect of incubation time on the binding of AgNPs to fibrinogen was examined, as illustrated in Figures 3g and 3h. The fractograms of fibrinogen are illustrated in Figure 3g (with UV detection at 280 nm) and Figure 3h (with ICP-MS detection). With UV detection (Figure 3g, red), the peak of fibrinogen appeared at retention time of 10.3 min. As expected, no signal was observed with the ICP-MS detection (Figure 3h, red). Fibrinogen was allowed to incubate with AgNPs for various incubation times at 5 min, 120 min, and 24 h. Comparing between Figure 3g and Figure 3h, the peak positions were not similar, suggesting that AgNPs were preferentially associated to the larger molecular weight fibrinogen. Considering Figure 3h, the binding occurred within 5 min of incubation time, as can be observed from the peak at 14.5 min, which slightly shifted toward larger size than the pure fibrinogen.

Effect of AgNPs concentration

To examine the effect of AgNPs concentration on the association between BSA and AgNPs, various concentrations of AgNPs were incubated with BSA at fixed time of 24 h. With increased concentration of AgNPs, the signal intensity was increased, suggesting that more AgNPs could be associated with BSA. The shoulder peak at around 10 min was observed when the concentration of AgNPs increased up to 4.9×10^{-7} M, suggesting that the enlargement of the particles depends on the concentration of AgNPs. The nanoparticle-protein corona formation, or the place-exchange reaction between BSA and tannic acid or the association between BSA and tannic acid was not taken place when the concentration of AgNPs was too low.

The binding of globulin to AgNPs with various AgNPs concentrations was also examined at a fixed incubation time of 24 h. When concentration of AgNPs was increased, the signal intensity of fractogram was increased. Broad distribution was observed at low

concentration of globulin. The distribution became bimodal showing distinct peaks at 6.6 and 13.2 min retention time when the concentration of AgNPs was increased to 4.6 x 10^{-7} M. This suggests that the dimerization of globulin induced by AgNPs is concentration dependent.

The binding of fibrinogen to AgNPs with various AgNPs concentrations is shown in Figure 4e and Figure 4f. With AgNPs of 9.2 x 10^{-8} M, the signal of Ag was quite negligible suggesting that this concentration might be too low to cause the binding with 2.9 x 10^{-3} M fibrinogen (Figure 4f). However, when the concentration of AgNPs increased to 2.7 x 10^{-7} M, the peak was observed at 16.6 min. Formation of nanoparticle-protein corona between AgNPs and fibrinogen is possible as reported by Cedervall et al [18]. With increasing AgNPs to 4.6 x 10^{-7} M, bimodal characteristic was observed at 10.5 and 14.2 min. The peak at 10.5 min is quite close to the peak of pure fibrinogen, suggesting the possible occurrence of fibrinogen binding with the released Ag ion from the AgNPs.

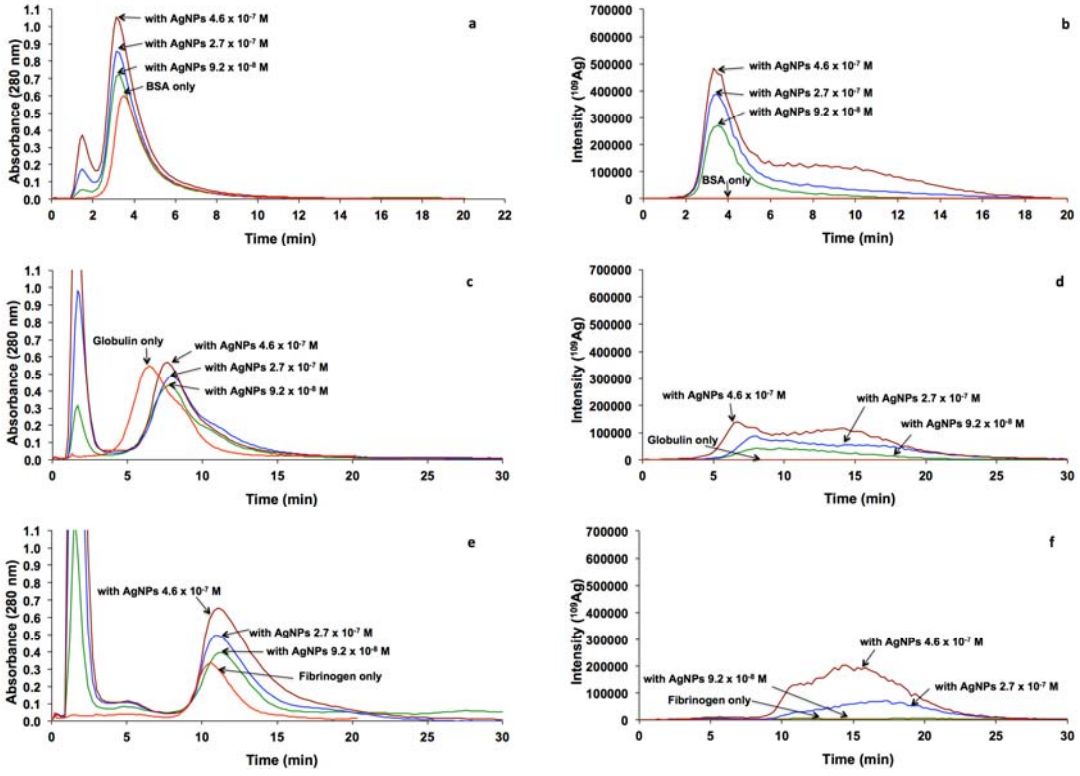

Figure 4 Fractograms of 2.6 x 10^{-1} M BSA (a and b, red); 3.1 x 10^{-2} M globulin (c and d, red); 2.9 x 10^{-3} M fibrinogen (e and f, red), incubated 24 h with 2.6 nm tannic stabilized AgNPs of various concentrations as (green) 9.2 x 10^{-8}; (blue) 2.7 x 10^{-7}; and (brown) 4.6 x 10^{-7} M: (a,c,e) with UV detection; and (b,d,f) with ICP-MS detection.

3.3.3 Binding stoichiometry between AgNPs and BSA

This is the first time that FlFFF-ICP-MS was applied to examine the stoichiometry of the binding of BSA with AgNPs. Various concentrations of BSA were incubated with AgNPs of 9.2 x 10^{-8} M. In order to differentiate the signal of Ag between the Ag binding to BSA and the Ag in the AgNPs, the fractogram of the mixture between BSA and AgNPs (Figure 5a) was deconvoluted using PeakFit® program (an automated peak separation analysis software). The deconvoluted peaks of the fractogram are illustrated in Figure 5b, which showed two distinct peaks at 3.6 and 5.9 min. The first peak was related to BSA binding and the second peak was contributed from AgNPs. The area under the first deconvoluted peak (peak I) of the Ag fractogram was observed. Using the mole-ratio method, the peak area under the first deconvoluted peak (peak I) of the Ag fractograms obtained from varying concentrations of BSA was plotted as a function of BSA concentration as illustrated in Figure 5c. At low concentration of BSA, the peak area of the first deconvoluted peak (peak I) of Ag fractogram was low and the peak area increased rapidly with increasing in BSA concentration from 7.46 x 10^{-2} to 1.49 x 10^{-1} M. After this point, the peak area under the first deconvoluted peak (peak I) of the Ag fractogram became relatively constant with increasing BSA, suggesting that the binding became constant. The stoichiometric binding between BSA and AgNPs was determined at the inflection point or the point where the two straight lines met, which was at the BSA concentration of 1.49 x 10^{-1} M, implying that the binding ratio between BSA and AgNPs was 1 : 6.2 x 10^{-7}. This is only a rough estimation as the increment of the concentration from 7.46 x 10^{-2} to 1.49 x 10^{-1} M was rather unrefined.

To confirm the stoichiometric binding between AgNPs and BSA, similar experiment was performed by varying AgNPs concentrations with fixed BSA concentration at 1.49 x 10^{-2} M. For very low concentrations of AgNPs, no signal of Ag was observed at the peak of BSA. Until at AgNPs of 7.4 x 10^{-9} M, the signal of Ag increased significantly and became relatively constant thereafter (Figure 5d). This suggests that the stoichiometric binding of BSA and AgNPs is 1 : 4.9 x 10^{-7}. Using the mole ratio method by keeping either AgNPs or BSA constant, the ratio of BSA and AgNPs were found to be approximately 1 : 5 x 10^{-7}, suggesting that approximately 2 x 10^{6} molecules of BSA adsorbed on a single AgNP with the size of 2.6 nm.

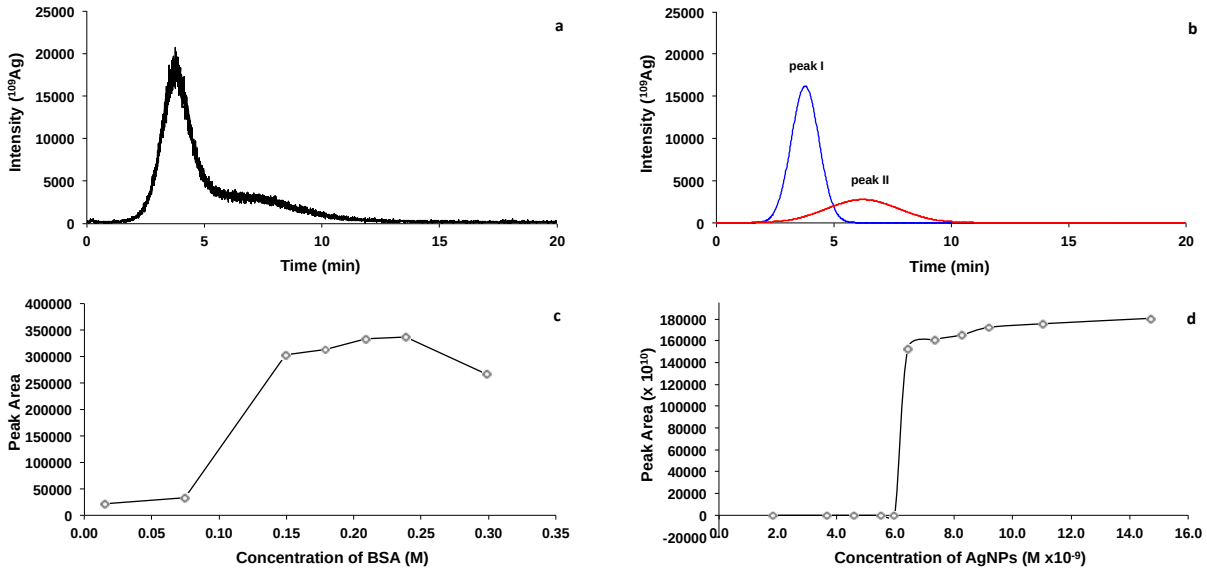

Figure 5 (a) Fractogram of the mixture between 1.49 x 10^{-2} M BSA and 9.2 x 10^{-8} M AgNPs, with ICP-MS detection. (b) The deconvoluted peaks of the fractogram, showing two peaks (Peak I, blue and Peak II, red). Plots of peak area under the deconvoluted peak I of the Ag fractograms versus concentrations of (c) BSA when the concentration of AgNPs was 9.2 x 10^{-8} M, and (d) AgNPs when the concentration of BSA was 1.49 x 10^{-2} M.

3.4 Summary

With the use of UV-visible spectrophotometry, complex formation of BSA and AgNPs could be observed and the apparent association constant (K_{app}) could be determined as reported by other investigators [7, 17]. The novel finding from this study, however, is that the K_{app} value was found to linearly depend on the particle volume ($K_{app} \propto d^3$). Furthermore, FlFFF-ICP-MS was demonstrated as an alternative method to monitor the protein-AgNPs association. Plasma proteins (BSA, globulin, and fibrinogen) were investigated for their formation of protein corona with AgNPs. The interaction between BSA and AgNPs was affected by both incubation time and concentration of AgNPs. The binding of plasma protein and AgNPs occurred rapidly within 5 min of incubation time. Additionally, the investigation of the stoichiometric binding between BSA and AgNPs was possible by FlFFF-ICP-MS, showing potential applications of the technique to study the complexation between other metals and macromolecules.

3.5 References

1. C.-F. Chau, S.-H. Wu and G.-C. Yen, *Trends Food Sci. Tech.*, 2007, **18**, 269-280.
2. Y. Li, Y. Zhang and B. Yan, *Int. J. Mol. Sci.*, 2014, **15**, 3671-3697.
3. Y. Teow, P. V. Asharani, M. P. Hande and S. Valiyaveettil, *Chem. Commun.*, 2011, **47**, 7025-7038.
4. S. Elodie, D. Julien, R.-L. Fernando and D. Jean-Marie, *J. Phys. Conf. Ser.*, 2011, **304**, 012039.
5. C. Beer, R. Foldbjerg, Y. Hayashi, D. S. Sutherland and H. Autrup, *Toxicol. Lett.*, 2012, **208**, 286-292.
6. L. Li, Q. Mu, B. Zhang and B. Yan, *Analyst*, 2010, **135**, 1519-1530.
7. J. Mariam, P. M. Dongre and D. C. Kothari, *J. Fluoresc.*, 2011, **21**, 2193-2199.
8. M. A. Dobrovolskaia, A. K. Patri, J. Zheng, J. D. Clogston, N. Ayub, P. Aggarwal, B. W. Neun, J. B. Hall and S. E. McNeil, *Nanomed.-Nanotechnol.*, 2009, **5**, 106-117.
9. Z. J. Deng, G. Mortimer, T. Schiller, A. Musumeci, D. Martin and R. F. Minchin, *Nanotechnology*, 2009, **20**.
10. I. Lynch and K. A. Dawson, *Nano Today*, 2008, **3**, 40-47.
11. A. R. Poda, A. J. Bednar, A. J. Kennedy, A. Harmon, M. Hull, D. M. Mitrano, J. F. Ranville and J. Steevens, *J. Chromatogr. A*, 2011, **1218**, 4219-4225.
12. J. G. Coleman, A. J. Kennedy, A. J. Bednar, J. F. Ranville, J. G. Laird, A. R. Harmon, C. A. Hayes, E. P. Gray, C. P. Higgins, G. Lotufo and J. A. Steevens, *Environ. Toxicol. Chem.*, 2013, **32**, 2069-2077.
13. A. R. Poda, A. J. Kennedy, M. F. Cuddy and A. J. Bednar, *J. Nanopart. Res.*, 2013, **15**, 1-10.

14. K. Loeschner, J. Navratilova, C. Købler, K. Mølhave, S. Wagner, F. von der Kammer and E. H. Larsen, *Anal. Bioanal. Chem.*, 2013, **405**, 8185-8195.

15. E. Bolea, J. Jimenez-Lamana, F. Laborda, I. Abad-Alvaro, C. Blade, L. Arola and J. R. Castillo, *Analyst*, 2014, **139**, 914-922.

16. S. K. Sivaraman, I. Elango, S. Kumar and V. Santhanam, *Curr. Sci.*, 2009, **97**, 1055-1059.

17. H. A. Benesi and J. H. Hildebrand, *J. Am. Chem. Soc.*, 1949, **71**, 2703-2707.

18. T. Cedervall, I. Lynch, S. Lindman, T. Berggård, E. Thulin, H. Nilsson, K. A. Dawson and S. Linse, *P. Natl. Acad. Sci. USA*, 2007, **104**, 2050-2055.

19. A. L. Capriotti, G. Caracciolo, C. Cavaliere, V. Colapicchioni, S. Piovesana, D. Pozzi and A. Laganà, *Chromatographia*, 2014, **77**, 755-769.

20. A. Ulrich, S. Losert, N. Bendixen, A. Al-Kattan, H. Hagendorfer, B. Nowack, C. Adlhart, J. Ebert, M. Lattuada and K. Hungerbühler, *J. Anal. At. Spectrom.*, 2012, **27**, 1120-1130.

21. A-K. Ostermeyer, C. K. Mumuper, L. Semprini and T. Radniecki, Environ. Sci. Technol., 2013, **47**, 14403-14410.

22. R. Sardar, J. W. Park and J. S. Shumaker-Parry, *Langmuir*, 2007, **23**, 11883-11889.

23. E. Obreque-Slier, C. Mateluna, A. Peña-Neira and R. López-Solís, *J. Agric. Food. Chem.*, 2010, **58**, 8375-8379.

24. S. Linse, C. Cabaleiro-Lago, W. F. Xue, I. Lynch, S. Lindman, E. Thulin, S. E. Radford and K. A. Dawson, *P. Natl. Acad. Sci. USA*, 2007, **104**, 8691-8696.

Output (RSA 5580011)

โครงการ การพัฒนาและการประยุกต์ใช้วิธีการทางเคมีวิเคราะห์ในการศึกษาการกระจายขนาดของอนุภาคขนาดนาโนเมตรในตัวอย่างอาหารเพื่อความเข้าใจเกี่ยวกับความสามารถในการนำไปใช้งานและความเป็นพิษของอนุภาคขนาดนาโนเมตร

ผลงานตีพิมพ์ในวารสารวิชาการนานาชาติ 3 เรื่อง

1. Wimuktiwan, P., Shiowatana, J., Siripinyanond, A., "Investigation of silver nanoparticles and plasma protein association using flow field-flow fractionation coupled with inductively coupled plasma mass spectrometry (FlFFF-ICP-MS)" (2015) Journal of Analytical Atomic Spectrometry, 30 (1), pp. 245-253. (impact factor 2013 = 3.396)
2. M-M, P., Somchue, W., Shiowatana, J., Siripinyanond, A., "Flow field-flow fractionation for particle size characterization of selenium nanoparticles incubated in gastrointestinal conditions" (2014) Food Research International, 57, pp. 208-209. (impact factor 2013 = 3.05)
3. M-M, P., Siripinyanond, A., "Field-flow fractionation with inductively coupled plasma mass spectrometry: Past, present, and future" (2014) Journal of Analytical Atomic Spectrometry, 29 (10), pp. 1739-1752. (impact factor 2013 = 3.396)

ผลงานตีพิมพ์ในรูปแบบ Book Chapter 1 เรื่อง

1. Suwanpetch, R., Techarang, T., Ornthai, M., M-M, P., Siripinyanond, A., "Field-flow fractionation with atomic spectrometric detection for characterization of engineered nanoparticles", in Encyclopedia of Analytical Chemistry, John Wiley & Sons, Ltd., DOI: 10.1002/9780470027318.a9427.

ผลงานเสนอในการประชุมวิชาการ 4 เรื่อง

1. Field-Flow Fractionation for Engineered Nanoparticles Characterization, The 2nd Taiwan-Thailand Bilateral Mini-Symposium: Chemistry for Creative Economy 17 - 18 January, 2013, Stang Mongkolsuk Building, Faculty of Science, Mahidol University, Thailand
2. Field-Flow Fractionation with Atomic Spectrometric Detection for Characterization of Engineered Nanoparticles, 2013 European Winter Conference on Plasma Spectrometry, 10 – 15 February, 2013, The Auditorium Maximum of Jagiellonian University, Krakow, Poland

3. Field-Flow Fractionation for Engineered Nanoparticles Characterization, The 1st Academic Science and Technology Conference (ASTC), 18 March, 2013, Ambassador Hotel Bangkok, Thailand
4. Hyphenated Inductively Coupled Plasma Mass Spectrometry Approaches for Bioaccessibility Study and Size-Based Fractionation, The 4th Asia Oceania Mass Spectrometry Conference and 10th Taiwan Society for Mass Spectrometry Annual Conference (4th AOMSC & 10th TSMS Annual Conference), 10 – 12 July, 2013, Taipei International Convention Center, Taipei, Taiwan

การบรรยายในสถาบันต่างๆ 6 เรื่อง

1. Field-Flow Fractionation for Engineered Nanoparticles Characterization, 21 January, 2013, Department of Food Engineering, King Mongkut's University of Technology Thonburi (KMUTT), Thailand
2. Field-Flow Fractionation for Size Characterization of Nanoparticles, 9 July, 2013, Department of Chemistry, National Sun Yat-Sen University, Kaohsiung, Taiwan
3. Field-flow fractionation for particle size characterization of nanoparticles, 19 September, 2013, ภาควิชาเคมี คณะวิทยาศาสตร์ มหาวิทยาลัยอุบลราชธานี
4. Applications of atomic spectroscopy and field-flow fractionation in the problem solving analytical chemistry (PSAC) research group, 14 November, 2013, TAB Research Forum ครั้งที่ 16 สถานวิจัยการวิเคราะห์สารปริมาณน้อยและไบโอเซนเซอร์ ภาควิชาเคมี คณะวิทยาศาสตร์ มหาวิทยาลัยสงขลานครินทร์
5. Applications of atomic spectroscopy and field-flow fractionation in the problem solving analytical chemistry research group, 17 February, 2014, ศูนย์เครื่องมือวิทยาศาสตร์และเทคโนโลยี คณะวิทยาศาสตร์ มหาวิทยาลัยศิลปากร
6. Size characterization of nanoparticles using field-flow fractionation, 20 March, 2014, การประชุมวิชาการระดับชาติ "วิทยาศาสตร์วิจัย" ครั้งที่ 6, คณะวิทยาศาสตร์ มหาวิทยาลัยบูรพา

JAAS

PAPER

Cite this: *J. Anal. At. Spectrom.*, 2015, **30**, 245

Investigation of silver nanoparticles and plasma protein association using flow field-flow fractionation coupled with inductively coupled plasma mass spectrometry (FlFFF-ICP-MS)†

Panida Wimuktiwan, Juwadee Shiowatana and Atitaya Siripinyanond*

Received 9th July 2014
Accepted 16th October 2014

DOI: 10.1039/c4ja00225c

www.rsc.org/jaas

Flow field-flow fractionation (FlFFF) with on-line inductively coupled plasma mass spectrometer (ICP-MS) was employed to investigate the association between protein and silver nanoparticles (AgNPs). In this work, bovine serum albumin (BSA), globulin, and fibrinogen were the model proteins studied. AgNPs were prepared by the reduction of silver nitrate using tannic acid as reducing and stabilizing agent. Various sizes (2.6, 10, and 26 nm) were obtained depending on the pH condition during particle preparation. The apparent association constants between BSA and AgNPs of various sizes were determined. Then, various concentrations of 2.6 nm AgNPs were incubated with plasma proteins, *i.e.*, albumin (2.6×10^{-1} M); globulin (3.1×10^{-2} M); and fibrinogen (2.9×10^{-3} M) at 37 °C for investigation of protein–AgNPs association. Factors influencing protein–AgNPs association were investigated, including the effect of incubation time and effect of AgNPs concentration. Association between protein and AgNPs increased as the incubation time and concentration of AgNPs increased. Further, the binding stoichiometry between BSA and AgNPs was determined to be approximately $1 : 5 \times 10^{-7}$.

Introduction

Many consumer products nowadays are claimed to contain engineered nanoparticles. Owing to its strong antimicrobial activity, silver nanoparticles (AgNPs) have been used in several applications, such as food packing materials, textiles, cosmetics, household items, and wound dressing. However, the wide usage of AgNPs increases the possibility for these nanomaterials to enter into the environment and human body. Human exposure to AgNPs can be from various routes, including ingestion, inhalation, dermal contact, and through therapeutic applications.[1,2]

Researchers have reported different transdermal penetration rates of AgNPs through intact and damaged skin, which are controlled by intrinsic parameters of the skin.[3] Upon entering the body, AgNPs rapidly come in contact with biological fluids such as saliva, mucus, lung lining fluid, and plasma protein.[4,5] Therefore, the assessment of the interactions between AgNPs and plasma proteins is a very important issue. The majority of the plasma proteins are comprised by albumin (55%), followed by globulin (38%) and fibrinogen (7%). Various analytical techniques have been exploited to examine plasma protein–nanoparticles association in order to gain an insight into the binding between plasma proteins and AgNPs. Those techniques include ultraviolet-visible spectroscopy (UV-vis),[6] fluorescence spectroscopy,[7] dynamic light scattering (DLS),[8] atomic force microscopy (AFM),[9] and size exclusion chromatography (SEC).[10] In this work, we propose the use of flow field-flow fractionation (FlFFF) on-line with inductively coupled plasma mass spectrometry (ICP-MS) as an alternative technique for investigation of AgNPs–plasma protein association. This hyphenated technique has been successfully applied to examine freshwater oligochaeta exposure to AgNPs,[11] study the effects of particle size and the coating on the bioaccumulation and depuration of AgNPs within the gut cavities of aquatic invertebrates,[12] investigate the effect of UV irradiation on the stability of AgNPs,[13] analyze AgNPs in chicken meat,[14] and examine the association of AgNPs with HepG2 cells.[15]

The aim of this work was to apply a conventional symmetrical flow field-flow fractionation (FlFFF) with on-line, inductively coupled plasma mass spectrometry (ICP-MS) to investigate the association between plasma protein and silver nanoparticles (AgNPs). Plasma proteins studied herein include bovine serum albumin (BSA), globulin, and fibrinogen. The key parameters affecting the association between plasma proteins and AgNPs were examined, including incubation time and concentration of AgNPs. The novel finding from this technique also includes the information on stoichiometric binding between AgNPs and BSA.

Department of Chemistry and Center for Innovation in Chemistry, Faculty of Science, Mahidol University, Rama VI Road, Bangkok 10400, Thailand. E-mail: atitaya.sir@mahidol.ac.th; Fax: +66-2-354-7151; Tel: +66-2-201-5195

† Electronic supplementary information (ESI) available. See DOI: 10.1039/c4ja00225c

Experimental

Instrumentation

A symmetrical FlFFF system (Model PN-1201-FO, Postnova Analytics, Landsberg, Germany) equipped with a 1000 Da molecular weight cut-off regenerated cellulose acetate membrane (Postnova) was used. The geometry of the FlFFF channel is 27.7 cm long, 2.0 cm wide, and 0.0254 cm thick. Sample volume of 20 μL was introduced into FlFFF *via* the Rheodyne® injector valve. Two high pressure liquid chromatography (HPLC) pumps (Model PN 2101, Postnova Analytics, Germany) were used to regulate the channel flow and the cross flow. In our experiment, channel flow was set at 1 mL min^{-1}, and a cross flow of 2 mL min^{-1} was used. After fractionation, the effluent was directed through a UV detector (Model Water 2487 Dual λ Absorbance Detector, Waters, Milford, MA, USA), which was set at 280 nm for detection of the plasma proteins. The UV detector outlet was coupled to an ICP-MS instrument (Sciex/Elan 6000, PerkinElmer Instruments, Shelton, CT, USA) using a cross-flow nebulizer with 50 cm poly (tetrafluoroethylene) tubing (PTFE, 0.58 mm id). The eluted fraction from FlFFF was introduced into the ICP-MS sample introduction system for further determination of elements. Both silver isotopes (^{107}Ag and ^{109}Ag) were monitored, and an integration dwell time of 25 ms was set for each isotope. The total number of readings per replicate was chosen such that data were collected for the entire fractograms. To assure no drift of instrument, 20 μg L^{-1} AgNPs was used to check the stability of the signal after every fifth run. The FlFFF-ICP-MS operating conditions are given in Table 1.

A UV/visible spectrophotometer (Model V-530, Jasco, Easton, Maryland, USA) was used for acquisition of the UV/visible absorption spectra of the AgNPs, plasma protein, and associated protein–AgNPs.

Chemicals

Bovine serum albumin (BSA) and tannic acid were purchased from Fluka (Buchs, Switzerland). γ-Globulin and fibrinogen were purchased from Sigma-Aldrich (Steinheim, Germany). Silver nitrate, sodium azide and nitric acid (65%) were from Merck (Darmstadt, Germany). Tris (hydroxymethyl aminomethane) and FL-70® detergent (AR 98% assay) were from Fisher Scientific (Leicestershire, UK). Deionized water (18.2 MΩ cm^{-1}) obtained from a water purification system (Barnstead International, Dubuque, IA, USA) was used throughout the experiment. All glassware was washed and soaked overnight in 30% HNO_3, and then rinsed again with deionized water before use.

Two types of carrier liquid were used in the experiment. A 0.02% (w/v) FL-70 with 0.02% (w/v) sodium azide was used for size characterization of AgNPs. Another carrier liquid was 30 mM Tris (hydroxymethyl aminomethane), buffered at pH 9, which was used in the investigation of AgNPs–plasma protein association.

Silver nanoparticles were prepared by using the method described by Sivaraman *et al.*[16] While stirring, 25 mL of 0.3 mM tannic acid, pH-adjusted with K_2CO_3, and 5 mL of 3 mM silver nitrate were mixed in a conical flask. Three pH conditions were used, including pH 8, 9, and 10, to prepare AgNPs of various sizes. A brownish yellow solution appeared immediately, indicating the formation of tannic-stabilized AgNPs. Albumin (5.2×10^{-1} M), γ-globulin (6.2×10^{-2} M), and fibrinogen (5.8×10^{-3} M) were prepared in Tris buffer.

Calculation of AgNPs concentration

The concentration of the synthesized AgNPs was calculated by the method described by Mariam *et al.*[7] By assuming that AgNPs are spherical in shape, the number of silver atoms was

Table 1 FlFFF-ICP-MS operating conditions

FlFFF: Model PN-1021-FO	
Channel flow rate/mL min^{-1}	1.0
Cross flow rate/mL min^{-1}	2.0
Equilibration time/min	1.1
Carrier liquid	30 mM Tris–HNO_3 (buffered at pH 9)
Membrane	1 kDa MWCO, poly(regenerated cellulose acetate)
ICP-MS: Sciex/Elan 6000 PerkinElmer	
RF generator frequency/MHz	40
RF power/W	1100–1300
Nebulizer gas flow rate/L min^{-1}	0.90–0.95
Coolant gas flow rate/L min^{-1}	15.0
Auxiliary gas flow rate/L min^{-1}	0.90
Mode	Peak hopping
Dwell time/measurement/isotope	25
Torch	Fassel type
Torch injector	Ceramic alumina
Spray chamber	Ryton®Scott-type
Nebulizer	Gem-tip® cross flow
Isotopes monitored	^{107}Ag, ^{109}Ag

calculated by considering that the volume ratio of silver atom to AgNPs is 74.1% in the cubic structure. The radius of silver atom is 0.144 nm, and therefore its volume is 0.0125 nm^3. For AgNPs with the diameter of d nm, the volume is $(\pi/6)d^3$ nm^3. Thus, the number of silver atoms (N) in each AgNP is equal to $\frac{74.1}{100} x \frac{\pi}{6} d^3 x \frac{1}{0.0125}$, which is calculated to be 31 d^3.[7] The concentration of the AgNPs was then calculated by taking the ratio of the total number of silver atoms added to the reaction solution (N_{Total}) and the product of the number of silver atoms present in each nanoparticle (N), the volume of the reaction solution in liters (V), and Avogadro's constant (N_A). By assuming that all silver atoms were converted to AgNPs completely, therefore, the concentrations of various AgNPs sizes of 2.6, 10, and 23 nm were calculated to be 9.2×10^{-7}, 1.6×10^{-8}, and 1.3×10^{-9} M, respectively. Calculations are given in the ESI.†

Observation of incubation time and concentration of AgNPs with plasma proteins

Two parameters influencing protein–nanoparticle association were investigated. These included the effects of incubation time and AgNPs concentration on protein binding. To examine the effect of incubation time, 4.6×10^{-7} M of 2.6 nm tannic-stabilized AgNPs was incubated with either 2.6×10^{-1} M BSA, 3.1×10^{-2} M globulin, or 2.9×10^{-3} M fibrinogen at 37 °C for 5 min, 2, and 24 h. To examine the effect of AgNPs concentration on their binding with proteins, various concentrations of 2.6 nm tannic-stabilized AgNPs: 9.2×10^{-8}, 2.7×10^{-7}, and 4.6×10^{-7} M, were incubated with either 2.6×10^{-1} M bovine serum albumin, 3.1×10^{-2} M globulin, or 2.9×10^{-3} M fibrinogen at 37 °C for 24 h. After incubation, the mixture was introduced into FlFFF for characterization. After fractionation, the effluent was directed through a UV detector and sequentially to ICP-MS.

Observation of stoichiometric binding between AgNPs and BSA

The stoichiometric binding between AgNPs with BSA was investigated by incubating different concentrations of bovine serum albumin with 9.2×10^{-8} M of 2.6 nm tannic-stabilized AgNPs at 37 °C for 5 min. To confirm the stoichiometric binding between AgNPs and BSA, various concentrations of tannic-stabilized AgNPs were incubated with 1.5×10^{-2} M BSA. After incubation, the mixture was introduced into FlFFF-ICP-MS. The mole ratio between AgNPs and BSA was examined by keeping AgNPs and BSA constant, as shown in Tables 2 and 3, respectively.

Table 2 Mole ratio method for determination of stoichiometric binding between BSA and AgNPs. The concentration of AgNPs was kept constant

Concentration of AgNPs (M)	Concentration of BSA (M)
9.2×10^{-8}	1.49×10^{-2}
	7.46×10^{-2}
	1.49×10^{-1}
	1.79×10^{-1}
	2.08×10^{-1}
	2.38×10^{-1}
	2.98×10^{-1}

Table 3 Mole ratio method for determination of stoichiometric binding between BSA and AgNPs. The concentration of BSA was kept constant

Concentration of BSA (M)	Concentration of AgNPs (M)
1.49×10^{-2}	1.84×10^{-9}
	3.68×10^{-9}
	4.60×10^{-9}
	5.52×10^{-9}
	5.98×10^{-9}
	6.44×10^{-9}
	7.36×10^{-9}
	8.28×10^{-9}
	9.20×10^{-9}
	1.10×10^{-8}

Results and discussion

Characterization of silver nanoparticles

Characterization of the synthesized AgNPs was performed using UV-visible absorption spectrophotometry and FlFFF. With UV-visible absorption spectrophotometry, the blank solution containing tannic acid at the same pH as the tannic-stabilized AgNPs was filled in a reference cuvette for background subtraction. The absorption spectra of AgNPs displayed surface plasmon resonance bands at 400, 410, and 420 nm for tannic-stabilized AgNPs at pH 8, 9, and 10, respectively, as displayed in Fig. 1a. These peaks indicated the formation of AgNPs. With FlFFF, the particle size distributions showed the peaks at 23.0 ± 0.2, 10.0 ± 0.3, and 2.6 ± 0.1 nm for tannic-stabilized AgNPs at pH 9, 10, and 11, respectively, as illustrated in Fig. 1b. The large void peaks observed in the fractograms shown in Fig. 1b were due to the incomplete removal of the negatively charged tannic acid through the negatively charged cellulose acetate membrane during a very short equilibration step (1.1 min, Table 1). The trends of particles sizes obtained from UV-visible absorption spectrophotometry and FlFFF were in good agreement. As can be seen, the smaller particle size of AgNPs exhibited plasmon resonance peaks at a shorter wavelength as compared to the bigger particle. These AgNPs were used in further experiments to observe the association between these particles and proteins.

As reported by other investigators,[7,17] the complex formation of BSA and AgNPs could be characterized by UV-visible absorption spectrophotometry. The absorption spectrum of BSA displayed a peak maximum at 278 nm (Fig. 2). In the presence of AgNPs as illustrated in Fig. 2a–c for AgNPs of 2.6, 10, and 23 nm size, respectively, the absorbance of BSA at 278 nm increased with increasing AgNPs concentration, suggesting the formation of the ground state complex between BSA and AgNPs.[7] The apparent association constant (K_{app}) for the complex formation

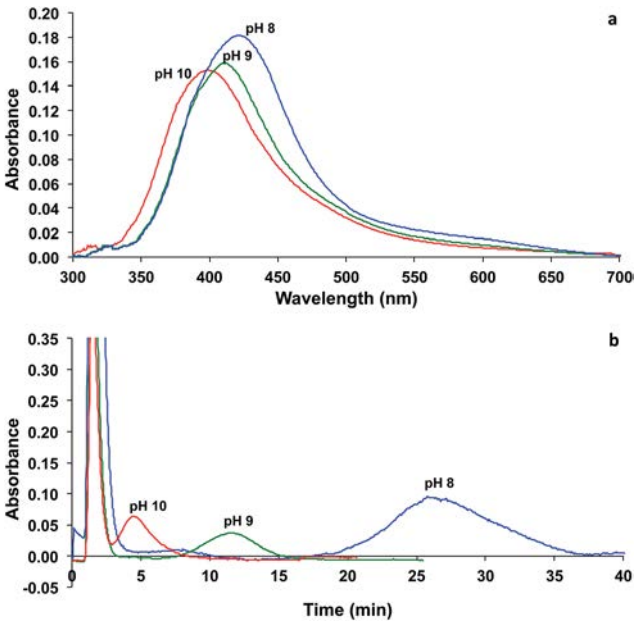

Fig. 1 (a) UV-visible absorption spectra and (b) fractograms of tannic-stabilized AgNPs synthesized at pH 8 (blue), 9 (green), 10 (red).

between BSA and AgNPs was then calculated using the method reported by Benesi and Hildebrand,[17] as illustrated in Fig. 2d. The slope of the graph represents the reciprocal of $K_{app}(A_c - A_0)$, and the intercept represents the reciprocal of $(A_c - A_0)$, where A_c is the absorbance of the AgNPs–BSA complex, and A_0 is the absorbance of BSA. Therefore, the values of K_{app} for AgNPs sized 2.6, 10, and 23 nm were calculated to be 5.2×10^7, 8.8×10^7, and 9.8×10^8 L mol^{-1}, respectively. This trend suggests that the bigger the particle size, the higher the value of the apparent association constant. The increase in K_{app} value was found to linearly depend on the increase of the particle volume ($K_{app} \propto d^3$).

FlFFF-ICP-MS for observation of protein–AgNPs association

The effects of incubation time and AgNPs concentration on the binding of the protein to AgNPs were examined using FlFFF-ICP-MS. The proteins investigated were BSA, globulin, and fibrinogen. The particle size of AgNPs was 2.6 nm. In order to understand if the binding was due to the binding between the proteins and AgNPs, or with the free dissolved Ag ions that were not converted into AgNPs, the remaining dissolved Ag ions were estimated. The estimation was performed by calculating the amount of Ag detected under the fractogram compared with the amount of Ag from the AgNPs suspension, which was nebulized directly into the ICP-MS without flowing through the FlFFF channel. By taking into consideration that the sample recovery of AgNPs fractionation in the FlFFF channel was approximately 80%, the remaining dissolved Ag ion in the AgNPs was estimated to be approximately 5%. Therefore, the binding behavior discussed hereafter is mainly due to the binding between the protein and AgNPs.

Effect of incubation time. The fractograms of tannic-stabilized AgNPs are illustrated in Fig. 3a (with UV detection at 400 nm) and Fig. 3b (with ICP-MS detection). Two peaks were observed in Fig. 3a, by which the first peak (1.6 min) was assigned to the excess tannic acid, whereas the second peak (4.8 min) was assigned to AgNPs, which was confirmed by one

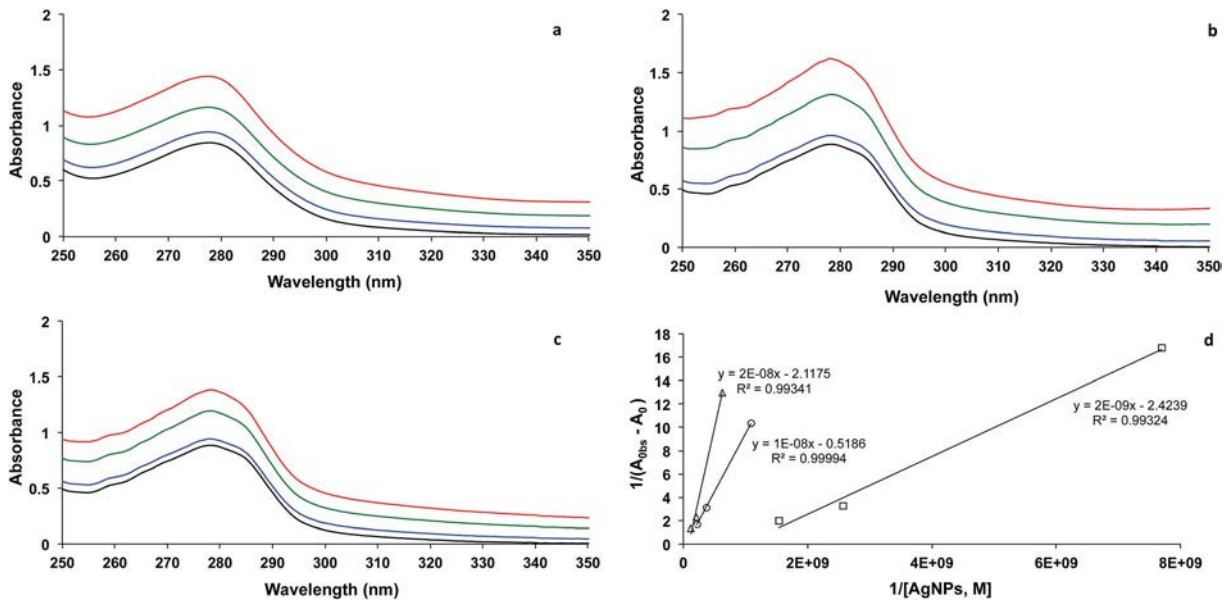

Fig. 2 UV-visible absorption spectra of 2.6×10^{-1} M BSA (black) and BSA in the presence of AgNPs of (a) 2.6 nm with the concentration of 9.2×10^{-8} M (blue), 2.7×10^{-7} M (green), and 4.6×10^{-7} M (red); (b) 10 nm with the concentration of 1.6×10^{-9} M (blue), 4.8×10^{-9} M (green), and 8.0×10^{-9} M (red); and (c) 23 nm with the concentration of 1.3×10^{-10} M (blue), 3.9×10^{-10} M (green), and 6.5×10^{-10} M (red) [Note – increasing concentration of AgNPs resulted in higher absorbance]. (d) Linear plots for calculation of K_{app} between BSA and AgNPs of 2.6 nm (○), 10 nm (△), and 23 nm (□).

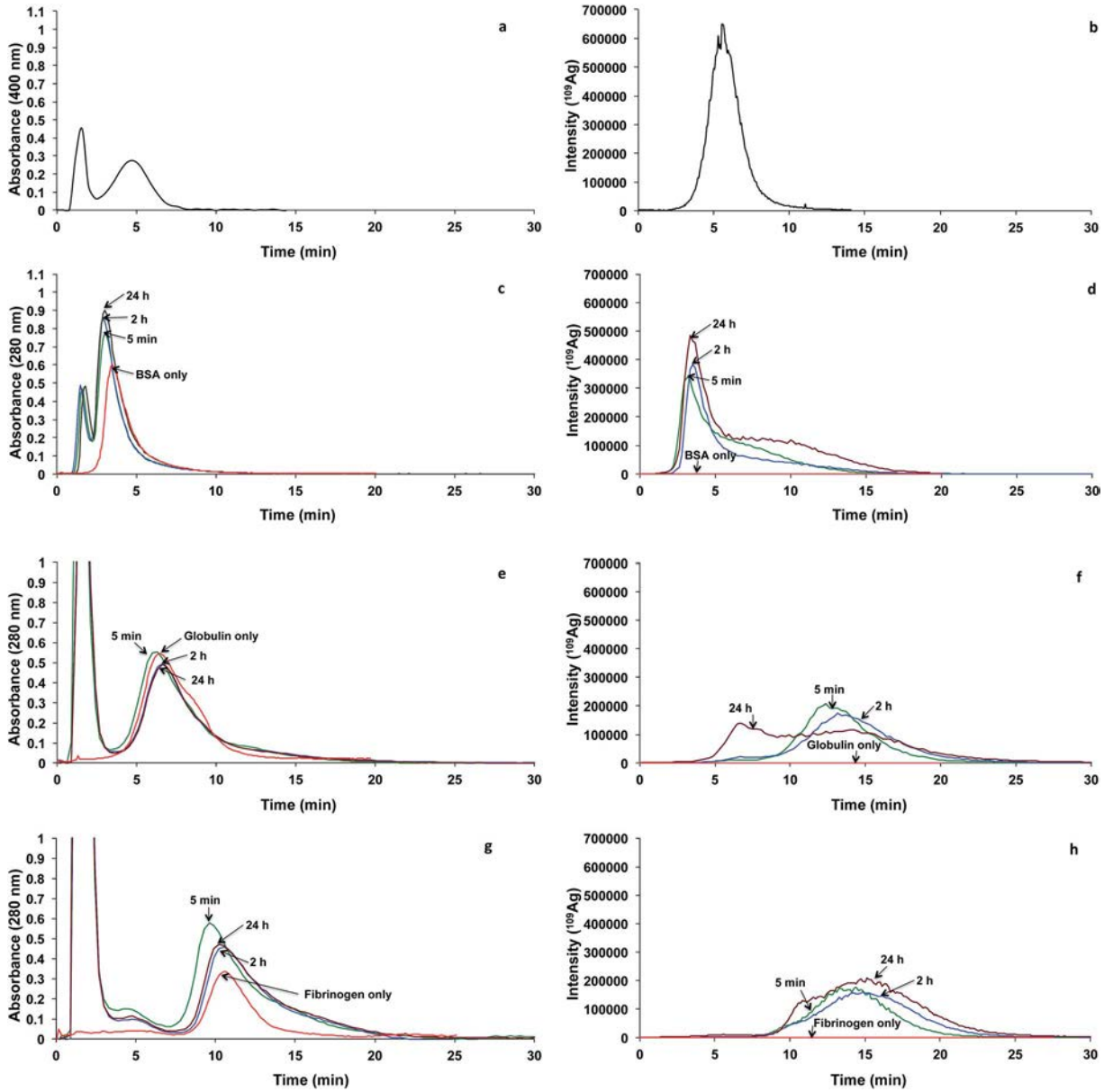

Fig. 3 Fractogram of 2.6 nm tannic-stabilized AgNPs at 4.6×10^{-7} M: (a) with UV detection, (b) with ICP-MS detection. Fractograms of (c and d, red) 2.6×10^{-1} M BSA; (e and f, red) 3.1×10^{-2} M globulin; and (g and h, red) 2.9×10^{-3} M fibrinogen, mixed with 2.6 nm tannic-stabilized 4.6×10^{-7} M AgNPs with (c, e and g) UV detection and (d, f and h) ICP-MS detection, at various incubation times of 5 min (green), 120 min (blue), and 24 h (brown).

distinct peak at 5.5 min as observed in Fig. 3b with ICP-MS detection. With UV detection, a large void peak was observed (1.6 min), owing to the incomplete removal of negatively charged tannic acid through the negatively charged cellulose acetate membrane during a 1.1 min equilibration step. No changes were observed upon incubation of this tannic acid-stabilized AgNPs at 37 °C for 24 h. The fractograms of BSA are illustrated in Fig. 3c (with UV detection at 280 nm) and Fig. 3d (with ICP-MS detection). One distinct peak was observed at 3.4 min with UV detection (Fig. 3c, red), and this was clearly the peak of BSA. No signal was observed with the ICP-MS detection (Fig. 3d, red). Different incubation times at 5 min, 120 min, and 24 h were given to allow BSA to interact with AgNPs. For the mixture, the fractograms with varying incubation times are shown in Fig. 3c (with UV detection at 280 nm) and Fig. 3d (with ICP-MS detection). With ICP-MS detection, it is clearly seen that the peaks illustrating the signal of Ag were shifted from 5.5 min (Fig. 3b) to approximately 3 min retention time (Fig. 3d), indicating the interaction between AgNPs and BSA. The association between AgNPs and BSA can be the formation of a "nanoparticle–protein corona," which has been documented in many published articles.[18,19] The formation of a "protein-corona" would affect the interactions with the membrane, resulting in a shift of the retention times.[14,20] Nonetheless, the formation of a

"nanoparticle–protein corona" was unlikely, as it should result in larger particle formation. Alternatively, the peak at 3 min might be due to the binding between BSA with the released Ag ion from the AgNPs, as reported by other investigators.[21]

As evidenced by Cedervall *et al.*,[18] the nanoparticle–protein corona formation is a complex and time-dependent process, which is governed by thermodynamic and kinetic factors. Under the condition studied herein, the association between BSA and AgNPs or the released Ag ion from the AgNPs occurred within 5 min of incubation time. With longer incubation time at 24 h, a bimodal characteristic was observed with the appearance of the peak at approximately 10 min, implying that AgNPs might grow bigger. The shift to bigger size may be caused by one of three reasons. The first plausible reason is nanoparticle–protein corona formation, yielding a larger particle size. The second plausible reason is the displacement of the tannic acid stabilizing agent by BSA, which is more steric, leading to larger particle size. The displacement of stabilizing agent by BSA might occur through the ligand-exchange or place-exchange reaction as reported by other investigators of AuNPs.[22] The third plausible reason is the interaction between tannic acid and BSA, as the association between tannic acid and proteins has been widely known by food scientists to cause astringency perception.[23]

To demonstrate the effect of incubation time on AgNPs binding with globulin, the fractograms shown in Fig. 3e and f are considered. The fractograms of globulin are illustrated in Fig. 3e (with UV detection at 280 nm) and Fig. 3f (with ICP-MS detection). With UV detection (Fig. 3e, red), the globulin peak appeared at the retention time of 6.2 min with a shoulder at 8.7 min. Clearly, no signal was observed with the ICP-MS detection (Fig. 3f, red). Different incubation times at 5 min, 120 min, and 24 h were given to allow globulin to interact with AgNPs. For the mixture, fractograms with varying incubation times are shown in Fig. 3e (with UV detection at 280 nm) and Fig. 3f (with ICP-MS detection). At incubation times of 5 and 120 min, monomodal distribution was observed at the retention time of 13.2 min. It is interesting to note that the peak at 13.2 min shifted significantly from the peak of individual AgNPs at 5.5 min (Fig. 3b), suggesting the rapid occurrence of binding between AgNPs and globulin. This globulin–AgNPs corona formation resulted in a larger particle size. Alternatively, the peak at 13.2 min might be assigned to the binding between the released Ag ion with the dimeric form of globulin, as the monomeric form of globulin displayed a peak at approximately 6.2 min (Fig. 3e). One might wonder why this dimeric peak was not distinct with the absorbance detection at 280 nm, as shown in Fig. 3e. We believe that the dimeric form was present in a relatively lower concentration than the monomeric form of globulin. Nonetheless, the released Ag ion from AgNPs showed preferential association with the globulin dimer, leading to the more distinct peak of the dimeric form when ICP-MS was used for silver detection. The dimerization of globulin on the AgNPs' surface might be caused by structural perturbation of globulin by the high surface-to-volume ratios of nanoparticles, which resulted in a high concentration of globulin adsorbed at the particle surface of low dimensionality, enhancing the probability of partial unfolding of globulin, as described by Linse *et al.*[24] Nonetheless, bimodal distribution was observed when the incubation time reached 24 h, with peaks at 6.6 and 13.2 min. This suggested that in our experiment, dimerization occurred rapidly within 5 min and was found reversible, as the monomeric peak at 6.6 min retention time was observed at the incubation time of 24 h. Alternatively, the peak at 6.6 min might be due to binding of the released Ag ion from AgNPs with the monomeric fraction.

The effect of incubation time on the binding of AgNPs to fibrinogen was examined, as illustrated in Fig. 3g and h. The fractograms of fibrinogen are illustrated in Fig. 3g (with UV detection at 280 nm) and Fig. 3h (with ICP-MS detection). With UV detection (Fig. 3g, red), the fibrinogen peak appeared at the retention time of 10.3 min. As expected, no signal was observed with the ICP-MS detection (Fig. 3h, red). Fibrinogen was allowed to incubate with AgNPs for various incubation times at 5 min, 120 min, and 24 h. Comparing Fig. 3g and h, the peak positions were not similar, suggesting that AgNPs preferentially associated with the larger molecular weight fibrinogen. Considering Fig. 3h, the binding occurred within 5 min of incubation time, as can be observed from the peak at 14.5 min, which slightly shifted toward a larger size than the pure fibrinogen.

Effect of AgNPs concentration. To examine the effect of AgNPs concentration on the association between BSA and AgNPs, various concentrations of AgNPs were incubated with BSA at a fixed time of 24 h. With increased concentration of AgNPs, the signal intensity increased, suggesting that more AgNPs could be associated with BSA. The shoulder peak at around 10 min was observed when the concentration of AgNPs increased up to 4.9×10^{-7} M, suggesting that the enlargement of the particles depends on the concentration of AgNPs. The nanoparticle–protein corona formation, the place-exchange reaction between BSA and tannic acid, or the association between BSA and tannic acid did not take place when the concentration of AgNPs was too low.

The binding of globulin to AgNPs with various AgNPs concentrations was also examined at a fixed incubation time of 24 h. When concentration of AgNPs was increased, the signal intensity of the fractogram increased. Broad distribution was observed at low globulin concentration. The distribution became bimodal, showing distinct peaks at 6.6 and 13.2 min retention time when the concentration of AgNPs was increased to 4.6×10^{-7} M. This suggests that the dimerization of globulin induced by AgNPs is concentration-dependent.

The binding of fibrinogen to AgNPs with various AgNPs concentrations is shown in Fig. 4e and f. With AgNPs concentration of 9.2×10^{-8} M, the Ag signal was quite negligible, suggesting that this concentration might be too low to cause binding with 2.9×10^{-3} M fibrinogen (Fig. 4f). However, when the concentration of AgNPs increased to 2.7×10^{-7} M, a peak was observed at 16.6 min. Formation of nanoparticle–protein corona between AgNPs and fibrinogen is possible as reported by Cedervall *et al.*[18] With increased concentration of AgNPs to 4.6×10^{-7} M, bimodal characteristic was observed at 10.5 and 14.2 min. The peak at 10.5 min is quite close to the peak of pure fibrinogen, suggesting the possible binding of fibrinogen with the released Ag ion from the AgNPs.

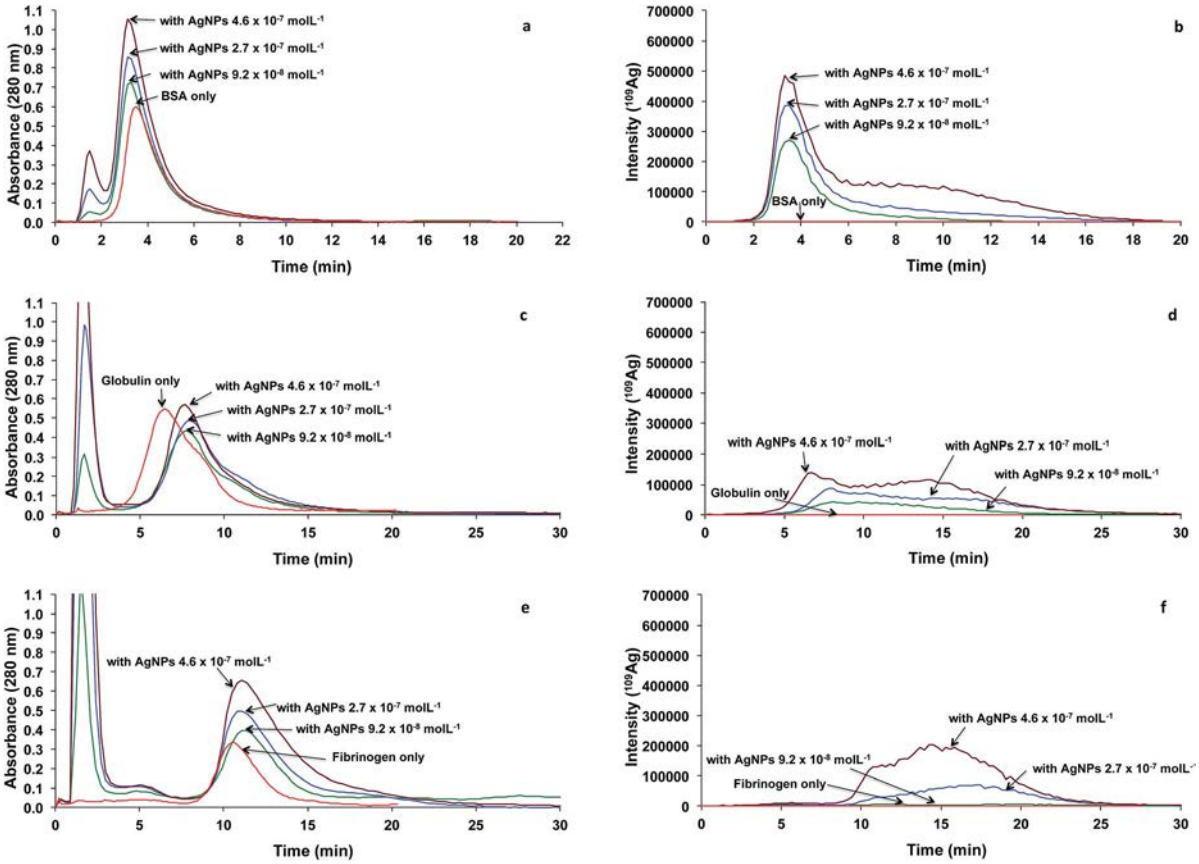

Fig. 4 Fractograms of (a and b, red) 2.6×10^{-1} M BSA; (c and d, red) 3.1×10^{-2} M globulin; (e and f, red) 2.9×10^{-3} M fibrinogen, incubated 24 h with 2.6 nm tannic-stabilized AgNPs of various concentrations: 9.2×10^{-8} (green), 2.7×10^{-7} (blue), and 4.6×10^{-7} M (brown); (a, c and e) with UV detection and (b, d and f) with ICP-MS detection.

Binding stoichiometry between AgNPs and BSA

This is the first time that FlFFF-ICP-MS was applied to examine the stoichiometry of the binding of BSA with AgNPs. Various concentrations of BSA were incubated with 9.2×10^{-8} M AgNPs. In order to differentiate the signal of Ag between that bound to BSA and the Ag in the AgNPs, the fractogram of the mixture between BSA and AgNPs (Fig. 5a) was deconvoluted using PeakFit® (an automated peak separation analysis software). The deconvoluted peaks of the fractogram are illustrated in Fig. 5b, which showed two distinct peaks at 3.6 and 5.9 min. The first peak is related to BSA binding, and the second peak is contributed by AgNPs. The area under the first deconvoluted peak (peak I) of the Ag fractogram was analyzed. Using the mole-ratio method, the peak area under the first deconvoluted peak (peak I) of the Ag fractograms obtained from varying concentrations of BSA was plotted as a function of BSA concentration as illustrated in Fig. 5c. At low BSA concentration, the peak area of the first deconvoluted peak (peak I) of the Ag fractogram was low, and the peak area increased rapidly with increasing BSA concentration from 7.46×10^{-2} to 1.49×10^{-1} M. After this point, the peak area under the first deconvoluted peak (peak I) of the Ag fractogram became relatively constant with increasing BSA, suggesting that the binding became constant. The stoichiometric binding between BSA and AgNPs was determined at the inflection point—the point where the two straight lines met—which was at the BSA concentration of 1.49×10^{-1} M, implying that the binding ratio between BSA and AgNPs was $1 : 6.2 \times 10^{-7}$. This is only a rough estimation, as the increment of the concentration from 7.46×10^{-2} to 1.49×10^{-1} M was rather unrefined.

To confirm the stoichiometric binding between AgNPs and BSA, a similar experiment was performed by varying AgNPs concentrations with fixed BSA concentration at 1.49×10^{-2} M. For very low concentrations of AgNPs, no Ag signal was observed at the BSA peak. The Ag signal increased significantly until the concentration of AgNPs was 7.4×10^{-9} M, and then became relatively constant thereafter (Fig. 5d). This suggests that the stoichiometric binding of BSA and AgNPs is $1 : 4.9 \times 10^{-7}$. Using the mole ratio method by keeping either AgNPs or BSA constant, the ratio of BSA and AgNPs were found to be approximately $1 : 5 \times 10^{-7}$, suggesting that approximately 2×10^{6} molecules of BSA adsorbed on a single AgNP with the size of 2.6 nm.

Conclusions

With the use of UV-visible spectrophotometry, complex formation of BSA and AgNPs could be observed, and the apparent

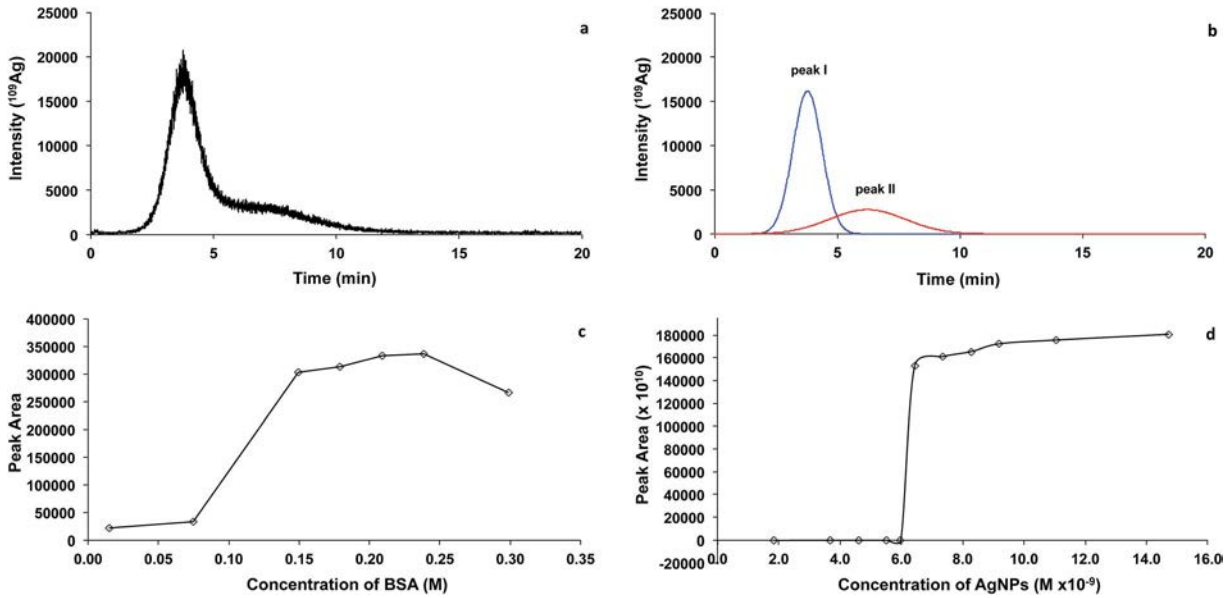

Fig. 5 (a) Fractogram of the mixture between 1.49×10^{-2} M BSA and 9.2×10^{-8} M AgNPs, with ICP-MS detection. (b) The deconvoluted peaks of the fractogram, showing two peaks (Peak I, blue, and Peak II, red). Plots of peak area under the deconvoluted peak I of the Ag fractograms *versus* concentrations of (c) BSA when the concentration of AgNPs was 9.2×10^{-8} M, and (d) AgNPs when the concentration of BSA was 1.49×10^{-2} M.

association constant (K_{app}) could be determined as reported by other investigators.[7,17] The novel finding from this study, however, is that the K_{app} value was found to linearly depend on the particle volume ($K_{app} \propto d^3$). Furthermore, FlFFF-ICP-MS was demonstrated as an alternative method to monitor the protein–AgNPs association. Plasma proteins (BSA, globulin, and fibrinogen) were investigated for their formation of protein corona with AgNPs. The interaction between BSA and AgNPs was affected by both incubation time and concentration of AgNPs. The binding of plasma protein and AgNPs occurred rapidly within 5 min of incubation time. Additionally, the investigation of the stoichiometric binding between BSA and AgNPs was possible by FlFFF-ICP-MS, showing potential applications of the technique in studying the complexation between other metals and macromolecules.

Acknowledgements

We sincerely thank the Office of the Higher Education Commission, Ministry of Education, Thailand through the Center for Innovation in Chemistry: Postgraduate Education and Research Program in Chemistry (PERCH-CIC) for the scholarship given to PW and funding for equipment. Financial supports from the Thailand Research Fund (TRF) and Mahidol University under the National Research Universities Initiative are gratefully acknowledged. Thanks are also due for the useful comments from anonymous reviewers.

References

1 C.-F. Chau, S.-H. Wu and G.-C. Yen, *Trends Food Sci. Technol.*, 2007, **18**, 269–280.
2 Y. Li, Y. Zhang and B. Yan, *Int. J. Mol. Sci.*, 2014, **15**, 3671–3697.
3 Y. Teow, P. V. Asharani, M. P. Hande and S. Valiyaveettil, *Chem. Commun.*, 2011, **47**, 7025–7038.
4 S. Elodie, D. Julien, R.-L. Fernando and D. Jean-Marie, *J. Phys.: Conf. Ser.*, 2011, **304**, 012039.
5 C. Beer, R. Foldbjerg, Y. Hayashi, D. S. Sutherland and H. Autrup, *Toxicol. Lett.*, 2012, **208**, 286–292.
6 L. Li, Q. Mu, B. Zhang and B. Yan, *Analyst*, 2010, **135**, 1519–1530.
7 J. Mariam, P. M. Dongre and D. C. Kothari, *J. Fluoresc.*, 2011, **21**, 2193–2199.
8 M. A. Dobrovolskaia, A. K. Patri, J. Zheng, J. D. Clogston, N. Ayub, P. Aggarwal, B. W. Neun, J. B. Hall and S. E. McNeil, *Nanomedicine*, 2009, **5**, 106–117.
9 Z. J. Deng, G. Mortimer, T. Schiller, A. Musumeci, D. Martin and R. F. Minchin, *Nanotechnology*, 2009, **20**, 455101.
10 I. Lynch and K. A. Dawson, *Nano Today*, 2008, **3**, 40–47.
11 A. R. Poda, A. J. Bednar, A. J. Kennedy, A. Harmon, M. Hull, D. M. Mitrano, J. F. Ranville and J. Steevens, *J. Chromatogr. A*, 2011, **1218**, 4219–4225.
12 J. G. Coleman, A. J. Kennedy, A. J. Bednar, J. F. Ranville, J. G. Laird, A. R. Harmon, C. A. Hayes, E. P. Gray, C. P. Higgins, G. Lotufo and J. A. Steevens, *Environ. Toxicol. Chem.*, 2013, **32**, 2069–2077.
13 A. R. Poda, A. J. Kennedy, M. F. Cuddy and A. J. Bednar, *J. Nanopart. Res.*, 2013, **15**, 1–10.
14 K. Loeschner, J. Navratilova, C. Købler, K. Mølhave, S. Wagner, F. von der Kammer and E. H. Larsen, *Anal. Bioanal. Chem.*, 2013, **405**, 8185–8195.
15 E. Bolea, J. Jimenez-Lamana, F. Laborda, I. Abad-Alvaro, C. Blade, L. Arola and J. R. Castillo, *Analyst*, 2014, **139**, 914–922.

16 S. K. Sivaraman, I. Elango, S. Kumar and V. Santhanam, *Curr. Sci.*, 2009, **97**, 1055–1059.
17 H. A. Benesi and J. H. Hildebrand, *J. Am. Chem. Soc.*, 1949, **71**, 2703–2707.
18 T. Cedervall, I. Lynch, S. Lindman, T. Berggård, E. Thulin, H. Nilsson, K. A. Dawson and S. Linse, *Proc. Natl. Acad. Sci. U. S. A.*, 2007, **104**, 2050–2055.
19 A. L. Capriotti, G. Caracciolo, C. Cavaliere, V. Colapicchioni, S. Piovesana, D. Pozzi and A. Laganà, *Chromatographia*, 2014, **77**, 755–769.
20 A. Ulrich, S. Losert, N. Bendixen, A. Al-Kattan, H. Hagendorfer, B. Nowack, C. Adlhart, J. Ebert, M. Lattuada and K. Hungerbühler, *J. Anal. At. Spectrom.*, 2012, **27**, 1120–1130.
21 A.-K. Ostermeyer, C. K. Mumuper, L. Semprini and T. Radniecki, *Environ. Sci. Technol.*, 2013, **47**, 14403–14410.
22 R. Sardar, J. W. Park and J. S. Shumaker-Parry, *Langmuir*, 2007, **23**, 11883–11889.
23 E. Obreque-Slier, C. Mateluna, A. Peña-Neira and R. López-Solís, *J. Agric. Food Chem.*, 2010, **58**, 8375–8379.
24 S. Linse, C. Cabaleiro-Lago, W. F. Xue, I. Lynch, S. Lindman, E. Thulin, S. E. Radford and K. A. Dawson, *Proc. Natl. Acad. Sci. U. S. A.*, 2007, **104**, 8691–8696.

Food Research International 57 (2014) 203–209

Contents lists available at ScienceDirect

Food Research International

journal homepage: www.elsevier.com/locate/foodres

Flow field-flow fractionation for particle size characterization of selenium nanoparticles incubated in gastrointestinal conditions

Pornwilard M-M, Wilaiwan Somchue, Juwadee Shiowatana, Atitaya Siripinyanond *

Department of Chemistry and Center for Innovation in Chemistry, Faculty of Science, Mahidol University, Rama VI Road, Bangkok 10400, Thailand

ARTICLE INFO

Article history:
Received 12 December 2013
Accepted 19 January 2014
Available online 23 January 2014

Keywords:
Selenium nanoparticles
Field-flow fractionation
Particle size
Inductively coupled plasma mass spectrometry
Gastrointestinal condition

ABSTRACT

An on-line flow field-flow fractionation (FlFFF) with inductively coupled plasma mass spectrometry (ICP-MS) was employed for particle size characterization of selenium nanoparticles stabilized by pectin, mixed alginate/pectin, ovalbumin, and β-lactoglobulin. Under the synthesis condition used herein, the particle size increased in the following order when β-lactoglobulin, ovalbumin, mixed alginate/pectin, and pectin was used as a stabilizing agent. Upon incubation of selenium nanoparticles in gastrointestinal conditions, both in enzymatic and non-enzymatic media, particle size distributions and the surface of selenium nanoparticles changed differently. Nonetheless, more than 90% of selenium was still presented in nanometer range after gastrointestinal digestion for the nanoparticles prepared by all types of stabilizers. In addition, the results show good agreement between the particle size observed from FlFFF and TEM techniques.

1. Introduction

Selenium is considered as an essential element and it can also be toxic. The recommended dietary allowances (RDAs) and maximum level of daily nutrient intake of selenium for both man and woman are 55–400 μg/day as specified by The Food and Nutrition Board of the US National Academy of Sciences (Monsen, 2000). Selenium is essential as it is an important component in many functional selenoproteins required for normal health (Combs & Combs, 1986; Dumont, Vanhaecke, & Cornelis, 2006; Navarro-Alarcon & Cabrera-Vique, 2008; Rayman, Infante, & Sargent, 2008; Thomson, 2004). Selenium nanoparticles show benefits as antioxidant and anticancer agents with low toxicity (Chen, Wong, Zheng, Bai, & Huang, 2008; Jia, Li, & Chen, 2005; Peng, Zhang, Liu, & Taylor, 2007; Wang, 2009; Wang, Zhang, & Yu, 2007; Zhang, Gao, Zhang, & Bao, 2001; Zhang, Wang, Bao, & Zhang, 2004; Zhang, Wang, Yan, & Zhang, 2005). At nutritional dose levels in mice, selenium nanoparticles (20–60 nm) were reported to have similar bioavailability to that of selenite, but the toxicity of selenium nanoparticles was 7-fold lower than sodium selenite considering the LD50 of 113 and 15 mg Se/kg body weight for selenium nanoparticles and selenite, respectively (Zhang et al., 2001). In the case of selenium nanoparticle ingestion into the human gastrointestinal tract, the absorption, translocation, and excretion of nanoparticles in the human body are controlled by various parameters including size and surface properties (Teow, Asharani, Prakash Hande, & Valiyaveettil, 2011).

The interaction with proteins influences the surface chemistry of nanoparticles and leads to changes in their charge and agglomeration state (Chithrani, Ghazani, & Chan, 2006; Kittler et al., 2010; Zook, MacCuspie, Locascio, Halter, & Elliott, 2011). Change in pH under the gastrointestinal condition may trigger the agglomeration of nanoparticles inside the gastrointestinal tract (Wang et al., 2006), and particle size influenced the efficiency of particle uptake (Desai, Labhasetwar, Amidon, & Levy, 1996). Size characterization of silver nanoparticles in the gastrointestinal tract was reported (Mwilu et al., 2013; Walczak et al., 2013). The rate of dye and dextran nanoparticle diffusion across the mucus layers to the enterocyte surface was determined (Hoet, Brüske-Hohlfeld, & Salata, 2004; Szentkuti, 1997). Particles with a 14 nm diameter permeated within 2 min, while 415 nm particles took 30 min, whereas 1000 nm particles were unable to translocate this barrier. Until now the information about the size characterization of selenium nanoparticles on human digestive conditions are still lacking. Therefore, changes in the particle size of selenium nanoparticles in gastrointestinal condition should be examined.

Selenium nanoparticles can be prepared by various methods. The most widely used method for the synthesis of selenium nanoparticles is the chemical reduction approach. Several exogenous reducing agents can be used such as ascorbic acid, glutathione, and sodium thiosulfate (Lin & Chris Wang, 2005; Mees, Pysto, & Tarcha, 1995; Zhang, Wang, Bao, & Zhang, 2004; Zhang et al., 2001). To control the formation and the dispersion of nanoparticles, stabilizing agents are normally required. Many reagents have been used for stabilizing selenium nanoparticles such as polyvinyl alcohol (Barnaby, Frayne, Fath, & Banerjee, 2011; Shah, Kumar, & Bajaj, 2007), chitosan (Bai, Wang, Zhou, Li, & Zheng, 2008; Zhang, Wang, Bao, & Zhang, 2004; Zhang et al., 2005), surfactant (Li & Hua, 2009; Mehta et al., 2008; Min-Hsiung, 2004), and bovine serum albumin (Zhang et al., 2001). In this work, stabilizing agents, which are generally recognized as safe (GRAS), were used for the preparation of selenium nanoparticles. These included pectin, mixed

* Corresponding author. Tel.: +662 201 5195: fax: 662 354 7151.
E-mail address: atitaya.sir@mahidol.ac.th (A. Siripinyanond).

0963-9969/$ – see front matter © 2014 Elsevier Ltd. All rights reserved.
http://dx.doi.org/10.1016/j.foodres.2014.01.040

alginate/pectin, ovalbumin, and β-lactoglobulin, as these reagents have been characterized and used as thickening, emulsifying, and stabilizing agents in food technology (Akhtara, Dickinson, Mazoyer, & Langendorff, 2002; Matto & Husain, 2006; Medina-Torres et al., 2010; Dickinson, 2010; respectively).

Several analytical techniques have been used for size characterization of nanoparticles. These include transmission electron microscopy (TEM) (Li & Hua, 2009; Lin & Chris Wang, 2005; Min-Hsiung, 2004), scanning electron microscopy (SEM) (Chen et al., 2008; Lee et al., 2008), and UV–visible spectrophotometry (UV–vis) (Lin & Chris Wang, 2005; Mees et al., 1995). With UV–vis absorption spectrophotometry, some researchers showed that the absorption peak of selenium nanoparticles was only observed when the particle size was larger than 100 nm (Lin & Chris Wang, 2005). Alternatively, flow field-flow fractionation (FlFFF) has been reported for characterization of several particles with nano scale range (Kammer, Legros, Hofmann, Larsen, & Loeschner, 2011; Poda et al., 2011). The FlFFF not only provides a relatively gentle separation process, but it also allows for collection of the fractionated samples for further analysis by other techniques.

Although size characterization of selenium nanoparticles has been documented, most publications focused on size in the as synthesized condition medium (Ingole, Thakare, Khati, Wankhade, & Burghate, 2010; Lin & Chris Wang, 2005). None has reported a size characterization of selenium nanoparticles in more complex gastrointestinal fluids. With these, the objectives of this work were two-fold. The first was to examine the feasibility of FlFFF for size characterization of selenium nanoparticles with subsequent ICP-MS to provide element specific detection of selenium, and the second was to examine the changes in particle size distribution of selenium under gastrointestinal conditions, both without and with digestive enzymes.

2. Materials and methods

2.1. Instrumentation

A symmetrical flow field-flow fractionation (FlFFF) system (Model PN-1021-FO; Postnova Analytics, Landsberg, Germany) coupled to an inductively coupled plasma quadrupole mass spectrometer (ICP-MS, Elan 6000 Perkin Elmer/Sciex, Toronto, Canada) was employed. The FlFFF system equipped with a 1 kDa molecular weight cut-off regenerated cellulose acetate membrane (RC) from Postnova Analytics was used for size characterization of selenium nanoparticles. The FlFFF channel was rectangular in shape with the dimensions being 27 cm long, 2.0 cm wide, and 0.0254 cm thick. A sample volume of 20 μL was introduced into FlFFF via the Rheodyne injector valve. A high-pressure liquid chromatography (HPLC) pump (Model PN 2101, Postnova Analytics, Germany) was used to deliver the channel flow. The cross flow rate was delivered by another HPLC pump of the same model. The optimum operating conditions of FlFFF–ICP-MS are listed in Table 1. A UV–visible detector (Model S3210, Postnova Analytics) was set at 410 nm for detection of the fractionated selenium nanoparticle samples, considering the absorption spectra of the synthesized selenium nanoparticles. The ICP-MS was used as an element detector sequentially after the UV–visible absorption detector. Owing to the similarity of the FlFFF channel and ICP-MS sample flow rates typically used for analysis, the ICP-MS cross-flow nebulizer was connected directly to the UV–visible detector outlet with a 60 cm length of poly(tetrafluoroethylene) tubing (PTFE, 0.58 mm id).

Zeta potential measurements were carried out using the Zetasizer Nano ZS (Malvern Instruments Zetasizer1000 Hs, Worcestershire, UK). A transmission electron microscope FEI model TECNAI T20 G^2 (FEI Company Corporate, Hillsboro, Oregon, USA) was used to observe the size and morphologies of selenium nanoparticles.

Table 1
FlFFF–ICP-MS operating condition.

FlFFF: PN-1021-FO	
Channel dimension/ cm × cm × cm	27.7 long × 2.0 wide × 0.02 thick
Carrier liquid	0.02% — FL-70 and 0.02 NaN_3 (pH 11.7)
Channel flow rate/mL min^{-1}	1.4
Cross flow rate/mL min^{-1}	0.8
Equilibration time/min	2.4
Membrane	1 kDa MWCO poly(regenerated cellulose acetate)
ICP-MS: Perkin Elmer ELAN 6000	
Torch	Fassel type with alumina ceramic injector
Rf generator frequency	40 MHz
Rf power	1100 W
Nebulizer gas flow rate	0.9 L/min
Coolant gas flow rate	15 L/min
Auxiliary gas flow rate	0.9 L/min
Scanning mode	Peak hopping
Isotopes monitored (m/z)	^{77}Se, ^{78}Se, ^{80}Se, ^{82}Se (^{78}Se for quantification)

2.2. Chemicals

The chemicals used in this study include sodium selenite, pectin from apples (30–100 kDa) with 70–75% degree of esterification, alginic acid sodium salt from brown algae (100–200 kDa), albumin from chicken egg white (ovalbumin) with molecular weight of 44.3 kDa, β-lactoglobulin from bovine milk (90% PAGE), pepsin (P-7000, porcine stomach mucosa), pancreatin (P-1750, porcine pancreas) and bile extract (B-6831, porcine). All aforementioned chemicals were purchased from Sigma-Aldrich, Inc., MO, USA. L-Ascorbic acid was purchased from Fisher Scientific UK Limited, Leicestershire, UK. De-ionized water (18.2 MΩ cm^{-1}) obtained from a water-purification system (Barnstead International, Dubuque, IA, USA) was used to prepare all chemical reagents. For the preparation of selenium nanoparticles, 2.5% (w/w) of stabilizers (pectin, alginate, ovalbumin, and β-lactoglobulin) and 300 m mol L^{-1} ascorbic acid as a reducing agent were dissolved in de-ionized water. FL-70, a mixture of anionic and non-ionic compounds, was purchased from Fisher Scientific UK Limited, Leicestershire, UK. A 0.02% (v/v) solution of FL-70 was prepared by diluting concentrated FL-70 with de-ionized water and was used as a carrier liquid. A commercial gold nanoparticle of 10 nm used for checking the performance of FlFFF channel was purchased from Sigma, St. Louis, MO, USA.

2.3. Preparation of selenium nanoparticles

Ascorbic acid was used as a reducing agent for synthesis of selenium nanoparticles. For the preparation of pectin, ovalbumin, and β-lactoglobulin stabilized selenium nanoparticles, 1 mL of 2.5% (w/w) stabilizing agent was mixed with 8 mL of 300 m mol L^{-1} ascorbic acid as a reducing agent under magnetic stirring at the speed of 1000 rpm. With the stirring speed reduced to 100 rpm, 1 mL of 30 m mol L^{-1} aqueous sodium selenite solution was slowly added into the mixtures to initiate the reaction (Chen et al., 2008). For mixed alginate/pectin stabilized selenium nanoparticles, 0.5 mL of 2.5% (w/w) alginate solution was mixed with 300 m mol L^{-1} ascorbic acid. Then, 1 mL of 30 m mol L^{-1} aqueous sodium selenite solution was slowly added into the mixtures to initiate the reaction, and 0.5 mL of 2.5% (w/w) pectin was added after 15 min incubation time. The reaction solution therefore contained 3 m mol L^{-1} sodium selenite, 0.25% (w/w) stabilizers, i.e., pectin; mixed alginate/pectin; ovalbumin; or β-lactoglobulin, and 240 m mol L^{-1} ascorbic acid. Upon mixing all reagents together at room temperature, the solutions

converted from colorless into red immediately with pH approximately 2.8–2.9. The obtained selenium nanoparticles were stored at 4 °C for 2 h (at least) before size characterization by FlFFF and TEM.

2.4. Gastrointestinal incubation of selenium nanoparticles

A pepsin solution was prepared by dissolving 0.16 g of pepsin in 1 mL of 0.1 mol L^{-1} HCl. A pancreatin–bile extract (PBE) mixture was prepared by dissolving 0.004 g of pancreatin and 0.025 g of bile extract in 5 mL of 0.001 mol L^{-1} $NaHCO_3$. Enzymatic digestion was performed according to the procedure of Miller (Miller, Schricker, Rasmussen, & Van Campen, 1981). 7.5 g of de-ionized water was added to 5 g of selenium nanoparticles as synthesized, adjusted to pH 2.0 with 6 mol L^{-1} HCl. To carry out pepsin–HCl digestion (gastric digestion), 375 μL of pepsin solution was added. The mixture was then incubated for 2 h at 37 °C in a shaking water bath. For intestinal digestion, a portion of the mixture after gastric digestion (5 g) was adjusted to pH 7.0 by 5 M NaOH solution. Then 625 μL of PBE mixture was added into the solution. The solution (intestinal fraction) was incubated for 2 h at 37 °C. Non-enzymatic digestion of selenium nanoparticles was also performed with the same procedure described above but without addition of pepsin and PBE mixture solution. These selenium nanoparticles after incubation in the gastrointestinal conditions were directly introduced into the FlFFF channel for particle size characterization. Duplicate experiments were performed for each type of selenium nanoparticles.

2.5. Quantification of fractionated selenium nanoparticles by ICP-MS

A fractogram from the FlFFF experiment was plotted between the intensity of selenium (y-axis) as a function of retention time (x-axis). The quantification of fractionated selenium from FlFFF was performed by an external calibration with sodium selenite standards using the peak height data from the ICP-MS peak profile. Therefore, the intensity of selenium in the fractogram was then translated into the concentration. With the fixed flow rate used in the FlFFF experiment, the retention time was then translated into the retention volume. The total concentration of selenium in the fractionated selenium nanoparticles was calculated by area integration of graph which was plotted between the concentration of Se and retention volume.

2.6. Data transformation from a fractogram to particle size distribution

The data transformation from a fractogram to particle size distribution was described previously (Dondi & Martin, 2000). In brief, raw fractograms were translated into mass size distribution profiles by using Microsoft Excel (Microsoft Excel 2007) spreadsheet software. Peak evaluation and baseline adjustment were performed by using PeakFit (SPSS, Chicago, IL, USA).

3. Results and discussion

3.1. Size characterization of selenium nanoparticles by FlFFF

In our work, selenium nanoparticles were prepared by using ascorbic acid to reduce selenite to selenium with zero valent as shown in the following chemical reaction (Lin & Chris Wang, 2005):

$$SeO_3^{2-} + 2C_6H_8O_6 + 2H^+ \rightarrow Se + 2C_6H_6O_6 + 3H_2O.$$

Various stabilizing agents were employed in the synthesis to control the formation and dispersion stability, and to prevent nanoparticles from aggregation (Donati et al., 2009). In this study, two types of stabilizing agents, which are generally recognized as safe (GRAS), were used. Those included the polysaccharide and protein types. The former included pectin and mixed alginate/pectin and the latter included ovalbumin and β-lactoglobulin. The reactive hydroxyl, carboxyl, and amino groups in polysaccharides and proteins show great potential for facilitating the formation and stabilization of selenium nanoparticles (Zhang, Zhang, Wang, & Chen, 2004). Without stabilizing agents, nanoparticles in solution are more susceptible to either oxidation or attractive interparticle Van der Waals forces which cause them to aggregate and precipitate (Cozzoli & Manna, 1996).

Particle size distributions of selenium nanoparticles prepared by ascorbic acid reducing agent with the use of various stabilizing agents are illustrated in Fig. 1. Two types of detectors were used including UV–visible (410 nm) and ICP-MS detectors, as illustrated in Fig. 1a and b, respectively. The peak profiles obtained from the two detectors were similar. Selenium nanoparticles stabilized with pectin yielded the peak maximum at 64 nm (Fig. 1, blue) and those stabilized with mixed alginate/pectin showed the peak maximum at 37 nm (Fig. 1, red). For protein based selenium nanoparticles, the peaks appeared at 30 nm (Fig. 1, green) and 23 nm for selenium nanoparticles with ovalbumin and β-lactoglobulin stabilizers (Fig. 1, purple), respectively. Nonetheless, the ICP-MS was used as a detector for further investigation as it provided element specific information. It is clear that the type of stabilizers shows significant effect on the obtained particle size, as different stabilizers resulted in different degrees of steric repulsion and charge stabilization or electrostatic interaction. Steric repulsion is normally governed by the molecular mass of the stabilizing agent. The differences in electrostatic interaction from various stabilizing agents are due to the differences in amino, hydroxyl, or carboxyl groups in different proteins and polysaccharides (Zhang, Zhang, Wang, & Chen, 2004).

FlFFF–ICP-MS not only provides particle size information, but it can also give quantitative information. To demonstrate this, the amount of selenium detected during fractionation was compared with the amount introduced into FlFFF. (The amount of selenium detected during fractionation was calculated based on the method described in Section 2.5, and the amount introduced into FlFFF was calculated

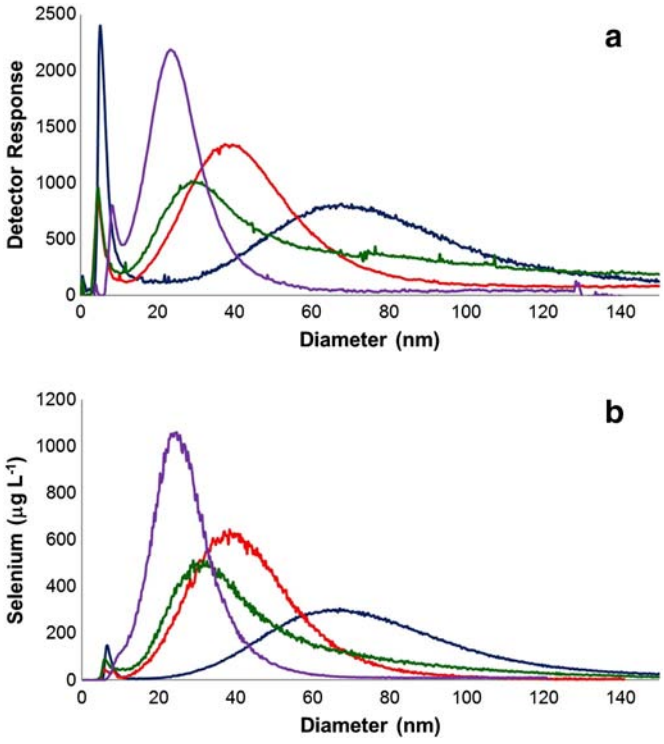

Fig. 1. Particle size distributions of selenium nanoparticles synthesized with various stabilizing agents: i.e., pectin (blue); mixed alginate/pectin (red); ovalbumin (green); and β-lactoglobulin (purple), characterized by FlFFF with a) UV–visible detector and b) ICP-MS. (For interpretation of the references to colors in this figure, the reader is referred to the web version of this article.)

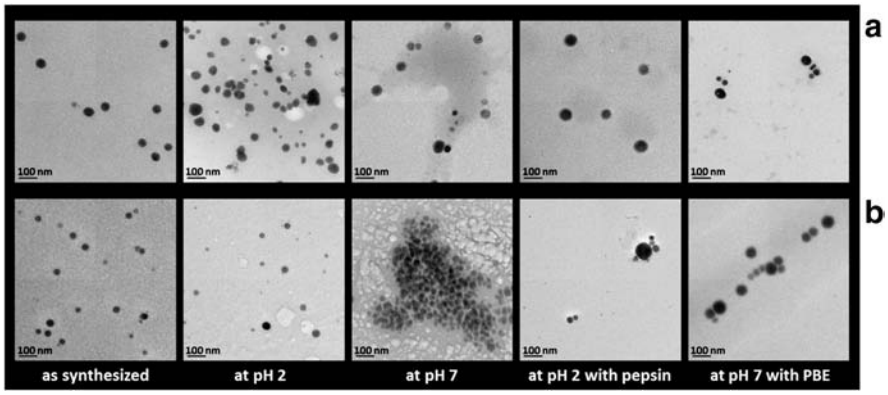

Fig. 2. TEM images of selenium nanoparticles under various conditions: a) pectin stabilized selenium nanoparticles; and b) ovalbumin stabilized selenium nanoparticles (PBE is pancreatin–bile extract).

based on the injection volume of 20 μL.) It was found that 88.4%, 102.5%, 100.5%, and 88.5% were detected during fractionation for pectin, mixed alginate/pectin, ovalbumin, and β-lactoglobulin, respectively.

In addition to the results observed by FlFFF, TEM was also used to monitor the size of selenium nanoparticles. Fig. 2a and b show the TEM images of pectin stabilized- and ovalbumin stabilized-selenium nanoparticles, respectively. The results show good agreement between the particle sizes observed from the two techniques, by comparing Fig. 1 (blue line) with Fig. 2a (as synthesized) for pectin stabilized selenium nanoparticles, and Fig. 1 (green line) with Fig. 2b (as synthesized) for ovalbumin stabilized selenium nanoparticles. With FlFFF, the peak particle sizes were 64 nm and 30 nm for pectin stabilized- and ovalbumin stabilized-selenium nanoparticles, respectively. TEM images also show that pectin gave a larger particle size than that with ovalbumin.

3.2. Selenium nanoparticles in gastrointestinal conditions: effect of pH (without enzyme addition)

To gain insight into changes in selenium nanoparticles in gastrointestinal conditions, selenium nanoparticles were incubated in the gastric (pH = 2) and intestinal pH (pH = 7), both with and without the addition of enzyme. These particles were subjected to FlFFF–ICP-MS, TEM characterization, and zeta potential measurement. The zeta potential values of selenium nanoparticles in various conditions are summarized in Table 2.

3.2.1. Selenium nanoparticles with polysaccharide-based stabilizing agents

Two types of polysaccharide-based stabilized selenium nanoparticles were examined with the particle size distributions shown in Fig. 3.

By adjusting the solution pH from 2 to 7, the zeta potential values of selenium nanoparticles with all stabilizers were more negatively charged. For polysaccharide stabilized selenium nanoparticles, increasing the pH value from 2 to 7 changed the zeta potential values from −14.2 mV to −20.4 mV and from −28.4 mV to −33.0 mV, for pectin stabilized and mixed alginate/pectin stabilized selenium nanoparticles, respectively. It can be realized that free carboxylic groups were deprotonated and changed to carboxylate anions at a pH value of 7 (pKa of pectin is between 3 and 4, and pKa of alginic acid is between 1.5 and 3.5). The more negative charge at pH 7 than at pH 2 indicates more electrostatic repulsion with increasing pH, which can inhibit the agglomeration of nanoparticles. Therefore, the particle size at peak of pectin stabilized selenium nanoparticles was smaller at pH 7 (72 nm as shown in Fig. 3a, brown) than that at pH 2 (84 nm as shown in Fig. 3a, purple). The TEM images of pectin stabilized selenium nanoparticles are illustrated in Fig. 2a, which show the same trend as the results from FlFFF.

Although selenium nanoparticles with mixed alginate/pectin stabilizer also exhibited slightly higher negative charge at pH of 7, the

Table 2
Zeta potential values of selenium nanoparticles in various conditions.

Condition	Zeta potential (mV)			
	Selenium nanoparticles with various stabilizing agents			
	Pectin	Mixed alginate/pectin	Ovalbumin	β-Lactoglobulin
As synthesized	−17.2	−27.6	33.3	24.3
At pH 2	−14.2	−28.4	37.9	25.8
At pH 7	−20.4	−33.0	−20.4	−35.0
At pH 2 with pepsin (gastric)	−11.4	−11.0	1.9	3.0
At pH 7 with PBE (intestinal)	−50.1	−47.0	−48.2	−43.1

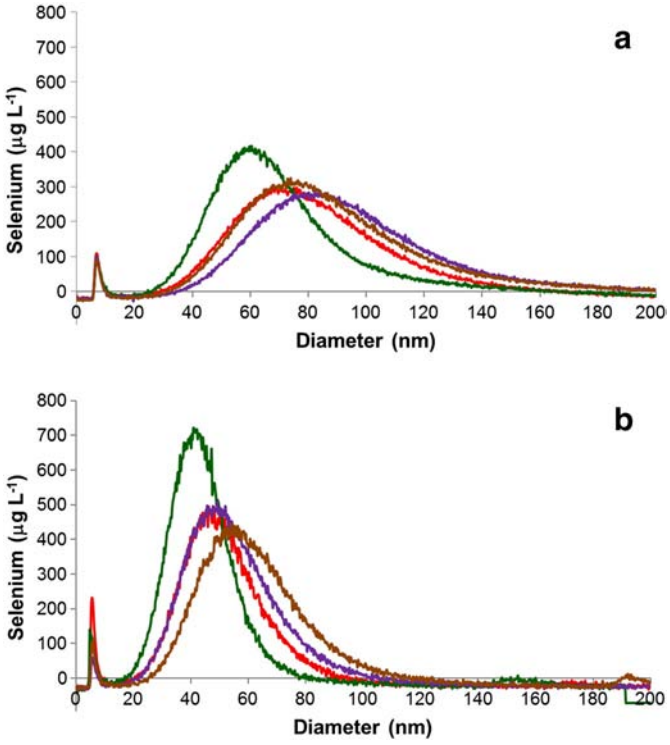

Fig. 3. Particle size distributions of a) pectin stabilized selenium nanoparticles and b) mixed alginate/pectin stabilized selenium nanoparticles, under various conditions: i.e., at pH 2 (purple); at pH 7 (brown); at pH 2 with pepsin (red); and at pH 7 with pancreatin–bile extract (green), characterized by FlFFF with ICP-MS. (For interpretation of the references to colors in this figure legend, the reader is referred to the web version of this article.)

particle size at peak was slightly larger than at pH of 2 (46 nm at pH 2 as shown in Fig. 3b, purple and 53 nm at pH 7 as shown in Fig. 3b, brown). This may be due to the nature of alginate that at a pH below 4 is likely to form a high-viscosity acid gel (Bu, Kjøniksen, Knudsen, & Nyström, 2004; Dentini, Rinaldi, Barbetta, Risica, & Skjåk-Bræk, 2006). Therefore, at pH 2, the solution was highly viscous, resulting in the decrease in the collision rate of molecule. At pH 7, however, the lowering in viscosity of the solution promoted the possibility for particle–particle collision, leading to a larger particle size.

3.2.2. Selenium nanoparticles with protein-based stabilizing agents

Ovalbumin and β-lactoglobulin were selected to be a model study of protein stabilized selenium nanoparticles. Gastrointestinal digestion of selenium nanoparticles with protein-based stabilizing agent was also performed in both non-enzymatic and enzymatic media. Two types of protein-based stabilized selenium nanoparticles were examined with the particle size distributions shown in Fig. 4. To understand the effect of pH on selenium nanoparticles, experiment without addition of enzymes is first considered.

By adjusting the solution pH from 2 to 7, the zeta potential values of selenium nanoparticles stabilized with proteins switched from the positive values to the negative values, as 37.9 to −20.4 and 25.8 to −35.0 mV for ovalbumin and β-lactoglobulin stabilized selenium nanoparticles, respectively (Table 2). This is due to the fact that the isoelectric points (pI) of both proteins are higher than 2 and lower than 7. The pI of ovalbumin is 4.75 and that of β-lactoglobulin is 5.2. Therefore, at pH 2, both proteins carry a net positive charge. At pH 7, both proteins exhibit a net negative charge.

Considering the particle size observed for ovalbumin stabilized selenium nanoparticles, increasing the pH from 2 to 7 caused the particle size at peak to shift from 52 nm (Fig. 4a, purple) to disappearance from the observable size range (1 to 160 nm) as shown in Fig. 4a (brown). Nonetheless, the signal of selenium showed up after stopping the cross flow indicating that the particle is larger than 160 nm (results not shown). This may be caused by the precipitation of ovalbumin during the pH adjustment from 2 to 7, causing agglomeration of selenium nanoparticles. The TEM image in Fig. 2b also implies that ovalbumin stabilized nanoparticles were agglomerated to larger size.

Considering the particle size observed for β-lactoglobulin stabilized selenium nanoparticles, particle size distribution exhibited a peak maximum at 46 nm with a shoulder at around 30 nm (Fig. 4b, purple). This bimodal characteristic may arise from the fact that β-lactoglobulin is normally found as dimers and other larger aggregates. However at pH below 3 and above pH 8, the dimers can be dissociated into monomers (Kuwata et al., 1999; Sakurai, Oobatake, & Goto, 2001). Therefore, at pH 2 β-lactoglobulin was presented as both monomer and other non-native larger aggregates causing the selenium nanoparticles to be stabilized by two different groups of stabilizer, leading to bimodal distribution. At pH 7, however, the shoulder peak at approximately 30 nm disappeared showing only monomodal peak at 46 nm (Fig. 4b, brown).

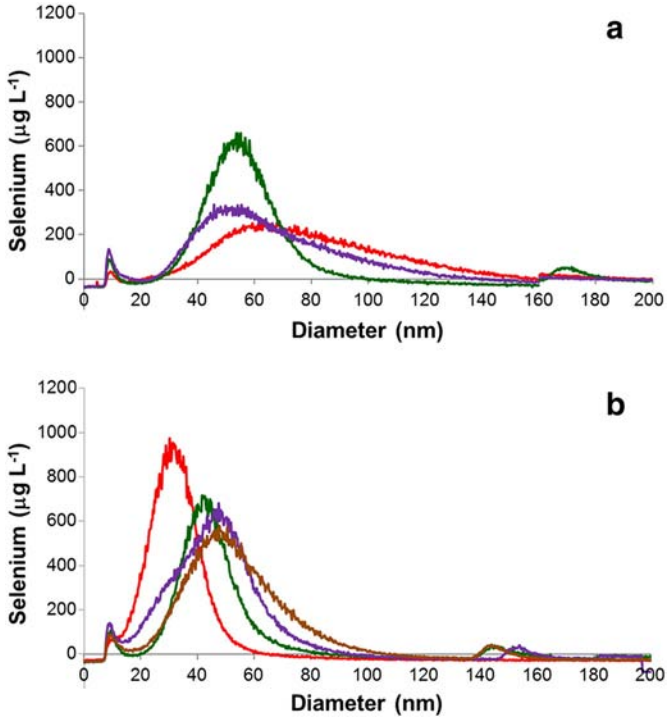

Fig. 4. Particle size distributions of a) ovalbumin stabilized selenium nanoparticles and b) β-lactoglobulin stabilized selenium nanoparticles, under various conditions: i.e., at pH 2 (purple); at pH 7 (brown); at pH 2 with pepsin (red); and at pH 7 with pancreatin–bile extract (green), characterized by FlFFF with ICP-MS. (For interpretation of the references to colors in this figure legend, the reader is referred to the web version of this article.)

3.3. Selenium nanoparticles in gastric conditions: pH 2 with and without pepsin addition

In gastric condition, not only should the pH be adjusted to 2, but pepsin should also be added to better mimic the digestive system. Pepsin is enzyme produced in the mucosal lining of the stomach that acts to degrade protein. Pepsin is negatively charged at a pH of 2 (pI of pepsin = 1) (Sepelyak, Feldkamp, Moody, White, & Hem, 1984). With pepsin addition, the surface charge of all types of selenium nanoparticles studied herein changed in such a way that the zeta potential values were less negative and less positive for polysaccharide stabilized and protein stabilized selenium nanoparticles, respectively (Table 2).

3.3.1. Selenium nanoparticles with polysaccharide-based stabilizing agents

Adding pepsin into polysaccharide stabilized selenium nanoparticles cannot digest pectin or mixed alginate/pectin to the smaller unit. Although pepsin addition caused the zeta potential values of polysaccharide stabilized selenium nanoparticles to become less negative (−14.2 to −11.4 mV and −28.4 to −11.0 mV for pectin stabilized and mixed alginate/pectin stabilized selenium nanoparticles, respectively), the particle size at peak of pectin stabilized selenium nanoparticles shifted to the smaller particle size (84 nm without pepsin as shown in the purple line to 72 nm with pepsin as shown in the red line of Fig. 3a) whereas that of the mixed alginate/pectin remained unchanged (48 nm in the purple and red lines in Fig. 3b). The decrease in particle size and the unchanged particle size, despite the less negatively surface charge, suggested that under this condition the particle stability of polysaccharide stabilized selenium nanoparticles was governed by steric stabilization rather than electrostatic repulsion. The TEM images of pectin stabilized selenium nanoparticles are illustrated in Fig. 2a, which show the same trend as the results from FlFFF.

3.3.2. Selenium nanoparticles with protein-based stabilizing agents

Addition of pepsin at stomach pH of 2 caused the zeta potential values of both protein stabilized selenium nanoparticles to become less positively charged (37.9 to 1.9 mV and 25.8 to 3.0 mV for ovalbumin and β-lactoglobulin stabilized selenium nanoparticles, respectively). It can be realized that at this pH both ovalbumin and β-lactoglobulin carry a net positive charge whereas pepsin carries a net positive charge. Therefore, the addition of negatively charged pepsin caused a charge neutralization of the positively charged proteins resulting in the overall reduction in the zeta potential values.

Ovalbumin is known to be resistant to pepsin digestion (Martos, Contreras, Molina, & López-FandiÑo, 2010). Considering ovalbumin stabilized selenium nanoparticles, the particle size was shifted to larger size (52 nm without pepsin as shown in the purple line and 64 nm with pepsin as shown in the red line in Fig. 4a). This may be due to the

decrease in electrostatic repulsion between the particles (as evidenced by the decrease in zeta potential values) causing particle agglomeration. The TEM images of ovalbumin stabilized selenium nanoparticles are illustrated in Fig. 2b, which show the same trend as the results from FlFFF.

Considering β-lactoglobulin stabilized selenium nanoparticles, the bimodal distribution at pH 2 without pepsin addition (30 and 46 nm as shown in Fig. 4b, purple) became monomodal at 30 nm with pepsin addition (Fig. 4b, red). The disappearance of the peak at 46 nm may be realized from the fact that the high-molecular weight nonnative aggregates were digested rapidly, whereas the dimers and monomer were resistant to peptic digestion (Peram, Loveday, Ye, & Singh, 2013). The resistance of native β-lactoglobulin to pepsin hydrolysis is attributed to its particular folded calyx structure where the target amino acid residues are buried in the protein core (Malaki Nik, Wright, & Corredig, 2010). Therefore, the peak at 46 nm which is believed to be the selenium nanoparticles stabilized by the high-molecular weight nonnative aggregates, was shifted to the smaller particles stabilized by only the dimeric and monomeric forms of β-lactoglobulin.

3.4. Selenium nanoparticles in intestinal conditions: pH 7 with and without pancreatin–bile extract addition

In the intestinal condition, not only should the pH be adjusted to 7, but pancreatin–bile extract should also be added to better mimic the intestinal system. Pancreatin is a mixture of several digestive enzymes produced by the exocrine cells of the pancreas. It is composed of amylase, trypsin, lipase, ribonuclease and protease. The amylase found in pancreatin works to hydrolyze carbohydrate into oligosaccharides and the disaccharide maltose. Moreover, the bile solution is hydrophilic on one side and hydrophobic on the other side. The hydrophilic side is negatively charged, and this charge can prevent the nanoparticles from aggregating. With the pancreatin–bile extract addition, the surface charge of all types of selenium nanoparticles studied herein became more negatively charged as evidenced by the zeta potential values shown in Table 2.

At pH 7, selenium nanoparticles stabilized with all types of stabilizing agents studied herein carry an overall negative charge. The addition of the pancreatin–bile extract, which consists of a group of negatively charged molecules, results in the overall increase in electrostatic repulsion of the same charged molecules. Therefore, the particles shifted to a smaller size as depicted in Figs. 3 and 4 (the brown lines and the green lines, without and with pancreatin–bile extract, respectively). The TEM images of pectin and ovalbumin stabilized selenium nanoparticles show the same trend as the results from FlFFF.

4. Conclusion

Flow field-flow fractionation was found effective for size characterization of selenium nanoparticles. With the use of an on-line ICP-MS detection, element specific information was obtained and the quantification of selenium indicated that a total of approximately 88–103% of the original selenium nanoparticles was detected during fractionation. Upon incubation of selenium nanoparticles in gastrointestinal conditions, particle size distributions shifted differently depending on the type of the stabilizing agent used in the preparation of selenium nanoparticles. The changes in particle size are governed by the resulting particle surface charge and the monomeric/dimeric nature of the stabilizing molecules at different pH values. Ionic strength and the presence of enzyme also affected the particle surface charge and electrostatic interaction. Despite the shift in particle size distribution, more than 90% of selenium was still present in nanometer range after gastrointestinal digestion.

Acknowledgments

We sincerely thank the Thailand Research Fund (TRF) for the research grants given to A. Siripinyanond and the scholarship given to P. M-M through the Royal Golden Jubilee Ph.D. Program (Grant No. PHD/0095/2553). Financial support from the Office of the Higher Education Commission, Ministry of Education, Thailand through the Center for Innovation in Chemistry: Postgraduate Education and Research Program in Chemistry (PERCH-CIC); and Mahidol University under the National Research Universities Initiative are gratefully acknowledged.

References

Akhtara, M., Dickinson, E., Mazoyer, J., & Langendorff, V. (2002). Emulsion stabilizing properties of depolymerized pectin. *Food Hydrocolloids*, *16*(3), 249–256.
Bai, Y., Wang, Y., Zhou, Y., Li, W., & Zheng, W. (2008). Modification and modulation of saccharides on elemental selenium nanoparticles in liquid phase. *Materials Letters*, *62*(15), 2311–2314.
Barnaby, S. N., Frayne, S. H., Fath, K. R., & Banerjee, I. A. (2011). Growth of Se nanoparticles on kinetin assemblies and their biocompatibility studies. *Soft Materials*, *9*(4), 313–334.
Bu, H., Kjøniksen, A. -L., Knudsen, K. D., & Nyström, B. (2004). Rheological and structural properties of aqueous alginate during gelation via the Ugi multicomponent condensation reaction. *Biomacromolecules*, *5*(4), 1470–1479.
Chen, T., Wong, Y. -S., Zheng, W., Bai, Y., & Huang, L. (2008). Selenium nanoparticles fabricated in *Undaria pinnatifida* polysaccharide solutions induce mitochondria-mediated apoptosis in A375 human melanoma cells. *Colloids and Surfaces B: Biointerfaces*, *67*(1), 26–31.
Chithrani, B.D., Ghazani, A. A., & Chan, W. C. (2006). Determining the size and shape dependence of gold nanoparticle uptake into mammalian cells. *Nano Letters*, *6*(4), 662–668.
Combs, G. F., Jr., & Combs, S. B. (1986). Selenium in human nutrition and health. In G. F. Combs, & S. B. Combs (Eds.), *The role of selenium in nutrition* (pp. 327–399). Academic Press.
Cozzoli, P. D., & Manna, L. (1996). Nanostructure and biomolecule synthesis. In W. C. Chan (Ed.), *Bio-applications of nanoparticles* (pp. 1–14). New York: Springer.
Dentini, M., Rinaldi, G., Barbetta, A., Risica, D., & Skjåk-Bræk, G. (2006). Acid gel formation in (pseudo) alginates with and without G blocks produced by epimerising mannuronan with C5 epimerases. *Carbohydrate Polymers*, *63*(4), 519–526.
Desai, M. P., Labhasetwar, V., Amidon, G. L., & Levy, R. J. (1996). Gastrointestinal uptake of biodegradable microparticles: Effect of particle size. *Pharmaceutical Research*, *13*(12), 1838–1845.
Dickinson, E. (2010). Flocculation of protein-stabilized oil-in-water emulsions. *Colloids and Surfaces B: Biointerfaces*, *81*(1), 130–140.
Donati, I., Travan, A., Pelillo, C., Scarpa, T., Coslovi, A., Bonifacio, A., et al. (2009). Polyol synthesis of silver nanoparticles: Mechanism of reduction by alditol bearing polysaccharides. *Biomacromolecules*, *10*(2), 210–213.
Dondi, F., & Martin, M. (2000). Physicochemical measurements and distributions from field-flow fractionation. In M. E. Schimpf, J. C. Caldwell, & J. C. Giddings (Eds.), *Field-flow fractionation handbook* (pp. 103–132). New York: Wiley.
Dumont, E., Vanhaecke, F., & Cornelis, R. (2006). Selenium speciation from food source to metabolites: A critical review. *Analytical and Bioanalytical Chemistry*, *385*(7), 1304–1323.
Hoet, P. H., Brüske-Hohlfeld, I., & Salata, O. V. (2004). Nanoparticles—Known and unknown health risks. *Journal of Nanobiotechnology*, *2*(1), 12.
Ingole, A.R., Thakare, S. R., Khati, N., Wankhade, A., & Burghate, D. (2010). Green synthesis of selenium nanoparticles under ambient condition. *Chalcogenide Letters*, *7*, 485–489.
Jia, X., Li, N., & Chen, J. (2005). A subchronic toxicity study of elemental Nano-Se in Sprague–Dawley rats. *Life Sciences*, *76*(17), 1989–2003.
Kammer, F. v. d., Legros, S., Hofmann, T., Larsen, E. H., & Loeschner, K. (2011). Separation and characterization of nanoparticles in complex food and environmental samples by field-flow fractionation. *TrAC Trends in Analytical Chemistry*, *30*(3), 425–436.
Kittler, S., Greulich, C., Gebauer, J., Diendorf, J., Treuel, L., Ruiz, L., et al. (2010). The influence of proteins on the dispersability and cell-biological activity of silver nanoparticles. *Journal of Materials Chemistry*, *20*(3), 512–518.
Kuwata, K., Era, S., Hoshino, M., Forge, V., Goto, Y., & Batt, C. A. (1999). Solution structure and dynamics of bovine β-lactoglobulin A. *Protein Science*, *8*(11), 2541–2545.
Lee, U., Choi, J., Myung, N., Kim, I. H., Chenthamarakshan, C. R. N., De Tacconi, N. R., et al. (2008). Synthesis of monodisperse selenium nanospheres and self-assembled monolayers using poly(vinyl pyrrolidone) as dual reductant/colloid stabilizer. *Bulletin of the Korean Chemical Society*, *29*(3), 689–692.
Li, Z. -L., & Hua, P. -M. (2009). Mixed surfactant template method for preparation of nanometer selenium. *Journal of Chemistry*, *6*(S1), S304–S310.
Lin, Z. -H., & Chris Wang, C. (2005). Evidence on the size-dependent absorption spectral evolution of selenium nanoparticles. *Materials Chemistry and Physics*, *92*(2), 591–594.
Malaki Nik, A., Wright, A. J., & Corredig, M. (2010). Surface adsorption alters the susceptibility of whey proteins to pepsin-digestion. *Journal of Colloid and Interface Science*, *344*(2), 372–381.
Martos, G., Contreras, P., Molina, E., & López-FandiÑo, R. (2010). Egg white ovalbumin digestion mimicking physiological conditions. *Journal of Agricultural and Food Chemistry*, *58*(9), 5640–5648.

Matto, M., & Husain, Q. (2006). Entrapment of porous and stable concanavalin A–peroxidase complex into hybrid calcium alginate–pectin gel. *Journal of Chemical Technology and Biotechnology*, *81*(7), 1316–1323.

Medina-Torres, L., Calderas, F., Gallegos-Infante, J. A., Gonzalez-Laredo, R. F., Rocha-Guzman, N. E., & Harte, F. (2010). Mechanical properties of ovalbumin gels formed at different conditions of concentration, ionic strength, pH, and aging time. *Food and Bioprocess Technology*, *3*(1), 150–154.

Mees, D. R., Pysto, W., & Tarcha, P. J. (1995). Formation of selenium colloids using sodium ascorbate as the reducing agent. *Journal of Colloid and Interface Science*, *170*(1), 254–260.

Mehta, S. K., Chaudhary, S., Kumar, S., Bhasin, K. K., Torigoe, K., Sakai, H., et al. (2008). Surfactant assisted synthesis and spectroscopic characterization of selenium nanoparticles in ambient conditions. *Nanotechnology*, *19*(29).

Miller, D.D., Schricker, B. R., Rasmussen, R. R., & Van Campen, D. (1981). An in vitro method for estimation of iron availability from meals. *The American Journal of Clinical Nutrition*, *34*(10), 2248–2256.

Min-Hsiung, C. -Y. (2004). Observation in the growth of selenium nanoparticles. *Journal of the Chinese Chemical Society*, *51*, 239–242.

Monsen, E. R. (2000). Dietary reference intakes for the antioxidant nutrients: Vitamin C, vitamin E, selenium, and carotenoids. *Journal of the American Dietetic Association*, *100*(6), 637–640.

Mwilu, S. K., El Badawy, A.M., Bradham, K., Nelson, C., Thomas, D., Scheckel, K. G., et al. (2013). Changes in silver nanoparticles exposed to human synthetic stomach fluid: Effects of particle size and surface chemistry. *Science of the Total Environment*, *447*, 90–98.

Navarro-Alarcon, M., & Cabrera-Vique, C. (2008). Selenium in food and the human body: A review. *Science of the Total Environment*, *400*(1), 115–141.

Peng, D., Zhang, J., Liu, Q., & Taylor, E. W. (2007). Size effect of elemental selenium nanoparticles (Nano-Se) at supranutritional levels on selenium accumulation and glutathione *S*-transferase activity. *Journal of Inorganic Biochemistry*, *101*(10), 1457–1463.

Peram, M. R., Loveday, S. M., Ye, A., & Singh, H. (2013). In vitro gastric digestion of heat-induced aggregates of β-lactoglobulin. *Journal of Dairy Science*, *96*(1), 63–74.

Poda, A.R., Bednar, A. J., Kennedy, A. J., Harmon, A., Hull, M., Mitrano, D., et al. (2011). Characterization of silver nanoparticles using flow-field flow fractionation interfaced to inductively coupled plasma mass spectrometry. *Journal of Chromatography A*, *1218*(27), 4219–4225.

Rayman, M. P., Infante, H. G., & Sargent, M. (2008). Food-chain selenium and human health: Spotlight on speciation. *British Journal of Nutrition*, *100*(02), 238–253.

Sakurai, K., Oobatake, M., & Goto, Y. (2001). Salt-dependent monomer–dimer equilibrium of bovine β-lactoglobulin at pH 3. *Protein Science*, *10*(11), 2325–2335.

Sepelyak, R. J., Feldkamp, J. R., Moody, T. E., White, J. L., & Hem, S. L. (1984). Adsorption of pepsin by aluminum hydroxide I: Adsorption mechanism. *Journal of Pharmaceutical Sciences*, *73*(11), 1514–1517.

Shah, C. P., Kumar, M., & Bajaj, P. N. (2007). Acid-induced synthesis of polyvinyl alcohol-stabilized selenium nanoparticles. *Nanotechnology*, *18*(38).

Szentkuti, L. (1997). Light microscopical observations on luminally administered dyes, dextrans, nanospheres and microspheres in the pre-epithelial mucus gel layer of the rat distal colon. *Journal of Controlled Release*, *46*(3), 233–242.

Teow, Y., Asharani, P. V., Prakash Hande, M., & Valiyaveettil, S. (2011). Health impact and safety of engineered nanomaterials. *Chemical Communications*, *47*(25), 7025–7038.

Thomson, C. (2004). Assessment of requirements for selenium and adequacy of selenium status: A review. *European Journal of Clinical Nutrition*, *58*(3), 391–402.

Walczak, A. P., Fokkink, R., Peters, R., Tromp, P., Herrera Rivera, Z. E., Rietjens, I. M. C. M., et al. (2013). Behaviour of silver nanoparticles and silver ions in an in vitro human gastrointestinal digestion model. *Nanotoxicology*, *7*(7), 1198–1210.

Wang, Y. (2009). Differential effects of sodium selenite and nano-Se on growth performance, tissue Se distribution, and glutathione peroxidase activity of avian broiler. *Biological Trace Element Research*, *128*(2), 184–190.

Wang, B., Feng, W. -Y., Wang, T. -C., Jia, G., Wang, M., Shi, J. -W., et al. (2006). Acute toxicity of nano-and micro-scale zinc powder in healthy adult mice. *Toxicology Letters*, *161*(2), 115–123.

Wang, H., Zhang, J., & Yu, H. (2007). Elemental selenium at nano size possesses lower toxicity without compromising the fundamental effect on selenoenzymes: Comparison with selenomethionine in mice. *Free Radical Biology and Medicine*, *42*(10), 1524–1533.

Zhang, J. S., Gao, X. Y., Zhang, L. D., & Bao, Y. P. (2001). Biological effects of a nano red elemental selenium. *BioFactors (Oxford, England)*, *15*(1), 27–38.

Zhang, J., Wang, H., Bao, Y., & Zhang, L. (2004). Nano red elemental selenium has no size effect in the induction of seleno-enzymes in both cultured cells and mice. *Life Sciences*, *75*(2), 237–244.

Zhang, J., Wang, H., Yan, X., & Zhang, L. (2005). Comparison of short-term toxicity between Nano-Se and selenite in mice. *Life Sciences*, *76*(10), 1099–1109.

Zhang, S. -Y., Zhang, J., Wang, H. -Y., & Chen, H. -Y. (2004). Synthesis of selenium nanoparticles in the presence of polysaccharides. *Materials Letters*, *58*(21), 2590–2594.

Zook, J. M., MacCuspie, R. I., Locascio, L. E., Halter, M.D., & Elliott, J. T. (2011). Stable nanoparticle aggregates/agglomerates of different sizes and the effect of their size on hemolytic cytotoxicity. *Nanotoxicology*, *5*(4), 517–530.

JAAS

CRITICAL REVIEW

View Article Online
View Journal | View Issue

Cite this: *J. Anal. At. Spectrom.*, 2014, **29**, 1739

Field-flow fractionation with inductively coupled plasma mass spectrometry: past, present, and future

Pornwilard M-M and Atitaya Siripinyanond*

Received 22nd June 2014
Accepted 25th July 2014

DOI: 10.1039/c4ja00207e

www.rsc.org/jaas

The hyphenated technique of field-flow fractionation (FFF) and inductively coupled plasma mass spectrometry (ICP-MS) is reviewed. FFF-ICP-MS provides unique information on elemental composition across size or molecular weight distributions. In the early stages of FFF-ICP-MS development, the technique was found to be useful for environmental applications. With the growth of nanotechnology, FFF-ICP-MS has gained increasing interest. The historical background of FFF-ICP-MS is summarized herein, including the key points reported in other previous reviews. Applications of FFF-ICP-MS are also reviewed to illustrate the potential of the technique for environmental colloids and nanoparticles. Finally, the future prospects for FFF-ICP-MS are considered.

Introduction

Among the analytical techniques providing particle size information, field-flow fractionation (FFF) is considered one of the major players. FFF is suitable for the size fractionation of nanometer and submicrometer particles and the molecular weight separation of macromolecules of various types, including environmental particulate materials, suspended clays, aquatic colloids, sediments, biological cells, viruses, and polysaccharides. When information on size-based elemental speciation is required, the coupling of FFF with atomic

Department of Chemistry and Center for Innovation in Chemistry, Faculty of Science, Mahidol University, Rama VI Road, Bangkok 10400, Thailand. E-mail: atitaya.sir@mahidol.ac.th; Fax: +662-354-7151; Tel: +662-201-5195

Pornwilard M-M is a Ph.D. student in the Analytical Chemistry Program at the Department of Chemistry, Faculty of Science, Mahidol University. She is a recipient of the Royal Golden Jubilee Ph.D. (RGJ-Ph.D.) program scholarship and is currently research training at the University of Florida at Gainesville, USA. Her previous experience included research training on the bioimaging of metals at the BrainMet, Research Center Jülich, Germany. Her main topics are elemental speciation by FFF and ICP-MS, and the development of analytical methods for the detection of metals and other analytes of biological relevance.

Atitaya Siripinyanond received her Ph.D. in Chemistry from the University of Massachusetts at Amherst, USA in 2002. She is currently an assistant professor at the Department of Chemistry, Faculty of Science, Mahidol University. She is a recipient of the 2007 Young Scientist Awards from the Foundation for the Promotion of Science and Technology under the Patronage of His Majesty the King, the 2011 TWAS Prize for Young Scientists in Thailand from the National Research Council of Thailand and The Academy of Sciences for the Developing World-TWAS, the 2012 L'ORÉAL-UNESCO award for Women in Science (Thailand) from the L'ORÉAL (Thailand) and the United Nations Educational, Scientific and Cultural Organization (UNESCO), and the 2012 Mahidol University Prize for Excellence in Teaching, Mahidol University, Thailand. Her research interests include elemental speciation by FFF and ICP-MS, characterization of engineered nanoparticles, and development of simple field test kits.

spectrometric techniques, such as ICP-OES and ICP-MS, is recommended, as it offers online capability with high selectivity. The combination of FFF with a sensitive multi-element detector like ICP-MS allows the determination of elemental composition across size or molecular weight distributions.[1] This information about elemental size distribution is useful for studying processes involving the formation of colloidal-size particulates and their chemical interactions with associated materials, such as in. the study of trace element contaminant transport in waterways,[2] and investigations in to the preferential binding of specific elements to proteins.[3]

Some key differences between FFF and chromatography are based on the types of force used to induce analyte retention. In chromatography, the forces are highly selective, but at the same time are so powerful that they cause irreversible adsorption and structural disruption, including denaturation. In contrast, the FFF retarding forces are much gentler in nature, and therefore, the molecular integrity of macromolecules can be retained during separation. Owing to the absence of a solid support in FFF, biological activity loss is minimized compared to chromatography where interactions between the analyte molecules and stationary phase are likely to occur. Therefore, FFF is considered a more gentle separation technique and can be invaluable in the separation of macromolecules, especially those with weakly bound or labile species. A schematic diagram representing the FFF separation principle is illustrated in Fig. 1.

After a decade of FFF-ICP-MS development from 1991, a summary of FFF combined with ICP was documented in a book chapter published in 2002,[4] which described many features and principles of FFF and highlighted a few examples of FFF-ICP-MS. At that time, only approximately 19 articles relating to the use of FFF and ICP had been reported. Moving up to date, it has been more than two decades now since the first work on FFF-ICP-MS was published, and using the Scopus database from 1991 to present (May 31, 2014), with the keywords "field-flow fractionation" and "inductively coupled plasma" searching for the article or review document type, a total of 119 outputs were found. The publication trend is illustrated in Fig. 2. After the early development of FFF-ICP, the technique grew quite slowly in the first decade, but since then a big jump of approximately a 400% increase in articles has been observed in the last ten years, suggesting the rapid growth of interest in this technique in the past decade. This may be due to the growing area of nanotechnology, where the particle size matters. This also expands the horizon of FFF applications from environmental colloids to nanoparticles (NPs). From the total of 119 articles published in our search timeframe, 12 articles are considered as review type articles, contributing to approximately 10% of the total number. Therefore, the key points in these previous review articles are summarized in this review.

Furthermore, this review describes the development and the status of FFF-ICP-MS in its early stages, the use of FFF and ICP in the first decades after the first report of the technique, and selected applications of the technique in the second decade for inorganic nanoparticles and environmental colloids. Also, we forecast the possible future trends and opportunities for the technique.

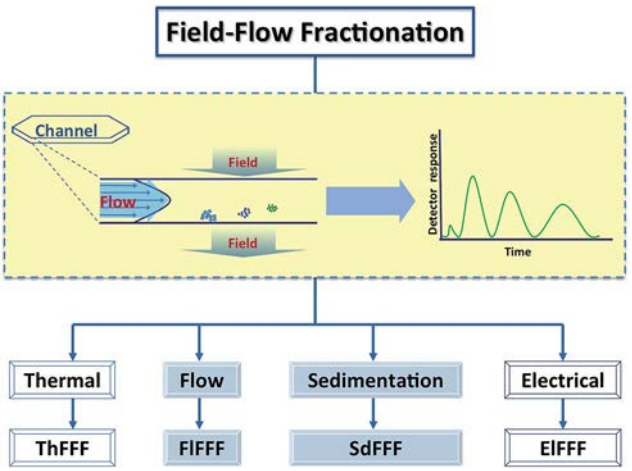

Fig. 1 FFF principle and subtechniques. In FFF, separations are achieved within a flat open channel with a rectangular cross-section and triangular end pieces where the sample and carrier liquid enter and leave. The essence of FFF is to apply a force perpendicular to the channel flow stream, which is a parabolic flow profile. This force drives the macromolecules or particles toward an accumulation wall where they encounter slow-moving laminar fluid streamlines. Fractionation is achieved by the balance between the applied field force pushing the sample particles toward the accumulation wall and the diffusivity of sample particles acting against the field force. Smaller species diffuse away from the accumulation wall into the carrier stream faster than larger species. Thus, various size sample components are driven into different average positions axially and laterally in the channel flow. Consequently, each sample component leaves the channel at a different time related to its diffusion coefficient and thus molecular weight. These primary driving forces can be generated by a number of fields or gradients, resulting in numerous FFF subtechniques that are generally applicable to different materials.

The invention and early stage development of FFF-ICP-MS

In 1991, Beckett introduced the first concepts and described his initial experience in linking FFF separation techniques with ICP-MS.[1] According to Beckett, FFF yielded accurate and high resolution particle size information for environmental samples (*e.g.*, suspended colloidal matter from rivers and lakes). Owing to the high degree of sample dilution taking place during separation in the FFF channel, a very sensitive analytical technique was needed for the subsequent characterization step. In order to gain morphological, compositional, and adsorption capacity information about various natural samples, various detection systems, (*e.g.*, optical microscopy, scanning and transmission electron microscopy, fluorescence, X-ray diffraction, atomic emission spectrometry, and radioactive tracer techniques), had been used;[1] until one day, Taylor of the US Geological Survey in Denver suggested that ICP-MS may be sensitive enough to give elemental information of the fractionated particles. In addition, he suggested that ICP-MS could provide multi-element concentration data across the size distribution of the fractionated sample. With these thoughts, experiments on FFF-ICP-MS were then conducted by Beckett, Taylor, and their coworkers.[5,6] In 1991, the first off-line

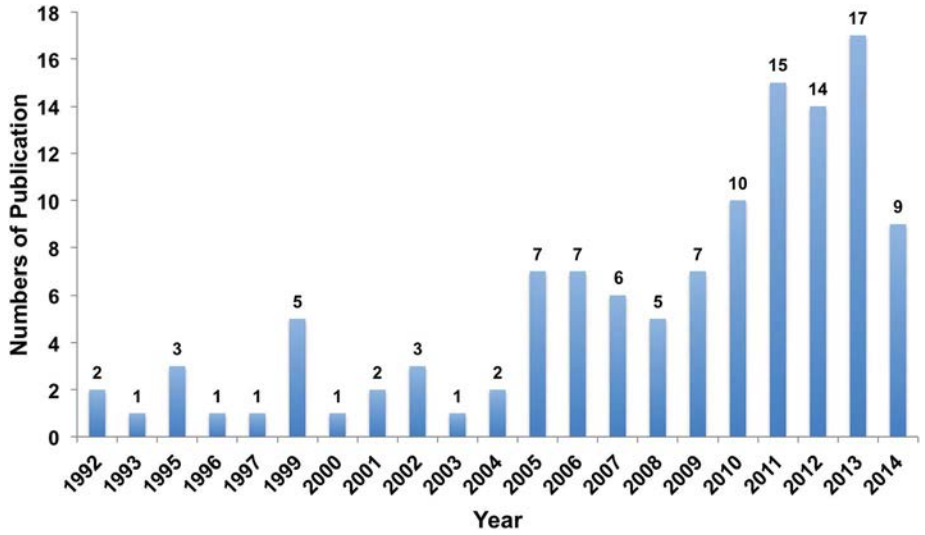

Fig. 2 Publication trend on "FFF" with "ICP" since 1992.

FFF-ICP-MS experiments were conducted, in which the FFF separation of suspended matter was carried out in Melbourne (Australia), and the fractionated components were sent to Denver (US) for off-line elemental characterization using ICP-MS. In the same year, the first online experiments were performed in Denver with the results reported by Taylor *et al.* in 1992.[5] In their work, SdFFF was used to separate three model inorganic solid compounds (*i.e.*, lead chromate, aluminum oxide, and iron oxide) suspended in 0.1% tetrasodium pyrophosphate. Another set of samples involved surface-water suspended matter collected from the Yarra and Darling rivers in Australia. Major, minor, and trace element compositions of the size-separated colloidal (<1 μm diameter) particulates were measured in the fractionated samples. In addition, the Cd adsorption characteristic in the Yarra river colloid concentrate was studied. The results showed that the amount of Cd adsorbed per mass of solid adsorbate increased as the particle size decreased. The authors demonstrated that FFF-ICP-MS was an important tool for studying processes involving the fractionation of colloidal-size particulates and their chemical interaction with associated materials. To avoid the risk of sample clogging, a Babington-type pneumatic nebulizer was used to introduce and nebulize suspended particulates into the ICP torch.

FFF-ICP-MS worldwide

Since its introduction in the early 1990s, FFF-ICP-MS has gradually attracted more attention. Only approximately 20 publications appeared in the peer-reviewed journals during the first 10 years after the first development of the technique, and the technique grew only relatively slowly as a consequence of the limited number of equipment manufacturers and their low marketing. Initially, only a few FFF manufacturers existed with many distributors worldwide. These manufacturers included: (1) Postnova Analytics, Munich, Germany and Postnova Analytics, Salt Lake City, Utah [http://www.postnova.com]; (2) Consenxus, Ober-Hilbersheim, Germany [http://www.consenxus.de]; and (3) Wyatt Technology Corporation, Santa Barbara, California [http://www.wyatt.com]. Another important reason why FFF-ICP-MS was of limited use, was possibly due to the fact that most ICP-MS users were not trained to be FFF practitioners, and likewise, most FFF users were not familiar with ICP-MS. Nonetheless, the situation changed when nanotechnology began to flourish since FFF-ICP-MS provides great merits and capabilities to solve important problems, and hence increasing research work has been observed that includes FFF-ICP-MS. Collaboration between research groups of different expertise is also helpful.

Current publications in FFF with ICP are mostly from researchers in the US, with Spain, Germany, and Australia, ranked as number two, also major contributors in publishing the applications of this technique, as shown in Fig. 3. In terms of the contributions from various research groups, the Colorado School of Mines rank number one, followed by Monash University as number two, and the University of Gothenburg together with Mahidol University as number three (Fig. 4). Both oral and poster presentations relating to the use of FFF and ICP have been made at many major conferences in the atomic spectroscopic community, including the 2013 European Winter Conference on Plasma Spectrochemistry in Krakow, Poland, and the 2014 Winter Conference on Plasma Spectrochemistry in Amelia Island, Florida, US.

In order to summarize the key points relating to FFF with ICP-MS detection given in the other review articles, the selected contents in those review articles are highlighted in the following section. Then, some selected recent applications of the technique for environmental colloids and engineered nanoparticles are discussed.

Review articles related to FFF-ICP-MS

Various review articles relating to the use of FFF and ICP in several investigations have been reported. However, a tutorial

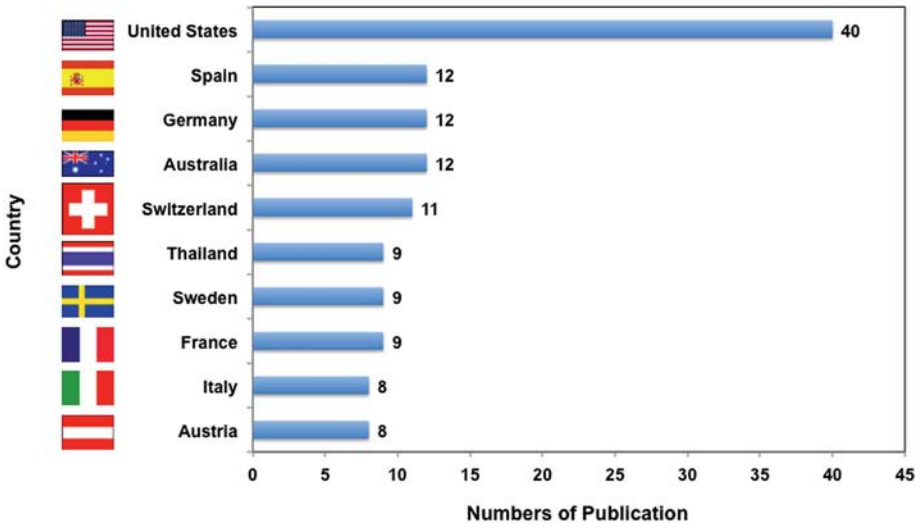

Fig. 3 Publications on "FFF" with "ICP" since 1992, as classified by country.

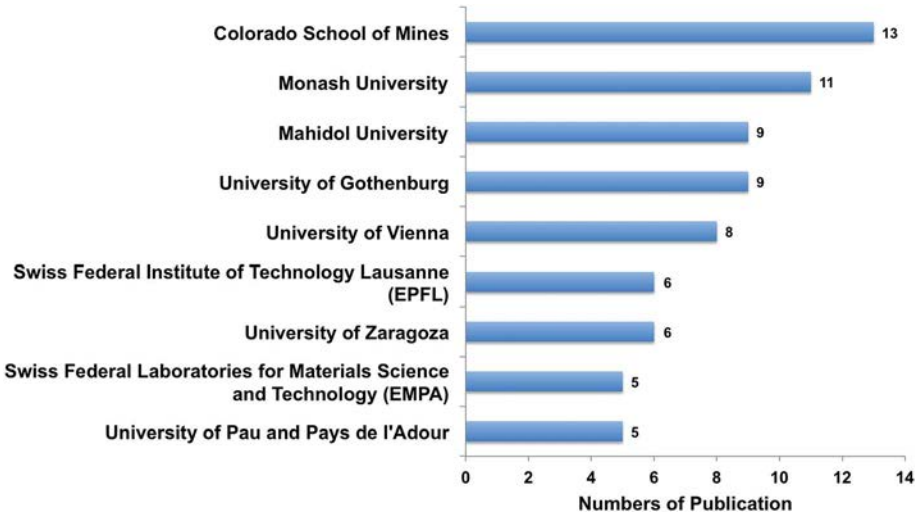

Fig. 4 Publications on "FFF" with "ICP" since 1992, as classified by the institution.

review directly devoted to FFF and ICP-MS coupling was reported in 2010 by Dubascoux *et al.*[7] This review emphasized some key elements regarding the interface between FFF and ICP-MS, including the history and practical aspects, but also described the applications of the technique for qualitative and quantitative analyses. It said that basically the interface between FFF and ICP-MS can be a simple connection through a PEEK (polyether ether ketone) or PFA (perfluoroalkoxy alkane) tube between the outlet of the FFF system and the sample nebulizer of the ICP-MS system, *i.e.*, when the flow rate outlets are compatible with the ICP-MS nebulizer. If not, a split connection may be used when the flow rate outlets were too high. The important thing to consider though is the issue of particle size selectivity in the nebulizer–spray chamber system. Regarding the applications of the technique, the authors stated that more than 90% of the papers were related to environmental applications, but few papers enlarged the application field with industrial applications, food sciences, and life sciences. The authors summarized some selected applications of FFF-ICP-MS in various applications, including in environmental, bio-applications, nanoparticles, and others. The feature of flow FFF to allow the sample preconcentration was also mentioned, to cope with the high dilutions associated with the inherent principle of the fractionation during FFF analyses.

The other review articles related to FFF with ICP-MS were not directly devoted to this hyphenated technique. However, FFF with ICP-MS was listed together with other techniques for certain applications, mainly focused either on engineered nanoparticles or environmental colloids.

For the engineered nanoparticles, various review articles were published.[8–10] The review by Tiede *et al.*[8] discussed different analytical techniques available for the detection, as well as physical and chemical characterization, of engineered nanoparticles in product formulations, environmental

matrices, and food materials. The authors emphasized the importance of the physical and chemical properties of the engineered nanoparticles within the sample and the chemical characteristics of any capping/functional layer on the particle surface. They stated that the analytical techniques should be sensitive enough to measure low concentrations and also to minimize sample disturbance. This review categorized a range of analytical techniques into various approaches, including microscopy, chromatography, centrifugation and filtration, spectroscopic techniques, and related techniques. Field-flow fractionation was listed as one of the chromatographic related techniques that could provide information on particle number concentration, shape, and size. In particular, the FFF technique was discussed as a highly promising technique for the size separation of ENPs in complex natural samples. Despite the fact that it is a mild and versatile fractionation technique, careful optimization of the carrier composition demands experience, and attention should be paid to minimize the membrane interactions. By coupling FFF with ICP-MS, not only is it possible to quantify different nanoparticles in food, water, biota and soil, but also to characterize or elementally analyze them.

Jiménez *et al.*[9] described the use of several separation techniques with ICP-MS detection for the analysis of natural and engineered nanoparticles in the environment. They categorized the review into different parts as follows: natural nanoparticles analysis by polyacrylamide gel electrophoresis laser ablation ICP-mass spectrometry (PAGE-LA-ICP-MS); engineered nanoparticle analysis by separation techniques coupled to ICP-MS; and the identification and characterization of engineered nanoparticles by single particle detection. When hyphenating with ICP-MS detection, FFF was described as one of separation techniques used for separation, apart from for size exclusion chromatography or hydrodynamic chromatography.

A critical review on the application of plasma spectrometry for the analysis of engineered nanoparticles was given by Krystek *et al.*[10] This review covered the use of the ICP technique for the determination of ENPs and its application in various consumer products, including its possible release during use. The authors stated the importance of sample handling and sample preparation for the analysis with plasma spectrometry, stating that care must be taken to preserve the size stability. Among all the hyphenated techniques for the analysis of ENPs, FFF coupled with ICP-OES or ICP-MS was also described in the review as a size fractionation technique for complex mixtures of NPs. With FFF, questions related to the membrane–nanoparticle interaction, the behaviors of different nanoparticle types in the FFF channel, and the influence of dilution of suspensions during separation should be considered, as well as, the development of suitable calibration strategies or recovery improvement.

Fedotov *et al.*[11] reviewed the techniques for the fractionation and characterization of nanoparticles and microparticles in liquid media. Among all other techniques, FFF was listed as one of the most versatile techniques for such purposes. Three modes of FFF separation were mentioned, including normal, steric, and hyperlayer. Various subtechniques of FFF were described. The authors mentioned that homogeneous samples should be used to obtain representative data, because in FFF the sample weight is less than 1 mg. Additionally, with only a very small sample weight, the detection techniques for the analysis of the separated fractions needs to be highly sensitive. Applications of asymmetrical flow FFF (AF4) coupled online with ICP-MS to study metal associations to different environmental microparticles, nanocolloids, and macromolecules were also mentioned.

The applications of flow FFF (FlFFF) for the characterization of natural colloids and natural and manufactured nanoparticles, with an emphasis on the detection systems, were reviewed by Baalousha *et al.*[12] Various detection techniques were mentioned, including UV-vis, organic carbon detector, fluorescence, ICP-MS and ICP-OES, laser-induced breakdown detection, multi angle light scattering, dynamic light scattering, transmission electron microscopy, and atomic force microscopy. With FlFFF, the calculation of the hydrodynamic diameter is based on applying Stokes' relationship and assuming that the particles are hard spheres. However, the particles are not spherical in shape in all cases, suggesting the need for a detector that could give an independent and complimentary measurement of the particle size distribution. The authors discussed the use of a multi detection approach to help verify any abnormalities and deviations from theoretical principles of the fractionation, and in some cases to help provide a wide range of information on other particle properties, such as composition, concentration, optical properties, interaction with trace metals, and structure. In their review, the operational conditions of FlFFF and the study of the analysis of natural colloids and natural nanoparticles were summarized. Natural colloids include extracted humic substances, river and lake waters, estuaries and marine water, wastewater, soil, sediment, and groundwater, as well as atmospheric particles. For manufactured nanoparticles, measurements of the thickness of surface coatings, structures, and aggregation behavior were discussed.

The review by Lespes and Gigault[13] also discussed the use of different hyphenated techniques to obtain multidimensional information for the characterization of submicron particles. Hyphenation of an online fractionation to one or several complementary detectors was illustrated to be useful. FFF was listed as one of the techniques that could provide separation before the detection. In comparison with other techniques, FFF offered the advantage that the fractionation power and dynamic range could be easily tuned by varying the field strength. Various subtechniques of FFF were mentioned. Detection was classified into the category that could provide particle concentration, particle size, elemental concentration, molecular structure information, and other more specific information. Where the information on elemental concentration was sought, inductively coupled plasma spectroscopy was listed as a technique of choice. Various other techniques were discussed and compared for their advantages and limitations.

For environmental samples, Contado *et al.*[14] discussed different methodologies to fractionate and characterize riverine suspended particulate matter. The review also described various experimental approaches to perform sampling and

preconcentration, including membrane filtration, tangential flow filtration, centrifugation, and continuous flow centrifugation. For size fractionation, sequential continuous flow centrifugation, tangential flow filtration, split-flow thin-channel fractionation (SPLITT), and FFF were mentioned. Among these techniques, FFF and SPLITT preserved the complexity of the colloidal feature and were useful for quantitative approaches to study the trace metal distribution on suspended particulate matter, particularly when element specific detectors such as GFAAS or ICP-MS were used.

Another review described the various components of FlFFF instrumentation, the nature of the separation process, and the theory for translating the retention time to relative molecular mass.[15] This review focused on the symmetrical FlFFF subtechnique. The use of frit inlet and frit outlet features was described. The frit inlet offers rapid hydrodynamic relaxation of the sample components to reach their equilibrium positions without having to stop the channel flow, thereby avoiding disruption in the channel. The frit outlet was used for skimming off the carrier liquid through the frit materials and thereby allowing the concentrated particles to flow to the detection system, whereby the detection sensitivity was increased. Regarding the carrier liquid, not only do the ionic strength and the effective dispersion of the particles need to be considered, also the liquid should be properly chosen to minimize swelling of the membrane, which otherwise could lead to nonuniform flows in the channel. Also, care must be taken to avoid potential interference with the detector response and interactions with the channel materials. Detectors should be selected according to the information sought for the sample being analyzed. Two operating modes, including normal and steric/hyperlayer modes were discussed. The applications of FlFFF to environmental and biological matrices and the detection of polymers and inorganic colloids were summarized by listing the analytes, the membrane, the carrier, and the detector used. The authors commented that in order to establish a broader user base with appropriate practical support, the publication of "standard" analytical methods for particular applications may be needed.

The review by von der Kammer *et al.*[16] presented the current status of FFF as an analytical separation technique for the study of NPs in complex food and environmental samples. The ability to identify the ENPs among the background of all other NPs in the sample is quite challenging. With this in mind, the development of a proper sample-preparation procedure or the use of element specific detector may need to be considered. Sample preparation should be carried out in such a way that a stable suspension of particles is obtained. The authors commented on different approaches to separate NPs from a certain matrix, such as particle settling, centrifugation, or filtration. Using settling and centrifugation minimized the risks of sample alterations, whereas for filtration, the membrane filter cannot guarantee that particles smaller than the membrane cut-off indeed pass the membrane quantitatively. For natural NPs, which are generally complex, heterogeneous, and present in a broad size range, careful optimization of the FFF operating conditions must be carried out in order to obtain the full range of sizing. In addition, optimization must be carried out to separate the analytical part of the fractogram completely from the void peak, and the mixed modes of elution (normal and steric mode) should be avoided. In general, the carrier liquid should prevent particle dissolution and aggregation. Normally, the carrier liquid should provide sufficient electrostatic repulsion to prevent attachment and loss of the particles to the membrane. The membrane should be chosen to provide enough repulsion between the particles and the membrane surface, but not too high to cause a repulsion-cushion effect causing the early elution of the particles. For the detection, FFF may be coupled with many types of detectors. When ICP-MS is used, the particle size dependent nebulization and ionization efficiencies in the ICP should be considered.

Selected applications of FFF-ICP-MS

Considering the applications of FFF-ICP-MS, most of the publications relate to environmental colloids and inorganic nanoparticles. Therefore, some more recent applications of the technique are reviewed in the following sections.

Environmental colloids

With FFF-ICP-MS, size-based elemental speciation can be performed. Information on elemental concentration across the size distribution is obtained. FFF-ICP-MS also allows the detection of the specific binding of elements to various nanocolloids subfractions. This information can be important and useful to gain an insight into metals' transport and their fate. Some brief findings of FFF-ICP-MS experiments on environmental applications are summarized as follows.

Bolea and Castillo[17] established a methodology based on asymmetrical flow FFF (AF4) coupled with ICP-MS to characterize metals associated with to environmental particles of a wide range sizes from 1 kDa to 50 μm. In AF4, both steric (microparticle) and normal (nanocolloids and macromolecules) modes of AF4 were performed with prefractionation steps, sedimentation, and centrifugation. Four cross-flow programs were used to classify environmental particles into four groups: microparticles eluted in the steric mode (>1 μm), nanocolloids eluted in the normal mode (15 nm to 1 μm), macromolecules up to 1000 kDa, and macromolecules less than 100 kDa. To correct for ICP-MS instrumental drift, a Cs internal standard solution was mixed with the outlet stream of AF4. Al and Si were mainly found with microparticles, with which Zn and Pb were also significantly associated, as compared to Cu, which was mainly associated with macromolecules.

Worms *et al.*[18] applied AF4-ICP-MS to examine the association of metals to the colloidal organic matter from a wastewater treatment plant. The colloidal organic matter was classified into low molecular mass and high molecular mass fractions. Most metals, including Ag, Cd, Cu, Cr, Mn, and Zn, were found to be associated only with the low molecular mass fraction, suggesting that the low molar mass fraction of the colloidal pool played a key role in controlling the distribution of metals in the colloidal phase. The exceptions included Al, Fe, and Pb, which

were found to be also associated with the high molecular mass fraction.

Krachler *et al.*[19] applied the coupling of AF4 with ICP-MS to characterize colloidal iron carriers in peat-draining rivers in North Scotland. The size distribution of natural organic matter determined by FFF-UV ($\lambda = 220$ nm) was merged with the Fe distribution by AF4-ICP-MS. The distribution of Fe was bimodal, whereby, the smaller particle size indicated iron complexed by natural organic matter, and the second peak was higher and represented a higher abundance of Fe, which may be iron oxides. However, for rivers with a high sodium concentration, the signal for the secondary Fe species became lower, implying that these iron species were more vulnerable to increases in salinity.

Plathe *et al.*[20] coupled AF4 to high-resolution ICP-MS to study the relationships between trace metals and nanoparticles in contaminated sediments. The signal of several elements including Al, Fe, Si, Mg, Ti, Zn, Cu, Mn, Ba, Pb, Sr, Cr, Ce, La, Co, Th, Bi, Pr, and In were monitored. Al and Si represented the peak maximum at particle sizes larger than 100 nm. The peak maximum of Fe was at particle sizes smaller than 100 nm. The peak maximum of Ti was between that of Al and Fe. The fractograms of Zn, Cu, and Pb were similar to that of Fe and Ti, implying that these elements were held on or were in nanoparticle minerals containing Fe and Ti as the major elements. The Al-rich minerals were much more depleted in the nanometer size fraction and showed a less important role in metal binding.

Neubauer *et al.*[21] investigated the effects of ionic strength and sample loading on the retention and recovery for the size characterization of natural nanoparticles by AF4 coupled with ICP-MS. A wide range of polystyrene sulfonate (PSS) molecular weight standards of 1100–145 000 g mol^{-1} were used to cover the particle size range of natural organic matter and its aggregates. To obtain reliable results, a higher ionic strength carrier solution with lower sample loading was recommended. Ammonium carbonate/ammonium carbamate solution was used as a carrier liquid due to its interference-free ICP-MS property. The Rh solution was added as an internal standard for ICP-MS detection. From the UV-vis fractogram, natural organic matter appeared only as one peak, which could bind with about 50% of Fe. However, two peaks were observed in the Fe fractogram, by which the other peak of Fe was defined as an iron-rich nanophase.

Claveranne-Lamolère *et al.*[22] exploited AF4-ICP-MS together with CE-ICP-MS coupling to characterize uranium–colloid interactions. With AF4-ICP-MS, the colloidal population in soil leachates appeared to be polydisperse, which was identified as aggregates probably constituted of inorganic colloidal Ti, Mg, Ca, Fe, Al-rich, and carbon-based particles, as well as organic matter. Uranium was associated with the whole colloidal population. Then, CE-ICP-MS was employed to examine the effect of pH on the affinity between uranium and colloid surface sites.

Brittain *et al.*[23] studied the chemical speciation of U and trace metals in depleted uranium (DU) contaminated soils. Soil samples were extracted with sodium pyrophosphate to remove the organic-bound fraction, followed by a further chemical extraction to separate humic and fulvic complexes. The majority of elements (Mn, Fe, Cu, Zn) gave monomodal fractograms for the soils studied, with the exception of Pb and U. Bimodal distribution was found for Pb in the sodium pyrophosphate extract of the Kirkcudbright soil, but Pb exhibited monomodal distribution in the fulvic and humic acid fractions. In the control soil, U was primarily associated with the sodium pyrophosphate fraction, with only a small amount of U associated with the humic acid fraction, whereas only a negligible amount of U was found in the fulvic acid fraction. In the Eskmeals soil, U displayed a monomodal peak in the sodium pyrophosphate fraction, and in the isolated humic fraction, whereas a bimodal peak was observed for the fulvic acid fraction.

Henderson *et al.*[24] exploited FlFFF-ICP-MS to characterize nanoparticles released during anoxia in grassland soils receiving biannual broiler litter amendments in 12 of the last 15 years. A bimodal distribution was observed at a very small size fraction and with approximately 400 nm particles or aggregates. High concentrations of Al and Si were found in these fractions, with minor contributions from Fe and Ti. The peak of Fe corresponded well with the peaks of Si and Al, whereas the peak of Ti was shifted toward later elution times. Nonetheless, P exhibited an elution peak slightly earlier than those of Si, Al, and Fe.

Saito *et al.*[25] employed FlFFF-ICP-MS to examine the size distributions and elemental compositions of nanocolloids in granitic groundwater. Owing to the relatively low concentration of colloids in groundwater, a three-step enrichment of colloids was carried out by ultrafiltration, a focusing technique with a large sample injection loop, and by the slot flow technique. In most cases, the size distributions of Al, Mg, and Lu corresponded well with that of organic colloids. Similarly, most other lanthanide and actinide elements were also shown to be associated with organic colloids, but with smaller size fractions. Sr was found to be associated with the Ca-dominant fraction, which may form a solid solution in $CaCO_3$.

Stolpe *et al.* reported various examples of FFF-ICP-MS to examine metal binding with environmental colloids.[26–28] They applied the online coupling of FlFFF to detectors, including UV-absorbance, fluorescence, and ICP-MS, to examine Fe, P, Mn, Cu, Zn, Pb, and U distributions, along with the 'nanocolloidal size distributions' (0.5–40 nm, hydrodynamic diameter) of chromophoric and fluorescent organic matter in the Mississippi river, the Pearl river, and the northern Gulf of Mexico.[26] The distributions of Cu and U in all rivers were monomodal in the 0.5–4 nm size range, matching the UV254 size spectrum. In the Pearl river, Zn also showed a similar distribution to Cu and U, but with a broader peak extending into sizes larger than 5 nm. For Mn and Pb, the distributions were similar to that of Fe, which showed an additional peak in the 5–25 nm size range, in comparison with those of Cu and U. The distribution of P resembled that of Fe in the Pearl river, with P distributed in both the 0.5–4 nm and the 5–25 nm peaks. In the Mississippi river, on the other hand, it resembled Cu and U, by which only the 0.5–4 nm peak could be distinguished.

Furthermore, the technique was also employed to examine Cr, Mn, Fe, Co, Ni, Cu, Zn, and Pb distributions along with

'nanocolloidal size distributions' (0.5–40 nm, hydrodynamic diameter) of humic-type and chromophoric dissolved organic matter (CDOM) in Alaskan rivers.[27] Similar to UV254 absorbance, carbon, and Fe distributions, during the spring flood, Cr, Co, Cu, Ni, Mn, Zn, and Pb showed one single peak centered at 1.5 nm, and were largely found in the 0.5–4 nm size fraction. During the summer, Cr, Co, Cu, and Ni showed the sharp peak at 1.5 nm, but with a narrower 0.5–3 nm width than during the spring flood. For the other elements, their signals were too low to be observed.

In another application, Stolpe *et al.*[28] used flow FFF-ICP-MS to characterize the binding between nanocolloids (0.5–40 nm) and Fe, La, Ce, Pr, Nd, Sm, Gd, Tb, Dy, Ho, Er, Tm, Yb, and Lu in six Alaskan rivers in the Yukon River basin, and where seasonal changes and rivers affected the REE-binding of the nanocolloids. Nanocolloids were classified as 'fulvic-rich', 'organic/iron-rich' or 'iron-rich' fractions. During the spring flood, the REEs were high in concentration and were largely associated with <8 nm organic/iron-rich nanocolloids. During the summer base flow, the concentrations of REEs were low and the REEs were mostly associated with small (<0.5 nm) organic and/or carbonate complexes, probably leached from deeper soil layers.

Inorganic nanoparticles

With the emergence of nanotechnology, the use of nanoparticles has increased tremendously. Inorganic nanoparticles can be detected by FFF-ICP-MS. This review highlights some selected applications of FFF-ICP-MS for various types of inorganic nanoparticles, including silver (AgNPs), gold (AuNPs), titanium dioxide (TiO_2), and other inorganic nanoparticles.

Bednar *et al.*[29] compared the sensitivity and selectivity obtained by various instruments (UV, DLS, ICP-MS, ICP-DRC-MS, and ICP-AES) as online detection systems for FFF. In their work, several types of inorganic nanoparticles were investigated, including AgNPs, AuNPs, and quantum dots. Among the detection techniques studied therein, ICP-MS and ICP-AES provided specific and simultaneous detection for AgNPs, with detection limits of 10 μg L^{-1} and 100 μg L^{-1}, respectively. For UV detection, even a detection limit of 100 μg L^{-1} was achieved, although the technique was not specific and could not differentiate between nanoparticles from different elements. For the DLS technique, the detection limit was as high as 1500 μg L^{-1}. Moreover, the impurities in the suspension or a few large particles skewed the DLS measurement to a larger size. Therefore, the advantages of ICP-MS and ICP-AES as online detection systems were emphasized and applied to detect multiple components of nanoparticle systems, including core–shell gold–silver nanoparticles, Cd–Se–Zn–S quantum dots, and silver nanoparticles after sulfidation.

The mixtures of 10, 30, and 60 nm AuNPs with 10, 30, and 60 nm AgNPs were separated by FFF with different detection techniques (UV, DLS, ICP-MS, and ICP-AES). ICP-MS provided the lowest detection limit at 10 μg L^{-1} for both AuNPs and AgNPs, compared with ICP-AES (200 μg L^{-1} for AuNPs and 100 μg L^{-1} for AgNPs), UV (400 μg L^{-1} for AuNPs and 100 μg L^{-1} for AgNPs), and DLS (4000 μg L^{-1} for AuNPs and 1500 μg L^{-1} for AgNPs).

ICP-MS, ICP-DRC-MS, and ICP-AES were coupled with FFF for the characterization of cadmium selenide–zinc sulfide core–shell quantum dots (CdSe–ZnS). For Cd and Zn, ICP-MS provided more detection capabilities over ICP-AES. However, sulfur could not be detected by standard mode ICP-MS (polyatomic interferences), whereas ICP-AES could measure sulfur. Moreover, DRC was used to overcome interferences for sulfur and for selenium detection.

Silver nanoparticles. Hoque *et al.*[30] reported the use of AF4 with online and off-line ICP-MS for the size characterization and quantitative analysis of AgNPs in aqueous matrices. For online AF4-ICP-MS, indium was selected as an internal standard to correct for signal drift during separation and analysis. External calibration was carried out by injecting a series of AgNPs standards into the AF4 system with ICP-MS detection. With this online detection procedure, a LOQ of 1.4 ng mL^{-1} (0.1 mL injection volume) and LOD of 0.8 ng mL^{-1} were obtained. Three calibration approaches for the quantification of AgNPs in water samples were evaluated. These include the external calibration with AgNPs standards, the standard addition of AgNPs in the samples injected into the AF4 channel, and the flow injection approach using a dissolved Ag^+ standard introduced into the eluent flow after the AF4 system *via* an online injector. The first two approaches provide information on both the particle size and concentration, whereas only the information on concentration was obtained from the last approach. Application of the three calibration approaches to a wastewater sample displayed good agreement between the external and standard addition calibration approaches. However, the flow injection approach gave different values, which may be due to the presence of various other insoluble forms of silver (*e.g.*, Ag_2S and AgCl) rather than AgNPs.

Ulrich and coworkers[31] stated the importance of sample handling and preparation on nanoparticle analysis. They studied the effect of dilution, pH, and ionic strength on nanoparticle analysis. Two types of nanosilvers were used in this study; AgNPs with citrate stabilized (Ag@citrate, electrostatic stabilization) and AgNPs with PVA stabilized (Ag@PVA, steric stabilization). With sample dilution, an increase of particle size was observed for both types of AgNPs, which may be due to an alteration of the ratio between the nanoparticles and the coating or functionalization agents bound to its surface. The effect of ionic surfactant or electrolyte addition into the carrier liquid was also investigated. Adding sodium nitrate into the carrier liquid resulted in an increase in size of both types of silver nanoparticles. The authors suggested that the addition of ions may change the electrostatic forces between the coating or functionalization agent and the nanoparticle core, where, generally, the sterically stabilized nanoparticles should be less sensitive to ionic strength changes than the electrostatically stabilized ones. Similarly, the effect of pH change had more impact on the electrostatically stabilized than the sterically stabilized nanoparticles. The time dependent curves showing the change in particle size upon pH change implied the kinetics of the agglomeration behavior. For Ag@PVA, a relatively steep increase was observed after 120 minutes, whereas it took only 60 minutes for Ag@citrate. Moreover, the charge of nanoparticles

also affected the separation efficiency and recovery rate in FFF-ICP-MS analysis. A shift in the retention time may be expected with different particle–membrane interactions.

Bolea *et al.*[32] reported the hyphenated techniques of AF4 and ICP-MS for the characterization and quantification of AgNPs standards and for AgNPs in consumer products. Various parameters, including the mobile phase composition (pH, ionic strength, and the presence of surfactants), the injection/focusing time, and the cross-flow were optimized. Different compositions of nonionic (Tween 20) and ionic surfactants (SDS) were compared in terms of colloid stabilization, based on the steric and electrostatic repulsion. Nonionic surfactants offered a shorter time elution peak with a narrower profile, which may be due to the weaker repulsion forces among AgNPs, whereby the particles are focused into a narrow area. Nonetheless, with nonionic surfactants, three different AgNPs standards (10, 20, and 80 nm) were eluted at the same retention times, suggesting that nonionic surfactants are not appropriate carrier liquids under this condition. In contrast, ionic surfactants promoted electrostatic repulsion forces, leading to longer retention times of the AgNPs. The best sample recovery for all AgNPs standards was observed when 0.01% SDS at pH 8 was used as a carrier liquid. Increasing the ionic strength of the carrier liquid led to the reduction in sample recovery, as the repulsion between AgNPs and the membrane surface was shielded, leading to nanoparticle adsorption on the membrane surface. With ultrapure water as a carrier liquid, conditioning of the membrane surface was necessary by repeated injections of concentrated AgNPs to reduce adsorption, by which recoveries of 98 $\pm$ 5% were obtained when four injections of AgNPs were applied to condition the membrane. Between the two commonly used membranes, poly(ether sulfone) and the PES membrane provided the higher recovery for AgNPs, as opposed to regenerated cellulose membrane. Under optimum conditions, FFF channel calibration was performed using various AgNPs standards with particle sizes between 10 and 80 nm, and consequently the method was applied to characterize the particle sizes of AgNPs in antiseptic and dietary supplements. ICP-MS was also used for elemental detection and quantitation purposes, and the results obtained from direct nebulization were agreeable with those from the digested sample analysis.

Poda *et al.*[33] reported the use of FFF-ICP-MS for the characterization of a AgNPs mixture and applied it to biological media samples. In their work, a symmetrical FlFFF equipped with a 10 kDa regenerated cellulose membrane was used with 0.025% FL-70 in the presence of 0.025% sodium azide as a carrier liquid. NIST-traceable polystyrene bead size standards (20, 50, and 100 nm) were used for the FlFFF channel calibration. Recoveries of 88–89% were obtained for the three sizes of AgNPs at 10, 40, and 70 nm. Recoveries of less than 100% may be due to the interaction of particles with the FFF membrane and particle loss during ICP-MS sample introduction. The sizes of AgNPs obtained from the FFF analysis agreed well with the results from DLS, but were larger than the TEM sizes, reflecting that the FFF and DLS techniques measure the hydrodynamic particle rather than the primary particle size. The injection of a mixture containing 10, 40, and 70 nm AgNPs at concentrations of 67 $\mu g\ L^{-1}$ showed clearly defined peaks, although the baseline resolution was not achieved. With an increase in the particle size, the noise signals also significantly increased. The authors hypothesized that this may be due to the delivery of larger amounts of Ag per particle unit into the plasma/detector system. At concentrations down to 6.7 $\mu g\ L^{-1}$ of mixed AgNPs, three peaks were quite noisy, but still sufficiently defined. However, increasing the cross-flow from 1 to 1.1 mL min^{-1} improved the peak separation, with minimal reductions in sensitivity and minor peak broadening. In addition, the study of biota exposure to AgNPs was carried out. The freshwater oligochaete, *Lumbriculus variegatus,* was exposed to PVP-coated AgNPs spiked sediment. The tissues were extracted after 28 days exposure, by deionized water using sonication. The authors found that AgNPs became bigger at 46 nm after biological exposure, compared to the original size of 31 nm, which may be from coating of the particles with proteins or other biological molecules. Alternatively, the PVP coating might have been removed as a result of biological mechanisms or abiotic reactions in the soil exposure medium, thereby resulting in an aggregation of the destabilized silver particles.

Coleman and coworkers[34] used FFF-ICP-MS to examine the effects of particle size and the coating on the bioaccumulation and depuration of AgNPs within the gut cavities of aquatic invertebrates (*L. variegatus*). Prior to analysis, the *L. variegatus* was homogenated and sonicated for 1 h in deionized water. After 48 h of depuration, FFF-ICP-MS fractograms showed a fraction of AgNPs, but which were smaller in size than the original particle sizes. This result agreed with the data from single particle (SP)-ICP-MS analysis performed for the collected fractions from FFF. The analysis of the collected fractions at the shouldered void peaks from FFF with the SP-ICP-MS revealed that this fraction could be either dissolved Ag, small particles, or Ag associated with organic moieties, such as proteins recovered from the tissue with the water sonication extraction. However, all dissolved Ag should be removed by cross-flow and filtered off through the membrane before reaching the detector. This study illustrated that with FFF-ICP-MS and SP-ICP-MS, AgNPs could be retained in the *L. variegatus* for longer than the standard 6 h depuration period, as indicated in the recommended procedure by USEPA for bioaccumulation testing.

Another work by Poda *et al.*[35] was to examine the effect of UV irradiation on the stability of AgNPs using FFF-ICP-MS. 50 nm polyvinylpyrrolidone-capped AgNPs in the presence and absence of dissolved organic carbon (DOC) were examined. AgNPs were prepared in three different media, including deionized (DI) water, moderately hard reconstituted water (MHW), and MHW with DOC. The ICP-MS response of AgNPs in MHW decreased, compared with AgNPs in DI water, as MHW triggered particle aggregation by charge neutralization. However, adding 4 mg L^{-1} DOC solution in the MHW caused an increase in the ICP-MS signal, as the DOC solution consists of negatively charged carboxylates that increase the nanoparticle dissolution, by scavenging and complexing Ag^{+} and possibly reducing Ag^{+} to Ag^{0}. To mimic the 24 h exposure of AgNPs to sunlight, photolysis with sixteen 14 W black lamps was set up for approximately 1 h. The photolysis resulted in a decrease in the average particle size of

AgNPs, which may be due to the photoinduced oxidation of the PVP and dissolution of the metallic silver. Moreover, it was observed that the particle size of AgNPs in MHW and DOC/MHW also decreased after the photolysis reaction. Moreover, not only did the particle size decrease after adding the DOC component in to the AgNPs solution, the overall particle concentration also decreased, which might be caused by the oxidation of silver to Ag_2O, followed by dissolution. In addition, the toxicity of AgNPs under light exposure was investigated using the standard zooplankton model.

Loeschner *et al.*[36] developed a method based on the use of AF4-ICP-MS for the analysis of AgNPs in chicken meat. To mimic a possible scenario where AgNPs may migrate from an antibacterial food packaging material into meat, AgNPs stabilized with polyvinylpyrrolidone (PVP) were spiked into chicken meat. Then, enzymolysis by Proteinase K for 40 min at 37 °C of the homogenized AgNPs-spiked chicken meat sample was performed to degrade the protein to peptides and amino acids. The fractogram of the enzymatically digested meat sample containing AgNPs displayed one large peak, with two smaller peaks eluting close to the void volume. The large peak was assigned to AgNPs, which eluted earlier than the pristine AgNPs without meat. This earlier elution hampers the accurate determination of the particle size distribution based on retention times.

Bolea *et al.*[37] applied AF4-ICP-MS to investigate the changes in the AgNPs particle size incubated in culture medium and cells to gain an insight into nanotoxicity. The particle size of AgNPs was bigger than the original size upon incubation in the culture medium, suggesting the occurrence of protein corona formation around the AgNPs. Using the appropriate operating conditions to accommodate protein fractionation (19, 53, 113 kDa), Ag signals appeared at the same retention time as the proteins, suggesting that the AgNPs were partially oxidized to Ag^+, which could then associate with proteins present in the culture medium. The association of AgNPs with HepG2 cells was examined by using AF4-ICP-MS after alkaline solubilization. The fractograms revealed the presence of AgNPs, but with a smaller size than the original size, implying that a dissolution process might have occurred. However, the presence of a AgNPs peak provided evidence of the AgNPs association with the cells.

Gold nanoparticles. Schmidt *et al.*[38] reported the use of FFF coupled with ICP-MS for the separation and quantification of 10, 20, and 60 nm AuNPs mixtures. The mean recoveries of 50%, 95%, and 67% were observed for 10, 20, and 60 nm AuNPs, respectively. It is thought that the incomplete recoveries were due to the possible adhesion of AuNPs on the membrane surface during separation process. The limits of detection varied between 0.02 ng Au to 0.4 ng Au, depending on nanoparticle diameter. The LODs increased with increasing particle size. AuNPs of 10 nm and/or 60 nm were injected in to sixteen female Wistar rats. After 24 h, the livers were taken out and solubilized in tetramethylammonium hydroxide. With ICP-MS detection using Rh as an internal standard after microwave-assisted wet ashing, the recoveries of AuNPs from the rat livers ranged from 86% to 123% of their total Au content. However, the 10 nm or 60 nm AuNPs could not be observed by FFF, due to the association of AuNPs with the remains of the liver tissue.

Gray *et al.*[39] compared the performances of hydrodynamic chromatography (HDC) and AF4 coupled with ICP-MS for the analysis of AuNPs. The resolution, recovery, and detection limit obtained by the two techniques were evaluated. Two types of AuNPs, namely tannic stabilized- and citrate stabilized-AuNPs of 5, 20, 50, and 100 nm, were examined. The resolution obtained from HDC was poorer than that from AF4, although the better resolution of AF4 over HDC came with the drawbacks of longer run time. With both techniques, different surface coatings on the AuNPs showed variability in the relationship between the time and diameter under identical operating conditions, implying that size calibration should be performed by using the particles with coatings that caused a similar retention behavior to that of the unknown sample. This problem should be paid greater attention in environmental and biological systems, as NPs are likely to accumulate coatings on their surface. Considering sample recovery during the separation process, HDC provided a higher recovery than AF4, as particle sorption on the separation membrane is the main cause of sample loss. The limits of detection for both techniques are approximately 5 $\mu g\ L^{-1}$.

Titanium dioxide nanoparticles. Owing to their several interesting properties, *i.e.*, insoluble; highly stable; nonreactive; thermally stable; nonflammable; low cost; and environmental friendly, TiO_2 nanoparticles are used in many applications. Various research groups have reported the use of FFF with element specific detectors for the size characterization of TiO_2 nanoparticles, particularly in cosmetic products.

In 2008, Contado and Pagnoni applied FFF with off-line ICP-AES detection for the size characterization of TiO_2 in commercial sunscreen lotion.[40] TiO_2 particles showed a strong affinity for each other and, in some cases, even for the accumulation wall of the FlFFF channel (membrane). In the case of a commercial sample, the Ti concentration profiles obtained by ICP-AES were in agreement with those from the UV detector. The authors mentioned that different sunscreen formulations required different sample preparation methods. In 2010, the same researchers proposed the use of square wave voltammetry as a lower cost technique to quantify the Ti concentration in commercial foundation creams.[41] In their study, the results obtained from square wave voltammetry were compared with ICP-AES. With square wave voltammetry, the presence of interfering elements, such as Pb^{2+} and Cu^{2+}, resulted in unexpectedly low values of the Ti concentration compared to the values obtained by ICP-AES. Therefore, ICP-AES was used as an off-line detector for the fractions collected from FFF. Furthermore, SdFFF and FlFFF were used to investigate the size of TiO_2 nanoparticles in the commercial foundation creams after solvent extraction. The mixture of water : methanol : hexane in a ratio of 1 : 4 : 1 was an optimum extractant, because the higher amount of methanol better dispersed the foundation, and was then evaporated off more rapidly than water. With SdFFF analysis, the void peaks for all six concentrated suspension samples were significantly higher, which might be due to the contributions from some particles with sizes smaller than 100 nm or even bigger sizes with a density lower than 4 $g\ mL^{-1}$. To analyze the smaller particle size fraction, FlFFF was

employed, and this subtechnique was density independent. With FlFFF, particles of about 2–3 nm and about 15 nm were detected in the samples.

Samontha *et al.*[42] reported the coupling between SdFFF and ICP-MS for the size characterization of TiO_2 nanoparticles in sunscreen samples after hexane extraction to remove organic components from the samples. Sunscreen products of various sun protection factor (SPF) values were used as samples. The particle size distributions of titanium dioxide in most sunscreen samples investigated were larger than 100 nm, which might be attributed to the secondary particles. The authors also carried out the quantitative analysis of titanium in the samples by comparing the results obtained from the online SdFFF-ICP-MS and those from the off-line ICP-MS determination of titanium after acid digestion. The concentrations of titanium found from both methods were in good agreement.

Nischwitz and Goenaga-Infante[43] described the first systematic comparison and optimization of extraction methods for titanium dioxide nanoparticles in sunscreen samples. They used FlFFF with online ICP-MS for the size characterization of titanium dioxide nanoparticles in sunscreens after defatting the sample with hexane, followed by bath sonication with an aqueous extractant. With this extraction procedure, stable suspensions of secondary titanium dioxide particles were obtained. To obtain the primary particle size, a further addition of a small amount of hexane to the aqueous extractant was recommended to disaggregate the particles. The developed sample preparation procedure prior to FFF-ICP-MS was applied to the analysis of commercial sunscreens with various sun protection factors.

Another recent published work on the use of AF4-ICP-MS for TiO_2 nanoparticles analysis in cosmetic and food products is given by López-Heras *et al.*[44] In their work, the experimental parameters affecting NPs separation and elemental quantification by AF4-UV/ICP-MS were optimized and discussed. Polystyrene latex standards of three known sizes (22, 54, and 100 nm) were used as calibrants. However, by collecting the fractions analyzed by AF4 for further characterization by TEM, it was found that erroneous results might be obtained when using the latex standards for calibrating rutile TiO_2 NPs size, due to the high aggregation state of TiO_2. To reduce agglomeration, the use of ultrasound energy was explored. Then, AF4-ICP-MS was applied to detect TiO_2 NPs in moisturizing cream, sugar glass, and in coffee cream. However, the Ti signal was negligible in food extracts, suggesting that although TiO_2 was commonly used as an anti-caking agent and food additive, the compound might not be present as NPs.

Ulrich and coworkers[31] examined the effects of pH, ionic strength, and dilution on the analysis of polyacrylate-functionalized TiO_2 nanoparticles. The size of the TiO_2 nanoparticles was not significantly changed after 1 : 50, 1 : 100, 1 : 500, 1 : 1000, and 1 : 5000 dilution. The change of TiO_2 particle size was also insignificant when changing the ionic strength with the addition of sodium nitrate. Nonetheless, the pH change affected the particle size of the TiO_2 nanoparticles. In this case, hydrolysis or other chemical interactions could influence the cross-linking or binding between the polymer coating component of the TiO_2 nanoparticles stabilized by polyacrylate.

Other inorganic nanoparticles. Pace *et al.*[45] applied FlFFF-ICP-MS for the characterization of four CdSe/ZnS quantum dots, including 2 nm QDs (green-emitting) and 5 nm QDs (red-emitting) with two different surface coatings, *i.e.*, polyethylene oxide (PEO); and 11-mercaptoundecanoic acid (MUA). The isotopes monitored included ^{64}Zn, ^{82}Se, and ^{114}Cd, using ^{45}Sc and ^{209}Bi as internal standards for all the samples. However, instrument drift during the FlFFF-ICP-MS analysis was not observed. Therefore, all elemental concentrations were not normalized by internal standard intensities. The signals from ^{64}Zn, ^{82}Se, and ^{114}Cd exhibited similar hydrodynamic diameters, with sizes of 23, 24, 24, and 29 nm for red MUA, green MUA, red PEO, and green PEO QDs, respectively. However, their elemental compositions were significantly different. The MUA-coated QDs provided a very large Cd signal compared to the Se signal. The ratios of Cd/Se were 2.1, 23, 1.3, and 11 for red PEO, red MUA, green PEO, and green MUA QDs, respectively. These QDs were subjected to acute toxicity test by exposure to *Daphnia magna* for 48 h.

Huang *et al.*[46] incubated Be-associated materials in synthetic lung fluid (SLF) to study their dissolution and nanoparticle generation behaviors. To mimic the inter- and intracellular environment in lung tissue, the pH of SLF was adjusted to 4.5 and 7.2, respectively. AF4-ICP-MS was utilized for the size characterization of the particles in incubated samples from days 0, 4, 8, 32, 49, and 149. Cs was selected as the internal standard for the ICP-MS elemental quantification. The time-dependent dissolution and particle generation were investigated for $Be(OH)_2$ suspension (pH = 4.5). No signals of Be, Al, and Si were detected in sizes less than 450 nm for $Be(OH)_2$ suspensions on day 4, whereas they were found at 10–60 nm by day 32. However, the signal intensities of the 10–60 nm particles decreased, whereas the larger particles were formed, suggesting the presence of particle aggregation in SLF. A similar trend was observed at day 149. For all Be-associated materials (bertrandite-containing ore, beryl-containing ore, frit, $Be(OH)_2$), they could significantly produce nanoparticles with the size distribution of 10–100 nm. However, fewer nanoparticles were observed for BeO, for which ionic Be were significantly produced after SLF incubation.

M-M *et al.*[47] exploited FlFFF-ICP-MS to study the particle size characterization of selenium nanoparticles stabilized by pectin, mixed alginate/pectin, ovalbumin, and β-lactoglobulin. Quantification of the selenium was performed and indicated that a total of approximately 88–103% of the original selenium nanoparticles was detected during fractionation. These nanoparticles were subjected to incubation in gastrointestinal conditions, both in enzymatic and non-enzymatic media. The particle size distributions shifted differently depending on the type of stabilizing agent used in the preparation of the selenium nanoparticles. Despite the shift in particle size distribution, more than 90% of the selenium was still present in the nanometer range after the gastrointestinal digestion.

Heroult *et al.*[48] reported the use of AF4-ICP-MS together with multi-angle light scattering (MALS) and off-line with

transmission electron microscopy (TEM) with energy-dispersive X-ray analysis (EDAX) to perform size-based elemental quantification and the size estimation of silica (SiO_2) nanoparticles in coffee creamer. For optimization, SiO_2 of 12 nm size was used and a baseline separation was achieved with a cross-flow rate of 2 mL min^{-1}. Increasing the cross-flow rate higher than2 mL min^{-1} resulted in a better separation but at the expense of poorer recovery. Interestingly, the elution time of 12 nm SiO_2 was shorter than that of the 10 nm AuNPs calibrant. The authors hypothesized that the different elution behaviors between the two particles might be caused by differences in particle–membrane interactions between these particles. For the analysis of SiO_2 in coffee creamer, the sample preparation was carried out by mixing the coffee creamer with water at different temperatures (40 °C and 60 °C) to mimic how coffee is prepared in real life. Silicon fractograms obtained by FFF-ICP-MS for the coffee creamer suspensions showed no significant effect of the water temperature on the particle size distribution of the silica nanoparticles in coffee creamer extracts.

FFF-ICP-MS: concluding remarks and future challenge

FFF-ICP-MS is regarded as a size-based elemental speciation tool, since it produces information on chemical composition across the size distribution of particulate and macromolecular samples. Various important applications of FFF-ICP-MS on the size characterization of environmental colloids and nanoparticles were reviewed, and showed that the technique provides unique and new information, which cannot be gained otherwise. The technique shows great potential to revolutionize our understanding of trace metal–colloid interactions in environmental studies. The chemical composition as a function of particle size can be determined and adsorption characteristics can be investigated. Also, it provides information about bioinorganic metal binding with macromolecules. FFF-ICP-MS can be used to study the competitive binding of several metal ions to particular macromolecules. Regarding the engineered nanoparticles, applications of FFF-ICP-MS for the detection of inorganic nanoparticles in complex matrices, such as in food or environmental samples, are useful. Furthermore, FFF-ICP-MS can be used to gain a greater understanding of how nanoparticles interact with biological systems, to provide evidence on the bioavailability and toxicity of nanoparticles.

Considering the applications of FFF to nanoparticles, a difficulty arises from the variability in the retention behaviors of the same nanoparticle core with different coatings. Different particle–membrane interactions can cause a shift in the elution time of the same size particles, and also variations in the sample recovery during the separation process. The former leads to the incorrect interpretation of particle size information, whereas the latter hinders the quantitative analysis of the nanoparticles. Solving these problems can be a challenge. To enable accurate interpretation of particle size, the use of single particle (SP)-ICP-MS in combination with FFF-ICP-MS is helpful. The works on FFF-ICP-MS with SP-ICP-MS can be found in several publications,[34,46,49,50] and many more publications on these techniques are expected. The use of matrix matched standards or the standard particles of the same coating are suggested. Nonetheless, it is difficult to match the type of particle coating between the standard and the unknown sample in practice. To overcome this problem, we therefore propose the concept of matrix modification by the addition of an appropriate amount of coating or stabilizing agent in the carrier liquid. Experiments to prove this concept are now being conducted in our laboratory.

The main goals of analytical chemistry are identification and quantification of samples. Most FFF-ICP-MS works have reported only species identification. Although a report on the quantitation by FFF-ICP-MS has been found, the quantitative information has not been emphasized in most of the published articles. The elemental speciation of macromolecular compounds is often involved with large carbon-rich molecules.[51,52] The presence of high carbon contents can hinder the accuracy of trace element determination by ICP-MS. As previously reported, carbon concentrations of higher than 1500 mg L^{-1} could cause serious non-spectroscopic interferences.[53] Although no clear evidence exists, varying compositions in fractionated peaks influence the ionization efficiency in the plasma, and therefore, can hinder the exact external calibration of fractograms. The prohibitive factor to obtain accurate quantification of elements in colloids or macromolecules is a lack of standards. To obtain accurate quantitative information of the trace elements bound to macromolecules or particles, standards or standard reference materials must be produced for a particular sample type. Alternatively a method that can overcome the matrix effects must be used. Another clever way to achieve high accuracy is to use ICP-isotope dilution MS (ICP-IDMS), where the sources of systematic error are well understood and can be controlled. Quantification by isotope dilution analysis is based on the measurement of an isotope ratio and not on the absolute ion intensity. The application of an online FFF-ICP-IDMS should be considered by adopting the concept of an online HPLC-ICP-IDMS suggested by Heumann *et al.*[54–59] Two different spiking modes are possible, one using species-specific and another using species-unspecific spike solutions of isotope-enriched labeled compounds. The species-specific mode is only possible for element species well-defined in their structure and composition, whereas the species-unspecific mode could be applied in all cases where the structure and composition of the species are unknown. In the case of FFF-ICP-MS work, the latter approach, *i.e.*, the species-unspecific mode, is suggested. With the latter approach, equilibration of the isotopes on-line is not necessary. Instead of the HPLC column, the FFF channel can be used. This concept has been successfully demonstrated recently by Meermann *et al.*[60] for quantification of AgNPs. The online isotope dilution appears to be an ideal approach for the accurate quantification of speciated elements. Nevertheless, the method is limited to only analyte elements with various sufficient isotopes. Monoisotopic elements (*e.g.*, Al, As, Au, and Mn) cannot be quantified by this approach.

Since the FFF-ICP-MS provides great merits and capabilities to solve important but unusual problems, analysts can expect to

see more and more research work on this hyphenated technique. Collaborative work between analytical chemists and biochemists, biologists, botanists, and nutritionists is suggested. With a fully developed FFF-ICP-MS technique, the role of trace metals and their isotopes in nutrition, health, and disease can be studied. With the use of enriched stable isotopes, differentiation between externally spiked elements and endogenous pools makes the investigation of the exchange between endogenous and exogenous elements of metal-containing macromolecules possible.

In most of the FFF-ICP-MS publications, only SdFFF and FlFFF subtechniques have been used. Coupling between ElFFF and ICP-MS may be seen in the future, as ElFFF has been shown to be able to separate nanoparticles.[61,62] Since the separation in FFF is driven by physical forces, less chemistry is involved in FFF compared to SEC or other chromatographic separations. To obtain elemental size separation without destroying the structure integrity of macromolecules or colloids, FFF-ICP-MS holds the best promise. Despite other advantages, FFF also suffers from limited separation resolution. Depending upon each FFF subtechnique, resolution might be improved by optimizing the parameters governing fractionation power. Analytical chemists can expect to see multidimensional FFF, especially FFF-CE, added to the specificity of their elemental analyses. Multidimensional, hyphenated systems like FFF-CE-ICP-MS or FFF-HPLC-ICP-MS might be necessary to gain detailed information on clinical and environmental studies, where elemental size distribution and its functionality information are sought. This idea was demonstrated by Dubascoux *et al.*[63] when analyzing the fractions collected from AF4 for the further speciation analysis of organotin in environmental colloids by using off-line headspace solid-phase microextraction-gas chromatography with pulsed-flame photometric detection. The work on the combination of FFF with other speciation techniques to provide more insightful information on elemental speciation should gain more interest in the future. Indeed, looking to the future, FFF-ICP-MS can offer a lot more than one might imagine at present. With our entry into the "proteomics era", it is essential to develop ideal assays for the detection and quantification of proteins.[64,65] The use of FFF-ICP-MS in combination with FFF and electrospray ionization mass spectrometry may be a useful additional approach for metalloproteomics.

Acknowledgements

The authors would like to acknowledge the Thailand Research Fund (TRF) for the research grants given to A. Siripinyanond and the scholarship given to P. M-M through the Royal Golden Jubilee Ph.D. Program (Grant no. PHD/0095/2553). We are also grateful for the financial support from the Office of the Higher Education Commission, Ministry of Education, Thailand through the Center for Innovation in Chemistry: Postgraduate Education and Research Program in Chemistry (PERCH-CIC); and Mahidol University under the National Research Universities Initiative.

References

1 R. Beckett, *At. Spectrosc.*, 1991, **12**, 228–232.
2 M. Hassellöv, B. Lyvén, C. Haraldsson and W. Sirinawin, *Anal. Chem.*, 1999, **71**, 3497–3502.
3 A. Siripinyanond and R. M. Barnes, *J. Anal. At. Spectrom.*, 1999, **14**, 1523–1526.
4 R. M. Barnes and A. Siripinyanond, in *Advances in Atomic Spectroscopy*, ed. J. Sneddon, Elsevier, Amsterdam, 2002, vol. 7, pp. 179–235.
5 H. E. Taylor, J. R. Garbarino, D. M. Murphy and R. Beckett, *Anal. Chem.*, 1992, **64**, 2036–2041.
6 D. M. Murphy, J. R. Garbarino, H. E. Taylor, B. T. Hart and R. Beckett, *J. Chromatogr.*, 1993, **642**, 459–467.
7 S. Dubascoux, I. Le Hécho, M. Hassellöv, F. von der Kammer, M. Potin Gautier and G. Lespes, *J. Anal. At. Spectrom.*, 2010, **25**, 613–623.
8 K. Tiede, A. B. Boxall, S. P. Tear, J. Lewis, H. David and M. Hassellöv, *Food Addit. Contam., Part A*, 2008, **25**, 795–821.
9 M. S. Jiménez, M. T. Gómez, E. Bolea, F. Laborda and J. Castillo, *Int. J. Mass Spectrom.*, 2011, **307**, 99–104.
10 P. Krystek, A. Ulrich, C. C. Garcia, S. Manohar and R. Ritsema, *J. Anal. At. Spectrom.*, 2011, **26**, 1701–1721.
11 P. S. Fedotov, N. G. Vanifatova, V. M. Shkinev and B. Y. Spivakov, *Anal. Bioanal. Chem.*, 2011, **400**, 1787–1804.
12 M. Baalousha, B. Stolpe and J. R. Lead, *J. Chromatogr. A*, 2011, **1218**, 4078–4103.
13 G. Lespes and J. Gigault, *Anal. Chim. Acta*, 2011, **692**, 26–41.
14 C. Contado, G. Blo, C. Conato, F. Dondi and R. Beckett, *J. Environ. Monit.*, 2003, **5**, 845–851.
15 L. J. Gimbert, K. N. Andrew, P. M. Haygarth and P. J. Worsfold, *TrAC, Trends Anal. Chem.*, 2003, **22**, 615–633.
16 F. von der Kammer, S. Legros, T. Hofmann, E. H. Larsen and K. Loeschner, *TrAC, Trends Anal. Chem.*, 2011, **30**, 425–436.
17 E. Bolea, F. Laborda and J. R. Castillo, *Anal. Chim. Acta*, 2010, **661**, 206–214.
18 I. A. M. Worms, Z. Al-Gorani Szigeti, S. Dubascoux, G. Lespes, J. Traber, L. Sigg and V. I. Slaveykova, *Water Res.*, 2010, **44**, 340–350.
19 R. Krachler, R. F. Krachler, F. von der Kammer, A. Süphandag, F. Jirsa, S. Ayromlou, T. Hofmann and B. K. Keppler, *Sci. Total Environ.*, 2010, **408**, 2402–2408.
20 K. L. Plathe, F. von der Kammer, M. Hassellöv, J. Moore, M. Murayama, T. Hofmann and M. F. Hochella, *Environ. Chem.*, 2010, **7**, 82–93.
21 E. Neubauer, F. von der Kammer and T. Hofmann, *J. Chromatogr. A*, 2011, **1218**, 6763–6773.
22 C. Claveranne-Lamolère, J. Aupiais, G. Lespes, J. Frayret, E. Pili, F. Pointurier and M. Potin-Gautier, *Talanta*, 2011, **85**, 2504–2510.
23 S. R. Brittain, A. G. Cox, A. D. Tomos, E. Paterson, A. Siripinyanond and C. W. McLeod, *J. Environ. Monit.*, 2012, **14**, 782–790.
24 R. Henderson, N. Kabengi, N. Mantripragada, M. Cabrera, S. Hassan and A. Thompson, *Environ. Sci. Technol.*, 2012, **46**, 11727–11734.

25 T. Saito, Y. Suzuki and T. Mizuno, *Colloids Surf., A*, 2013, **435**, 48–55.
26 B. Stolpe, L. Guo, A. M. Shiller and M. Hassellöv, *Mar. Chem.*, 2010, **118**, 119–128.
27 B. Stolpe, L. Guo, A. M. Shiller and G. R. Aiken, *Geochim. Cosmochim. Acta*, 2013, **105**, 221–239.
28 B. Stolpe, L. Guo and A. M. Shiller, *Geochim. Cosmochim. Acta*, 2013, **106**, 446–462.
29 A. J. Bednar, A. R. Poda, D. M. Mitrano, A. J. Kennedy, E. P. Gray, J. F. Ranville, C. A. Hayes, F. H. Crocker and J. A. Steevens, *Talanta*, 2013, **104**, 140–148.
30 M. E. Hoque, K. Khosravi, K. Newman and C. D. Metcalfe, *J. Chromatogr. A*, 2012, **1233**, 109–115.
31 A. Ulrich, S. Losert, N. Bendixen, A. Al-Kattan, H. Hagendorfer, B. Nowack, C. Adlhart, J. Ebert, M. Lattuada and K. Hungerbühler, *J. Anal. At. Spectrom.*, 2012, **27**, 1120–1130.
32 E. Bolea, J. Jiménez-Lamana, F. Laborda and J. R. Castillo, *Anal. Bioanal. Chem.*, 2011, **401**, 2723–2732.
33 A. R. Poda, A. J. Bednar, A. J. Kennedy, A. Harmon, M. Hull, D. M. Mitrano, J. F. Ranville and J. Steevens, *J. Chromatogr. A*, 2011, **1218**, 4219–4225.
34 J. G. Coleman, A. J. Kennedy, A. J. Bednar, J. F. Ranville, J. G. Laird, A. R. Harmon, C. A. Hayes, E. P. Gray, C. P. Higgins, G. Lotufo and J. A. Steevens, *Environ. Toxicol. Chem.*, 2013, **32**, 2069–2077.
35 A. R. Poda, A. J. Kennedy, M. F. Cuddy and A. J. Bednar, *J. Nanopart. Res.*, 2013, **15**, 1673.
36 K. Loeschner, J. Navratilova, C. Købler, K. Mølhave, S. Wagner, F. von der Kammer and E. H. Larsen, *Anal. Bioanal. Chem.*, 2013, **405**, 8185–8195.
37 E. Bolea, J. Jimenez-Lamana, F. Laborda, I. Abad-Alvaro, C. Blade, L. Arola and J. R. Castillo, *Analyst*, 2014, **139**, 914–922.
38 B. Schmidt, K. Loeschner, N. Hadrup, A. Mortensen, J. J. Sloth, C. Bender Koch and E. H. Larsen, *Anal. Chem.*, 2011, **83**, 2461–2468.
39 E. P. Gray, T. A. Bruton, C. P. Higgins, R. U. Halden, P. Westerhoff and J. F. Ranville, *J. Anal. At. Spectrom.*, 2012, **27**, 1532–1539.
40 C. Contado and A. Pagnoni, *Anal. Chem.*, 2008, **80**, 7594–7608.
41 C. Contado and A. Pagnoni, *Anal. Methods*, 2010, **2**, 1112–1124.
42 A. Samontha, J. Shiowatana and A. Siripinyanond, *Anal. Bioanal. Chem.*, 2011, **399**, 973–978.
43 V. Nischwitz and H. Goenaga-Infante, *J. Anal. At. Spectrom.*, 2012, **27**, 1084–1092.
44 I. López-Heras, Y. Madrid and C. Cámara, *Talanta*, 2014, **124**, 71–78.
45 H. E. Pace, E. K. Lesher and J. F. Ranville, *Environ. Toxicol. Chem.*, 2010, **29**, 1338–1344.
46 W. Huang, D. Fernandez, A. Rudd, W. P. Johnson, D. Deubner, P. Sabey, J. Storrs and R. Larsen, *J. Chromatogr. A*, 2011, **1218**, 4149–4159.
47 P. M-M, W. Somchue, J. Shiowatana and A. Siripinyanond, *Food Res. Int.*, 2014, **57**, 203–209.
48 J. Heroult, V. Nischwitz, D. Bartczak and H. Goenaga-Infante, *Anal. Bioanal. Chem.*, 2014, **406**, 3919–3927.
49 R. B. Reed, C. P. Higgins, P. Westerhoff, S. Tadjiki and J. F. Ranville, *J. Anal. At. Spectrom.*, 2012, **27**, 1093–1100.
50 D. M. Mitrano, A. Barber, A. Bednar, P. Westerhoff, C. P. Higgins and J. F. Ranville, *J. Anal. At. Spectrom.*, 2012, **27**, 1131–1142.
51 J. Szpunar, *TrAC, Trends Anal. Chem.*, 2000, **19**, 127–137.
52 J. Szpunar, *Analyst*, 2000, **125**, 963–988.
53 A. S. Al-Ammar, E. Reitznerová and R. M. Barnes, *Spectrochim. Acta, Part B*, 1999, **54**, 1813–1820.
54 L. Rottmann and K. G. Heumann, *Fresenius. J. Anal. Chem.*, 1994, **350**, 221–227.
55 L. Rottmann and K. G. Heumann, *Anal. Chem.*, 1994, **66**, 3709–3715.
56 J. Vogl and K. G. Heumann, *Fresenius. J. Anal. Chem.*, 1997, **359**, 438–441.
57 J. Vogl and K. G. Heumann, *Anal. Chem.*, 1998, **70**, 2038–2043.
58 K. G. Heumann, S. M. Gallus, G. Raedlinger and J. Vogl, *Spectrochim. Acta, Part B*, 1998, **53**, 273–287.
59 K. G. Heumann, *Anal. Bioanal. Chem.*, 2004, **378**, 318–329.
60 B. Meermann, A. L. Fabricius, L. Duester, F. Vanhaecke and T. Ternes, *J. Anal. At. Spectrom.*, 2014, **29**, 287–296.
61 J. Gigault, B. K. Gale, I. Le Hecho and G. Lespes, *Anal. Chem.*, 2011, **83**, 6565–6572.
62 W. Somchue, A. Siripinyanond and B. K. Gale, *Anal. Chem.*, 2012, **84**, 4993–4998.
63 S. Dubascoux, J. Heroult, I. Le Hécho, M. Potin-Gautier and G. Lespes, *Anal. Bioanal. Chem.*, 2008, **390**, 1805–1813.
64 M. Abu-Farha, F. Elisma, H. Zhou, R. Tian, H. Zhou, M. S. Asmer and D. Figeys, *Anal. Chem.*, 2009, **81**, 4585–4599.
65 Z. Ning, H. Zhou, F. Wang, M. Abu-Farha and D. Figeys, *Anal. Chem.*, 2011, **83**, 4407–4426.

Field-Flow Fractionation with Atomic Spectrometric Detection for Characterization of Engineered Nanoparticles

Rabiab Suwanpetch, Takdanai Techarang, Mathuros Ornthai, Pornwilard M-M, and Atitaya Siripinyanond

Mahidol University, Bangkok, Thailand

Engineered nanoparticles (ENPs) have been applied in various applications: biomedical, consumer products, electronic devices, and sensors. Field-flow fractionation (FFF) is an interesting nonchromatographic technique for size characterization of materials with nanometer range. Various subtechniques of FFF including flow, sedimentation, and electrical are described with some selected applications reviewed. Moreover, FFF can be used via off-line and on-line with many elemental detection techniques: GFAAS, ICP-OES, ICP-MS, and SP-ICP-MS to provide more information in term of quantification and element-specific detection. In this article, applications of FFF with atomic spectrometric detection for environmental and biological samples and consumer products and food-related samples are discussed.

1 INTRODUCTION

ENPs have been increasingly used in our daily life. Therefore, suitable analytical techniques for ENPs characterization are of great demands. Choices of analytical techniques for nanoparticle (NP) characterization are various. Selection of proper analytical techniques depends on the information sought. FFF is a technique of choice when the particle size information is required.

This article is categorized into six parts. In the first part, the applications of ENPs are reviewed. The second part describes the principle of FFF techniques and summarizes the applications of FFF for size characterization of ENPs. The third part describes the principle of various atomic spectrometric techniques by showing some selected applications of the techniques to ENPs. The fourth part discusses about the hyphenation between FFF with atomic spectrometric detection, with selected applications in biological, environmental, and industrial samples reviewed. The fifth part consists of the applications of FFF with atomic spectrometric detection for ENPs. The concluding remarks are given in the sixth part.

2 ENGINEERED NANOPARTICLES

ENPs are the synthetic particles composed of variety of materials. The size, shape, and surface of the particles can be controlled during the synthesis process. Various types

Encyclopedia of Analytical Chemistry, Online © 2006–2015 John Wiley & Sons, Ltd.

This article was published in the *Encyclopedia of Analytical Chemistry* in 2015 by John Wiley & Sons, Ltd.
DOI: 10.1002/9780470027318.a9427

of ENPs exist and can be categorized into three classes. The first class is the carbon-based materials such as carbon nanotubes (CNTs), fullerenes, and nanowires. The second class is inorganic NPs including metal nanoparticles: silver nanoparticles and gold nanoparticles; metal oxide nanoparticles: CeO_2, SiO_2, TiO_2, and ZnO NPs; quantum dots (QDs): CdSe and CdS. The last class is polymer and dendrimer-based NPs.

In this article, only inorganic NPs are discussed. Metal NPs are fabricated from elemental metals to produce particles in the nanometer scale with new chemical and physical properties. Examples of metal NPs include gold nanoparticles (AuNPs), silver nanoparticles (AgNPs), copper nanoparticles (CuNPs), and platinum nanoparticles (PtNPs). Metal oxide NPs are NPs of metal oxide such as silicon dioxide (SiO_2), titanium dioxide (TiO_2), zinc oxide (ZnO), and iron oxide (Fe_2O_3/Fe_3O_4). Metal oxide NPs are often used as coating and compost agent in various material and devices. QDs are 1–10 nm of particles made from semiconductor materials. QDs show unique electronic and optical properties owing to the electrons transfer as quantum confinement in small limited area fixed by their nanosize. For optical property, QDs absorb wide spectral range and emit the light in ultraviolet to infrared regions, which depend on their size and elemental compositions form core. QDs are used as bioprobes such as bioimaging in medical application. In addition, QDs are used in electronic application such as solar cell, optical sensor, light-emitting diode (LED), telecommunication device, and quantum computer.[1,2] Applications of inorganic NPs are various as shown in Figure 1. In this article, applications of inorganic NPs in biomedical, consumer products, electronics, and sensor are summarized.

2.1 Biomedical Application

Nowadays, people concern much about health problems including cancers, tumors, infectious diseases, and antibiotic-resistant problems. Since the beginning of twenty-first century, nanotechnology has been of interest for health and treatment applications using their benefits to the treatment of human diseases. Various types of ENPs were used in medical application. Regarding the inorganic NPs, the use of silver nanoparticles (AgNPs), gold nanoparticles (AuNPs), metal oxide NPs, and many types of QDs has been reported in the applications as antibiotic, cancers and tumors treatment, cell imaging and biomarker, drug delivery, and nanocoating medical device such as catheter, tube, and dressing. Inorganic NPs are easy to synthesize and can be readily functionalized, and they are biocompatible. Consequently, they have been used for cellular delivery, targeted delivery, and controlled release.[3–6]

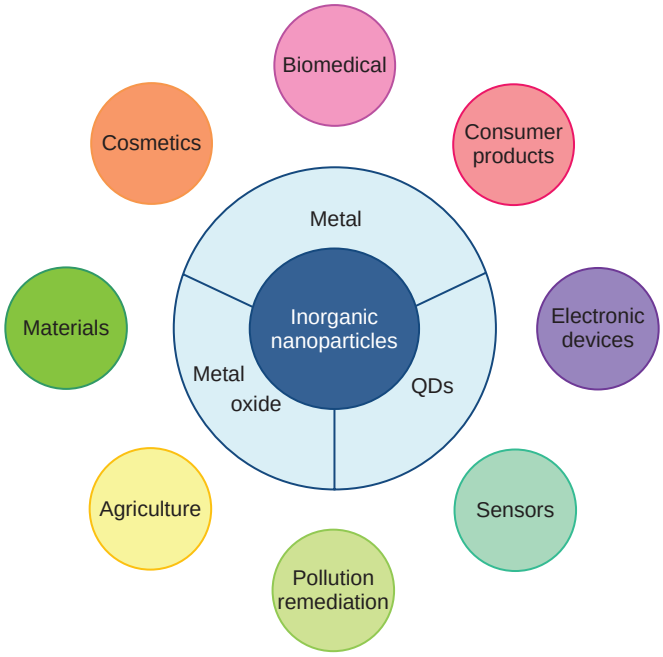

Figure 1 Inorganic nanoparticles and their applications.

2.1.1 *Gold Nanoparticles*

Gold NPs were used as cancer marker and therapy.[7–9] Surface-modified AuNPs were used to deliver gene and drug to the target cells.[3–6] In addition, the use of AuNPs, with and without stabilizers, as an antibacterial agent was reported and it was proved that AuNPs could be used as an alternative for the development of new antibacterial drugs to combat resistance problem.[10,11] Moreover, AuNPs were used in biosensing applications for diagnostic purposes. Špringer et al.[12] created novel biofunctionalized surface-modified AuNPs (bio-AuNPs) to detect carcinoembryonic antigen, a biomarker of cancer of tumor, in human blood plasma. In addition, Zhang et al.[13] developed AuNPs for selective and sensitive sensing of prion protein sensing.

2.1.2 *Silver Nanoparticles*

Silver NPs are well known for their resistance to the bacterial cell both Gram-negative and positive bacteria.[14,15] They are often used in medical application to inhibit bacterial growth that causes infectious diseases. Synthesis of AgNPs is aimed toward using green methodology to be noncytotoxic to provide stable particles with narrow size distribution. Examples included the synthesis of AgNPs using cysteine as reducing agent and cetyltrimethylammonium bromide (CTAB) as stabilizing agent. These synthesized AgNPs were

Encyclopedia of Analytical Chemistry, Online © 2006–2015 John Wiley & Sons, Ltd.

This article was published in the *Encyclopedia of Analytical Chemistry* in 2015 by John Wiley & Sons, Ltd.
DOI: 10.1002/9780470027318.a9427

tested for their antibacterial properties with *Escherichia coli* O157:H7, and high antibacterial efficiency was obtained as reported by Paredes et al.[16] Another investigation was reported by Thomas et al.[17] to study antibacterial property of biosynthesized AgNPs and AgNPs combined with antibiotics. Both AgNPs exhibited inhibitory effect against *Staphylococcus aureus*, *Vibrio cholerae*, *Salmonellatyphi*, *Salmonella paratyphi*, and multidrug-resistant biofilm-forming coagulase-negative *Staphylococcus epidermidis* 73, 145, and 152. In addition, AgNPs were applied to use as wound treatments, by which Tian et al.[18] demonstrated that AgNPs could heal wounds and reduce inflammation in the animal model. In addition, AgNPs were coated on medical devices as antibiofilm to inhibit dispersion of bacteria in medical activity such as catheters[19−22] or orthopedics and dentistry for prosthesis implantation.[23] For therapeutic purpose, the use of AgNPs as tumor and cancer treatment was also reported, by which AgNPs possessed antiangiogenic properties to block growth of tumor cell[24,25] and AgNPs could damage cell membrane and disturb into cell leading to cancer cell death.[26−29] Future interest included the modification of AgNPs surface to be selective to cancer cell and nontoxic to normal cell.

2.1.3 Zinc Oxide Nanoparticles

Zinc oxide NPs were used for wound healing, cell imaging, cancer therapy, and drug delivery. In 2013, Sudheesh Kumar et al.[30] fabricated bandage from β-chitin hydrogel and ZnO NPs composites to enhance antibacterial and speed up the wound healing process. Depending on the concentration of ZnO NPs, the composite bandages showed in vitro antibacterial and antifungal activities against *Candida albicans*, *E. coli*, and *S. aureus*. They also studied cell viability using human dermal fibroblast (HDF) cells and found that higher concentration of ZnO NPs resulted in reduction of cell viability. In addition, composite bandages were studied in vivo for their antibacterial activity and wound healing using Sprague Dawley rats. The wound treated with the composite bandages was healed faster with high collagen deposition. Furthermore, the composites of ZnO NPs with chitosan gel and gentamicin antibiotic were prepared to offer cutaneous healing with controlled release of antibacterial agent.[31] The use of regenerated bacterial cellulose (RBC) combined with ZnO NPs was also demonstrated for wound dressing with biocompatibility and nontoxicity to cell.[32] In addition, ZnO NPs were used as biomedical therapeutic[33,34] and imaging agents.[34,35] The cytotoxicity of ZnO NPs depended on size, shape, and their concentration. Zn^{2+} released from ZnO NPs and reactive oxygen species (ROS) species caused cytogenetic damage and induced apoptosis of cancer cell.[35−38]

Other metal oxide NPs include manganese oxide (MnO) and iron oxide (Fe_3O_4). With surface modification, they were used as biomedical imaging and drug delivery applications.[39,40] Iron oxide NPs showed unique properties such as superparamagnetism, and they were used in bioseparation. Furthermore, the applications of iron oxide NPs included multimodality imaging, therapy, biophotonics, diagnostic, and drug delivery agent. Combination with specific targeting agent on the surface of NPs was reported to solve the problem of specificity lacking.[41−44] Moreover, as antimicrobial activity, AgNPs, AuNPs, SiO_2 NPs, TiO_2 NPs, and ZnO NPs were studied and used in dentistry as control of oral infections.[45−47]

2.1.4 Quantum Dots

QDs were useful as fluorescence probes owing to their unique optical properties such as photoluminescence, high photobleaching threshold, and excellent chemical stability. In addition, QDs functionalized with targeting agent were also applied in biomedical field to function as cell imaging, biomedical sensor, and biodiagnostic. The use of QDs as a probe for liver cancer cell[48] and tumor monitoring[49] was reported. In addition, the QD-loaded micelles were used as cancer therapeutic and imaging agents in mice model.[50]

2.1.5 Nanoparticle-Encapsulated Platinum

NP-encapsulated platinum was interested for its therapeutic application as cancer treatment agent, because platinum compounds such as cisplatin have shown anticancer property toward germ cell tumors and bladder, ovarian, testes, lung, head, and neck cancers. However, they exhibited unfavorable pharmacokinetic profile, short half-life in blood system, and toxic side effects to liver, kidney, and nerves system.[51−55] In order to attain enhanced efficiency against cancer with lower dose, targeting, and reduced side effect, development of platinum drug encapsulated in NPs for cancer therapy was studied. Encapsulation of prodrug or other Pt complexes in polymer as drug carrier, which could target, control release, minimize dose with low toxic side effect was considered.[53,55−58] Dhar et al. encapsulated Pt(IV) complex: *c*,*t*,*c*-$Pt(NH_3)_2(O_2CCH_2CH_2CH_2CH_2CH_3)_2Cl_2$ as cancer prodrug agent, which generated cisplatin after reduction in cell, using poly(D,L-lactic-*co*-glycolic acid)-*b*-poly(ethylene glycol) (PLGA-*b*-PEG) to form NPs. This was to deliver the drug to prostate cancer cell. The test was carried out in mouse and rat models with the result

Encyclopedia of Analytical Chemistry, Online © 2006–2015 John Wiley & Sons, Ltd.

This article was published in the *Encyclopedia of Analytical Chemistry* in 2015 by John Wiley & Sons, Ltd.
DOI: 10.1002/9780470027318.a9427

shown that the developed drug showed higher anticancer efficiency than that of the cisplatin conventional drug. The lower dose of drug was required, and the drug residence in blood was prolonged.[56]

2.2 Consumer Products

Inorganic NPs have been applied to various consumer products. In textile industry, inorganic NPs (silver, copper dioxide, silicon dioxide, and titanium dioxide) were used as coating materials on the textile fibers.[59−63] TiO_2 and SiO_2 NPs were coated on cotton textile surface to enhance self-cleaning.[59] Fabrication of antibacterial, conductive, and super hydrophobic textiles was possible by coating of AgNPs.[64] ZnO NPs coated silk fabrics showed UV blocking, self-cleaning, and antibacterial activity against *E. coli* and *S. aureus*.[65] AuNPs were coated on cotton and silk fabrics to protect UV radiation and provide antimicrobial ability.[66]

In cosmetic and sunscreen products, nanomaterials (gold, silver, titanium dioxide, and zinc oxide) were used as ingredients to show protections of acne and dermatitis, UV radiation, dark spot, blemish, and freckles.[67−69]

In food and beverage industries, NPs were used for various purposes. AgNPs, TiO_2, and ZnO NPs were used as antimicrobial agents and UV blocker and used for maintaining freshness and nutrient in food storage and in packaging. They were also used in bake wares, chopsticks, kitchen tools, and cutting boards as sterilizing agents to prevent digestive diseases. NPs of copper, gold, iridium, palladium, platinum, silica, silver, and zinc were added in beverage as supplements to promote human health and also for antibacterial protection.[67,70,71] Silica NPs were added in food as anticlumping and anticaking agent in powder food products such as milk powder, chocolate powder, coffee creamer, pancake and cake mix, and instant soups.[72]

In personal care products such as toothpastes, soap, shampoos, and spray, nanomaterials such as silver, titanium dioxide, and zinc oxide were added as antibacterial and antifungal agents to neutralize odor and prevent oral and skin infection.[67]

In paint, pigment, building, and furniture materials, metal oxide NPs such as titanium dioxide, silicon dioxide, indium tin oxide (ITO), and zinc oxide were used for self-cleaning, antifogging, UV protection, and antibacterial and antifungal purposes.[67,73−77]

In addition, home and electronic appliances were coated with nanomaterials as disinfectant and purificant. These appliances include air conditioner, iron, vacuum cleaner, refrigerators, computer equipment, water purifier, and hair dryer and roll.[67]

2.3 Electronic Devices

Owing to the physical properties, size, structure, surface area, and morphology, and chemical properties, electrical, optical, semiconductivity, and mechanical properties, NPs were applied in various electronic-related devices. For examples, NPs were used as electrode materials in solar cell to enhance efficiency of solar cell such as light-harvesting efficiency, electron injection efficiency, and electrons collection efficiency.[78−80] Another example is the use of NPs as anode and cathode materials in lithium-ion batteries and electrodes in super-capacitors because NPs exhibited enhanced capacitance, long cycle life, high power, and high-energy density.[78,81,82] Furthermore, NPs were used in electronic devices such as computers, transistors, televisions, robots, mobile phones, and LED for the purpose of downsizing of the devices and providing lightweight.[81,83,84]

2.4 Sensors

ENPs have been widely used as sensor, owing to their low cost and simple preparation. Moreover, they are less toxic, eco-friendly, chemically stable, with fast response, high sensitivity, selectivity, and simple detection.[85] For example, AgNPs were applied to detect Ba^{2+}, Cr^{3+}, Hg^{2+}, anions, and organic molecules: glucose, triptans, tryptophan, pesticides, melamine, and quaternary ammonium surfactants.[85−92] AuNPs were used for detection of Ag^{+}, Cd^{2+}, Cr^{3+}, Hg^{2+}, NO_2^{-}, and NO_3^{-}.[93−97] Moreover, AuNPs were modified as electrochemical sensor of organic molecules.[98,99] NPs of metal oxide (Cu_2O, Fe_2O_3, MoO_3, SiO_2, SnO_2, TiO_2, WO_3, and ZnO) were used as gas detection (C_2H_2, CO, VOCs, H_2, H_2O_2, H_2S, NO_2, ammonia, and ethanol)[63,99−102] and humidity sensor.[103] Metal oxide NPs functionalized with organic ligands were developed as luminescent ion probes for detection of Cu^{2+}.[104] QDs were used as luminescence probe, owing to their broad absorption and narrow emission spectra, resistance to photobleaching, and long fluorescence lifetime.[105] The surface modification of QDs gave high sensitivity and selectivity for ion detection.[106] CdSe/CdS QDs were functionalized using diethyldithiocarbamate for Cu^{2+} detection.[105] CdS:Eu QDs with L-cysteine capping were used as Hg^{2+} detection.[107] CdTe QDs capped by mercaptopropionic acid (MPA) were used as Ag^{+} detection.[108] CdTe QDs capped by glutathione were used as Cr(VI) fluorescence probes.[109] CdSe QDs capped by 2-mercaptoethanol were used for Ba^{2+} detection.[110]

Encyclopedia of Analytical Chemistry, Online © 2006–2015 John Wiley & Sons, Ltd.

This article was published in the *Encyclopedia of Analytical Chemistry* in 2015 by John Wiley & Sons, Ltd.
DOI: 10.1002/9780470027318.a9427

3 FIELD-FLOW FRACTIONATION FOR ENGINEERED NANOPARTICLES

FFF is a nonchromatographic flow-assisted hydrodynamic separation technique. In FFF, an open channel is used instead of a column, and the external physical force is applied to drive separation. Thus, nonspecific interaction between sample and column materials, which normally occur in other chromatographic techniques, is avoided. Many subtechniques are available depending on the field applied to cause separation. If the cross flow is used, the technique is called flow field-flow fractionation (FlFFF). With centrifugal field force, the technique is called sedimentation field-flow fractionation (SdFFF). These two subtechniques are quite common. More details regarding the FFF theory are described elsewhere.[111–113] In this article, only the general principles and the applications of FFF for ENPs characterization are discussed.

The FFF separation principle is illustrated in Figure 2. During sample introduction, mixed particles are introduced into the FFF channel, the perpendicular external field is applied to the channel, causing particles move toward accumulation wall. Then, a counteracting diffusive force drives the particles back toward the center of the channel. The diffusive force directly relates to the diffusion coefficient and the hydrodynamic diameter by which smaller particles can move faster than bigger particles. Therefore, the smaller particles are lifted away from the accumulation wall at a higher position than that of the bigger particles. As the flow profile of carrier liquid is parabolic by which the maximal velocity is in the middle of the channel, the particles are then carried downstream through the channel at different speeds and exit the channel at different times.

In a general system set-up, ultraviolet/visible spectrophotometer (UV/VIS) is used as a detector to detect the eluted particles. Nonetheless, various types of other detectors can be used depending on the purpose of the analysis. For example, inductively coupled plasma-optical emission spectrometry (ICP-OES) or inductively coupled plasma mass spectrometry (ICP-MS) is used for element detection, and dynamic light scattering (DLS) is used for size characterization. These two types of detectors can be used both on-line and off-line modes. Transmission electron microscope (TEM) and scanning electron microscope (SEM) can be used as off-line detection system to observe the size and morphology of the particles.

In FFF, separation mechanism can be achieved in normal or steric modes, depending on the particle size and the field condition used. In the normal or Brownian mode, particle sizes of samples are negligible when compared to the diffusional cloud. With the normal mode, smaller particles elute earlier than the bigger particles. Generally,

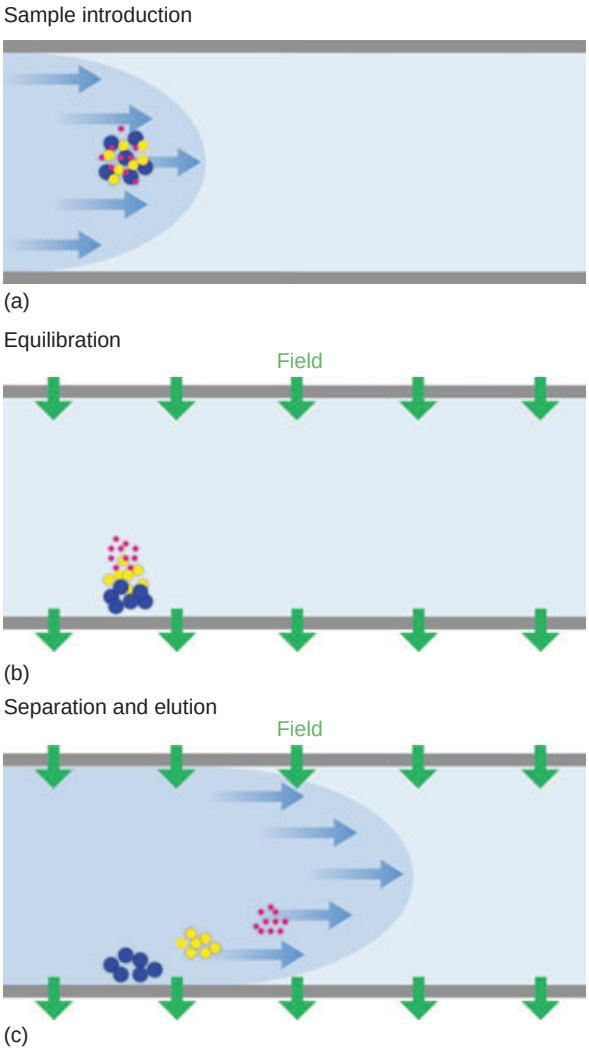

Figure 2 Illustration of field-flow fractionation principle. The separation consists of three steps including (a) sample introduction, (b) equilibration, and (c) separation and elution.

particles of ~1–1000 nm are separated in this mode. The steric mode is considered for separation of particle sizes larger than 1 μm. With this size range, the particle sizes are not negligible when compared to the diffusional cloud. The larger particles protrude from the accumulation wall toward the upper part at a higher position than that of the smaller particles. Then, larger particles elute before the smaller ones. Thus, NPs are generally separated in the normal elution mode.

3.1 FFF Subtechniques

The perpendicular external field can be of various kinds, resulting in various FFF subtechniques, as illustrated in

Encyclopedia of Analytical Chemistry, Online © 2006–2015 John Wiley & Sons, Ltd.

This article was published in the *Encyclopedia of Analytical Chemistry* in 2015 by John Wiley & Sons, Ltd.
DOI: 10.1002/9780470027318.a9427

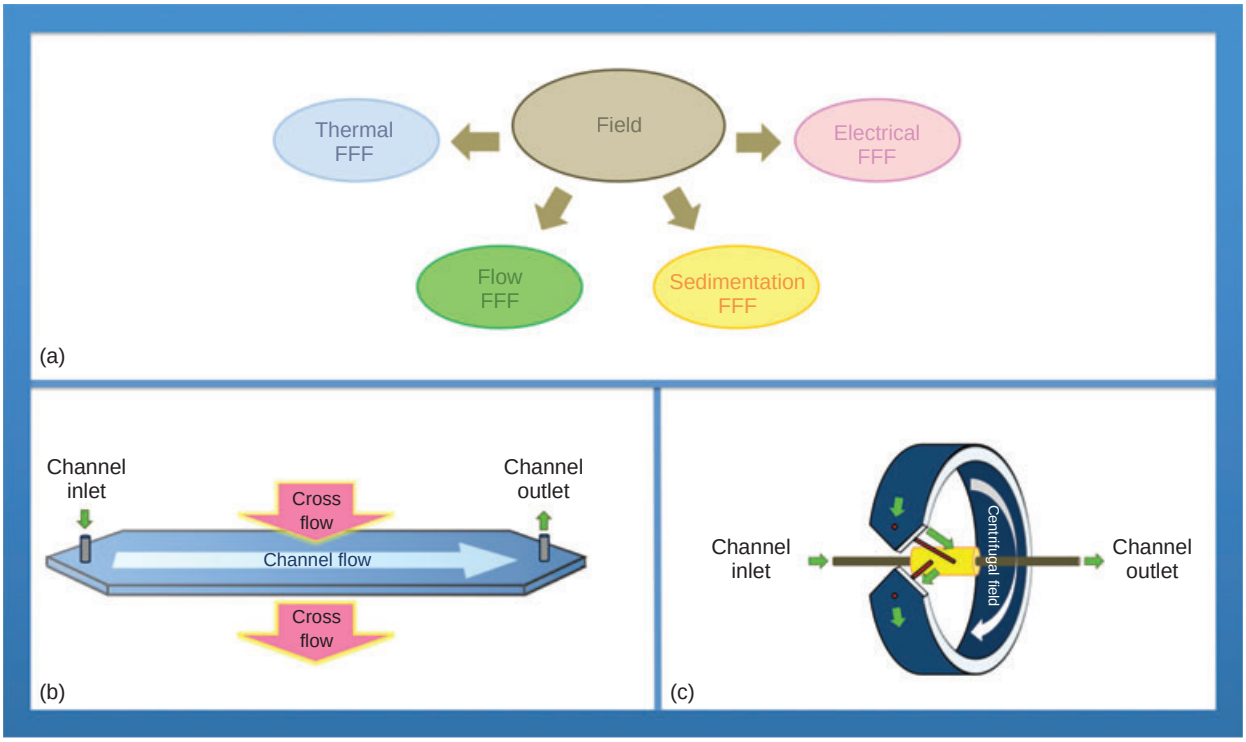

Figure 3 (a) Various FFF subtechniques. (b) Flow field-flow fractionation (FlFFF). (c) Sedimentation field-flow fractionation (SdFFF).

Figure 3. Two most commonly used subtechniques are FlFFF and SdFFF. However, the use of electrical field-flow fractionation (ElFFF) for ENPs was also reported. Therefore, the principles of these three subtechniques are described.

3.1.1 *Flow Field-Flow Fractionation*

FlFFF (or F4) is the most commonly used subtechnique. With FlFFF, a perpendicular secondary flow is applied as the perpendicular external field. Depending on where the secondary flow is generated, FlFFF can be divided into two types: symmetric flow field-flow fractionation (SF4) and asymmetric flow field-flow fractionation (AF4).

In SF4, the carrier flow rates at the inlet and the outlet of the channel are identical. The cross flow is generated by another HPLC pump that propels liquid through the top permeable ceramic frit and the bottom membrane. In AF4, the carrier flow rates at the inlet and the outlet of the channel are not equal. The top wall of the channel is impermeable, and the cross flow is generated by an excess flow rate at the channel inlet, making the carrier flow rate at the outlet smaller than that at the inlet.

3.1.2 *Sedimentation Field-Flow Fractionation*

SdFFF was developed for the separation and size determination of particle in the submicrometer to micrometer scale size range.[114,115] Similar to other FFF subtechniques, separation in SdFFF is carried out in a thin flow channel under an applied field directing perpendicular to the channel flow. The type of force applied to the particles in SdFFF is a centrifugal acceleration generated by rotating the circular channel.

3.1.3 *Electrical Field-Flow Fractionation*

ElFFF is a technique, which can separate analytes on the basis of their electrophoretic mobility and size by electric field as external field. The ElFFF separation channel is consisted of solid graphite blocks as channel walls and also acting as electrodes that are separated by Mylar spacer.[116] Two modes of separation are considered including normal ElFFF and cyclical electrical field-flow fractionation (CyElFFF). In the normal ElFFF, the constant direct current field is used to provide a perpendicular electric field across the flow channel that can separate particles in the basis of ratio between electrophoretic mobility and the size of particles. In the

Encyclopedia of Analytical Chemistry, Online © 2006–2015 John Wiley & Sons, Ltd.

This article was published in the *Encyclopedia of Analytical Chemistry* in 2015 by John Wiley & Sons, Ltd.
DOI: 10.1002/9780470027318.a9427

CyElFFF, cyclical electrical field is applied instead of the steady direct current field. The cyclical electrical field causes particles to oscillate across the channel width. Separation in CyElFFF is theoretically based on the difference in electrophoretic mobilities.[117]

3.2 Practical Considerations for Successful FFF Experiment

Several practices and precautions for experimental FFF were nicely overviewed by Moon and Myers.[118] In order to be successful in FFF experiment, several things need to be considered, i.e. carrier preparation, start-up process, sample overloading effect, and channel maintenance. Carriers used in FFF experiment should be free of particulate material and dissolved gas. Bubbles should all be removed from the channel. All carriers should be filtered through 0.2 μm filter to provide particle-free carrier liquid. Ionic strength should be carefully controlled, owing to the fact that at high ionic strength aggregation might occur. The channel should be flushed daily using carrier liquid introduced by a channel flow rate of 2–3 mL min^{-1} for an hour to stabilize the baseline. It is recommended to add an antibacterial carrier liquid within the FFF channel when the FFF channel is not used for an extended time. As the separation in FFF occurs in a very thin region (cloud layer thickness), very large amount of sample materials can cause insufficient room for particles to reach and establish equilibrium. This sample overloading subsequently affects retention level and hence physicochemical information obtained from the FFF experiment. To check the presence of sample overloading, for every unknown sample, several runs should be made with different sample loads to verify that retention times obtained from different amounts of sample injected are the same. Further, the FFF channel should be occasionally cleaned to remove all the materials that adhere to the accumulation wall over time. Excessive accumulation of sample materials can lead to a disruption and blockage of the channel flow path. Once this happens, the FFF channel should be opened up and the FFF accumulation surface should be gently rubbed and cleaned.

3.3 Applications of FFF for Engineered Nanoparticles

Using the Scopus database searching for the keywords on 'FFF' and 'nanoparticles' in recent two decades (1994 and 2004), the total numbers of 221 publications were found, as summarized in Figure 4. It is clearly seen that before the year of 2000 the report on the application of FFF for nanoparticles was not available. Nonetheless, the numbers of publication related to FFF and nanoparticles increased significantly in recent decade. Some selected applications of FFF to ENPs are summarized as follows:

Baalousha et al.[119] investigated the interactions between unpurified manufactured iron oxide NPs (~7 nm, pH ~2) and standard Suwannee river humic acid (SRHA) under a range of environmentally relevant conditions. Increasing the pH from 3 to 5, iron oxide

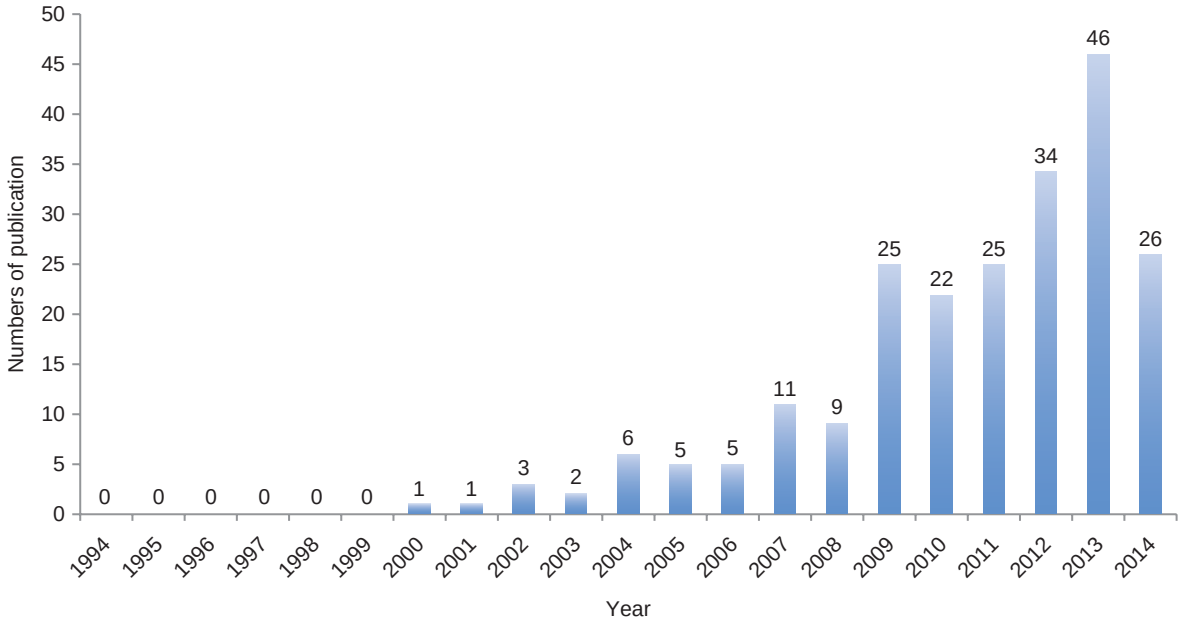

Figure 4 Publication trend on 'FFF' for 'nanoparticles' since 1994.

Encyclopedia of Analytical Chemistry, Online © 2006–2015 John Wiley & Sons, Ltd.

This article was published in the *Encyclopedia of Analytical Chemistry* in 2015 by John Wiley & Sons, Ltd.
DOI: 10.1002/9780470027318.a9427

NPs shifted to larger size and extensive aggregation was observed with the increased pH and reached a maximum at approximately pH 8.5. The adverse effect was observed with addition of SRHA, whereby aggregation was observed with lowering pH values of 4–5, which was also affected by SRHA concentration. Both pH and SRHA concentration affected on the structure and aggregation mechanism of these aggregates.

Cumberland and Lead[120] employed SF4/UV/VIS along with DLS and TEM to study the effects of pH, dissolved organic carbon, and calcium concentration for size distribution of 15-nm citrate-stabilized silver nanoparticles (AgNPs). Increasing the pH from 5 to 8 at low ionic strength (10^{-3} M of $Ca(NO_3)_2$) caused the increase in size of AgNPs. However, AgNPs were not stable at pH 5 in high ionic strength (10^{-2} M of $Ca(NO_3)_2$) at which loss of AgNPs peak was observed. In case of low ionic strength, adding the humic substance resulted in the reduction in AgNPs size, whereas at high ionic strength, the AgNPs peak disappeared almost completely, which was most likely due to aggregation.

Sermsri et al.[121] employed SF4/UV/Vis for size characterization of α-tocopherol-induced enlargement of AuNPs. α-Tocopherol played the role as catalyst for citrate reduction of $AuCl_4^-$ resulting in larger AuNPs. This catalytic effect also depended on the incubation time and concentration. Longer incubation time and higher concentration of α-tocopherol resulted in larger AuNPs.

Cho and Hackley[122] optimized the measurement conditions for analysis of AuNPs using AF4 coupled on-line with multiangle light scattering (MALS) to give the radius of gyration and with DLS to give the hydrodynamic size, and UV/Vis detectors to observe the elution of the particles. The mixture of 10–60 nm AuNPs and the mixture of AuNPs functionalized with polyethylene glycol and their unconjugated AuNPs were fractionated.

Römer et al.[123] incubated the monodisperse 7-, 10-, and 20-nm citrate-stabilized AgNPs in the *Daphnia magna* exposure media as used in (eco) toxicity studies. In the undiluted media, rapid aggregation of all AgNPs was observed. However, dilution of the media by a factor of 2, 5, or 10 could minimize aggregation. However, the smallest NPs were unstable under all media conditions. The authors concluded that dilution by ∼10 times of standard media could reduce the aggregation of AgNPs without affecting the viability of the test organism.

Calzolai et al.[124] used nuclear magnetic resonance (NMR) for analysis of citrate stabilized-AuNPs (5–60 nm) before and after fractionation by AF4. They found that the original synthetic AuNPs contained an excess of citrate; however, the free citrate was not present in the fraction from AF4. Then, it was possible to identify the presence or absence of free citrate in the various AuNPs samples.

Gigault et al.[125] demonstrated the use of AF4 for fractionation of positively charged gold nanorods (GNRs). The critical parameter was the components of carrier liquid. A mixture of ammonium nitrate and CTAB at different molar ratios enabled separation of GNRs with high recovery. Moreover, GNRs of different shapes could be fractionated. The fractionation depended on the aspect ratio (length divided by diameter) and a steric-entropic contribution, by which the higher aspect ratio eluted earlier.

Kim et al.[126] demonstrated the application of SdFFF for separation of bimodal mixtures AgNPs in the sizes range about 100 nm. The types of carrier liquid were studied and water with 0.1% FL-70 provided a good resolution. Separation could be speeded up by exploiting a flow programming, where the flow rate was linearly increased during separation, without losing much in resolution.

Böhmert et al.[127] set-up an in vitro digestion models mimicking mouth, stomach, and intestine for determination of physicochemical properties of AgNPs. A separation technique, AF4, was coupled with two different detection methods: SAXS and DLS. In saliva fluid, most AgNPs were not aggregated to larger nanoparticle size as shown by AF4 results. Owing to strongly acidic stomach and basic intestinal environment, hydrodynamic sizes of AgNPs became larger with DLS detection. With SAXS data, only small portion of AgNPs were aggregated and formed dimeric stage.

Cardot et al.[128] employed SdFFF to fractionate polydisperse TiO_2 colloidal suspension. The collected fractions were analyzed for the size distributions by electron microscopy (EM) that showed sizes between 0.2 and 0.4 μm. Further, they performed the reinjection of the collected fraction by both direct injection and preconcentration before injection. The particle size of the collected fractions appeared accurately.

Tadjiki and Deering[129] applied SdFFF to fractionate the unlabeled silica nanoparticles in the size of 70 nm, which were extracted from human endothelial cell lysate and rat lung tissue. Quantifications were obtained by considering from the area under the fractogram. The subsequent work was carried out by fractionation of a mixture of nanosized (70 nm) and submicrometer(250 nm) silicon dioxide particles added to mammalian tissue.[130] They also used fluorescence microscopy and TEM for particle-treated cell culture samples in order to allow comparison of the SdFFF results.

Contado and Argazzi[131] applied SdFFF in order to study size distributions of AuNPs that were prepared by citrate reduction method to the particles sizes around 12–65 nm. The size of AuNPs depended on the ratio of citrate/gold(III) by which the particles size decreased in the citrate/gold(III) ratio of 1 : 1 to 3 : 1 and then increased

Encyclopedia of Analytical Chemistry, Online © 2006–2015 John Wiley & Sons, Ltd.

This article was published in the *Encyclopedia of Analytical Chemistry* in 2015 by John Wiley & Sons, Ltd.
DOI: 10.1002/9780470027318.a9427

from 5 : 1 to 10 : 1 and passing through a plateau region in between.

Gigault et al.[132] demonstrated the fractionation of many kinds of nanomaterials including Fe_3O_4 and AgNPs (50 and 10 nm, respectively) by CyElFFF. Different operating parameters were investigated including the voltage, frequency, and flow rate of carrier liquid.

Somchue et al.[133] showed the applicability of ElFFF for separation and characterization of AuNPs stabilized by citrate and tannic acid. The effective field and plate height were calculated by varying the applied DC voltage and flow rate. With the same particle size, particles with lower electrophoretic mobility eluted earlier than those with higher electrophoretic mobility. For particles with the same stabilizing agent, particles with smaller size eluted earlier than the bigger particles.

Tasci et al.[134] demonstrated that using biased cyclical electric fields, by which the duration of the positive cycle voltage was applied longer than the negative cycle voltage, were able to separate nanoparticles smaller than 50 nm. They were able to separate a mixture of 15- and 40-nm AuNPs in high resolution by varying the voltages, frequency, and the magnitude of percentage duty cycle. A theoretical analysis to accomplish these separations was also given.

Rasouliet al.[135] showed the applicability of gravitational field-flow fractionation (GrFFF) for separation and characterization of polydisperse submicrometer TiO_2 powder into two groups: spherical particles with an average diameter of 0.31 mm and ellipsoidal particles with a 0.45-mm hydrodynamic diameter. Electrolyte and surfactant characteristics in the carrier phase and the sample concentration strongly affected on the elution peaks.

4 ELEMENT DETECTION OF ENGINEERED NANOPARTICLES

Various analytical methods are available for element detection of ENPs. However, this article focuses on atomic spectrometric techniques, such as graphite furnace atomic absorption spectrometry (GFAAS), ICP-OES, ICP-MS, and single-particle inductively coupled plasma mass spectrometry (SP-ICP-MS), which are widely used as quantitative detection of ENPs as either on-line or off-line coupling to FFF. The brief principles of each technique and their applications on ENPs are summarized.

4.1 Graphite Furnace Atomic Absorption Spectrometry

GFAAS is a powerful atomic spectroscopic technique based on electrothermal atomic absorption spectrometry (ETAAS) in a graphite furnace. GFAAS differs from flame atomic absorption spectrometry (FAAS) by the use of much higher atomization temperature (up to 3000 K). The operation in GFAAS determination starts by dispensing a known volume of sample into a graphite tube (3–5 cm in length and a few millimeters in diameter) through a tiny hole in the center of the tube wall. Both ends of the tube are open to allow the light from the radiation source to pass through and for the removal of sample constituents after the analysis. The sample is then subjected to electrical heat controlled by a multistep temperature program including drying, pyrolysis, and atomization. The limit of detection (LOD) of GFAAS is 10–100 times better than FAAS.[136,137] Two examples of GFAAS for detection of ENPs are summarized as follows:

For GFAAS detection, Gagné et al.[138] stated that the particle size of ENPs affected on the sensitivity of detection. In their study, the effects of atomization temperatures were examined on Ag of different sizes (20, 60, and 80 nm) at the same nominal Ag concentration of 10 ng mL^{-1}. The dissolved Ag (0.15 nm) was also investigated for comparison purpose. The increase in the molecular size of Ag led to increased atomization temperatures: ionic Ag readily atomized at $1400 \pm 25^{\circ}C$, whereas 20-, 60-, and 80-nm nano-Ag readily atomized at $1550 \pm 30^{\circ}C$, $1600 \pm 20^{\circ}C$, and $1700 \pm 33^{\circ}C$, respectively.

Hartmann et al.[139,140] developed cloud point extraction (CPE) method for the extraction of ionic silver species, silver nanoparticles, ionic gold species, and gold nanoparticles with further detection by ETAAS. Separation of ionic silver species was achieved by addition of EDTA as a ligand to chelate silver ion, whereas silver nanoparticles (AgNPs) in environmental samples were extracted using Triton X-114 to form cloud. For gold species, Triton X-114 was used as a collecting phase for AuNPs, whereas sodium thiosulfate was used as a complexing agent for ionic gold species.

4.2 Inductively Coupled Plasma Optical Emission Spectrometry and Inductively Coupled Plasma Mass Spectrometry

Both ICP-OES and ICP-MS exploit plasma as a high-energy source to accommodate desolvation, vaporization, atomization, ionization, and excitation. Liquid sample is nebulized using a nebulizer to produce fine aerosols that are further transported with argon into the ICP torch. With high temperature of around 5000–8000 K in the ICP plasma, the sample aerosols undergo evaporation, atomization with subsequent excitation and ionization.[141] With ICP-OES, the light emission at a specific wavelength, induced by excitation of atoms or ions in the plasma, is detected. With ICP-MS, a mass

Encyclopedia of Analytical Chemistry, Online © 2006–2015 John Wiley & Sons, Ltd.

This article was published in the *Encyclopedia of Analytical Chemistry* in 2015 by John Wiley & Sons, Ltd.
DOI: 10.1002/9780470027318.a9427

spectrometer is used to separate and quantify the ions of different elements.[142] Two applications of ICP-OES and ICP-MS for detection of ENPs are given as examples as follows:

Helfrich and Bettmer[143] applied liquid chromatography (LC) and gel electrophoresis (GE) coupled to ICP-MS for the characterization of synthesized AuNPs. The LC-ICP-MS approach was optimized for monitoring the formation of citrated-stabilized AuNPs. With GE-ICP-MS, the Au^+/S^+-ratios in AuNPs covered by mercapto succinic acid (MSA) were determined. These ratios were used for further characterization of the nanoparticles. In addition, electrospray ionization-mass spectrometry (ESI-MS) was applied as a complementary technique for detection of molecular components of AuNPs.

Geertsen et al.[144] performed the systematic study based on the ICP-OES and ICP-MS measurement of TiO_2 NPs suspensions. Sample treatment was examined and the measurement was performed in the concentration range from 10 ppb to 30 ppm. Soft sonication was used during sample treatment, and internal standard addition was used during measurement. The procedure was applied to detect titanium in Seine River water with the total amount of 48.7 ppb titanium found. The result was in good agreement with the result of the reference method.

4.3 Single-Particle Inductively Coupled Plasma Mass Spectrometry

SP-ICP-MS provides information about particle size distribution and particle number concentration. In SP-ICP-MS operation, sample needs to be very diluted and the sample introduction flow rate is set to be relatively slow to attain very low particle number concentration. A very short dwell time (10 ms or less) is acquired for each reading. The intensity from each reading is plotted individually as a function of time. The intensity is related to particle mass and hence particle diameter, whereas the frequency of the pulses is directly related to the number concentration of the particles.[145] A brief concept of SP-ICP-MS is illustrated in Figure 5.

In 2003, Degueldre and Favarger[146–148] reported the first application of SP-ICP-MS for the study of model colloids (rutile, alumina, and goethite) and natural clay (montmorillonite). Thorium colloid particles or thorium sorbed on clay colloids in water were analyzed. With the plasma design used in their experiment, thorium colloids down to 10 fg and gold colloid suspension in water of sizes ranging from 80 to 250 nm were detectable. The size detection limit was around 25 nm corresponding to 0.15 fg colloids.

Hu et al.[149] proposed a highly sensitive immunoassay based on SP-ICP-MS using AuNPs with an average

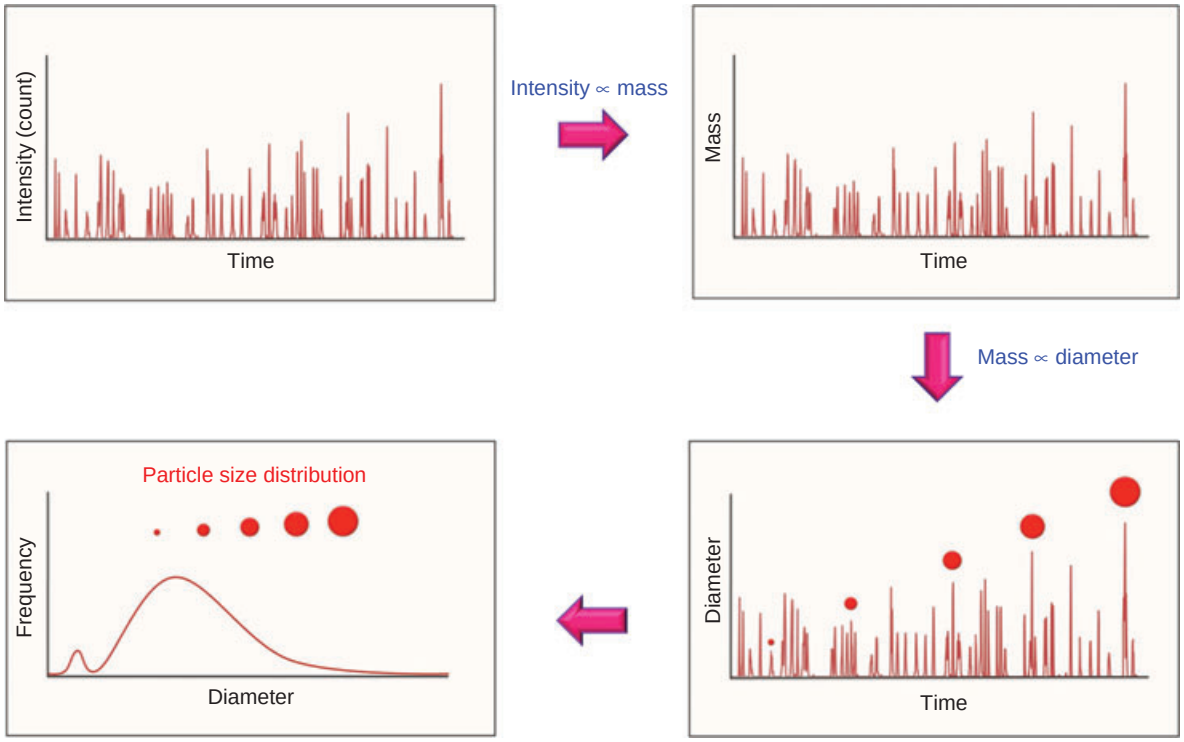

Figure 5 Schematic diagram representing the concept of SP-ICP-MS.

Encyclopedia of Analytical Chemistry, Online © 2006–2015 John Wiley & Sons, Ltd.

This article was published in the *Encyclopedia of Analytical Chemistry* in 2015 by John Wiley & Sons, Ltd.
DOI: 10.1002/9780470027318.a9427

diameter of about 20, 45, and 80 nm serving as model tags. The antibodies tagged with AuNPs were quantitatively detected based on the good correlation between the frequency of transient signals and the concentration of antibodies. The smallest detectable size of AuNPs tags was approximately 15 nm. The developed protocol was applied for a competitive immunoassay of α-fetoprotein with the linear range 0.016–6.8 μg L^{-1} (between 20% and 80% inhibition). The limit of quantification was 0.016 μg L^{-1} (20% inhibition, IC_{20}) with a relative standard deviation of 4.2% (20% inhibition, 4 replicates) for α-fetoprotein.

Pace et al.[145,150] reported a practical guide on how to count and size nanoparticles using SP-ICP-MS. The developed protocol was used for characterization of mono-dispersed AgNPs. Furthermore, the same group of the authors also assessed the sizing capabilities of SP-ICP-MS for four AgNPs dispersions (nominal diameters of 40, 60, 80, and 100 nm) compared to DLS, differential centrifugal sedimentation (DCS), nanoparticles tracking analysis (NTA), and transmission electron microscopy (TEM). With SP-ICP-MS, size characterization of AgNPs together with particle number concentrations was possible. The accuracy obtained from the developed SP-ICP-MS was similar to the other commercially available techniques.

Mitrano et al.[151] demonstrated the use of SP-ICP-MS to detect and quantify two products containing AgNPs. The first product was AgNPs with precisely manufactured size and shape, and the second product was a commercial health product containing AgNPs. Dissolved and particulate silver (Ag) could be differentiated. The developed SP-ICP-MS was applied to two wastewater samples containing Ag concentrations at nanograms per liter level. AgNP was found at 100–200 ng L^{-1} in the presence of 50–500 ng L^{-1} dissolved Ag.

Reed et al.[152] reported the feasibility of SP-ICP-MS for detection and size characterization of metal-containing ENPs such as Ag nanowires, TiO_2, ZnO, and CeO_2. The particle size distributions obtained from SP-ICP-MS were in good agreement with those from SdFFF.

Gray and coworkers[153] applied SP-ICP-MS to investigate ENPs in various biological tissue samples including, beef, *Daphnia magna*, and *Lumbriculus variegatus.* The tissues were extracted by alkaline digestion procedure before SP-ICP-MS detection. From the results, Ag could be separated from AgNPs of 60 and 100 nm particles by extraction procedure. The authors mentioned that this established method could be applied to a wide range of tissues.

Tuoriniemi et al.[154] investigated the potential of SP-ICP-MS for detection of AgNPs in waste water treatment plant effluent sample. To minimize the size detection limit, the shortest possible dwell time of 0.1 ms was used. The authors commented that it would be interesting to adapt the developed concepts for simultaneous multielement detection.

5 HYPHENATION BETWEEN FFF WITH ATOMIC SPECTROMETRIC DETECTION

Coupling between FFF with atomic spectrometric detection can be as either off-line or on-line, as illustrated in Figure 6. With off-line detection, the fraction from FFF is collected for further detection by atomic spectrometric techniques. The element fractogram is not a continuous plot. However, with on-line detection, the eluted fraction is introduced directly into the sample introduction part of the atomic spectrometric techniques, and therefore, the element fractogram is a continuous plot.

5.1 FFF with ETAAS

Although ICP-MS is extremely sensitive and is considered as a speedy way to acquire analytical information, the limited availability of ICP-MS and its relatively high equipment cost reduced its broad applicability. As an alternative approach, ETAAS has been used as an element detector after size separation. Electrothermal AAS also offers good sensitivity and slurry analysis capability. Nonetheless, most ETAAS instruments are not equipped with simultaneous multielement analysis features. Therefore, this can limit the use of ETAAS as compared to ICP-MS. Yet, when the information of only a few elements is sought, ETAAS can be quite useful.

In 1995, a group of researchers from Italy and Spain first introduced ETAAS as an off-line detection for SdFFF of clay analysis.[155] Aluminum and Si were determined quantitatively, and the limits of detection were 63.6 and 212.4 ng for Al and Si, respectively. Two years later, the same research group, together with Beckett, extended their work to the elemental characterization of water-borne river particles (Po river).[156] The first on-line SdFFF–ETAAS was reported in 2001 for the analyses of Fe in a synthetic model colloid and a reservoir sediment and Cu in a soil sample.[157] Those applications were limited to the particle size of <1 μm. Applications of GrFFF[158] and split flow thin cell fractionation (SPLITT)[159] with ETAAS were reported. In the GrFFF experiment, size separation was tested for 5- and 10-μm HPLC silica particles coated with a thin layer of goethite.[158] With SPLITT fractionation, the applicability range was extended to 25-μm particle size.[159,160]

Encyclopedia of Analytical Chemistry, Online © 2006–2015 John Wiley & Sons, Ltd.

This article was published in the *Encyclopedia of Analytical Chemistry* in 2015 by John Wiley & Sons, Ltd.
DOI: 10.1002/9780470027318.a9427

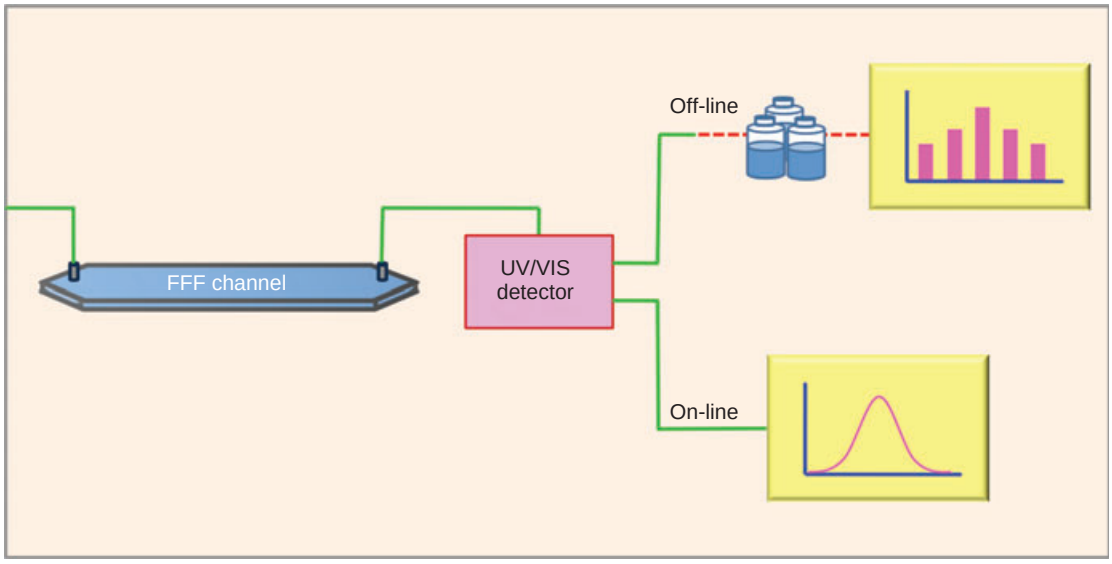

Figure 6 Hyphenation between FFF and atomic spectrometric detection.

5.2 FFF with ICP-OES

In practice, ICP-OES offers advantages over ICP-MS and ETAAS in some circumstances. For instance, ICP-OES is capable of determining major elements, e.g. K and Ca, which are difficult to be determined even with high-resolution ICP-MS. For minor and trace constituents, however, the higher sensitivity of ICP-MS or ETAAS is often required. One might argue that ETAAS is only more sensitive than the ICP-radial view-OES but not the ICP-axial view-OES. The classical ICP-axial-view-OES suffered greatly from matrix interferences, which might make the technique less attractive. Nonetheless, with ICP-axial view-OES, matrix interferences are significantly reduced and hence could improve detection limits of many elements, the FFF-ICP-OES should also be considered, as it provides multielements detection capability with lower cost than FFF-ICP-MS. Some of the literatures reported the use of the FFF-ICP-OES.[160,161]

5.3 FFF with ICP-MS

Optical detectors (spectrophotometric and light-scattering detectors) have been generally used to detect the fractionated materials eluted from the FFF channel.[162] However, this detector type gives information only on the size distribution of the macromolecules or colloidal materials that interact with light. To obtain information about the chemical composition of the colloids or macromolecules in different size ranges, element-specific detectors (e.g. atomic absorption, X-ray fluorescence, or inductively coupled plasma spectrometries) must be used. Practically, only less than 1 mg of sample is required for fractionation in carrier stream flows of 1–2 mL min^{-1}. High sample concentration may cause overloading effects in the FFF channel. With low sample concentration (e.g. < 0.5 mg mL^{-1}), however, very sensitive analytical techniques must be used. As ICP-MS provides excellent sensitivity, low detection limits, extended linear dynamic range, and multielement analysis with limited interferences,[163] ICP-MS is an ideal element-specific detector for FFF.[164] In addition, slurry atomization from solid-phase particulate matter can be achieved in the plasma source.[163] At the same time, FFF adds a dimension of selectivity to ICP-MS measurement by separating the individual elemental species into different size fractions. The combination of the two techniques offers size-based elemental speciation in a single run. Furthermore, the interface between the FFF system and the ICP-MS instrument is rather straightforward owing to the compatibility between the flow rates generally used in the FFF separation and the ICP-MS sample uptake rate. Therefore, no major instrumentation modification is needed to couple FFF directly to ICP-MS.

FFF-ICP-MS can be applied in numerous fields. As can be seen in Figure 4, the applications of FFF to nanoparticles were not available before the year of 2000. Therefore, the applications of FFF-ICP-MS before the millennium were mostly related to environmental samples but not ENPs. The analyses of natural suspended particulate matter, soil, and clay minerals by SdFFF-ICP-MS[161,165–167] and by FlFFF-ICP-MS[168,169] were described. Applications

Encyclopedia of Analytical Chemistry, Online © 2006–2015 John Wiley & Sons, Ltd.

This article was published in the *Encyclopedia of Analytical Chemistry* in 2015 by John Wiley & Sons, Ltd.
DOI: 10.1002/9780470027318.a9427

of FFF-ICP-MS to biological[170,171] and industrial materials[172] were also reported.

5.3.1 Biological Applications

Although several biological applications of FFF were reported as reviewed by Levin[173], only one application of FFF-ICP-MS to biological samples was reported before the millennium.[171] In 1993, Barnes briefly predicted that FFF-ICP-MS should be an alternative technique for elemental speciation in biomedical samples.[174] The idea was also suggested in the review on analytical plasma source mass spectrometry in biomedical research in 1996.[175] A feasibility study of FFF-ICP-MS was first reported for protein standards.[171] In this preliminary work, the effect of the FlFFF cross flow rate was examined for separation of a carbonic anhydrase and alcohol dehydrogenase mixture. Preliminary studies with FlFFF-ICP-MS were applied to several protein standards including metallothionein, carbonic anhydrase, ceruloplasmin, alcohol dehydrogenase, and thyroglobulin. Cadmium was detected in metallothionein; Cu and Zn in carbonic anhydrase, alcohol dehydrogenase, and ceruloplasmin; and I in thyroglobulin. As the coupling between FFF and ICP-MS was quite simple and FFF was capable of protein fractionation, FFF-ICP-MS was expected to be a valuable tool for speciation of metal binding proteins.

5.3.2 Environmental Applications

FFF-ICP-MS provides size-based elemental speciation information. This approach was applied successfully to various environmental and geological samples. In general, elemental concentration across size distribution information is obtained. This information can be important and useful to gain insight into metal transport and fate. Brief findings of FFF-ICP-MS experiments on environmental applications are summarized in the following sections.

5.3.2.1 Aquatic Samples In 1993, Murphy et al.[176] investigated changes in elemental composition as a function of particle sizes of suspended particulates from the Darling River. Atomic ratio distribution plots were illustrated for various pairs of elements (Al, Mg, Rb, and Si). All the element atomic ratios with Si showed substantial decrease with larger particle sizes. This might be due to an increase amount of SiO_2 fractions with increased particle size. The Mg:Al ratio showed significant decrease with increased particle sizes, whereas the Rb:Al ratio was almost constant throughout the whole particle size range (0.08–0.45 μm). These findings suggested that Mg and Rb were not present in the same proportion.

The effect of colloidal surface coatings on the adsorptive behavior of orthophosphate in river was investigated.[177] The surface adsorption density of orthophosphate increased with increased particle size.

Hassellöv et al.[166] applied SdFFF-ICP-MS to study trace metal adsorption processes onto aquatic colloids. The elements investigated included Cd, Cs, Cu, La, Pb, and Zn. Adsorption experiments were conducted with various amounts of metal loadings and at different pH conditions. The goal was to examine whether the adsorption occurred at a certain size range. Experiments at different pH distinguished between surface complexation (pH dependent) and ion exchange adsorption (pH independent). The aims were to get insightful information on the uptake processes, the transport, and fate of trace metals in aquatic systems.

Early FFF-ICP-MS studies were reported for SdFFF. In 1999, the first application of FlFFF-ICP-MS was described by Hassellöv et al.[168] for elemental size characterization of colloids in natural water. Twenty-eight elements in a small freshwater creek in Sweden were determined, and the results of six selected elements were illustrated. In their experiment, an on-channel preconcentration procedure allowing large volume sample introduction was used to provide preconcentration factor of about 1000 times. Different distribution patterns were observed for each element, indicating their dissimilar behaviors in aquatic environment. According to Hassellöv et al.,[168] colloidal nickel was mainly associated with the carbon and possibly with the smaller iron fraction. Lead was associated with the larger iron-based colloids, whereas La was bound to both the organic and inorganic colloids. Molybdenum coemerged with the void peak, suggesting that Mo occurred as dissolved molybdate ions, which were partially retained in the channel during the preconcentration step by charge repulsion from the membrane surface.

Similar investigations using an on-channel preconcentration FFF before ICP-MS detection were applied to characterize colloidal samples in sewage water from Amherst wastewater treatment plant (WWTP).[169] Three types of water, including influent sewage water, sewage after primary treatment, and effluent water, were tested for 10 different elements. A 1.0-mL aliquot of wastewater samples was introduced into the FlFFF channel instead of the typical injection volume (20 μL). With this, preconcentration factor of 50-fold was obtained. The entire volume of sample was loaded through the back end of the channel using focusing flows. Then, the cross flow stream was introduced, so that the sample could reach steady-state equilibrium. Reasonable trends of decreasing elemental and colloidal concentrations as the water treatment process proceed were achieved.

Encyclopedia of Analytical Chemistry, Online © 2006–2015 John Wiley & Sons, Ltd.

This article was published in the *Encyclopedia of Analytical Chemistry* in 2015 by John Wiley & Sons, Ltd.
DOI: 10.1002/9780470027318.a9427

In addition, elemental distribution patterns also changed along the course of the treatment.

5.3.2.2 Clay Minerals, Soil, and Sediment Samples Murphy et al.[176] studied the changes in chemical composition of clay minerals kaolinite and illite, as a function of particle size by plotting appropriate element atomic ratio distributions. Atomic ratio distribution plots were illustrated for Si:Al, Mg:Al, and Rb:Al in an illite sample. Those atomic ratios were constant across the entire size distribution showing that the illite sample had a uniform composition. The authors further suggested the use of a tracer element, so that the size distribution of one component could be singled out from a mixture. Plots of atomic ratio against particle size for appropriate elements were constructed to monitor the changes in elemental composition as a function of particle size.

In 1999, Ranville et al.[165] examined the applicability of SdFFF-ICP-MS to the analysis of horizon soils collected from Mountain Bold in South Australia. They used a 1 mmol L^{-1} sodium pyrophosphate solution with 0.02% sodium azide as a carrier liquid for SdFFF with 100 ng mL^{-1} In as an internal standard for ICP-MS to correct for noise and drift. Attempts to determine Si ($m/z = 28$), another major element present in the sample, were unsuccessful owing to spectral interferences from diatomic species (N_2^+ and NO^+). They compared the results of direct slurry with digested sample nebulization. Disagreement between the two approaches occurred when particles of larger than 1 μm were introduced into the ICP-MS, indicating that either the transfer of particles through the spray chamber or the atomization of the particles in the plasma was incomplete. Yet, the results for particles smaller than 1 μm by the two sample introduction techniques agreed, confirming the quantitative nature of direct particle analysis by ICP-MS for colloidal samples.

Schmitt et al.[178] investigated the influence of natural organic matter on the adsorption of Al, Fe, Pb, and Zn onto clay minerals. Aggregation of clay particles decreased in the presence of natural organic matter and at high pH values.

The scope of FFF-ICP-MS was further extended not only to study elemental size distribution but also to determine the distribution of potentially available heavy metals within the colloidal fractions (0.05–1 μm) in Cu- and Pb-contaminated soils.[167,179] The metal bioavailability was assessed using a selective extraction. To identify the exchangeable, reducible, or complexed target phases, diluted acetic acid, hydroxylamine hydrochloride, or ethylene diamine tetraacetic acid (EDTA) disodium salt, respectively, was used as extractants. Size distributions of Al, Cu, Fe, Mn, and Pb in colloidal fractions were characterized before and after EDTA extraction. With these chemical pretreatments, the authors were able to identify which size fractions of soil colloids contained the largest fraction of potentially bioavailable heavy metals. The element atomic ratio distributions (i.e. Cu:Al, Fe:Al, Mn:Al, and Pb:Al) were used to follow the changes in soil colloid chemistry.

Elemental size distributions were characterized for river and estuarine sediment core samples collected from two sites in New Jersey.[180] Sediment samples were extracted using sodium pyrophosphate. Distributions of analyte elements as functions of hydrodynamic diameters and core depth levels (depth profile fractograms) were represented as the three-dimensional surface plots. Patterns of these two samples were significantly different by which the size distributions of Cape May sediments were slightly broader than those of Hackensack sediments. Differences in humic acid sizes found in two sediments probably were due to different types of humic acids or aggregate formation.

5.3.2.3 Humic Substances Humic substances are well known for their ability to bind and form complexes with metal ions. Flow FFF coupled with ICP-MS enables the simultaneous characterization of molecular weight distribution of humic acid macromolecules and investigation of heavy metals bound to them. Size characterization of trace metals (Al, Cu, Cd, Pb, and Zn) complexed to soil-, peat-, and compost-derived humic acids was reported.[169] Furthermore, physical parameters such as the diffusion coefficient (D) and hydrodynamic diameter (d_h) were determined. For all humic acids studied, fractograms were found to be monomodal with good reproducibility. The molecular weights at peak maximum (M_p) for all humic acids studied were about 3850 Da and their M_p ranged from 3950 to 3790 Da indicating a very small variation in molecular sizes. The diffusion coefficients of humic acids varied from 1.66×10^6 to 1.72×10^6 cm^2 s^1. The study demonstrated how the FlFFF-ICP-MS could be used not only to acquire elemental speciation and molecular weight information under gentle separation conditions presumably without perturbing the humic molecules but also to obtain the important physical and chemical information about the mobility characteristics of humic substances. Moreover, possibilities of using FFF-ICP-MS to study the aggregation of humic acids in the presence of divalent metal ions were also suggested.[169,181]

Crude isolation of humic substances from the sediment samples was also investigated.[180] By adjusting the pH of sediment extracts, humic and fulvic acids were isolated. Size distributions of Fe, Ni, and Pb in extracted fulvic and humic fractions were characterized. Distinct peaks of fulvic ($d_p \sim 3$ nm) and humic acids ($d_p \sim 5$ nm) were obtained, providing evidence that sediment extracts

Encyclopedia of Analytical Chemistry, Online © 2006–2015 John Wiley & Sons, Ltd.

This article was published in the *Encyclopedia of Analytical Chemistry* in 2015 by John Wiley & Sons, Ltd.
DOI: 10.1002/9780470027318.a9427

contained both fulvic and humic components. Humic acids were well resolved from the void peak. Under the operating conditions used, fulvic fractions partly coeluted with the void peak. The observation of two distinct peaks of fulvic and humic acids provided clear proof that FlFFF was capable of separating humic substances. Individual peaks at 3 (fulvic) and 5 nm (humic) after chemical isolation of these two macromolecules by pH adjustment confirmed their coexistence in the sediments.

5.3.3 *Industrial Applications*

Flow FFF-ICP-MS was applied to study elemental size distributions of chemical mechanical polishing slurries to demonstrate the scope of the technique with industrial materials.[172] Particle size information, including size distribution, minimum and maximum particle sizes, average and mean diameters, polydispersity, and breadth of distribution, were characterized for 18 alumina and silica slurry samples. Iron, Pb, Ti, and Zr were also detected by ICP-MS after on-line size separation by FlFFF to evaluate the presence of coexisting elements with alumina and silica polishing slurries. By knowing the exact geometry of FlFFF channel, experimental retention time can be converted into hydrodynamic diameter (d_h) without standards of known diameters to calibrate the FlFFF channel.

Mixed mode retention (normal and steric modes) might occur in the separation of these chemical mechanical polishing slurries. Steric inversion is the point where particles of larger size elute earlier than the smaller components.[182] This steric inversion, which is usually taken place at around 1 μm, could lead to inaccurate particle size information. Nonetheless, to avoid steric effects, sample filtration was necessary before sample injection to remove particles of larger than 500 nm. However, particle size distribution of chemical mechanical polishing slurry might be changed upon sample pretreatment. To obtain accurate and reliable size information, independent methods (e.g. light scattering) might be used to verify the analytical results obtained.

Considering the particle size limitations with ICP sample introduction, small diameter particulates ($\leq$8 μm) can be introduced directly into the plasma as long as the amount of the solids injected is relatively small. With the particle diameter of larger than 8 μm, plasma energy might not be sufficient to evaporate and decompose the sample matrices.[183] Therefore, applicable particle size range is limited between 2 and 500 nm, when the normal-mode FFF separation with direct ICP-MS detection is used. Nonetheless, for submicrometer-sized industrial particles, the steric-mode FFF separation with electrothermal vaporization (ETV)-ICP-MS might be considered. On the basis of other FFF reports, despite its limited documentation, numerous applications of FFF to the characterization of industrial products were carried out.[184] Most of those applications were of proprietary materials and hence were not reported in the scientific literature. The proposed FFF-ETV-ICP-MS or FFF-ETV-ICP-OES provides the potential for process control applications of raw and processed materials (e.g. cement, nanoparticles, and pigments)

6 APPLICATIONS OF FFF WITH ATOMIC SPECTROMETRIC DETECTION FOR ENGINEERED NANOPARTICLES

The use of FFF coupled with atomic spectrometric detection has been reported. Some researchers examined the advantages and disadvantages of the technique compared with other techniques. The analytical features of the techniques were evaluated. The hyphenated techniques of FFF with atomic spectrometric detection were found useful in various applications for detection of ENPs in food, consumer products, and biological and environmental samples.

Hagendorfer et al.[185] placed an on-line DLS detector between AF4 and on-line ICP-MS in order to determine the mass and number size distributions simultaneously without the need of either size or mass calibration. The results showed a good size characterization in AgNPs containing products although the samples have different degrees of polydispersities. This proposed method was shown to be more reliable than using the batch-DLS and clearly faster than using TEM. However, the limitation of this method was due to poor sensitivity of the on-line light-scattering detector for nanoparticles smaller than 10 nm. Then, higher concentration was required for injection in order to obtain reliable results for such small particles.

Mitrano et al.[186] compared the advantages and limitations of SP-ICP-MS and AF4-ICP-MS for silver nanoparticles detection. SP-ICP-MS was considerably more sensitive than AF4-ICP-MS (ng L^{-1} vs μg L^{-1}, respectively) and offered the unique ability to differentiate dissolved and nanoparticulate fractions of total metal. AF4-ICP-MS could detect a much smaller NP size (2 nm vs 20 nm for SP-ICP-MS) and provide better size resolution.

Geiss et al.[187] described a method based on AF4 with ICP-MS and UV/VIS detection. Prechannel injections were developed to measure size and mass of nanoparticles by simultaneously injection several sizes and concentration of AgNPs standard reference materials. Comparing to postcolumn with ionic standard solution, a series of standards could be analyzed under exactly the same conditions. However, the limitation of this method was

Encyclopedia of Analytical Chemistry, Online © 2006–2015 John Wiley & Sons, Ltd.

This article was published in the *Encyclopedia of Analytical Chemistry* in 2015 by John Wiley & Sons, Ltd.
DOI: 10.1002/9780470027318.a9427

due to the lacking of AgNPs with different sizes and concentrations.

6.1 Environmental and Biological Samples

Songsilawat et al.[188] used SF4/UV/VIS with off-line electrothermal atomic absorption spectrometry for size characterization of AgNPs in the aquatic system. Upon incubation of three types of AgNPs (9 nm of citrate, 19 nm of pectin, and 45 nm of alginate-stabilized AgNPs) with natural waters, i.e. tap water, seawater, and ground water, rapid changes in particle size of AgNPs were observed. Citrate-stabilized AgNPs were the least stable in comparison with that of pectin stabilized and alginate-stabilized AgNPs, respectively. The results suggested that the surface property was the key factor that controlled the stability of AgNPs in aquatic system and humic acid was found to prolong the stability of AgNPs in the environment.

Poda et al.[189] developed an SF4–ICP-MS method for the characterization of AgNPs mixtures and applied to AgNPs suspensions and those in biological tissue. They spiked the polyvinylpyrrolidone (PVP)-coated AgNPs to freshwater sediment for 2 weeks. Then, the freshwater oligochaete *Lytechinus variegatus* was left in the sediment for 28 days. After that, the freshwater oligochaetes were removed from the sediment and AgNPs were extracted from these tissues which were then analyzed by FFF-ICP-MS. The size of AgNPs increased from approximately 31–46 nm. The increase in AgNPs size might be due to the removal of PVP coating by biological mechanisms or abiotic reactions in the soil exposure medium resulting in destabilized AgNPs.

Hoque et al.[190] applied AF4 for size characterization of AgNPs in aqueous matrices, lakes, river, and untreated wastewater, collected from a municipal WWTP. Off-line ICP-MS was used in order to quantify AgNPs. The fractionation of a mixture of AgNPs standards (20, 40, and 60 nm) showed a well-resolved fractogram. AgNPs were not detectable in the surface water; however, they were detected in the untreated wastewater in the size of 9.3 nm (The method detection limit was 0.80 ng mL^{-1}). The size of 9.3 nm was measured by comparing the retention time with the particle size calibration curve. However, this value was not corresponded with the value obtained using the Stokes–Einstein equation to calculate the size, which yielded the size of 3.2 nm. This error might be due to the use of an inappropriate value for viscosity in the Stokes–Einstein equation.

Gondikas et al.[191] examined several methodological approaches to detect TiO_2 nanomaterials released from sunscreen products into the Old Danube Lake (Vienna, Austria) and able to identify TiO_2 NPs stemming from sunscreens in the suspended matter of the lake using EM. Bulk analysis of suspended particulate matter clearly showed an increase in Ti-containing particles during the summer season.

Schmidt et al.[192] connected the ICP-MS with AF4-MALS-DLS in order to measure the amount of AuNPs in the sizes of 10–60 nm after fractionation. The LOD of 0.02–0.4 ng Au was obtained, but the LOD increased when the particle sizes were larger. Further, they applied this system to characterize AuNPs in livers of rats after intravenous injection. The livers were solubilized in tetra methyl ammonium hydroxide (TMAH). The bovine serum albumin (BSA) was used for stabilization in the TMAH medium to prevent the aggregation of AuNPs. The soluble AuNPs from rat livers could not be fractionated, owing to their elution in the non-Brownian (steric) elution in AF4. TEM results indicated that AuNPs were associated with undissolved portion, which remained in the liver tissues.

6.2 Consumer Products and Food-Related Samples

Contado and Pagnoni[193] showed the ability of SF4 for fractionation of titanium dioxide particles in the range 0.1–0.2 μm and proposed an extraction method for determining the size and amount of titanium dioxide particles in a commercial sunscreen product (with sun protection factor of 50). The fractions of TiO_2 were collected after fractionation by SF4 and measured the amount of TiO_2 by ICP-OES.

Contado and Pagnoni[194] reported the use of ICP-MS for nano- or micro-TiO_2 particles determination in commercial cosmetic formulations. Square wave voltammetry (SWV) and ICP-OES were employed to determine the amount of TiO_2 in six foundation creams sold in Italy and the United States. SdFFF and FlFFF were exploited to characterize the sizes of the particles contained in the foundations by analyzing aqueous slurries obtained from solvent extraction procedure. The higher amount of TiO_2 was found in the sample commercialized in the United States with the TiO_2 declared as ~11% w/w, whereas all samples commercialized in Europe (Italy) had a lower TiO_2 content of approximately <8% w/w.

Samontha et al.[195] determined the size distributions of TiO_2 in sunscreen products. They used hexane for removal of organic components before fractionation by SdFFF. ICP-MS was used in order to determine the concentrations of TiO_2. The concentrations of TiO_2 analyzed by both on-line SdFFF-ICP-MS and off-line SdFFF-ICP-MS after acid digestion were in good agreement, indicating that ICP-MS could atomize and ionize the TiO_2 particle without the need for acid digestion of the samples. The obtained size distributions of TiO_2 were larger than 100 nm in most sunscreen

Encyclopedia of Analytical Chemistry, Online © 2006–2015 John Wiley & Sons, Ltd.

This article was published in the *Encyclopedia of Analytical Chemistry* in 2015 by John Wiley & Sons, Ltd.
DOI: 10.1002/9780470027318.a9427

samples and concentrations of TiO_2 were higher for the products of higher sun protection factor values.

Nischwitz and Goenaga-Infante[196] compared and optimized two extraction methods for titanium dioxide nanoparticles analysis in sunscreen samples using AF4-ICP-MS (steric elution mode). The first method was applied for particles that were resuspended by tip sonication before defatting by hexane. The second method was applied for particles that were defatted first and then the residue was suspended in water without any sonication. The authors suggested that using hexane for defatting first followed by reextraction by bath sonication offered clear advantages in terms of simplicity, relatively low cost, and high compatibility with the FFF conditions. Further, they presented a novel approach by spiking with aluminum-labeled titanium dioxide reference particles for studying the effect of extraction and separation conditions in real sample matrix.

Kim et al.[197] demonstrated the use of SP-ICP-MS for the analysis of size distributions and concentrations of two types of TiO_2 nanoparticles, rutile and anatase, after fractionation by SdFFF. The results suggested that SP-ICP-MS could be a powerful tool for broad size distribution analysis of nanoparticles when combined with a particle separator such as SdFFF.

López-Heras et al.[198] proposed the method based on AF4-ICP-MS for size characterization and element quantification of rutile titanium dioxide nanoparticles (TiO_2 NPs) in cosmetic and food products. Size characterization was carried out using particle size calibration curve constructed from polystyrene latex standards and compared with the size observed by TEM. However, one problem for quantification was the differences in nebulization efficiencies between NPs and the ionic standard solutions. They solved this problem using the titanium standard in the form of rutile TiO_2 NPs. The results were in good agreement with the quantity of Ti analyzed by FIA-ICP-MS. Moreover, using tip sonicator method for preparing NPs dispersions provided better linearity of concentration calibration curve, as opposed to the ultrasonic bath method.

Contado et al.[199] demonstrated the use of SdFFF for size fractionations of four types of SiO_2 available in the market as additives in food and personal care products in the size range 7 nm to 9 μm. TEM and photon correlation spectroscopy (PCS) were also used for detection. The content of SiO_2 in different powdered foodstuffs was determined by GFAAS that showed the concentration in the range 0.006–0.35% (w/w).

Bolea et al.[200] reported the development of a method for size characterization and quantification of AgNPs by AF4 coupled with ICP-MS. They found that the PES membrane and a mobile phase containing an anionic surfactant such as SDS at pH 8 were the optimal conditions for the characterization of AgNPs. The method was applied for the analysis of AgNPs in two consumer products: a strong antiseptic and dietary supplement. The sizes obtained by this system were in good agreement with those obtained by TEM.

Loeschner et al.[201] demonstrated the application of AF4-ICP-MS for characterization of AgNPs in chicken meat. AgNPs were extracted from chicken meat by enzymatic digestion using Proteinase K and subsequently introduced into the AF4. Similar size distributions were observed in the digestive meat and aqueous suspension of AgNPs used for spiking into the meat. No dissolution of AgNPs in the preparation step was observed. Further, off-line single particle ICP-MS was used for determination of the number-based particle size distribution.

M-M et al.[202] investigated the changes in the size distribution of selenium nanoparticles (SeNPs) in the environment of gastrointestinal conditions by on-line SF4-ICP-MS. The pectin, mixed alginate/pectin, ovalbumin, and β-lactoglobulinstabilized-SeNPs (the particle sizes are 64, 37, 30, and 23 nm, respectively) showed different size changes in both enzymatic and nonenzymatic media. However, SeNPs in all types of stabilizing agents were still in nanometer-sized range although they were incubated in the gastrointestinal condition.

Grombe et al.[203] used AF4-ICP-MS as a confirmation method for characterization of silica nanoparticles that were used as reference materials in synthetic tomato soup. Silica nanoparticles were isolated from tomato soup by heating the soup for 30 min at 50°C, homogenization in a glass beaker (Ultra Turrax, IKA-T10; 30 s at 20,000–25,000 rpm), removal of the organic materials by acid digestion and stabilization of the remaining particle suspension by pH adjustment, and probe sonication before fractionation by AF4.

Heroult et al.[204] investigated the application of AF4 with multiple detectors for size characterization of silica nanoparticles in coffee creamer. The probable parameters affecting the change in particle size changing from the original size were examined. These included the coffee creamer matrix components, extraction method, and cooking. The combination of AF4 with ICP-MS and TEM/EDAX was proved essential to provide reliable information of nanoparticle size in the complex food matrix.

Peters et al.[205] applied AF4-ICP-MS and single-particle ICP-MS to characterize TiO_2 particles in several products: 7 food grade materials (E171), 24 food products, and 3 personal care products. Size distribution between 60 and 300 nm was found for all seven food grade materials. Approximately 10–15% and 5–10% of particles with particle sizes smaller than 100 nm were detected in all food grade, food, and personal care products. The authors mentioned that size limits of TiO_2 detection were in the

Encyclopedia of Analytical Chemistry, Online © 2006–2015 John Wiley & Sons, Ltd.

This article was published in the *Encyclopedia of Analytical Chemistry* in 2015 by John Wiley & Sons, Ltd.
DOI: 10.1002/9780470027318.a9427

range 20–50 nm. In term of concentration, 0.02–9 mg TiO_2/g product was detected in 24 of 27 food and personal care products.

7 CONCLUDING REMARKS

Owing to the expanding applications of ENPs and their properties depend greatly on size, the analytical techniques used for size characterization of ENPs are necessary. FFF has been increasingly used for particle size characterization of nanoparticles. Hyphenation between FFF and atomic spectrometric detection adds the specificity for the detection. The element-specific detection is particularly useful when the samples contain mixed ENPs, such as AuNPs and AgNPs. With some size characterization techniques, DLS, TEM, only the information on the overall particle size are gained. Nonetheless, with the use of FFF coupled with atomic spectrometric detection, it is possible to differentiate the particle sizes of AuNPs and AgNPs in the mixture. Furthermore, adding the dimension on element-specific detection to the FFF size separation facilitates the characterization of ENPs in complex matrices containing natural nanoparticles. Therefore, FFF with atomic spectrometric detection should be considered as a convenient and effective tool for ENPs characterization.

ACKNOWLEDGMENTS

The authors would like to acknowledge the support from the Office of the Higher Education Commission, Ministry of Education, Thailand through the Strategic Scholarships Fellowships Frontier Research Networks (Specific for Southern Region) given to R. Suwanpetch; the Center for Innovation in Chemistry: Postgraduate Education and Research Program in Chemistry (PERCH-CIC); and Mahidol University under the National Research Universities Initiative. We are also grateful for the support from the Thailand Research Fund (TRF) for the research grants given to A. Siripinyanond and the scholarships given to M. Ornthai and P. M-M through the Royal Golden Jubilee PhD Program.

ABBREVIATIONS AND ACRONYMS

AF4	Asymmetric Flow Field-flow Fractionation
BSA	Bovine Serum Albumin
CNT	Carbon Nanotube
CPE	Cloud Point Extraction
CTAB	Cetyltrimethylammonium Bromide
CyElFFF	Cyclical Electrical Field-flow Fractionation
DCS	Differential Centrifugal Sedimentation
DLS	Dynamic Light Scattering
EDTA	Ethylene Diamine Tetraacetic Acid
ElFFF	Electrical Field-flow Fractionation
EM	Electron Microscopy
ENP	Engineered Nanoparticle
ESI-MS	Electrospray Ionization-mass Spectrometry
ETAAS	Electrothermal Atomic Absorption Spectrometry
ETV	Electrothermal Vaporization
FAAS	Flame Atomic Absorption Spectrometry
FFF	Field-flow Fractionation
FlFFF	Flow Field-flow Fractionation
GE	Gel Electrophoresis
GFAAS	Graphite Furnace Atomic Absorption Spectrometry
GNR	Gold Nanorod
GrFFF	Gravitational Field-flow Fractionation
HDF	Human Dermal Fibroblast
ICP-MS	Inductively Coupled Plasma Mass Spectrometry
ICP-OES	Inductively Coupled Plasma-optical Emission Spectrometry
ITO	Indium Tin Oxide
LC	Liquid Chromatography
LED	Light-emitting Diode
LOD	Limit of Detection
MALS	Multiangle Light Scattering
MPA	Mercaptopropionic Acid
MSA	Mercapto Succinic Acid
NMR	Nuclear Magnetic Resonance
NP	Nanoparticle
NTA	Nanoparticles Tracking Analysis
PCS	Photon Correlation Spectroscopy
PLGA-*b*-PEG	poly(D,L-lactic-*co*-glycolic acid)-*b*-poly(ethylene glycol
PVP	Polyvinylpyrrolidone
QD	Quantum Dot
RBC	Regenerated Bacterial Cellulose
ROS	Reactive Oxygen Species
SdFFF	Sedimentation Field-flow Fractionation
SEM	Scanning Electron Microscope
SeNP	Selenium Nanoparticle

Encyclopedia of Analytical Chemistry, Online © 2006–2015 John Wiley & Sons, Ltd.

This article was published in the *Encyclopedia of Analytical Chemistry* in 2015 by John Wiley & Sons, Ltd.
DOI: 10.1002/9780470027318.a9427

SF4	Symmetric Flow Field-flow Fractionation
SP-ICP-MS	Single-particle Inductively Coupled Plasma Mass Spectrometry
SPLITT	Split Flow Thin Cell Fractionation
SRHA	Suwannee River Humic Acid
SWV	Square Wave Voltammetry
TEM	Transmission Electron Microscope
TMAH	Tetra Methyl Ammonium Hydroxide
UV/VIS	Ultraviolet/Visible
WWTP	Wastewater Treatment Plant

RELATED ARTICLES

Environment: Trace Gas Monitoring **(Volume 3)**
Environmental Trace Species Monitoring: Introduction

Environment: Water and Waste **(Volume 3)**
Flame and Graphite Furnace Atomic Absorption Spectrometry in Environmental Analysis • Inductively Coupled Plasma Mass Spectrometry in Environmental Analysis

Food **(Volume 5)**
Atomic Spectroscopy in Food Analysis

Particle Size Analysis **(Volume 6)**
Particle Size Analysis: Introduction • Field-flow Fractionation in Particle Size Analysis

Atomic Spectroscopy **(Volume 11)**
Graphite Furnace Atomic Absorption Spectrometry • Inductively Coupled Plasma/Optical Emission Spectrometry

Liquid Chromatography
Asymmetric Flow Field Flow Fractionation

Food
Nanoparticles in Foods, Determination of

Environment: Water and Waste
Hyphenated methods for speciation analysis

REFERENCES

1. T.M. Jovin, 'Quantum Dots Finally Come of Age', *Nat. Biotechnol.*, **21**, 32–33 (2003).
2. E.C. Wang, A.Z. Wang, 'Nanoparticles and Their Applications in Cell and Molecular Biology', *Integr. Biol.*, **6**, 9–26 (2014).
3. Z.P. Xu, Q.H. Zeng, G.Q. Lu, A.B. Yu, 'Inorganic Nanoparticles as Carriers for Efficient Cellular Delivery', *Chem. Eng. Sci.*, **61**, 1027–1040 (2006).
4. L. Matthews, R.K. Kanwar, S. Zhou, V. Punj, J.R. Kanwar, 'Applications of Nanomedicine in Antibacterial Medical Therapeutics and Diagnostics', *Open Trop. Med. J.*, **3**, 1–9 (2010).
5. D. Pissuwan, T. Niidome, M.B. Cortie, 'The Forthcoming Applications of Gold Nanoparticles in Drug and Gene Delivery Systems', *J. Controlled Release*, **149**, 65–71 (2011).
6. E.H. Jeong, G. Jung, C.A. Hong, H. Lee, 'Gold Nanoparticle (AuNP)-Based Drug Delivery and Molecular Imaging for Biomedical Applications', *Arch. Pharmacal Res.*, **37**, 53–59 (2014).
7. Y. Ge, B. Kang, 'Surface Plasmon Resonance Scattering and Absorption of Biofunctionalized Gold Nanoparticles for Targeted Cancer Imaging and Laser Therapy', *Sci. China Technol. Sci.*, **54**, 2358–2362 (2011).
8. T. Okuno, S. Kato, Y. Hatakeyama, J. Okajima, S. Maruyama, M. Sakamoto, S. Mori, T. Kodama, 'Photothermal Therapy of Tumors in Lymph Nodes Using Gold Nanorods and Near-Infrared Laser Light', *J. Controlled Release*, **172**, 879–884 (2013).
9. L. Zhao, T.H. Kim, J.C. Ahn, H.W. Kim, S.Y. Kim, 'Highly Efficient ''Theranostics'' System Based on Surface-Modified Gold Nanocarriers for Imaging and Photodynamic Therapy of Cancer', *J. Mater. Chem. B*, **1**, 5806–5817 (2013).
10. P. Prema, S. Thangapandiyan, 'In-Vitro Antibacterial Activity of Gold Nanoparticles Capped with Polysaccharide Stabilizing Agents', *Int. J. Pharm. Pharm. Sci.*, **5**, 310–314 (2013).
11. S.L. Smitha, K.G. Gopchandran, 'Surface Enhanced Raman Scattering, Antibacterial and Antifungal Active Triangular Gold Nanoparticles', *Spectrochim. Acta, Part A*, **102**, 114–119 (2013).
12. T. Špringer, J. Homola, 'Biofunctionalized Gold Nanoparticles for SPR-Biosensor-Based Detection of CEA in Blood Plasma', *Anal. Bioanal. Chem.*, **404**, 2869–2875 (2012).
13. H.J. Zhang, Y.H. Lu, Y.J. Long, Q.L. Wang, X.X. Huang, R. Zhu, X.L. Wang, L.P. Liang, P. Teng, H.Z. Zheng, 'An Aptamer-Functionalized Gold Nanoparticle Biosensor for the Detection of Prion Protein', *Anal. Methods*, **6**, 2982–2987 (2014).
14. I. Sondi, B. Salopek-Sondi, 'Silver Nanoparticles as Antimicrobial Agent: A Case Study on *E. Coli* as a Model for Gram-Negative Bacteria', *J. Colloid Interface Sci.*, **275**, 177–182 (2004).
15. M. Rai, A. Yadav, A. Gade, 'Silver Nanoparticles as a New Generation of Antimicrobials', *Biotechnol. Adv.*, **27**, 76–83 (2009).

Encyclopedia of Analytical Chemistry, Online © 2006–2015 John Wiley & Sons, Ltd.

This article was published in the *Encyclopedia of Analytical Chemistry* in 2015 by John Wiley & Sons, Ltd.
DOI: 10.1002/9780470027318.a9427

16. D. Paredes, C. Ortiz, R. Torres, 'Synthesis, Characterization, and Evaluation of Antibacterial Effect of Ag Nanoparticles against *Escherichia Coli* O157:H7 and Methicillin-Resistant *Staphylococcus aureus* (MRSA)', *Int. J. Nanomed.*, **9**, 1717–1729 (2014).

17. R. Thomas, A.P. Nair, S. Kr, J. Mathew, R. Ek, 'Antibacterial Activity and Synergistic Effect of Biosynthesized AgNPs with Antibiotics against Multidrug-Resistant Biofilm-Forming Coagulase-Negative Staphylococci Isolated from Clinical Samples', *Appl. Biochem. Biotechnol.*, **173**, 449–460 (2014).

18. J. Tian, K.K.Y. Wong, C.M. Ho, C.N. Lok, W.Y. Yu, C.M. Che, J.F. Chiu, P.K.H. Tam, 'Topical Delivery of Silver Nanoparticles Promotes Wound Healing', *ChemMedChem*, **2**, 129–136 (2007).

19. M. Pollini, F. Paladini, M. Catalano, A. Taurino, A. Licciulli, A. Maffezzoli, A. Sannino, 'Antibacterial Coatings on Haemodialysis Catheters by Photochemical Deposition of Silver Nanoparticles', *J. Mater. Sci. - Mater. Med.*, **22**, 2005–2012 (2011).

20. T. Furuzono, T. Iwamoto, Y. Azuma, M. Okada, Y. Sawa, 'Preparation of Carboxylated Ag Nanoparticles as a Coating Material for Medical Devices and Control of Antibacterial Activity', *J. Artif. Organs*, **16**, 451–457 (2013).

21. F. Martinez-Gutierrez, L. Boegli, A. Agostinho, E.M. Sánchez, H. Bach, F. Ruiz, G. James, 'Anti-Biofilm Activity of Silver Nanoparticles Against Different Microorganisms', *Biofouling*, **29**, 651–660 (2013).

22. M. Agarwala, T. Barman, D. Gogoi, B. Choudhury, A.R. Pal, R.N.S. Yadav, 'Highly Effective Antibiofilm Coating of Silver-Polymer Nanocomposite on Polymeric Medical Devices Deposited by One Step Plasma Process', *J. Biomed. Mater. Res. Part B*, **102**, 1223–1235 (2014).

23. A. Travan, E. Marsich, I. Donati, M. Benincasa, M. Giazzon, L. Felisari, S. Paoletti, 'Silver-Polysaccharide Nanocomposite Antimicrobial Coatings for Methacrylic Thermosets', *Acta Biomater.*, **7**, 337–346 (2011).

24. S. Gurunathan, K.J. Lee, K. Kalishwaralal, S. Sheikpranbabu, R. Vaidyanathan, S.H. Eom, 'Antiangiogenic Properties of Silver Nanoparticles', *Biomaterials*, **30**, 6341–6350 (2009).

25. M.I. Sriram, S.B.M. Kanth, K. Kalishwaralal, S. Gurunathan, 'Antitumor Activity of Silver Nanoparticles in Dalton's Lymphoma Ascites Tumor Model', *Int. J. Nanomed.*, **5**, 753–762 (2010).

26. E. Locatelli, F. Broggi, J. Ponti, P. Marmorato, F. Franchini, S. Lena, M.C. Franchini, 'Lipophilic Silver Nanoparticles and Their Polymeric Entrapment into Targeted-PEG-Based Micelles for the Treatment of Glioblastoma', *Adv. Healthc. Mater.*, **1**, 342–347 (2012).

27. R. Govender, A. Phulukdaree, R.M. Gengan, K. Anand, A.A. Chuturgoon, 'Silver Nanoparticles of *Albizia Adianthifolia*: The Induction of Apoptosis in Human Lung Carcinoma Cell Line', *J. Nanobiotechnol.*, **11**, 5 (2013).

28. S. Gurunathan, J. Raman, S.N. Abd Malek, P.A. John, S. Vikineswary, 'Green Synthesis of Silver Nanoparticles Using *Ganoderma Neo-Japonicum* Imazeki: A Potential Cytotoxic Agent against Breast Cancer Cells', *Int. J. Nanomed.*, **8**, 4399–4413 (2013).

29. G. Sathishkumar, C. Gobinath, A. Wilson, S. Sivaramakrishnan, '*Dendrophthoe Falcata* (L.f) Ettingsh (Neem Mistletoe): A Potent Bioresource to Fabricate Silver Nanoparticles for Anticancer Effect against Human Breast Cancer Cells (MCF-7)', *Spectrochim. Acta, Part A*, **128**, 285–290 (2014).

30. P.T. Sudheesh Kumar, V.K. Lakshmanan, M. Raj, R. Biswas, T. Hiroshi, S.V. Nair, R. Jayakumar, 'Evaluation of Wound Healing Potential of β-Chitin Hydrogel/Nano Zinc Oxide Composite Bandage', *Pharm. Res.*, **30**, 523–537 (2013).

31. B.S. Vasile, O. Oprea, G. Voicu, A. Ficai, E. Andronescu, A. Teodorescu, A. Holban, 'Synthesis and Characterization of a Novel Controlled Release Zinc Oxide/Gentamicin-Chitosan Composite with Potential Applications in Wounds Care', *Int. J. Pharm.*, **463**, 161–169 (2014).

32. M. Ul-Islam, W.A. Khattak, M.W. Ullah, S. Khan, J.K. Park, 'Synthesis of Regenerated Bacterial Cellulose-Zinc Oxide Nanocomposite Films for Biomedical Applications', *Cellulose*, **21**, 433–447 (2014).

33. T. Chen, T. Zhao, D. Wei, Y. Wei, Y. Li, H. Zhang, 'Core-Shell Nanocarriers with ZnO Quantum Dots-Conjugated Au Nanoparticle for Tumor-Targeted Drug Delivery', *Carbohydr. Polym.*, **92**, 1124–1132 (2013).

34. H.M. Xiong, 'ZnO Nanoparticles Applied to Bioimaging and Drug Delivery', *Adv. Mater.*, **25**, 5329–5335 (2013).

35. I. Balti, A. Barrère, V. Gueguen, L. Poussard, G. Pavon-Djavid, A. Meddahi-Pellé, P. Rabu, L.S. Smiri, N. Jouini, F. Chaubet, 'Preparation of Cytocompatible Luminescent and Magnetic Nanohybrids Based on Zno, Zn0.95Ni0.05O and Core@Shell ZnO@Fe_2O_3 Polymer Grafted Nanoparticles for Biomedical Imaging', *J. Nanopart. Res.*, **14**, 1–15 (2012). doi:10.1007/s11051-012-1266-x.

36. J.W. Rasmussen, E. Martinez, P. Louka, D.G. Wingett, 'Zinc Oxide Nanoparticles for Selective Destruction of Tumor Cells and Potential for Drug Delivery Applications', *Expert Opin. Drug Delivery*, **7**, 1063–1077 (2010).

37. R. Wahab, N.K. Kaushik, A.K. Verma, A. Mishra, I.H. Hwang, Y.B. Yang, H.S. Shin, Y.S. Kim, 'Fabrication and Growth Mechanism of ZnO Nanostructures and Their Cytotoxic Effect on Human Brain Tumor U87, Cervical Cancer Hela, and Normal HEK Cells', *J. Biol. Inorg. Chem.*, **16**, 431–442 (2011).

Encyclopedia of Analytical Chemistry, Online © 2006–2015 John Wiley & Sons, Ltd.

This article was published in the *Encyclopedia of Analytical Chemistry* in 2015 by John Wiley & Sons, Ltd.
DOI: 10.1002/9780470027318.a9427

38. M.J. Akhtar, M. Ahamed, S. Kumar, M.A. Majeed Khan, J. Ahmad, S.A. Alrokayan, 'Zinc Oxide Nanoparticles Selectively Induce Apoptosis in Human Cancer Cells through Reactive Oxygen Species', *Int. J. Nanomed.*, **7**, 845–857 (2012).
39. I. Schick, S. Lorenz, D. Gehrig, A.M. Schilmann, H. Bauer, M. Panthöfer, K. Fischer, D. Strand, F. Laquai, W. Tremel, 'Multifunctional Two-Photon Active Silica-Coated Au@MnO Janus Particles for Selective Dual Functionalization and Imaging', *J. Am. Chem. Soc.*, **136**, 2473–2483 (2014).
40. S.N. Sun, C. Wei, Z.Z. Zhu, Y.L. Hou, S.S. Venkatraman, Z.C. Xu, 'Magnetic Iron Oxide Nanoparticles: Synthesis and Surface Coating Techniques for Biomedical Applications', *Chin. Phys. B*, **23**, 037503 (2014).
41. M. Mahmoudi, S. Sant, B. Wang, S. Laurent, T. Sen, 'Superparamagnetic Iron Oxide Nanoparticles (Spions): Development, Surface Modification and Applications in Chemotherapy', *Adv. Drug Delivery Rev.*, **63**, 24–46 (2011).
42. T. Heidt, M. Nahrendorf, 'Multimodal Iron Oxide Nanoparticles for Hybrid Biomedical Imaging', *NMR Biomed.*, **26**, 756–765 (2013).
43. J. Huang, L. Wang, R. Lin, A.Y. Wang, L. Yang, M. Kuang, W. Qian, H. Mao, 'Casein-Coated Iron Oxide Nanoparticles for High MRI Contrast Enhancement and Efficient Cell Targeting', *ACS Appl. Mater. Interfaces*, **5**, 4632–4639 (2013).
44. L. Zhang, W.F. Dong, H.B. Sun, 'Multifunctional Superparamagnetic Iron Oxide Nanoparticles: Design, Synthesis and Biomedical Photonic Applications', *Nanoscale*, **5**, 7664–7684 (2013).
45. I.M. Hamouda, 'Current Perspectives of Nanoparticles in Medical and Dental Biomaterials', *J. Biomed. Res.*, **26**, 143–151 (2012).
46. R.P. Allaker, K. Memarzadeh, 'Nanoparticles and the Control of Oral Infections', *Int. J. Antimicrob. Agents*, **43**, 95–104 (2014).
47. Z. Wang, Y. Shen, M. Haapasalo, 'Dental Materials with Antibiofilm Properties', *Dent. Mater.*, **30**, e1–e16 (2014).
48. X. Sun, Y. Li, H. Huang, B. Yang, Y. Wang, 'Synthesis and Application of a Targeting Diagnosis System Via Quantum Dots Coated by Amphiphilic Polymer for the Detection of Liver Cancer Cells', *Luminescence*, **29**(7), 831–836 (2014).
49. X. Li, D. Deng, J. Xue, L. Qu, S. Achilefu, Y. Gu, 'Quantum Dots Based Molecular Beacons for in Vitro and in Vivo Detection of MMP-2 on Tumor', *Biosens. Bioelectron.*, **61**, 512–518 (2014).
50. M. Nurunnabi, K.J. Cho, J.S. Choi, K.M. Huh, Y.K. Lee, 'Targeted near-IR QDs-Loaded Micelles for Cancer Therapy and Imaging', *Biomaterials*, **31**, 5436–5444 (2010).
51. J. Lokich, N. Anderson, 'Carboplatin Versus Cisplatin in Solid Tumors: An Analysis of the Literature', *Ann. Oncol.*, **9**, 13–21 (1998).
52. S. Wang, J.B. Mi, Y.Z. Li, W.B. Chang, Y.X. Ci, M.Z. Zhao, Y.K. Zhao, L.Y. Zhu, G. Xu, 'Pharmacokinetics and Tissue Distribution of Iv Injection of Polyphase Liposome-Encapsulated Cisplatin (KM-1) in Rats', *Acta Pharmacol. Sin.*, **24**, 589–592+623 (2003).
53. J.Y. Yu, Y.J. Jun, S.H. Jang, H.J. Lee, Y.S. Sohn, 'Nanoparticulate Platinum(II) Anticancer Drug: Synthesis and Characterization of Amphiphilic Cyclotriphosphazene-Platinum(II) Conjugates', *J. Inorg. Biochem.*, **101**, 1931–1936 (2007).
54. K.J. Haxton, H.M. Burt, 'Polymeric Drug Delivery of Platinum-Based Anticancer Agents', *J. Pharm. Sci.*, **98**, 2299–2316 (2009).
55. H.S. Oberoi, N.V. Nukolova, A.V. Kabanov, T.K. Bronich, 'Nanocarriers for Delivery of Platinum Anticancer Drugs', *Adv. Drug Delivery Rev.*, **65**, 1667–1685 (2013).
56. S. Dhar, N. Kolishetti, S.J. Lippard, O.C. Farokhzad, 'Targeted Delivery of a Cisplatin Prodrug for Safer and More Effective Prostate Cancer Therapy in Vivo', *Proc. Natl. Acad. Sci. U.S.A.*, **108**, 1850–1855 (2011).
57. N. Graf, D.R. Bielenberg, N. Kolishetti, C. Muus, J. Banyard, O.C. Farokhzad, S.J. Lippard, '$\alpha_v\beta_3$ Integrin-Targeted PLGA-PEG Nanoparticles for Enhanced Anti-Tumor Efficacy of a Pt(IV) Prodrug', *ACS Nano*, **6**, 4530–4539 (2012).
58. Y. Mi, J. Zhao, S.S. Feng, 'Targeted Co-Delivery of Docetaxel, Cisplatin and Herceptin by Vitamin E TPGS-Cisplatin Prodrug Nanoparticles for Multimodality Treatment of Cancer', *J. Controlled Release*, **169**, 185–192 (2013).
59. T. Yuranova, R. Mosteo, J. Bandara, D. Laub, J. Kiwi, 'Self-Cleaning Cotton Textiles Surfaces Modified by Photoactive SiO_2/TiO_2 Coating', *J. Mol. Catal. A: Chem.*, **244**, 160–167 (2006).
60. I. Perelshtein, G. Applerot, N. Perkas, E. Wehrschuetz-Sigl, A. Hasmann, G. Guebitz, A. Gedanken, 'CuO-Cotton Nanocomposite: Formation, Morphology, and Antibacterial Activity', *Surf. Coat. Technol.*, **204**, 54–57 (2009).
61. A. Hebeish, M.E. El-Naggar, M.M.G. Fouda, M.A. Ramadan, S.S. Al-Deyab, M.H. El-Rafie, 'Highly Effective Antibacterial Textiles Containing Green Synthesized Silver Nanoparticles', *Carbohydr. Polym.*, **86**, 936–940 (2011).
62. A. Behzadnia, M. Montazer, A. Rashidi, M.M. Rad, 'Sonosynthesis of Nano TiO_2 on Wool Using Titanium Isopropoxide or Butoxide in Acidic Media Producing Multifunctional Fabric', *Ultrason. Sonochem.*, **21**, 1815–1826 (2014).

Encyclopedia of Analytical Chemistry, Online © 2006–2015 John Wiley & Sons, Ltd.

This article was published in the *Encyclopedia of Analytical Chemistry* in 2015 by John Wiley & Sons, Ltd.
DOI: 10.1002/9780470027318.a9427

63. A. Sedighi, M. Montazer, N. Samadi, 'Synthesis of Nano Cu_2O on Cotton: Morphological, Physical, Biological and Optical Sensing Characterizations', *Carbohydr. Polym.*, **110**, 489–498 (2014).
64. C.H. Xue, J. Chen, W. Yin, S.T. Jia, J.Z. Ma, 'Superhydrophobic Conductive Textiles with Antibacterial Property by Coating Fibers with Silver Nanoparticles', *Appl. Surf. Sci.*, **258**, 2468–2472 (2012).
65. B.A. Çakir, L. Budama, Ö. Topel, N. Hoda, 'Synthesis of Zno Nanoparticles Using PS-b-PAA Reverse Micelle Cores for UV Protective, Self-Cleaning and Antibacterial Textile Applications', *Colloids Surf., A*, **414**, 132–139 (2012).
66. Y. Zheng, M. Xiao, S. Jiang, F. Ding, J. Wang, 'Coating Fabrics with Gold Nanorods for Colouring, UV-Protection, and Antibacterial Functions', *Nanoscale*, **5**, 788–795 (2013).
67. The Project on Emerging Nanotechnology, Nanomaterials, http://www.nanotechproject.org/cpi/browse/nanomaterials/ (accessed 8 December 2014).
68. G.J. Nohynek, E.K. Dufour, M.S. Roberts, 'Nanotechnology, Cosmetics and the Skin: Is There a Health Risk?', *Skin Pharmacol. Physiol.*, **21**, 136–149 (2008).
69. T.G. Smijs, S. Pavel, 'Titanium Dioxide and Zinc Oxide Nanoparticles in Sunscreens: Focus on Their Safety and Effectiveness', *Nanotechnol. Sci. Appl.*, **4**, 95–112 (2011).
70. Purest Colloids, Products of Purest Colloids, http://www.purestcolloids.com/products.php (accessed 8 December 2014).
71. A. Martirosyan, Y.J. Schneider, 'Engineered Nanomaterials in Food: Implications for Food Safety and Consumer Health', *Int. J. Environ. Res. Public Health*, **11**, 5720–5750 (2014).
72. S. Dekkers, P. Krystek, R.J.B. Peters, D.P.K. Lankveld, B.G.H. Bokkers, P.H. Van Hoeven-Arentzen, H. Bouwmeester, A.G. Oomen, 'Presence and Risks of Nanosilica in Food Products', *Nanotoxicology*, **5**, 393–405 (2011).
73. D. Ebert, B. Bhushan, 'Transparent, Superhydrophobic, and Wear-Resistant Coatings on Glass and Polymer Substrates Using SiO_2, ZnO, and Ito Nanoparticles', *Langmuir*, **28**, 11391–11399 (2012).
74. S.H. Nam, J.H. Boo, 'Growth and Surface Treatment of TiO_2 Nanorods Using Stearic Acid Solution', *Thin Solid Films*, **546**, 35–37 (2013).
75. X. Zhang, Y. Guo, Z. Zhang, P. Zhang, 'Self-Cleaning Superhydrophobic Surface Based on Titanium Dioxide Nanowires Combined with Polydimethylsiloxane', *Appl. Surf. Sci.*, **284**, 319–323 (2013).
76. X. Zhang, L. Wang, E. Levänen, 'Superhydrophobic Surfaces for the Reduction of Bacterial Adhesion', *RSC Adv.*, **3**, 12003–12020 (2013).
77. Y. Zhang, D. Ge, S. Yang, 'Spray-Coating of Superhydrophobic Aluminum Alloys with Enhanced Mechanical Robustness', *J. Colloid Interface Sci.*, **423**, 101–107 (2014).
78. C. Cheng, H.J. Fan, 'Branched Nanowires: Synthesis and Energy Applications', *Nano Today*, **7**, 327–343 (2012).
79. Y. Feng, J. Zhu, J. Jiang, W. Wang, G. Meng, F. Wu, Y. Gao, X. Huang, 'Building Smart TiO_2 Nanorod Networks in/on the Film of P25 Nanoparticles for High-Efficiency Dye Sensitized Solar Cells', *RSC Adv.*, **4**, 12944–12949 (2014).
80. L. Ming, H. Yang, W. Zhang, X. Zeng, D. Xiong, Z. Xu, H. Wang, W. Chen, X. Xu, M. Wang, J. Duan, Y.B. Cheng, J. Zhang, Q. Bao, Z. Wei, S. Yang, 'Selective Laser Sintering of TiO_2 Nanoparticle Film on Plastic Conductive Substrate for Highly Efficient Flexible Dye-Sensitized Solar Cell Application', *J. Mater. Chem. A*, **2**, 4566–4573 (2014).
81. C. Buzea, I.I. Pacheco, K. Robbie, 'Nanomaterials and Nanoparticles: Sources and Toxicity', *Biointerphases*, **2**, MR17–MR71 (2007).
82. H.J. Zhang, K.X. Wang, X.Y. Wu, Y.M. Jiang, Y.B. Zhai, C. Wang, X. Wei, J.S. Chen, 'MoO_2/Mo_2C Heteronanotubes Function as High-Performance Li-Ion Battery Electrode', *Adv. Funct. Mater.*, **24**, 3399–3404 (2014).
83. T.S. Kang, T.Y. Kim, G.M. Lee, H.C. Sohn, J.P. Hong, 'Highly Stable Solution-Processed ZnO Thin Film Transistors Prepared Via a Simple Al Evaporation Process', *J. Mater. Chem. C*, **2**, 1390–1395 (2014).
84. S.J. Lee, C.S. Hwang, J.E. Pi, M.K. Ryu, H. Oh, S.H. Cho, J.H. Yang, S.H. Ko Park, H.Y. Chu, 'Characterization of ZnO-SnO_2 Nanocomposite Thin Films Deposited by Pulsed Laser Ablation and Their Field Effect Electronic Properties', *Mater. Lett.*, **122**, 94–97 (2014).
85. H.P. Borase, C.D. Patil, R.B. Salunkhe, R.K. Suryawanshi, B.K. Salunke, S.V. Patil, 'Mercury Sensing and Toxicity Studies of Novel Latex Fabricated Silver Nanoparticles', *Bioprocess. Biosyst. Eng.*, **37**(11), 2223–2233 (2014).
86. D. Xiong, H. Li, 'Colorimetric Detection of Pesticides Based on Calixarene Modified Silver Nanoparticles in Water', *Nanotechnology*, **19**, 465502–465507 (2008).
87. C. Han, H. Li, 'Visual Detection of Melamine in Infant Formula at 0.1 ppm Level Based on Silver Nanoparticles', *Analyst*, **135**, 583–588 (2010).
88. H. Li, F. Li, C. Han, Z. Cui, G. Xie, A. Zhang, 'Highly Sensitive and Selective Tryptophan Colorimetric Sensor Based on 4,4-Bipyridine-Functionalized Silver Nanoparticles', *Sens. Actuators, B*, **145**, 194–199 (2010).
89. Y. Fu, F. Liang, H. Tian, J. Hu, 'Nonenzymatic Glucose Sensor Based on ITO Electrode Modified with Gold Nanoparticles by Ion Implantation', *Electrochim. Acta*, **120**, 314–318 (2014).

Encyclopedia of Analytical Chemistry, Online © 2006–2015 John Wiley & Sons, Ltd.

This article was published in the *Encyclopedia of Analytical Chemistry* in 2015 by John Wiley & Sons, Ltd.
DOI: 10.1002/9780470027318.a9427

90. S.K. Laliwala, V.N. Mehta, J.V. Rohit, S.K. Kailasa, 'Citrate-Modified Silver Nanoparticles as a Colorimetric Probe for Simultaneous Detection of Four Triptan-Family Drugs', *Sens. Actuators, B*, **197**, 254–263 (2014).
91. R.P. Modi, V.N. Mehta, S.K. Kailasa, 'Bifunctionalization of Silver Nanoparticles with 6-Mercaptonicotinic Acid and Melamine for Simultaneous Colorimetric Sensing of Cr^{3+} and Ba^{2+} Ions', *Sens. Actuators, B*, **195**, 562–571 (2014).
92. L.Q. Zheng, X.D. Yu, J.J. Xu, H.Y. Chen, 'Rapid Visual Detection of Quaternary Ammonium Surfactants Using Citrate-Capped Silver Nanoparticles (AgNPs) Based on Hydrophobic Effect', *Talanta*, **118**, 90–95 (2014).
93. W.L. Daniel, M.S. Han, J.S. Lee, C.A. Mirkin, 'Colorimetric Nitrite and Nitrate Detection with Gold Nanoparticle Probes and Kinetic End Points', *J. Am. Chem. Soc.*, **131**, 6362–6363 (2009).
94. L. Chen, T. Lou, C. Yu, Q. Kang, L. Chen, 'N-1-(2-Mercaptoethyl)Thymine Modification of Gold Nanoparticles: A Highly Selective and Sensitive Colorimetric Chemosensor for Hg^{2+}', *Analyst*, **136**, 4770–4773 (2011).
95. Y.C. Chen, I.L. Lee, Y.M. Sung, S.P. Wu, 'Triazole Functionalized Gold Nanoparticles for Colorimetric Cr^{3+} Sensing', *Sens. Actuators, B*, **188**, 354–359 (2013).
96. Y.M. Sung, S.P. Wu, 'Colorimetric Detection of Cd(II) Ions Based on Di-(1H-pyrrol-2-yl) Methanethione Functionalized Gold Nanoparticles', *Sens. Actuators, B*, **201**, 86–91 (2014).
97. Y.M. Sung, S.P. Wu, 'Highly Selective and Sensitive Colorimetric Detection of Ag(I) Using N-1-(2-Mercaptoethyl)Adenine Functionalized Gold Nanoparticles', *Sens. Actuators, B*, **197**, 172–176 (2014).
98. P.S. Dorraji, F. Jalali, 'Novel Sensitive Electrochemical Sensor for Simultaneous Determination of Epinephrine and Uric Acid by Using a Nanocomposite of MWCNTs-Chitosan and Gold Nanoparticles Attached to Thioglycolic Acid', *Sens. Actuators, B*, **200**, 251–258 (2014).
99. X. Zhang, Y. Peng, J. Bai, B. Ning, S. Sun, X. Hong, Y. Liu, Y. Liu, Z. Gao, 'A Novel Electrochemical Sensor Based on Electropolymerized Molecularly Imprinted Polymer and Gold Nanomaterials Amplification for Estradiol Detection', *Sens. Actuators, B*, **200**, 69–75 (2014).
100. Y.J. Chen, X.M. Gao, X.P. Di, Q.Y. Ouyang, P. Gao, L.H. Qi, C.Y. Li, C.L. Zhu, 'Porous Iron Molybdate Nanorods: In Situ Diffusion Synthesis and Low-Temperature H_2S Gas Sensing', *ACS Appl. Mater. Interfaces*, **5**, 3267–3274 (2013).
101. I. Lee, S.J. Choi, K.M. Park, S.S. Lee, S. Choi, I.D. Kim, C.O. Park, 'The Stability, Sensitivity and Response Transients of ZnO, SnO_2 and WO_3 Sensors under Acetone, Toluene and H_2S Environments', *Sens. Actuators, B*, **197**, 300–307 (2014).
102. S. Radhakrishnan, K. Krishnamoorthy, C. Sekar, J. Wilson, S.J. Kim, 'A Highly Sensitive Electrochemical Sensor for Nitrite Detection Based on Fe_2O_3 Nanoparticles Decorated Reduced Graphene Oxide Nanosheets', *Appl. Catal., B*, **148–149**, 22–28 (2014).
103. J. Herrán, I. Fernández, E. Ochoteco, G. Cabañero, H. Grande, 'The Role of Water Vapour in ZnO Nanostructures for Humidity Sensing at Room Temperature', *Sens. Actuators, B*, **198**, 239–242 (2014).
104. Z. Chen, D. Wu, 'Monodisperse BSA-Conjugated Zinc Oxide Nanoparticles Based Fluorescence Sensors for Cu^{2+} Ions', *Sens. Actuators, B*, **192**, 83–91 (2014).
105. J. Wang, X. Zhou, H. Ma, G. Tao, 'Diethyldithiocarbamate Functionalized CdSe/CdS Quantum Dots as a Fluorescent Probe for Copper Ion Detection', *Spectrochim. Acta, Part A*, **81**, 178–183 (2011).
106. L. Ding, P.J. Zhou, H.J. Zhan, C. Chen, W. Hu, T.F. Zhou, C.W. Lin, 'Microwave-Assisted Synthesis of L-glutathione Capped ZnSe QDs and Its Interaction with BSA by Spectroscopy', *J. Lumin.*, **142**, 167–172 (2013).
107. K. Zhang, Y. Yu, S. Sun, 'Facile Synthesis L-Cysteine Capped CdS:Eu Quantum Dots and Their Hg^{2+} Sensitive Properties', *Appl. Surf. Sci.*, **276**, 333–339 (2013).
108. T.T. Gan, Y.J. Zhang, N.J. Zhao, X. Xiao, G.F. Yin, S.H. Yu, H.B. Wang, J.B. Duan, C.Y. Shi, W.Q. Liu, 'Hydrothermal Synthetic Mercaptopropionic Acid Stabled CdTe Quantum Dots as Fluorescent Probes for Detection of Ag^{+}', *Spectrochim. Acta, Part A*, **99**, 62–68 (2012).
109. L. Zhang, C. Xu, B. Li, 'Simple and Sensitive Detection Method for Chromium(VI) in Water Using Glutathione-Capped CdTe Quantum Dots as Fluorescent Probes', *Microchim. Acta*, **166**, 61–68 (2009).
110. W.E. Mahmoud, 'Functionalized Me-Capped CdSe Quantum Dots Based Luminescence Probe for Detection of Ba^{2+} Ions', *Sens. Actuators, B*, **164**, 76–81 (2012).
111. J.C. Giddings, 'A New Separation Concept Based on a Coupling of Concentration and Flow Nonuniformities', *Sep. Sci.*, **1**, 123–125 (1966).
112. J.C. Giddings, F.J. Yang, M.N. Myers, 'Theoretical and Experimental Characterization of Flow Field-Flow Fractionation', *Anal. Chem.*, **48**, 1126–1132 (1976).
113. M.E. Schimpf, K. Caldwell, J.C. Giddings, *Field-Flow Fractionation Handbook*, Wiley-Interscience, New York, 2000.
114. J.C. Giddings, 'Field-Flow Fractionation: Analysis of Macromolecular, Colloidal, and Particulate Materials', *Science*, **260**, 1456–1465 (1993).
115. M.H. Moon, J.C. Giddings, 'Extension of Sedimentation/Steric Field-Flow Fractionation into the Submicrometer Range: Size Analysis of 0.2-15-μm Metal Particles', *Anal. Chem.*, **64**, 3029–3037 (1992).

Encyclopedia of Analytical Chemistry, Online © 2006–2015 John Wiley & Sons, Ltd.

This article was published in the *Encyclopedia of Analytical Chemistry* in 2015 by John Wiley & Sons, Ltd.
DOI: 10.1002/9780470027318.a9427

116. K.D. Caldwell, Y.S. Gao, 'Electrical Field-Flow Fractionation in Particle Separation. 1. Monodisperse Standards', *Anal. Chem.*, **65**, 1764–1772 (1993).

117. B.K. Gale, M. Srinivas, 'Cyclical Electrical Field Flow Fractionation', *Electrophoresis*, **26**, 1623–1632 (2005).

118. M.H. Moon, M.N. Myers, in *Field-Flow Fractionation Handbook*, eds M. Schimpf, K. Caldwell, J.C. Giddings, Wiley-Interscience, New York, 199–211, 2000.

119. M. Baalousha, A. Manciulea, S. Cumberland, K. Kendall, J.R. Lead, 'Aggregation and Surface Properties of Iron Oxide Nanoparticles: Influence of pH and Natural Organic Matter', *Environ. Toxicol. Chem.*, **27**, 1875–1882 (2008).

120. S.A. Cumberland, J.R. Lead, 'Particle Size Distributions of Silver Nanoparticles at Environmentally Relevant Conditions', *J. Chromatogr. A*, **1216**, 9099–9105 (2009).

121. W. Sermsri, P. Jarujamrus, J. Shiowatana, A. Siripinyanond, 'Flow Field-Flow Fractionation: A Versatile Approach for Size Characterization of α-Tocopherol-Induced Enlargement of Gold Nanoparticles', *Anal. Bioanal. Chem.*, **396**, 3079–3085 (2010).

122. T.J. Cho, V.A. Hackley, 'Fractionation and Characterization of Gold Nanoparticles in Aqueous Solution: Asymmetric-Flow Field Flow Fractionation with MALS, DLS, and UV–vis Detection', *Anal. Bioanal. Chem.*, **398**, 2003–2018 (2010).

123. I. Römer, T.A. White, M. Baalousha, K. Chipman, M.R. Viant, J.R. Lead, 'Aggregation and Dispersion of Silver Nanoparticles in Exposure Media for Aquatic Toxicity Tests', *J. Chromatogr. A*, **1218**, 4226–4233 (2011).

124. L. Calzolai, D. Gilliland, C.P. Garcìa, F. Rossi, 'Separation and Characterization of Gold Nanoparticle Mixtures by Flow-Field-Flow Fractionation', *J. Chromatogr. A*, **1218**, 4234–4239 (2011).

125. J. Gigault, T.J. Cho, R.I. MacCuspie, V.A. Hackley, 'Gold Nanorod Separation and Characterization by Asymmetric-Flow Field Flow Fractionation with UV–vis Detection', *Anal. Bioanal. Chem.*, **405**, 1191–1202 (2013).

126. S.T. Kim, D.Y. Kang, S. Lee, W.S. Kim, J.T. Lee, H.S. Cho, S.H. Kim, 'Separation and Quantitation of Silver Nanoparticles Using Sedimentation Field-Flow Fractionation', *J. Liq. Chromatogr. Related Technol.*, **30**, 2533–2544 (2007).

127. L. Böhmert, M. Girod, U. Hansen, R. Maul, P. Knappe, B. Niemann, S.M. Weidner, A.F. Thünemann, A. Lampen, 'Analytically Monitored Digestion of Silver Nanoparticles and Their Toxicity on Human Intestinal Cells', *Nanotoxicology*, **8**, 631–642 (2014).

128. P.J.P. Cardot, S. Rasouli, P. Blanchart, 'TiO_2 Colloidal Suspension Polydispersity Analysed with Sedimentation Field Flow Fractionation and Electron Microscopy', *J. Chromatogr. A*, **905**, 163–173 (2001).

129. S. Tadjiki, S. Assemi, C. Deering, J. Veranth, J. Miller, 'Detection, Separation, and Quantification of Unlabeled Silica Nanoparticles in Biological Media Using Sedimentation Field-Flow Fractionation', *J. Nanopart. Res.*, **11**, 981–988 (2009).

130. C.E. Deering, S. Tadjiki, S. Assemi, J.D. Miller, G.S. Yost, J.M. Veranth, 'A Novel Method to Detect Unlabeled Inorganic Nanoparticles and Submicron Particles in Tissue by Sedimentation Field-Flow Fractionation', *Part. Fibre Toxicol.*, **5**, 18 (2008).

131. C. Contado, R. Argazzi, 'Size Sorting of Citrate Reduced Gold Nanoparticles by Sedimentation Field-Flow Fractionation', *J. Chromatogr. A*, **1216**, 9088–9098 (2009).

132. J. Gigault, B.K. Gale, I. Le Hecho, G. Lespes, 'Nanoparticle Characterization by Cyclical Electrical Field-Flow Fractionation', *Anal. Chem.*, **83**, 6565–6572 (2011).

133. W. Somchue, A. Siripinyanond, B.K. Gale, 'Electrical Field-Flow Fractionation for Metal Nanoparticle Characterization', *Anal. Chem.*, **84**, 4993–4998 (2012).

134. T.O. Tasci, W.P. Johnson, D.P. Fernandez, E. Manangon, B.K. Gale, 'Biased Cyclical Electrical Field Flow Fractionation for Separation of Sub 50 nm Particles', *Anal. Chem.*, **85**, 11225–11232 (2013).

135. S. Rasouli, P. Blanchart, D. Clédat, P.J.P. Cardot, 'Size- and Shape-Dependent Separation of TiO_2 Colloidal Subpopulations with Gravitational Field Flow Fractionation', *J. Chromatogr. A*, **923**, 119–126 (2001).

136. A. Sanz-Medel, R. Pereiro, J. Manuel Costa-Fernandez, 'An Overview of Atomic Spectrometric Techniques', in *Basic Chemometric Techniques in Atomic Spectroscopy*, 2nd edition, The Royal Society of Chemistry, Cambridge, 1–51, Chapter 1, , 2013.

137. R.J.C. Brown, M.J.T. Milton, 'Analytical Techniques for Trace Element Analysis: An Overview', *TrAC, Trends Anal. Chem.*, **24**, 266–274 (2005).

138. F. Gagné, P. Turcotte, C. Gagnon, 'Screening Test of Silver Nanoparticles in Biological Samples by Graphite Furnace-Atomic Absorption Spectrometry', *Anal. Bioanal. Chem.*, **404**, 2067–2072 (2012).

139. G. Hartmann, C. Hutterer, M. Schuster, 'Ultra-Trace Determination of Silver Nanoparticles in Water Samples Using Cloud Point Extraction and ETAAS', *J. Anal. At. Spectrom.*, **28**, 567–572 (2013).

140. G. Hartmann, M. Schuster, 'Species Selective Preconcentration and Quantification of Gold Nanoparticles Using Cloud Point Extraction and Electrothermal Atomic Absorption Spectrometry', *Anal. Chim. Acta*, **761**, 27–33 (2013).

141. J.S. Becker, 'Trace and Ultratrace Analysis in Liquids by Atomic Spectrometry, *TrAC*', *Trends Anal. Chem.*, **24**, 243–254 (2005).

Encyclopedia of Analytical Chemistry, Online © 2006–2015 John Wiley & Sons, Ltd.

This article was published in the *Encyclopedia of Analytical Chemistry* in 2015 by John Wiley & Sons, Ltd.
DOI: 10.1002/9780470027318.a9427

142. M. Baalousha, B. Stolpe, J.R. Lead, 'Flow Field-Flow Fractionation for the Analysis and Characterization of Natural Colloids and Manufactured Nanoparticles in Environmental Systems: A Critical Review', *J. Chromatogr. A*, **1218**, 4078–4103 (2011).

143. A. Helfrich, J. Bettmer, 'Analysis of Gold Nanoparticles Using ICP-MS-Based Hyphenated and Complementary ESI-MS Techniques', *Int. J. Mass Spectrom.*, **307**, 92–98 (2011).

144. V. Geertsen, M. Tabarant, O. Spalla, 'Behavior and Determination of Titanium Dioxide Nanoparticles in Nitric Acid and River Water by ICP Spectrometry', *Anal. Chem.*, **86**, 3453–3460 (2014).

145. H.E. Pace, N.J. Rogers, C. Jarolimek, V.A. Coleman, C.P. Higgins, J.F. Ranville, 'Determining Transport Efficiency for the Purpose of Counting and Sizing Nanoparticles Via Single Particle Inductively Coupled Plasma Mass Spectrometry', *Anal. Chem.*, **83**, 9361–9369 (2011).

146. C. Degueldre, P.Y. Favarger, 'Colloid Analysis by Single Particle Inductively Coupled Plasma-Mass Spectroscopy: A Feasibility Study', *Colloids Surf., A*, **217**, 137–142 (2003).

147. C. Degueldre, P.Y. Favarger, 'Thorium Colloid Analysis by Single Particle Inductively Coupled Plasma-Mass Spectrometry', *Talanta*, **62**, 1051–1054 (2004).

148. C. Degueldre, P.Y. Favarger, S. Wold, 'Gold Colloid Analysis by Inductively Coupled Plasma-Mass Spectrometry in a Single Particle Mode', *Anal. Chim. Acta*, **555**, 263–268 (2006).

149. S. Hu, R. Liu, S. Zhang, Z. Huang, Z. Xing, X. Zhang, 'A New Strategy for Highly Sensitive Immunoassay Based on Single-Particle Mode Detection by Inductively Coupled Plasma Mass Spectrometry', *J. Am. Soc. Mass Spectrom.*, **20**, 1096–1103 (2009).

150. H.E. Pace, N.J. Rogers, C. Jarolimek, V.A. Coleman, E.P. Gray, C.P. Higgins, J.F. Ranville, 'Single Particle Inductively Coupled Plasma-Mass Spectrometry: A Performance Evaluation and Method Comparison in the Determination of Nanoparticle Size', *Environ. Sci. Technol.*, **46**, 12272–12280 (2012).

151. D.M. Mitrano, E.K. Lesher, A. Bednar, J. Monserud, C.P. Higgins, J.F. Ranville, 'Detecting Nanoparticulate Silver Using Single-Particle Inductively Coupled Plasma–Mass Spectrometry', *Environ. Toxicol. Chem.*, **31**, 115–121 (2012).

152. R.B. Reed, C.P. Higgins, P. Westerhoff, S. Tadjiki, J.F. Ranville, 'Overcoming Challenges in Analysis of Polydisperse Metal-Containing Nanoparticles by Single Particle Inductively Coupled Plasma Mass Spectrometry', *J. Anal. At. Spectrom.*, **27**, 1093–1100 (2012).

153. E.P. Gray, J.G. Coleman, A.J. Bednar, A.J. Kennedy, J.F. Ranville, C.P. Higgins, 'Extraction and Analysis of Silver and Gold Nanoparticles from Biological Tissues Using Single Particle Inductively Coupled Plasma Mass Spectrometry', *Environ. Sci. Technol.*, **47**, 14315–14323 (2013).

154. J. Tuoriniemi, G. Cornelis, M. Hassellöv, 'Size Discrimination and Detection Capabilities of Single-Particle ICP-MS for Environmental Analysis of Silver Nanoparticles', *Anal. Chem.*, **84**, 3965–3972 (2012).

155. G. Blo, C. Contado, F. Fagioli, M.H. Bollain Rodriguez, F. Dondi, 'Analysis of Kaolin by Sedimentation Field-Flow Fractionation and Electrothermal Atomic Absorption Spectrometry Detection', *Chromatographia*, **41**, 715–721 (1995).

156. C. Contado, G. Blo, F. Fagioli, F. Dondi, R. Beckett, 'Characterisation of River Po Particles by Sedimentation Field-Flow Fractionation Coupled to GFAAS and ICP-MS', *Colloids Surf., A*, **120**, 47–59 (1997).

157. B. Chen, R. Beckett, 'Development of SdFFF-ETAAS for Characterising Soil and Sediment Colloids', *Analyst*, **126**, 1588–1593 (2001).

158. R. Chantiwas, R. Beckett, J. Jakmunee, I.D. McKelvie, K. Grudpan, 'Gravitational Field-Flow Fractionation in Combination with Flow Injection Analysis or Electrothermal AAS for Size Based Iron Speciation of Particles', *Talanta*, **58**, 1375–1383 (2002).

159. G. Blo, C. Contado, F. Fagioli, F. Dondi, 'Size-Elemental Characterization of Suspended Particle Matter by Split-Flow Thin Cell Fractionation and Slurry Analysis-Electrothermal Atomic Absorption Spectrometry', *Analyst*, **125**, 1335–1339 (2000).

160. G. Blo, C. Contado, D. Grandi, F. Fagioli, F. Dondi, 'Dimensional and Elemental Characterization of Suspended Particulate Matter in Natural Waters: Quantitative Aspects in the Integrated Ultrafiltration, Splitt-Flow Thin Cell and Inductively Coupled Plasma–Atomic Emission Spectrometry Approach', *Anal. Chim. Acta*, **470**, 253–262 (2002).

161. D.J. Chittleborough, D.M. Hotchin, R. Beckett, 'Sedimentation Field-Flow Fractionation: A New Technique for the Fractionation of Soil Colloids', *Soil Sci.*, **153**, 341–348 (1992).

162. H. Cölfen, M. Antonietti, 'Field-Flow Fractionation Techniques for Polymer and Colloid Analysis', in *New Developments in Polymer Analytics I*, ed. M. Schmidt, Springer Berlin Heidelberg, New York, 67–187, 2000.

163. H.E. Taylor, J.R. Garbarino, D.M. Murphy, R. Beckett, 'Inductively Coupled Plasma-Mass Spectrometry as an Element-Specific Detector for Field-Flow Fractionation Particle Separation', *Anal. Chem.*, **64**, 2036–2041 (1992).

164. R. Beckett, 'Field-Flow Fractionation-ICP-MS: A Powerful New Analytical Tool for Characterizing Macromolecules and Particles', *At. Spectrosc.*, **12**, 228–232 (1991).

Encyclopedia of Analytical Chemistry, Online © 2006–2015 John Wiley & Sons, Ltd.

This article was published in the *Encyclopedia of Analytical Chemistry* in 2015 by John Wiley & Sons, Ltd.
DOI: 10.1002/9780470027318.a9427

165. J.F. Ranville, D.J. Chittleborough, F. Shanks, R.J.S. Morrison, T. Harris, F. Doss, R. Beckett, 'Development of Sedimentation Field-Flow Fractionation-Inductively Coupled Plasma Mass-Spectrometry for the Characterization of Environmental Colloids', *Anal. Chim. Acta*, **381**, 315–329 (1999).

166. M. Hassellöv, B. Lyvén, R. Beckett, 'Sedimentation Field-Flow Fractionation Coupled Online to Inductively Coupled Plasma Mass Spectrometry New Possibilities for Studies of Trace Metal Adsorption onto Natural Colloids', *Environ. Sci. Technol.*, **33**, 4528–4531 (1999).

167. B. Chen, C.A. Shand, R. Beckett, 'Determination of Total and EDTA Extractable Metal Distributions in the Colloidal Fraction of Contaminated Soils Using SdFFF-ICP-HRMS', *J. Environ. Monit.*, **3**, 7–14 (2001).

168. M. Hassellöv, B. Lyvén, C. Haraldsson, W. Sirinawin, 'Determination of Continuous Size and Trace Element Distribution of Colloidal Material in Natural Water by on-Line Coupling of Flow Field-Flow Fractionation with ICPMS', *Anal. Chem.*, **71**, 3497–3502 (1999).

169. D. Amarasiriwardena, A. Siripinyanond, R.M. Barnes, 'Trace Elemental Distribution in Soil and Compost-Derived Humic Acid Molecular Fractions and Colloidal Organic Matter in Municipal Wastewater by Flow Field-Flow Fractionation-Inductively Coupled Plasma Mass Spectrometry (Flow FFF-ICP-MS)', *J. Anal. At. Spectrom.*, **16**, 978–986 (2001).

170. A. Siripinyanond, Flow Field-Flow Fractionation-Inductively Coupled Plasma Mass Spectrometry, PhD Thesis, University of Massachusetts, Amherst, 2002.

171. A. Siripinyanond, R.M. Barnes, 'Flow Field-Flow Fractionation-Inductively Coupled Plasma Mass Spectrometry and Metal Speciation in Proteins: A Feasibility Study', *J. Anal. At. Spectrom.*, **14**, 1527–1531 (1999).

172. A. Siripinyanond, R.M. Barnes, 'Flow Field-Flow Fractionation-Inductively Coupled Plasma Mass Spectrometry of Chemical Mechanical Polishing Slurries', *Spectrochim. Acta, Part B*, **57**, 1885–1896 (2002).

173. S. Levin, 'Field Flow Fractionation in Biomedical Analysis', *Biomed. Chromatogr.*, **5**, 133–138 (1991).

174. R.M. Barnes, 'Advances in Inductively Coupled Plasma Mass Spectrometry: Human Nutrition and Toxicology', *Anal. Chim. Acta*, **283**, 115–130 (1993).

175. R.M. Barnes, 'Analytical Plasma Source Mass Spectrometry in Biomedical Research', *Fresenius J. Anal. Chem.*, **355**, 433–441 (1996).

176. D.M. Murphy, J.R. Garbarino, H.E. Taylor, B.T. Hart, R. Beckett, 'Determination of Size and Element Composition Distributions of Complex Colloids by Sedimentation Field-Flow Fractionation-Inductively Coupled Plasma Mass Spectrometry', *J. Chromatogr. A*, **642**, 459–467 (1993).

177. J. Van Berkel, R. Beckett, 'Estimating the Effect of Particle Surface Coatings on the Adsorption of Orthophosphate Using Sedimentation Field-Flow Fractionation', *J. Liq. Chromatogr. Related Technol.*, **20**, 2647–2667 (1997).

178. D. Schmitt, H.E. Taylor, G.R. Aiken, D.A. Roth, F.H. Frimmel, 'Influence of Natural Organic Matter on the Adsorption of Metal Ions onto Clay Minerals', *Environ. Sci. Technol.*, **36**, 2932–2938 (2002).

179. B. Chen, J. Hulston, R. Beckett, 'The Effect of Surface Coatings on the Association of Orthophosphate with Natural Colloids', *Sci. Total Environ.*, **263**, 23–35 (2000).

180. A. Siripinyanond, R.M. Barnes, D. Amarasiriwardena, 'Flow Field-Flow Fractionation-Inductively Coupled Plasma Mass Spectrometry for Sediment Bound Trace Metal Characterization', *J. Anal. At. Spectrom.*, **17**, 1055–1064 (2002).

181. D. Amarasiriwardena, A. Siripinyanond, R.M. Barnes, in *Humic Substances: Versatile Components of Plants, Soil and Water*, eds E.A. Ghabbour, G. Davies, The Royal Society of Chemistry, Cambridge, 214–226, 2000.

182. K.D. Caldwell, in *Field-Flow Fractionation Handbook*, eds M. Schimpf, K. Caldwell, J.C. Giddings, Wiley-Interscience, New York, 79–94, 2000.

183. H.E. Taylor, R.A. Huff, A. Montaser, in *Inductively Coupled Plasma Mass Spectrometry*, ed. A. Montaser, Wiley-VCH, New York, 681–807, 1998.

184. B.N. Barman, in *Field-Flow Fractionation Handbook*, eds M. Schimpf, K. Caldwell, J.C. Giddings, Wiley-Interscience, New York, 373–382, 2000.

185. H. Hagendorfer, R. Kaegi, M. Parlinska, B. Sinnet, C. Ludwig, A. Ulrich, 'Characterization of Silver Nanoparticle Products Using Asymmetric Flow Field Flow Fractionation with a Multidetector Approach – a Comparison to Transmission Electron Microscopy and Batch Dynamic Light Scattering', *Anal. Chem.*, **84**, 2678–2685 (2012).

186. D.M. Mitrano, A. Barber, A. Bednar, P. Westerhoff, C.P. Higgins, J.F. Ranville, 'Silver Nanoparticle Characterization Using Single Particle ICP-MS (SP-ICP-MS) and Asymmetrical Flow Field Flow Fractionation ICP-MS (AF4-ICP-MS)', *J. Anal. At. Spectrom.*, **27**, 1131–1142 (2012).

187. O. Geiss, C. Cascio, D. Gilliland, F. Franchini, J. Barrero-Moreno, 'Size and Mass Determination of Silver Nanoparticles in an Aqueous Matrix Using Asymmetric Flow Field Flow Fractionation Coupled to Inductively Coupled Plasma Mass Spectrometer and Ultraviolet–Visible Detectors', *J. Chromatogr. A*, **1321**, 100–108 (2013).

188. K. Songsilawat, J. Shiowatana, A. Siripinyanond, 'Flow Field-Flow Fractionation with Off-line Electrothermal

Encyclopedia of Analytical Chemistry, Online © 2006–2015 John Wiley & Sons, Ltd.

This article was published in the *Encyclopedia of Analytical Chemistry* in 2015 by John Wiley & Sons, Ltd.
DOI: 10.1002/9780470027318.a9427

Atomic Absorption Spectrometry for Size Characterization of Silver Nanoparticles', *J. Chromatogr. A*, **1218**, 4213–4218 (2011).

189. A.R. Poda, A.J. Bednar, A.J. Kennedy, A. Harmon, M. Hull, D.M. Mitrano, J.F. Ranville, J. Steevens, 'Characterization of Silver Nanoparticles Using Flow-Field Flow Fractionation Interfaced to Inductively Coupled Plasma Mass Spectrometry', *J. Chromatogr. A*, **1218**, 4219–4225 (2011).
190. M.E. Hoque, K. Khosravi, K. Newman, C.D. Metcalfe, 'Detection and Characterization of Silver Nanoparticles in Aqueous Matrices Using Asymmetric-Flow Field Flow Fractionation with Inductively Coupled Plasma Mass Spectrometry', *J. Chromatogr. A*, **1233**, 109–115 (2012).
191. A.P. Gondikas, F.V.D. Kammer, R.B. Reed, S. Wagner, J.F. Ranville, T. Hofmann, 'Release of TiO_2 Nanoparticles from Sunscreens into Surface Waters: A One-Year Survey at the Old Danube Recreational Lake', *Environ. Sci. Technol.*, **48**, 5415–5422 (2014).
192. B. Schmidt, K. Loeschner, N. Hadrup, A. Mortensen, J.J. Sloth, C. Bender Koch, E.H. Larsen, 'Quantitative Characterization of Gold Nanoparticles by Field-Flow Fractionation Coupled Online with Light Scattering Detection and Inductively Coupled Plasma Mass Spectrometry', *Anal. Chem.*, **83**, 2461–2468 (2011).
193. C. Contado, A. Pagnoni, 'TiO_2 in Commercial Sunscreen Lotion: Flow Field-Flow Fractionation and ICP-AES Together for Size Analysis', *Anal. Chem.*, **80**, 7594–7608 (2008).
194. C. Contado, A. Pagnoni, 'TiO_2 Nano- and Micro-Particles in Commercial Foundation Creams: Field Flow-Fractionation Techniques Together with ICP-AES and SQW Voltammetry for Their Characterization', *Anal. Methods*, **2**, 1112–1124 (2010).
195. A. Samontha, J. Shiowatana, A. Siripinyanond, 'Particle Size Characterization of Titanium Dioxide in Sunscreen Products Using Sedimentation Field-Flow Fractionation–Inductively Coupled Plasma–Mass Spectrometry', *Anal. Bioanal. Chem.*, **399**, 973–978 (2011).
196. V. Nischwitz, H. Goenaga-Infante, 'Improved Sample Preparation and Quality Control for the Characterisation of Titanium Dioxide Nanoparticles in Sunscreens Using Flow Field Flow Fractionation on-Line with Inductively Coupled Plasma Mass Spectrometry', *J. Anal. At. Spectrom.*, **27**, 1084–1092 (2012).
197. S.T. Kim, H.K. Kim, S.H. Han, E.C. Jung, S. Lee, 'Determination of Size Distribution of Colloidal TiO_2 Nanoparticles Using Sedimentation Field-Flow Fractionation Combined with Single Particle Mode of Inductively Coupled Plasma-Mass Spectrometry', *Microchem. J.*, **110**, 636–642 (2013).
198. I. López-Heras, Y. Madrid, C. Cámara, 'Prospects and Difficulties in TiO_2 Nanoparticles Analysis in Cosmetic and Food Products Using Asymmetrical Flow Field-Flow Fractionation Hyphenated to Inductively Coupled Plasma Mass Spectrometry', *Talanta*, **124**, 71–78 (2014).
199. C. Contado, L. Ravani, M. Passarella, 'Size Characterization by Sedimentation Field Flow Fractionation of Silica Particles Used as Food Additives', *Anal. Chim. Acta*, **788**, 183–192 (2013).
200. E. Bolea, J. Jiménez-Lamana, F. Laborda, J.R. Castillo, 'Size Characterization and Quantification of Silver Nanoparticles by Asymmetric Flow Field-Flow Fractionation Coupled with Inductively Coupled Plasma Mass Spectrometry', *Anal. Bioanal. Chem.*, **401**, 2723–2732 (2011).
201. K. Loeschner, J. Navratilova, C. Købler, K. Mølhave, S. Wagner, F. von der Kammer, E. Larsen, 'Detection and Characterization of Silver Nanoparticles in Chicken Meat by Asymmetric Flow Field Flow Fractionation with Detection by Conventional or Single Particle ICP-MS', *Anal. Bioanal. Chem.*, **405**, 8185–8195 (2013).
202. P. M-M, W. Somchue, J. Shiowatana, A. Siripinyanond, 'Flow Field-Flow Fractionation for Particle Size Characterization of Selenium Nanoparticles Incubated in Gastrointestinal Conditions', *Food Res. Int.*, **57**, 203–209 (2014).
203. R. Grombe, J. Charoud-Got, H. Emteborg, T.J. Linsinger, J. Seghers, S. Wagner, F. von der Kammer, T. Hofmann, A. Dudkiewicz, M. Llinas, C. Solans, A. Lehner, G. Allmaier, 'Production of Reference Materials for the Detection and Size Determination of Silica Nanoparticles in Tomato Soup', *Anal. Bioanal. Chem.*, **406**, 3895–3907 (2014).
204. J. Herould, V. Nischwitz, D. Bartczak, H. Goenaga-Infante, 'The Potential of Asymmetric Flow Field-Flow Fractionation Hyphenated to Multiple Detectors for the Quantification and Size Estimation of Silica Nanoparticles in a Food Matrix', *Anal. Bioanal. Chem.*, **406**, 3919–3927 (2014).
205. R.J.B. Peters, G. Van Bemmel, Z. Herrera-Rivera, H.P.F.G. Helsper, H.J.P. Marvin, S. Weigel, P.C. Tromp, A.G. Oomen, A.G. Rietveld, H. Bouwmeester, 'Characterization of Titanium Dioxide Nanoparticles in Food Products: Analytical Methods to Define Nanoparticles', *J. Agric. Food Chem.*, **62**, 6285–6293 (2014).

Encyclopedia of Analytical Chemistry, Online © 2006–2015 John Wiley & Sons, Ltd.

This article was published in the *Encyclopedia of Analytical Chemistry* in 2015 by John Wiley & Sons, Ltd.
DOI: 10.1002/9780470027318.a9427